MAY 1988
ENVIRONMENTAL SCIENCE & TECHNOLOGY
ES&T

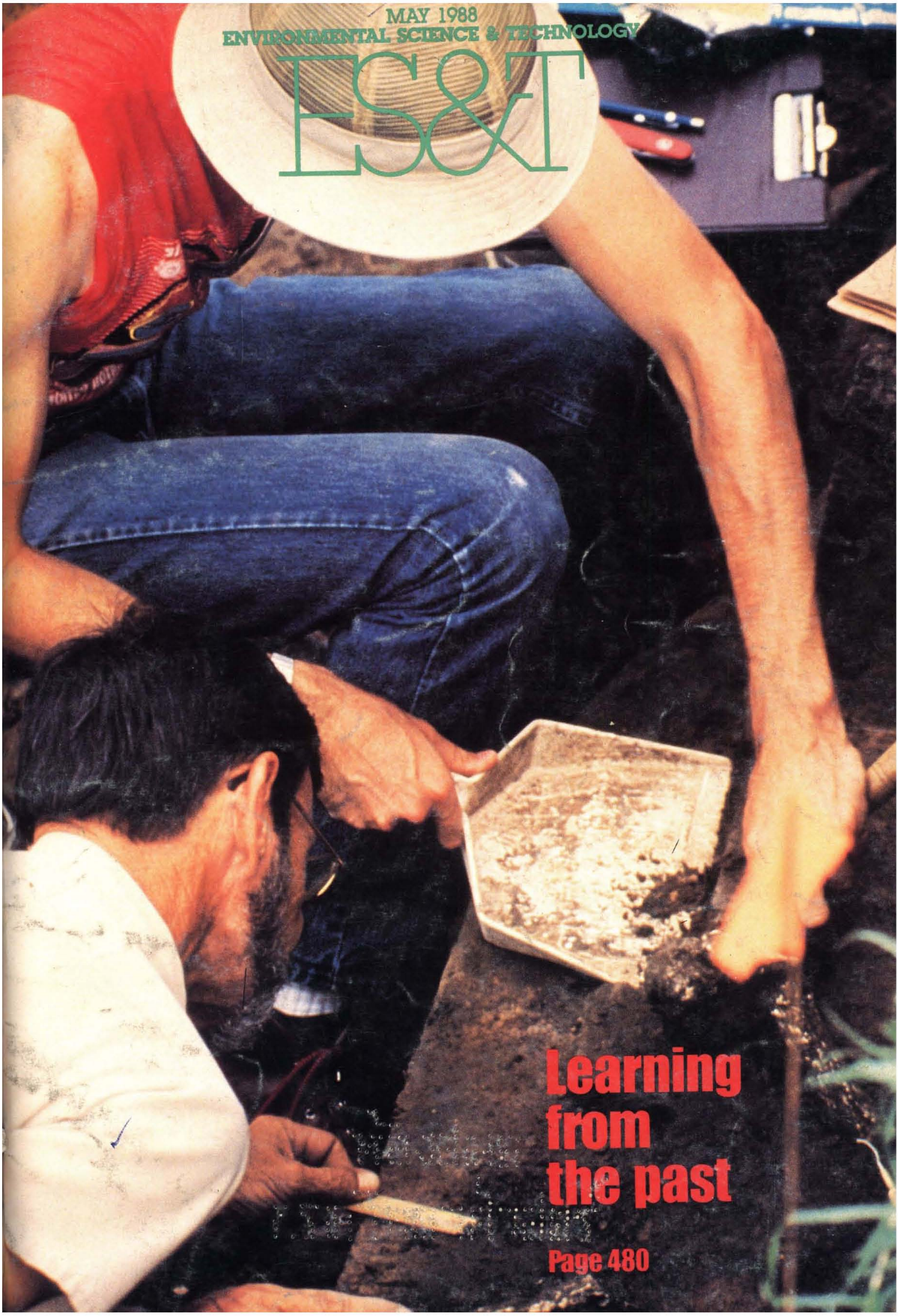

Learning from the past

Page 480

ARE YOU ALL THAT STANDS BETWEEN YOUR COMPANY AND DISASTER?

DON'T STAND ALONE.

Call Environmental Health Associates. We're the nation's most experienced provider of occupational and environmental health services. In the past ten years, we've probably completed more epidemiologic studies than any single group. Our physicians serve as corporate medical consultants to industries worldwide. We want to help you do an even better job protecting your employees, community, and company.

WE'RE HEALTH RISK ASSESSMENT SPECIALISTS.

We identify and measure the risk from chemical, biological, and physical hazards in the workplace and in the environment. We analyze the immediate impact of toxic exposure, and help you limit losses. We can place a team on site within days.

AND EFFECTIVE RISK MANAGERS.

At EHA, we're creative problem-solvers. We develop cost-effective strategies to increase safety and reduce risk, including EHA-CHIMES, our PC program for health data management. We explain our findings to your managers in terms they can understand, and help you communicate to the public.

EHA
WHEN IT'S A MATTER OF LIFE.[SM]

WE LISTEN.

Even if you think no one else does. Our permanent staff of over 50 physicians and specialists work well with industrial hygienists, law firms, government agencies, corporate medical departments, and management. You can call on your EHA team 24 hours a day.

WE'RE YOUR INFORMATION RESOURCE.

We keep you up to date with changing regulations. You'll have access to information on any health-related subject when you call our toll-free hotlines. EHA-INFO can give you complete information within 24 hours. Our board-certified physicians are always available to answer questions.

CALL TOLL-FREE FOR OUR COMPLETE INFORMATION PACKAGE.

Ask for extension 602.

1 (800) EHA-INFO in California

1 (800) 922-INFO nationwide

1 (415) 451-1888 worldwide

ENVIRONMENTAL HEALTH ASSOCIATES, INC.
520 THIRD STREET, SUITE 208
OAKLAND, CA 94607

Environmental Science & Technology

Please send *research* manuscripts to Manuscript Reviewing, *feature* manuscripts to Managing Editor. For editorial policy, author's guide, and peer review policy, see the January 1988 issue, page 31, or write Monica Creamer, Manuscript Reviewing Office, *ES&T.* A sample copyright transfer form, which may be copied, appears on the inside back cover of the January 1988 issue.

Environmental Science & Technology, ES&T (ISSN 0013-936X), is published monthly by the American Chemical Society at 1155 16th Street, N.W., Washington, D.C. 20036. Second-class postage paid at Washington, D.C., and at additional mailing offices. POSTMASTER: Send address changes to *Environmental Science & Technology,* Membership & Subscription Services, P.O. Box 3337, Columbus, Ohio 43210.

SUBSCRIPTION PRICES 1988: Members, $30 per year; nonmembers (for personal use), $55 per year; institutions, $192 per year. Foreign postage, $8 additional for Canada and Mexico, $18 additional for Europe including air service, and $24 additional for all other countries including air service. Single issues, $15 for current year; $19 for prior years. Back volumes, $219 each. For foreign rates add $2 for single issues and $10 for back volumes. Rates above do not apply to nonmember subscribers in Japan, who must enter subscription orders with Maruzen Company Ltd., 3-10 Nihon bashi 2 chome, Chuo-ku, Tokyo 103, Japan. Tel: (03) 272-7211.

SUBSCRIPTION SERVICE: Orders for new subscriptions, single issues, back volumes, and microform editions should be sent with payment to Office of the Treasurer, Financial Operations, ACS, 1155 16th St., N.W., Washington, D.C. 20036. Phone orders may be placed, using Visa, Master Card, or American Express, by calling the ACS Sales Office toll free (800) ACS-5558 from anywhere in the continental U.S. (In the Washington, D.C., area call 872-4600.) Changes of address, subscription renewals, claims for missing issues, and inquiries concerning records and accounts should be directed to Manager, Membership and Subscription Services, ACS, P.O. Box 3337, Columbus, Ohio 43210. Changes of address should allow six weeks and be accompanied by old and new addresses and a recent mailing label. Claims for missing issues will not be allowed if loss was due to insufficient notice of change of address, if claim is dated more than 90 days after the issue date for North American subscribers or more than one year for foreign subscribers, or if the reason given is "missing from files."

ES&T CONTENTS

Volume 22, Number 5, May 1988

FEATURES

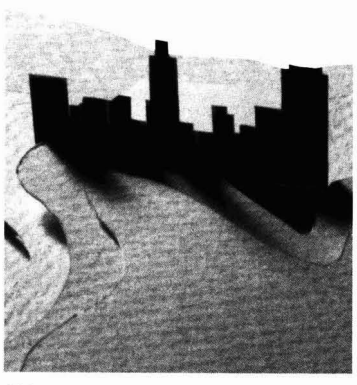

REGULATORY FOCUS

DEPARTMENTS

UPCOMING

RESEARCH

Cover: Ann F. Ramenofsky. Excavation of an archaeological site in central Louisiana under an investigation led by Ann Ramenofsky.

Credits: Fred Mang, Jr., National Park Service, p. 478; Ann Ramenofsky (two photos), p. 480.

ESTHAG 22(5)473–568 (1988)
ISSN 0013 936X

510
Chernobyl radionuclides in the environment: Tracers for the tight coupling of atmospheric, terrestrial, and aquatic geochemical processes. Peter H. Santschi,* Silvia Bollhalder, Klaus Farrenkothen, Alfred Lueck, Stefan Zingg, and Michael Sturm

The processes that influenced the mobility of Chernobyl radionuclides in air, soil, and aquatic reservoirs are investigated.

517
Atmospheric speciation and wet deposition of alkyllead compounds. Andrew G. Allen, Miroslav Radojevic, and Roy M. Harrison*

Concentrations and speciation of alkyllead compounds in air and total deposition are measured at urban and rural sites.

523
Nature and properties of some chlorinated lipophilic organic compounds in spent liquors from pulp bleaching. 1. Liquors from conventional bleaching of softwood kraft pulp. A. Bruce McKague,* Marie-Claude Kolar, and Knut B. Kringstad

RPTLC plays a key role in the isolation and identification of new chlorinated organics in spent chlorination liquor from pulp bleaching.

527
Rainwater analysis: a comparison between proton-induced X-ray emission and graphite furnace atomic absorption spectroscopy. Hans-Christen Hansson,* Ann Kristin C. Ekholm, and Howard B. Ross

One advantage of PIXE analysis is that 26 elements can be determined simultaneously.

532
Trace-element partitioning during the retorting of Condor and Rundle oil shales. John H. Patterson,* Leslie S. Dale, and James F. Chapman

The results show that arsenic is the most significant element in relation to both shale oil refining and disposal of retort waters.

537
Proteins in natural waters and their relation to the formation of chlorinated organics during water disinfection. Frank E. Scully, Jr.,* G. Dean Howell, Robert Kravitz, Jeffrey T. Jewell, Victor Hahn, and Mark Speed

Proteins may make a significant contribution to the trihalomethane formation potential of a surface water during algal blooms.

543
Occurrence and bioaccumulation of organochlorine compounds in fishes from Siskiwit Lake, Isle Royale, Lake Superior. Deborah L. Swackhamer and Ronald A. Hites*

These results, which confirm the long-range transport of several chlorinated pesticides and PCBs, indicate that technical chlordane constituents also are transported to remote locations.

548
Comparative toxicology for risk assessment of marine fishes and crustaceans. Glenn W. Suter II* and Aaron E. Rosen

Acute and chronic toxic effects data for marine fishes and crustaceans are analyzed to reveal patterns of relative sensitivity for risk assessment of coastal pollution.

557
Catalytic oxidation of polychlorinated biphenyls in a monolithic reactor system. Prasad Subbana, Howard Greene,* and Faredoon Desai

PCB destruction efficiencies and product selectivities for five catalysts are studied at temperatures between 500 °C and 600 °C.

561
A numerical solution for mass transport in membrane-based diffusion scrubbers. Richard L. Corsi,* Daniel P. Y. Chang, and Bruce E. Larock

A finite element model provides a tool for designing membrane-based diffusion scrubbers for which no existing analytical solutions are applicable.

565
Development and evaluation of a procedure for determining volatile organics in water. Larry C. Michael, Edo D. Pellizzari,* and Roger W. Wiseman

Volatile organic compounds from various waters are analyzed by coupled purge and trap-GC/MS/DS using the comprehensive EPA Master Analytical Scheme approach.

571
Influence of vapor-phase sorption and diffusion on the fate of trichloroethylene in an unsaturated aquifer system. Michele S. Peterson, Leonard W. Lion,* and Christine A. Shoemaker

Linear partition coefficients for binding of TCE vapor under a range of unsaturated conditions are 1–4 orders of magnitude greater than the value measured for the saturated sorbent.

578
Atmospheric reactions of a series of dimethyl phosphoroamidates and dimethyl phosphorothioamidates. Mark A. Goodman, Sara M. Aschmann, Roger Atkinson,* and Arthur M. Winer

The kinetics of the atmospherically important gas-phase reactions of a series of dimethyl phosphoroamidates and phosphorothioamidates with OH and NO_3 radicals and O_3 are investigated.

583
Xenon-133 in California, Nevada, and Utah from the Chernobyl accident. Robert W. Holloway* and Chunk-King Liu

The observed activity was much less than the peak xenon-133 activity detected in New York state after the Three Mile Island accident.

586
Rate constant for the reaction of NO_2 with sulfur(IV) over the pH range 5.3–13. Carol L. Clifton, Nisan Altstein, and Robert E. Huie*

A pulse radiolysis apparatus with signal averaging is used to monitor the decay of NO_2 directly and measure rate constants.

NOTES

590
Gran's titrations and ion balances: Some analytical control limits for precipitation and surface waters. Neil R. McQuaker* and Douglas K. Sandberg

Analytical results provided by weakly buffered samples are used to define control limits for cation–anion balances when the combined cation plus anion concentration is below 700 μeq/L.

*To whom correspondence should be addressed.

This issue contains no papers for which there is supplementary material in microform.

ES&T
EDITORIAL

Notes, correspondence, and communications

The research section of *ES&T* is devoted to the publication of critically reviewed Articles, Notes, and Correspondence. Articles, or full research papers, form the bulk of the research section; Notes are defined as short research reports describing preliminary results of unusual significance or studies of small scope; and Correspondence is significant comment on work published in the research section, with the original author given the opportunity for rebuttal.

Currently, the Notes section is not given special editorial treatment for more expeditious publication. Review proceeds on the same time scale as full research papers. As a result, Notes usually serve only one purpose: to report studies of small scope. Many Notes are originally submitted in the form of full papers and, as a consequence of review, the authors are encouraged to shorten the paper and resubmit it as a Note. In a few cases authors intend for their paper to be considered as a Note and construct it accordingly.

ES&T does not yet have a mechanism for facilitating rapid publication of articles "of unusual significance." From time to time, authors request rapid review of their manuscript, but few Notes are submitted with rapid publication specifically in mind. It is not clear if this is because there is little need for rapid publication in the field of environmental science and technology, or because our editorial policy has discouraged such attempts.

At the annual meeting of the *ES&T* Editorial Advisory Board in March, the Board discussed this issue and decided to pursue a course that will lead to a rapid communications section of *ES&T*. The consensus of the Board was that such a section is needed and that it would be enthusiastically received by our constituency. A second proposal discussed by the board was discontinuation of the Notes section because Notes, although somewhat shorter, are often similar to the full papers.

In addition, I discussed with the Board the prospect of discontinuing the Correspondence section. My view is that the practice of printing comments and rebuttals, although sometimes enlightening, often does not present a comprehensive argument of the issues and seldom serves to reconcile differences. Moreover, the Correspondence section creates editorial problems, such as ensuring adequate, but not excessive, response time for the original authors' rebuttal. In general, I feel that the refereed literature is the place for such debates; that is, good science eventually will prevail. Some members of the Board expressed support for continuing the Correspondence section in some form. One method for handling debates of broad interest might be to publish point–counterpoint articles in the Views section in the front of the journal.

The editors and the Board have made no firm decisions on these matters, but we plan to do so within the next few months. I would be pleased to hear your views on these proposals.

0013-936X/88/0922-0475$01.50/0

For Over Six Decades...

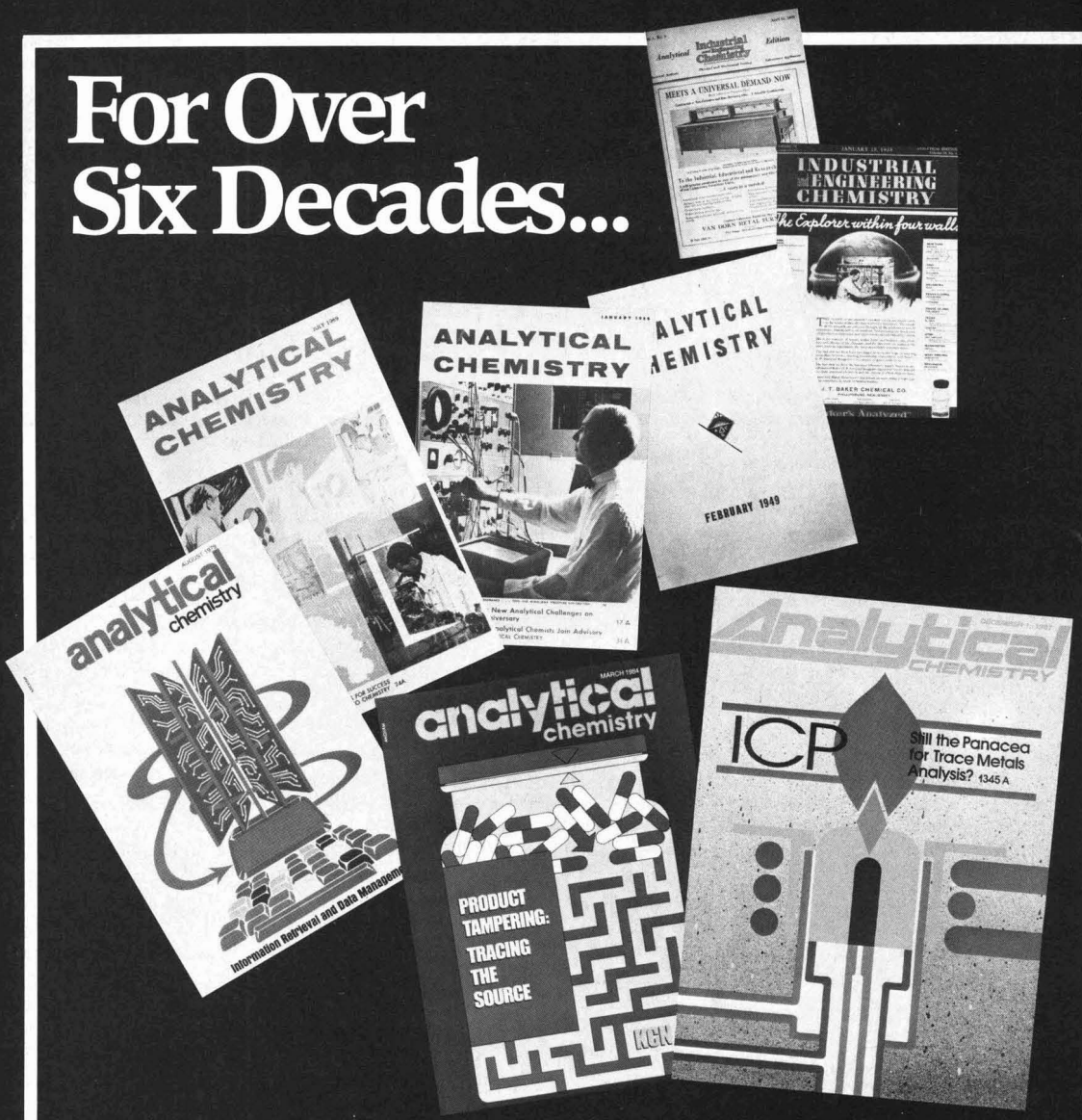

The Leader in the Field.

Now twice a month!

ANALYTICAL CHEMISTRY the world's foremost publication in the vital field of measurement science is now coming to you semi-monthly.

Keeping pace with these changes has continued to make *ANALYTICAL CHEMISTRY* the pinnacle of publications in the field . . . for over 6 decades.

Call now for your own personal subscription

CALL TOLL FREE (800) 227-5558

American Chemical Society
1155 16th St., NW
Washington, DC 20036

INTERNATIONAL

Acid rain can harm aquatic ecosystems severely in about 46% of Canada's land area (about 4 million km^2) according to the report "Acid Rain: A National Sensitivity Assessment" by Environment Canada. The most sensitive areas are found where granitic bedrock of the Canadian Shield is exposed and where shallow, coarse-textured soils are prevalent. Such rocks and soils are found in parts of British Columbia, the Northwest Territories, Ontario, and Yukon, but especially in Newfoundland, Nova Scotia, and Quebec. These areas contain much water in which the potential to combat and reduce acidity is generally low. An additional 1.8 million km^2 in British Columbia, New Brunswick, Ontario, and Quebec are classified as "moderately sensitive" to acid rain.

FEDERAL

The Senate ratified a treaty that requires its signatories to cut by 50% their consumption of chlorofluorocarbons (CFCs) by 1999. The March 14 vote was 83 to 0. Used as refrigerants, spray can propellants, and solvents, CFCs have been blamed for damaging the stratospheric ozone layer that shields Earth from harmful solar ultraviolet light. If 11 countries, representing two-thirds of the world's CFC consumers, ratify the treaty this year, it will take effect Jan. 1, 1989; otherwise, implementation must begin April 1, 1989. The treaty had been signed last September by 30 nations that met in Montreal.

It could cost the Department of Defense (DOD) and the Department of Energy (DOE) $100 billion to clean up their radioactive- and hazardous-waste sites, Energy Undersecretary Joseph Salgado told a House subcommittee March 10. Salient examples of highly contaminated DOD and DOE sites are the Rocky Mountain Arsenal (Colo.) and nuclear weapons production plants near Richland, Wash., Aiken, S.C., and Oak Ridge, Tenn. For instance, groundwater contamination near Oak Ridge by hazardous solvents could exceed drinking-water standards by as much as 1000 times, and radionuclide contamination of groundwater at the South Carolina and Washington sites may exceed drinking-water standards by 400 times. Forcing DOD, DOE, or any other federal agency to clean up a hazardous-waste site is difficult because one executive branch agency may not sue or issue orders to another agency.

***Thomas:** No FIFRA change this year*

EPA Administrator Lee Thomas does not expect Congress to reauthorize the Federal Insecticide, Fungicide, and Rodenticide Act (FIFRA) in 1988. He told the National Association of State Departments of Agriculture March 8 that one major impediment to reauthorization is the exemption of farmers from liability for damage from pesticides that are applied according to label instructions; another obstacle involves the right of states to set pesticide residue levels that are more stringent than federally mandated levels. Two reauthorization bills have been introduced—one by Sens. Patrick Leahy (D-Vt.) and Richard Lugar (R-Ind.) and the other by Sens. Howell Heflin (D-Ala.) and Jesse Helms (R-N.C.).

The General Accounting Office (GAO) notes that no federal program for establishing groundwater contaminant standards currently exists. In a report to Sen. Max Baucus (D-Mont.) (GAO/PEMD-88-6, March 1988), GAO says many states have developed their own standards; however, state officials often had less information than needed and had to duplicate efforts to develop their standards. The GAO report says state officials need more information on subjects such as the analytical chemistry of contaminants, human exposure, fate of substances, and the technological feasibility of control. GAO also recommends that EPA establish a criteria document for groundwater contaminants, with emphasis on those that pose the greatest risks.

An EPA report describes the steps toward a nonpoint source water pollution control strategy that the agency and states have taken. The March 2 report to Congress explains that EPA plans to issue guidance to the states clarifying nonpoint source control requirements of the Clean Water Act amendments of 1987. Funds are being distributed to 31 states for the preparation of assessment reports and the development of management programs. The report also sets forth the current status of state programs and major issues to be dealt with during the next year. Copies of the report, "A Report to Congress, Activities and Programs Implemented under Section 319 of the Clean Water Act as Amended by the Water Quality Act of 1987, December 1987," can be obtained from the Nonpoint Sources Branch, Office of Water Regulations and Standards, U.S. EPA, Washington, D.C. 20460.

EPA may sharply tighten standards for lead in drinking water, possibly as early as January 1989, according to preliminary proposals the agency has drafted. The maximum contaminant level (MCL) could be reduced from 50 ppb to as little as 5 ppb. How this new standard would be enforced is problematic. For example, if the lead originates in pipes in a private home, the agency has no power to require the homeowner to treat the water or replace the pipes. Thus the current focus is on improving treatment techniques that the supplier must use. EPA also will encourage states to mandate the replacement of service lines in cases in which anticorrosion methods have not reduced lead contamination to acceptable levels (average 10 ppb, maximum 20 ppb). EPA also is considering an alternative MCL of 8 ppb and an MCL of 10 ppb enforceable at the tap.

STATES

The attorneys general of Maine and Ohio have called upon Congress to force federal agencies to comply with hazardous-waste laws

0013-936X/88/0922-0477$01.50/0

by enacting new legislation. Under current law, the doctrine of sovereign immunity severely limits actions states can take to force these clean-ups. One bill now before Congress (H.R. 3781) would expand the waiver of sovereign immunity under the Resource Conservation and Recovery Act to allow states to issue administrative orders and sanctions and to impose fines and prison terms for violations of hazardous-waste laws at federal installations. Other bills, not as controversial, would establish a special environmental counsel to pressure federal agencies to clean up, create separate federal agency funds, or give EPA the power to enforce hazardous-waste laws at federal facilities.

Saguaros: Threat from air pollution?

Are Arizona's saguaro cacti declining partly because of air pollution? Scientists from Los Alamos National Laboratory and the National Park Service are studying the effects caused by emissions from copper smelters and the "brown haze" from the Tucson metropolitan area. They observe that the older plants are losing spines, turning brown, and dying and that the young cacti are few in number. The researchers are collecting samples from both healthy and unhealthy saguaros in the Saguaro National Monument near Tucson. They also are sampling the soil to ascertain whether pollutants are making nutrients such as nitrogen and potassium less available to the cacti. In addition, the scientists are analyzing the cores of trees in the area to determine what air pollution may have existed during the past century.

California's sweeping Proposition 65, which requires businesses to warn the public of any exposure to certain chemicals above a defined level, is now being enforced. Proposition 65 had been opposed by California Gov. George Deukmejian, but after the proposition was voted into law by referendum with a 2-to-1 margin, Deukmejian said he would enforce its provisions. The portion of Proposition 65 that requires the warnings of possible exposure to any of the 31 listed substances went into effect Feb. 27. Another provision, which takes effect in October, forbids the discharge of chemicals on the Proposition 65 list into drinking-water sources. The food, drug, and cosmetic industries have been granted a temporary exemption from the new law.

Partly because of Florida's system of environmental regulations, environmental engineering graduates have few problems finding jobs in that state, says Warren Viessman, chairman of the Department of Environmental Engineering Sciences at the University of Florida. Viessman adds that they normally can expect salaries of $20,000–$30,000 to start and that specialists in groundwater contamination are much in demand (these jobs usually require a master's degree). The training of environmental technicians also is a rapidly expanding field in Florida. In 1987, for example, the university's Center for Training Research and Education for Environmental Occupations (TREEO) offered 72 courses and trained 2700 professionals. This year TREEO is offering 100 courses and expects an enrollment of 4000.

The Groundwater Education in Michigan (GEM) Program has been launched at Michigan State University (MSU) under the sponsorship of the W. K. Kellogg Foundation (Battle Creek, Mich.). The Foundation is working with MSU's Institute of Water Research, which will provide the technical expertise necessary to help combat groundwater contamination in the state. Foundation funding will be used to foster individual and community action. Among projects under consideration are improved septic-system maintenance, proper handling of household and agricultural wastes, and training of local officials and community leaders.

AWARDS

Robert M. White received the Kenneth Andrew Roe Award of the American Association of Engineering Societies April 6. The award is one of several given each year for advancing the knowledge, understanding, and practice of engineering in the public interest. White has been president of the National Academy of Engineering since 1983. From 1970 to 1977, he was administrator of the National Oceanic and Atmospheric Administration (NOAA) of the Department of Commerce, and he served as administrator of NOAA's predecessor, the Environmental Science Services Administration, between 1965 and 1970.

SCIENCE

Stratospheric ozone levels over urban areas of North America and Europe have decreased by as much as 3%, according to results of an international study by scientists from U.S. and U.N. agencies. Moreover, stratospheric ozone levels over Alaska and Scandinavia have been observed to drop by more than 6% during the winter months. Robert Watson of NASA says the scientists believe that the decrease in ozone levels "is wholly or in large part due to man-made chlorine [from chlorofluorocarbons]." The 3% drop, calculated on a year-round basis, has been observed between latitudes 40° N and 53° N, comprising some of the world's most populated areas. The observed ozone decline in winter in these latitudes has been as high as 4.7%.

No increase in human birth defects resulted from exposure to 2,3,7,8-tetrachlorodibenzo-*p*-dioxin (TCDD) following the July 1976 accident in and around Seveso, Italy. According to the *Journal of the American Medical Association* (March 1988), researchers at Catholic University in Rome have found that children born in the contaminated area after the accident showed no abnormalities attributable to TCDD. Their study of more than 15,000 children—especially those born during the first three months of 1977—found no more malformations than in control populations. Moreover, the scientists report that not one baby born in the contaminated zone had a major malformation. Also, EPA has provisionally put its estimate of the carcinogenicity of TCDD at 6.2% of the previous figure.

The atmosphere can carry hazardous wastes long distances—even thousands of miles, says Steve Eisenreich of the University of Minnesota. He and other scientists estimate that as much as 90% of the polychlorinated biphenyls (PCBs), as well as much of the lead and benzo[*a*]pyrene found in Lake Superior, fell from the air. More confirmation of the air's ability to carry contaminants has been found in samples of

fish taken from Siskiwit Lake, a lake in the middle of the uninhabited Isle Royale in Lake Superior. No industry is nearby, gasoline engines are forbidden on the island, and aircraft may not fly over it. Nevertheless, fish taken from Siskiwit Lake contained PCBs, leading scientists to the conclusion that atmospheric transport is the only possible source of the contaminants.

TECHNOLOGY

A groundwater and soil data base that can store data for an unlimited number of wells and chemical parameters has been developed to provide data input and validation, tracking and reporting of well installations, field monitoring, and laboratory results. The program, known as EnviroBase III, is designed to manage environmental data for engineering consulting firms and for generators of hazardous waste. It is written in dBase III+ language, is compiled in Clipper, and can be used on IBM and compatible computers. The program requires a minimum of 640 kB of memory and a hard disk. Introduced by EnviroBase Systems Inc. (Englewood, Colo.), the program can do statistical analysis and plotting together with other software and currently is being used by a large chemical company to handle soil and groundwater data.

A particulate control technology: ceramic membrane filter[a]

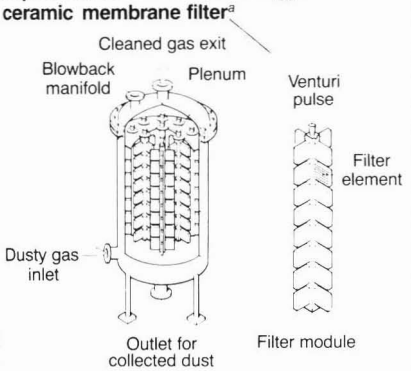

[a]Applicable to new coal use technologies
Source: U.S. Department of Energy

The control of particulate matter from coal combustion "is a mature technology," according to a report published in February by IEA Coal Research (London). Nevertheless, "a wide range of work is under way to improve the applicability, performance, and cost-effectiveness of particulate control equipment." The report, "Particulate Control for Coal Combustion," covers existing technologies and ongoing advances in mechanical collectors, electrostatic precipitators, fabric filters, and wet scrubbers. It also discusses particulate control for new coal utilization technologies and the interaction between particulate removal and sulfur control. The new technologies covered include coal–liquid mixtures, fluidized-bed combustion, gasification, and combined-cycle systems.

Three approaches to removing radon from community water supplies are being tested by Nancy Kinner of the University of New Hampshire. One technique involves the use of granular activated carbon (GAC). This method creates a problem, however, because removal rates with GAC decrease with time and radon emitters concentrated in the filter—such as uranium and radium—emit enough radiation to qualify the used carbon as a hazardous waste. Another approach involves packed tower and diffused bubble aeration, by which 98–99% of the radon emitters are removed. Radon-containing air, however, must be vented out, and other contaminants may accumulate on the packing material. The third approach uses "low-tech" systems such as spray nozzles and bubble aeration systems. Kinner currently believes that aeration systems show the most promise.

Electric utilities can assess exposure levels associated with chemical spills by means of the POSSM (PCB on-site spill model) developed by CH2M Hill under contract to the Electric Power Research Institute (EPRI, Palo Alto, Calif.). Although the model was designed to evaluate exposure levels and alternative cleanup strategies for polychlorinated biphenyls (PCBs), it is applicable to other contaminants. The model also may be used to address the extent of exposure from chemical residues at old spill sites and the effectiveness of cleanup and containment alternatives. Software for POSSM is available for use with IBM personal computers and compatible devices, according to EPRI spokesmen.

BUSINESS

Gladys Berchtold, chairman of Standard Laboratories (Charleston, W. Va.) called for the establishment of a single government laboratory accreditation board. Testifying for the American Council of Independent Laboratories, Berchtold told a House subcommittee that this board would "resolve difficulties that have arisen because of the proliferation of accrediting practices throughout the country." She proposed that the board be authorized to examine accreditation systems and "withhold approval from inadequate or marginally adequate systems." She added that the board should assign areas of accreditation and carry out those functions needed to produce "a comprehensive, technically competent system for laboratory accreditation." Berchtold said that "Congress needs to recognize the serious problem that exists because the country is without a national accreditation program."

Pollution control expenditures could increase by at least $32 billion a year and as many as 600,000 jobs could be lost if proposed amendments to the Clean Air Act (S. 1894) become law, warns the Business Roundtable (New York). The total annual environmental control cost to industry would exceed $100 billion, or about 2.5% of the Gross National Product, says David Roderick, chairman of USX and of the Business Roundtable's Environmental Task Force. He notes that S. 1894, introduced by Sen. George Mitchell (D-Me.) contains provisions addressing acid rain, mobile-source emissions, and the failure of many cities to meet ozone standards. Roderick notes that the $32 billion cost estimate covers only 21 of the 43 provisions because estimates for the remaining ones are not yet available.

The Fertilizer Institute (FI) has blasted the U.S. Department of Agriculture for seeking ways to replace synthetic chemical fertilizers and pesticides. Orville Bentley, assistant secretary for science and education, explained that the department is seeking "more harmless [farming] methods" in an effort to reduce human health hazards and water contamination associated with the "excessive use of these substances." The increased moves toward "low-input" farming, however, are reducing the revenues of agricultural chemical manufacturers. For example, the fertilizer industry enjoyed annual revenues of $10 billion during the early 1980s, but last year these revenues decreased to $7 billion because of reduced planting and costs of chemicals and environmental concerns. FI president Gary Myers charged that Bentley's statements were based on "no facts" and that the department "is advocating one farming system at the expense of another."

ES&T
FEATURES

Archaeological chemistry

The long-term migration of metals from archaeological contexts affects the movement of hazardous wastes

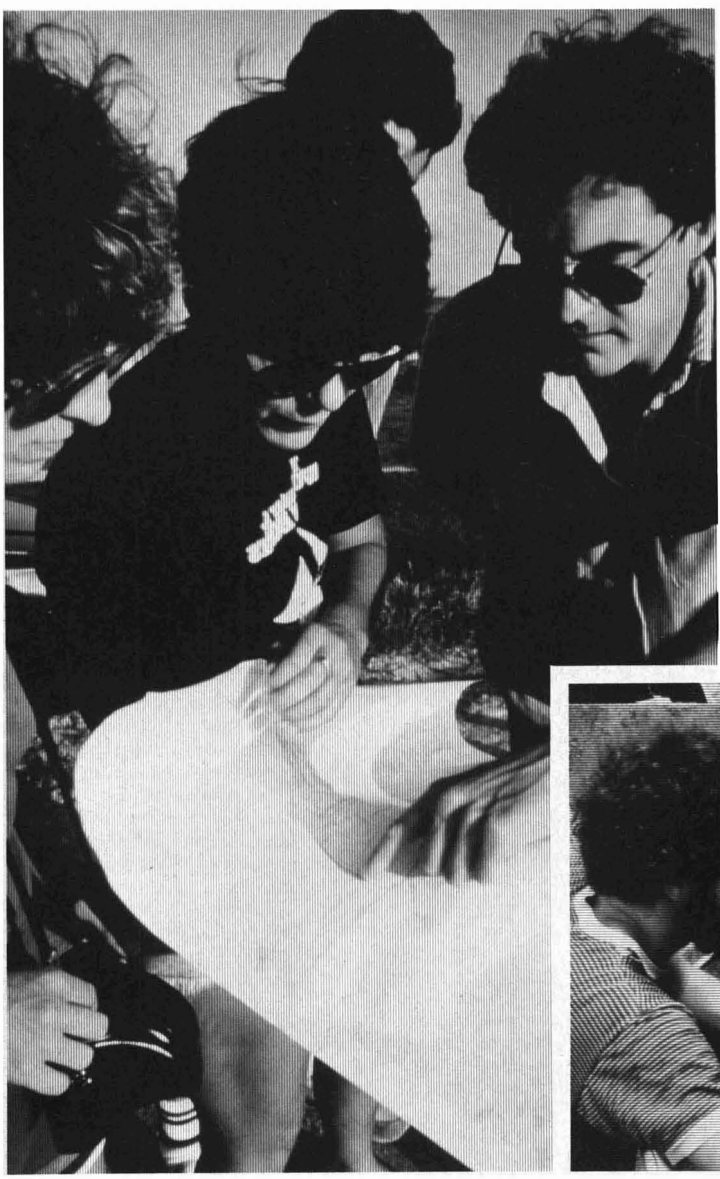

Jacob Thomas
Louis J. Thibodeaux
Ann F. Ramenofsky
Stephen P. Field
Bob J. Miller
Ann M. Whitmer
Hazardous Waste Research Center
Louisiana State University
Baton Rouge, La. 70803

The chemistry of archaeological sites may provide key information concerning the long-term movement of inorganic and organic constituents in soils. A scientific study of the soil surrounding material remains—such as fossilized or nonfossilized bone and lithic or ceramic artifacts, monuments, and the remains of daily living—may reveal important information on the likely future behavior of chemicals escaping landfills and similar waste-disposal sites.

The deposition of waste in or on the earth is not merely a recent human activity. Wastes generated from early factories or cottage industries were dis-

0013-936X/88/0922-0480$01.50/0

FIGURE 1
Concentration of elements above the Mucking silhouette

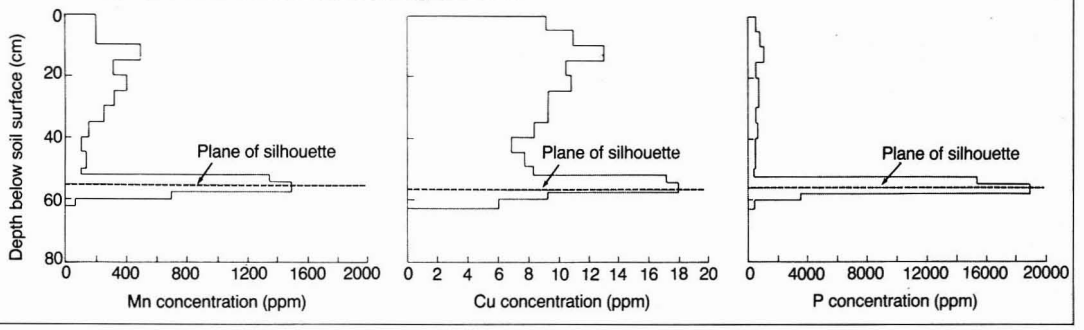

posed on-site or very near such operations. Because the material record of the human past—the archaeological record—currently exists on or below the surface of the earth, it includes chemical residues of past human activity. Although wholly new compounds have been produced during the last four decades that are not specifically analogous to chemicals produced in the past, it is possible that the study of chemical residues at archaeological sites could provide useful information for the future.

Archaeological investigation coupled with the chemical analysis of selected metal species has relevance for the deposition of hazardous materials, both in the surrounding soil and in the artifact (i.e., bone, metal, storage pit, or mound). Such investigations can yield data on long-term transport and fate of hazardous substances. Anthropogenic organic compounds, like metal species, are deposited in soil, but they are less likely to be preserved in appreciable quantities over long periods of time. Organic decomposition in most environmental settings is more rapid than inorganic transformation. The only exceptions to this statement are organics deposited in anaerobic environments or buried in contact with metals such as copper. The association of a metal with an organic reduces the probability of microbial activity.

The object of this paper is to show how the profile of metal concentration in the soil near bone from archaeological sites can be used, along with the appropriate mathematical model, to extract transport parameters. These parameters can then be used to predict long-term migration rates of chemical species associated with the burial of hazardous wastes in similar environmental settings.

Metal concentration profiles in soil

Although a number of archaeological studies have considered the question of elemental movement into and away from bone, only a few studies have considered the interactions between soil and bone (*1–7*). Fewer still have collected large soil samples and reported their results in a way that could be analyzed for information on chemical transport. We have located two such studies that meet the latter criterion.

One involves human remains, referred to as the Illinois Femurs (*8*), of the Middle Woodland Period in west-central Illinois (100 B.C.–400 A.D.). The study of four burials at the Illinois site demonstrated that, under certain environmental conditions, some metals (e.g., Ca and Mg) can be leached from bone, whereas others (e.g., Fe, Al, and K) adsorb into the bone. Unfortunately, certain anomalies in the chemical profiles required that we exclude these data from our analysis. The second study of a fifth-century Anglo-Saxon burial from Mucking, Essex, U.K. proved most useful for our purposes and became the basis of our analysis (*9*).

The Mucking silhouette

Bone preservation in archaeological sites varies considerably according to soil conditions. In general, bone is preserved well in soils of neutral or slightly alkaline pH and poorly in acidic soils. In certain circumstances the bone itself may nearly disappear, leaving a dark stain, or "silhouette," in the ground. The following is a summary of the findings on metal mobility around the Mucking silhouette (*9*).

Dedication

This feature article is dedicated to the memory of Professor Bob J. Miller, a coauthor on this paper, who died suddenly during an operation for an aneurysm. A recognized authority on soil acidity, Miller was an active force behind curriculum changes at LSU and had been nominated as Outstanding Professor in the LSU College of Agriculture.

A single grave was chosen for detailed analysis. It contained a fifth-century Saxon burial without grave goods at a depth of 60 cm (after removal of the topsoil). The grave was located in the gravel subsoil. All that remained of the body was a soil silhouette and some disintegrated bone. Part of the left leg below the knee was present, as were parts of the skull, jaw, and some teeth. Samples were taken systematically throughout the excavation of the grave at intervals of 5 cm vertically and in three positions horizontally to a depth of 50 cm, below which samples were taken at 2.5-cm intervals for an additional 7.5 cm. At 60-cm depth, samples were taken from the silhouette. Three more samples were taken 2.5 cm below the silhouette. Samples were analyzed by atomic adsorption spectrophotometry for elements of particular interest. Phosphorus was determined colorimetrically. Samples analyzed for Mn, Cu, and P from the leg region are shown in the form of histograms in Figure 1.

Concentrations of phosphorus, manganese, and copper were found to be higher in the body silhouette than in the surrounding soil; phosphorus levels were particularly high where bone survived. Manganese concentrations in samples from the silhouette were considerably higher than those normally found in bone, whereas copper concentrations were slightly lower. Keeley et al. noted that there was no evidence for Cu accumulation in the silhouette; however, Mn showed considerable accumulation in the silhouette (*9*). Relatively low Mn concentrations were found in soil immediately above and below the silhouette, suggesting that Mn had withdrawn from these areas. It was concluded that the body silhouette in the grave at Mucking was characterized by accumulation of Mn in the skeletal area and that P and Cu do not show this enhancement.

We are not in total agreement with the above conclusions of Keeley and co-workers. Based on the concentration

profiles of Mn and Cu immediately above the silhouette, we are of the opinion that these two metals are migrating from the soil toward the bone. This tentative conclusion is based on the position and shapes of the depleted zones immediately above the silhouette plane and the fact that Cu tends to sorb in bone. The concentration profile of P is nearly constant above the bone and, based on these concentration profiles, no mobility direction can be inferred.

The original investigators based their conclusions about Cu on average concentrations in the bone and soil. If Cu is highly sorbed in the surface layers of the bone, averaging will mask the sorption and mobility potential. Keeley and co-workers are not to be faulted, however, because evidence that bone sorbs Cu in the outer layers was found only recently (*10*). In the following section we propose a fairly complex historic scenario for the creation of the Cu and Mn profiles shown in Figure 1.

Modeling of silhouette data

A chemodynamic model was used to interpret the Mucking silhouette data. The Mucking data set has several characteristics that make it particularly well-suited for consistent, qualitative interpretation and quantitative modeling of long-term metal transport in soils. The Mucking silhouette constitutes a simple geometric plane; its soil zone is thin and contains decayed bone remains. Samples were obtained vertically from the center of the body near the leg region. The perpendicular orientation of the sampling axis with respect to the body plane allowed for the use of a one-dimensional model with a high degree of confidence.

From the histograms of depth vs. concentration for Cu and Mn (Figure 1) the following observations may be made. In the case of Mn, the concentrations decrease uniformly from 10 cm below the soil surface to 50 cm. For Cu, the concentrations decrease uniformly between 10 cm and 45 cm. This indicates a concentration gradient that favors transport of the elements toward and into the bone. However, from the plane of the silhouette upward 5 cm for Mn and upward 15 cm for Cu, the concentration gradients are reversed, indicating transport of the metals away from the bone. These two directions of transport may represent two different diagenetic processes. Consider the following hypothesis of soil and bone processes during the period from burial to soil sampling.

At time $t = 0$, the body is placed in a grave and soil cover is provided. The process of excavating and filling the pit mixes the soil column somewhat. It can therefore be assumed that a fairly uniform metal concentration profile exists in the soil at this point (Figure 2a).

During the course of decades, the organic portions of the body decay and other products move from the site. A drop in pH would accompany the anaerobic decomposition of organic matter, and this drop would likely increase the mobility of most metals in the surrounding soil and bone. The exposed, intact bone becomes a sink for the metals in the surrounding soil. For a period of time t_o (thousands of years), the bone is in the adsorption phase and the concentration profile shown in Figure 2b develops. The metal concentrations are low near the bone and increase with distance upward from the bone.

FIGURE 2
Chemodynamic model for the Mucking data

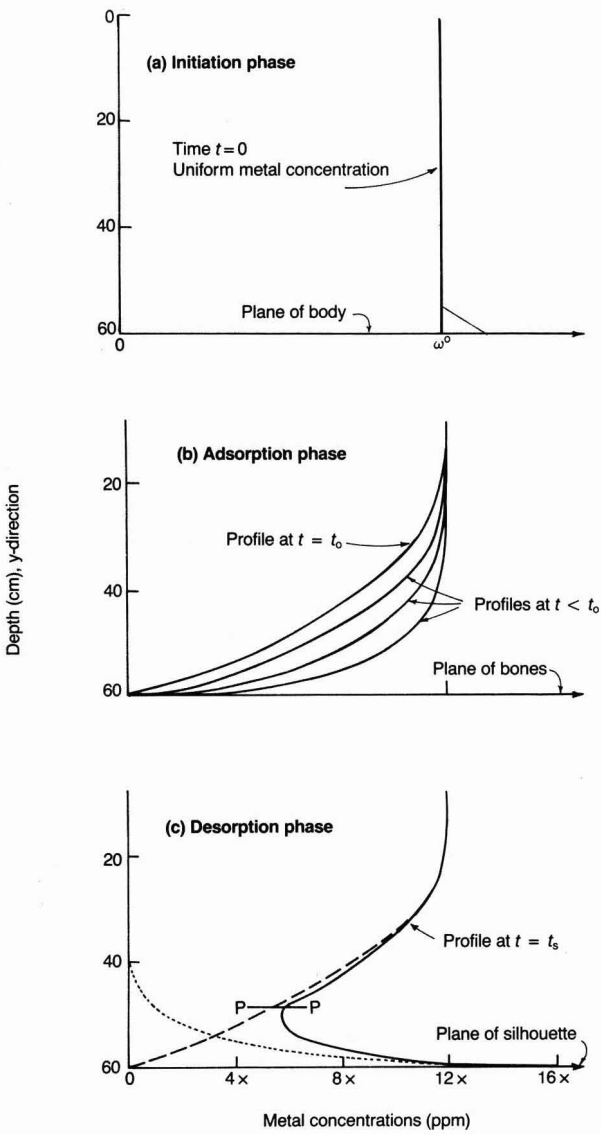

During this adsorption phase the bones are substantially intact, although still decomposing, and provide a highly adsorptive plane for the metals.

Commencing about time t_o, the bone begins to undergo substantial decomposition. This may result as the bone loses a substantial amount of the structural component hydroxyapatite, which tends to neutralize the acidic effects of adjacent soil. The loss of neutralizing capacity of the bone would create a drop in pH at the bone surface, which would result in metals release and increased mobility from the silhouette back to the soil. Because metals are sorbed onto the outer surface of the bone, a decay process coming from the outside would result in fairly instantaneous release for the metals.

For the time period from the onset of decomposition (t_o) to the sampling time (t_s), the metals are assumed to be continuously released to the soil and to migrate away from the bone. Figure 2c illustrates the effects of the desorption phase (dashed line), which is equivalent to the concentration histogram at the time of sampling (solid line) only for the region above the silhouette. Presumably a mirror image profile exists below the plane of the silhouette, but there are insufficient data to confirm this.

Although the above hypothesized description for the histograms of Cu and Mn contains several assumptions and three separate diagenetic processes involving bone, soil, and the silhouette, a simple hindered-diffusion transport model containing one adjustable parameter is sufficient to reproduce the data. The following section is a mathematical description of the chemodynamic model interpretation of the Mucking silhouette.

A transport model

A hindered-diffusion transport model is available for transport of metals in soils. The mathematical description for the soil region above the plane of the burial should be the simplest model with the minimum number of adjustable parameters sufficient to reproduce the data. The following assumptions produce the simplest hindered-diffusion transport model: one-dimensional transport; no metal movement by groundwater or other advective effects; transport by diffusion in the soil pore spaces; and equilibrium between the metal on the soil, in the solids, and in the adjoining pore water.

Combining simplified forms of the continuity equation for the metal species on the soil and in the pore water yields:

$$\delta\omega/\delta t = D(\delta^2\omega/\delta y^2) \qquad (1)$$

when Fick's first law is used for closure.

In Equation 1, ω is the concentration of the metal on the soil (mg/kg), t is time (s), y is the distance from the plane of the body (cm), and D is the effective diffusion coefficient for the metal (cm^2/s).

The model is Fick's second law. The effective diffusion coefficient consists of both transport and equilibrium parameters:

$$D \equiv D_m/[\tau(K_d\rho/\epsilon + 1)] \qquad (2)$$

where D_m is the molecular diffusivity of the metal species in water (cm^2/s), τ is the tortuosity factor of the porous media, and $K_d\rho/\epsilon + 1$ is the retardation factor. This factor contains the partition coefficient, K_d, for the metal between soil and water (L/kg), the bulk soil density, ρ (kg/L), and the effective soil porosity, ϵ (L/L).

The model is a version of the classical transport model for hindered diffusion of chemical species in groundwater. Metal concentration in soil, rather than in pore water, is used. The two are related linearly by K_d. This transformation makes the model compatible with the existing data. Formica and Thibodeaux used this approach in interpreting the effective diffusivity of a polychlorinated biphenyl in lake bottom sediments (*11*).

Diffusion coefficients

Effective diffusion coefficients were found for the adsorption phase. The geometric orientation and the depth of burial of the Mucking silhouette are ideal for invoking the semi-infinite slab solution to Fick's second law. That solution is:

$$\frac{\omega^o - \omega}{\omega^o - \omega^*} = 1 - \text{erf}\,(y/\sqrt{4Dt_s}) \qquad (3)$$

where erf is the error function. Use of Equation 3 requires that the background concentration, ω^o (ppm), of metal in the soil far removed from the plane of the silhouette be uniform at the time of burial and remain constant. In addition, the plane of the burial (i.e., bones at $y = 0$) must provide conditions that maintain the metal at a constant concentration, ω^* (ppm), that is less than ω^o, and the histogram data must be ω vs. y at t_s for the adsorption phase.

The process of burial, as was noted earlier, mixes the soil above the body; therefore, uniform initial metal concentrations are likely achieved. In the case of the Mucking silhouette, the depth of burial, 60 cm, appears to provide a sufficient distance between the plane of the bone and the soil surface so that ω^o is effectively constant at $y = \infty$. An inspection of the histogram data for both Mn and Cu (Figure 1) shows that the metal concentrations in the top 10 cm are not constant but decrease toward the surface. This may be an indication of an active leaching zone or biological uptake, both of which depend on ground cover and soil type. This is somewhat worrisome but, as mathematical analysis will show, apparently has little effect on model utility. It appears that the depletion of the metal zone near the soil surface either occurred shortly before the sampling time or was not severe enough to have an apparent effect on the results.

Bones apparently provide a highly sorptive medium for both Cu and Mn. This is evident from the high concentration gradients displayed in the histograms of Figure 1, in the soil data on other metals gathered by Lambert and co-workers, and in the studies that show high concentrations of Cu in bone adjacent to soil that has low Cu concentrations (*10*). In the absence of measured partition coefficients for Cu and Mn between bone and damp soil, but based on the above evidence, we assume the concentration gradient to be very large. This being the case, we can make the value for ω^* very small. We chose $\omega^* = 0$ for both Cu and Mn at the plane of the bones.

The data applicable to the adsorption phase need to be chosen carefully for two reasons. The concentration data near the soil surface must not be used. As discussed above, the data represented surface-related processes or other recent environmental occurrences that rendered the gradients wholly unrelated to the adsorption process at the plane of the body. The concentration data associated with the metal desorption phase (i.e., with bone decay and concomitant metal release) also must not be used; these data will be used with the model later in a desorption mode as an independent verification. In summary, only the data for depths between 12.5 cm and 42.5 cm for Cu, and between 12.5 cm and 57.25 cm for Mn, are applicable to the bone adsorption phase. The plane of the silhouette was placed at a depth of 56.25 cm.

Interpretation of the model

If the Mucking silhouette is a fifth-century Saxon burial, then the time of burial (or sampling), t_s, is approximately 1400 years, plus or minus a few hundred years. Assuming $t = 1400$ years (4.42×10^{10} s), the concentrations (ω) and distances above the silhouette (y) can be used in Equation 3 to extract numerical values of the effective diffusion coefficient. The basic data and calculated D values for Cu and Mn were reported by Thomas (*12*). Because of uncertainties as to the actual

value of the background metal concentrations, ω^o, as reflected in a depleted metal zone near the soil surface, a mathematical optimization process was used to arrive at the effective ω^o value. This technique involves a one-dimensional search over a reasonable expected range of ω^o values, minimizing the coefficient of variation (COV) of the D values. This mathematical technique has been used successfully in another study (*13*). In both cases minimum values of COV were found.

The effective diffusion coefficient is 7.9×10^{-9} cm^2/s for Cu and 1.0×10^{-7} cm^2/s for Mn. It appears that Mn moves approximately 100 times more rapidly than Cu. The effective background concentrations were 14 ppm for Cu and 1200 ppm for Mn. The copper value is in the range of the measured values, but that of Mn exceeds the measured value by a factor of 2.5. This occurrence with Mn suggests that the background concentration could not have remained constant; therefore, the semi-infinite boundary conditions were not met. Because of this, the effective diffusion coefficient for Mn is only a rough approximation. It should be noted also that the absolute value of COV for Mn is approximately twice that of Cu value. This indicates further suspicion of the D value for Mn.

From the goodness-of-fit of the model to the data using only the diffusion coefficient, it appears that a two-parameter model involving advection is not necessary in this case. Thus the simple hindered-diffusion transport model can be used to estimate key parameters related to the long-term mobility of metals in soils.

Bone decay time and desorption

As illustrated in Figure 2c of the interpretative model, the adsorption phase profile is essentially above the horizontal line P—P. This model assumes that the bone effectively decays at some time t_o before the sampling time t_s. Over time, $t_s - t_o$, the metals are free to move again. The desorption portion of the profile is shown below the P—P line of Figure 2c. If this new period of movement is characterized by the same numerical value of the effective diffusivity found in the adsorption phase but with gradients in the opposite direction, then the use of another version of the semi-infinite slab model equation is appropriate:

$$\frac{\omega - \omega^*}{\omega^o - \omega^*} = \text{erf}\,[y/\sqrt{4D(t_s - t_o)}] \quad (4)$$

The general limitations applied to Equation 3 also apply to Equation 4. The following conditions reverse the gradients: ω^* is now the high metal concentration at the plane of the decayed bone, and ω^o is the effective metal concentration that surrounds the bone and was depleted during the adsorption phase. The value for ω^o is taken as zero. Under the above conditions, Equation 4 becomes:

$$\frac{\omega}{\omega^*} = 1 - \text{erf}\,[y/\sqrt{4D(t_s - t_o)}] \quad (5)$$

This now can be used for the desorption phase.

An estimate of the time of bone decay is needed. Because the desorption profile is very near the plane of the silhouette, as is the point of minimum concentration, $t_s - t_o$ is likely a short period of time compared to t_s. The maximum concentrations at the plane of the silhouette in the field data will be used for estimating ω^*. From Figure 1, $\omega^* = 18$ ppm for Cu, and $\omega^* = 1500$ ppm for Mn. Figure 3 shows the results of the separate calculations for Cu during the adsorption and desorption processes, respectively, with t_o values of 1300, 1200, and 1100 years, and $t_s - t_o$ values of 100, 200, and 300 years. When the model calculations are compared with the data indicated, the effective time of adsorption is relatively insensitive to 100-year intervals; desorption is more sensitive. Based on

FIGURE 3
Estimating bone decay time

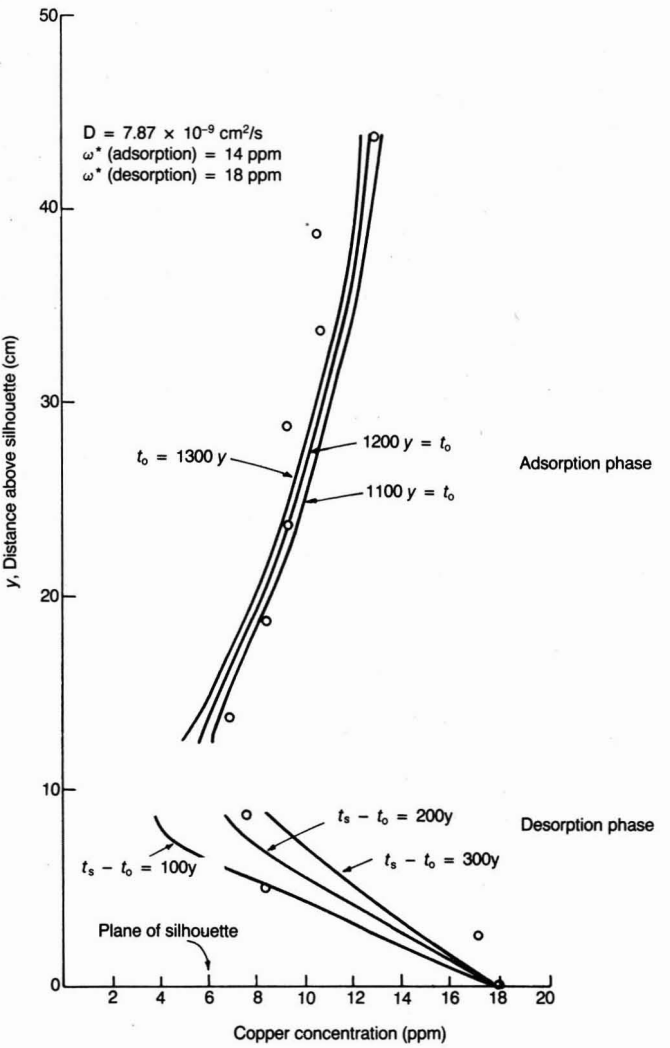

desorption alone, the effective time of bone decay was tentatively estimated at 200 years prior to the sampling time. The decay time was based on Cu data only. The desorption data for Mn are limited, with only one data point clearly identified.

Adsorption–desorption phases

It is a property of linear partial differential equations that the solutions of two simultaneous processes are the sum of each, so an independent test of the model is to add the results of the adsorption phase to the results of the desorption phase at depths. Quantitatively, the concentrations of ω values from Equations 3 and 5 are added together. The success of this particularly severe test of a simple model is illustrated in Figure 4, which contains the field data and the model-calculated concentrations for Cu and Mn. In the calculations for Cu, $t_s = 1300$ years; $t_s - t_o = 100$ years; $D = 7.87 \times 10^{-9}$ cm^2/s; and $\omega^* = 0$ and $\omega^o = 14$ ppm for the adsorption phase, $\omega^* = 18$ ppm and $\omega^o = 0$ for the desorption phase. The combined model refines the $t_s - t_o$ value to 100 years. The tentative estimate of $t_s - t_o$, calculated using the desorption model alone, was 200 years. In summary, it appears that the bone decay–Cu release process occurred 1300 years after burial and 100 years before sampling. Although the data set for Mn desorption is limited to a single value, the summed model component value and the data are shown in Figure 4. The data were calculated using $t_s - t_o = 100$ years, which is the value determined for Cu. These calculated values closely agree with the data.

The degree of correlation between calculated values and the data is a necessary test for a model. Another test of the model and the associated hypothesis concerns the range of numerical values for the particular adjustable parameters. The key parameter in this case is the effective diffusion coefficient, defined by Equation 2. This equation provides an independent means of estimating D. Reported ranges of K_d for Cu in streams and lakes with low sediment (i.e., soil) concentrations are from 2.5×10^3 to 2×10^4 L/kg and from 8.6×10^3 to 5×10^4, respectively (*14*). For Cu^{2+} in aqueous solution at 18 °C and 25 °C, tracer diffusion coefficients have been determined as 3.41×10^{-6}, 5.88×10^{-6}, and 7.33×10^{-6} cm^2/s (*15*). A soil bulk density of 1.5 kg/L and 50% porosity with the diffusivity data at 18 °C yields D values of 5.5×10^{-10} to 2.8×10^{-11} cm^2/s for a tortuosity of $\sqrt{2}$. Although the K_d values used were for low sediment concentrations and the expected K_d for the Mucking soil likely is lower, the range of D values is in general agreement with the silhouette data for Cu. Because similar independent data were not available for Mn, comparisons were not possible.

In summary, then, the basic hypothesis is valid: A one-parameter, hindered-diffusion, metal-transport model without an advection term is sufficient to account for adsorption and desorption phases in the diagenetic processes of buried bone.

Migration of hazardous substances

Archaeological data can be used as evidence for the long-term migration of hazardous substances in the soil. As demonstrated by our analysis, investigations of archaeological deposits are appropriate for problems of elemental movement for two reasons: They contain chemical concentrations that vary with depth and they can incorporate long time scales. Consequently, with appropriate transport models these data can be used to extract key parameters regarding elemental movement that are unobtainable by any other investigative means. In the Mucking case, for instance, data collected for purposes

FIGURE 4
Model vs. data for Cu and Mn

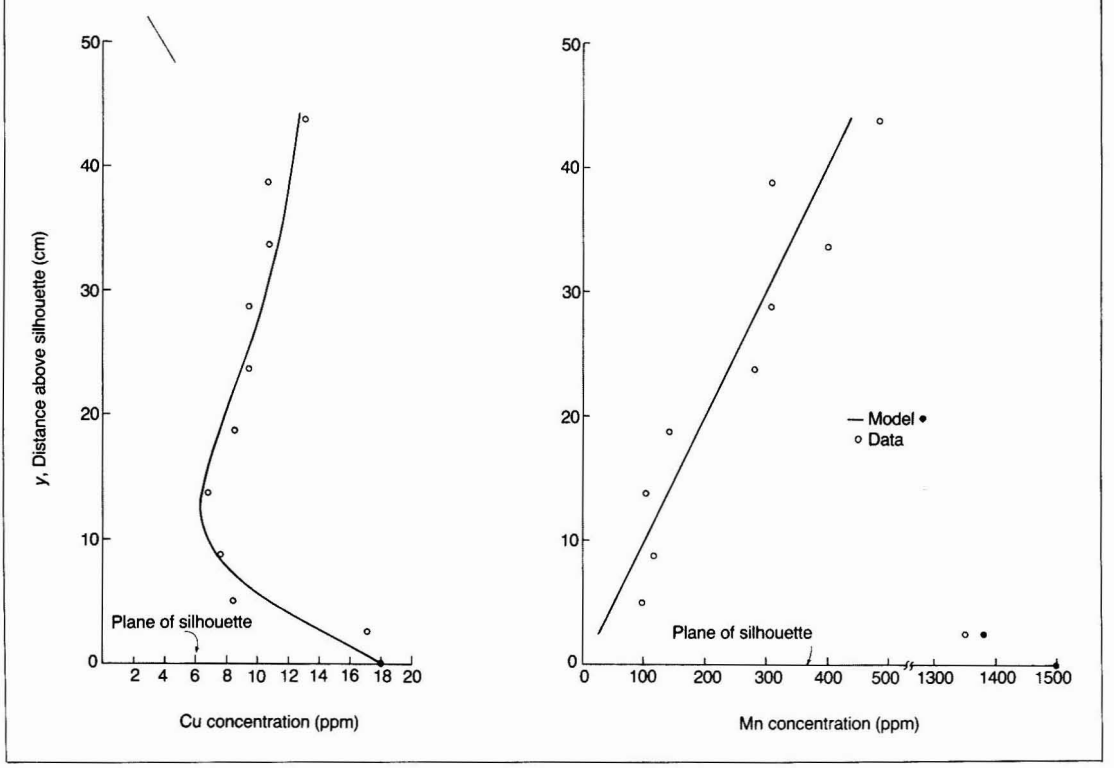

other than the problem of migration of hazardous substances in soils were adequate for demonstrating adsorption and desorption and for extracting diffusion coefficients. Because of this success, it seems worthwhile to pursue the problem of elemental mobility, transformation, or loss in archaeological contexts with a research strategy specifically designed to obtain appropriate data. Such research must be interdisciplinary and incorporate both field and laboratory phases (*15*). The remainder of this paper outlines how such research might be undertaken and what we might expect in return.

Scope of research activity

Research activity in the future should include field work at the site, retrieval of historic information, and specific laboratory studies. The field work should commence with known sites. There seems to be a sufficient number of open and partially excavated archaeological sites; therefore, a search for new sites is not necessary at this time. Existing sites will likely contain the needed information. The planning and execution of sampling protocols is easier at existing archaeological sites because the types, positions, and extent of artifacts can be predicted somewhat. The field work will involve the collection of appropriate samples from on and off the site. The extent of sampling should reflect the type of study involved. Samples should be collected from the artifacts, from the soil that surrounds the artifacts, and from pore water. Samples for classifying the soil and stratigraphic mapping of soil horizons also need to be taken.

Some laboratory research such as tests or simulations involving the artifact or its soil environment will likely need accompany the field investigations. For example, laboratory investigations may study the leachability and adsorptivity of elements from the artifact to water and the soil matrix. In the case where bone provides the sink or source for metal transport, the respective partition coefficients between bone and pore water need to be measured. Some specific laboratory investigations should explore the fate hypothesis developed from inspection and study of the chemical record within or surrounding the artifacts.

Historic information about the hazardous-waste site is also necessary to establish the time of entry of the artifact or the incidence of chemical perturbation and subsequent activities that may have affected the archaeological record. Time can be established by radiocarbon, thermoluminescence, or other dating techniques. Climatological information can be obtained from recorded history or inferred from tree rings, pollen, or plant macrofossils. In the case of prehistoric sites, the archaeological record of human inhabitation may be the only source of information.

Information derived and its uses

The information derived from such a research activity is a product of the basic data and the models, scenarios, and the hypotheses employed in interpreting the data. The basic data consist of chemical concentrations, time, environmental setting, and type of human activity. The interpretation of this evidence will involve many of the same general procedures used in forensic chemistry to reconstruct prior events. This particular manuscript illustrates how a mathematical transport model can be used as an interpretative tool.

Depending upon the methods used, information can be obtained on element or substance migration distances and rates over time; effective transport and transformation rate parameters; field verification, in both space and time, of laboratory experiment and theoretical models; soil types and conditions that retard or enhance element or substances migration; and the correlations of climate, terrain, and other environment factors to species movement.

There are many specific uses that can be made of the information. The following is a list of uses specific to hazardous-waste fixation, disposal, and containment: the prediction of distances and times for hazardous substances traveling from abandoned dump sites to sensitive targets; the design of containment barriers for landfills and other so-called long-term disposal facilities; calculation of the relative mobility and fate of metals and organics in sediment over long time periods; estimates of the significance of catastrophic environmental events (e.g., acid rain or flooding) on containment and disposal strategies; the formulation of waste into soil-like matrices and the maintenance of certain environmental conditions to minimize migration rates; and establishment of siting requirements based on soil properties for disposal and containment facilities.

Problems and uncertainties

Although the results of this preliminary study are encouraging, the exploitation of the archaeological record for purposes of hazardous-waste disposal is not without its problems. It is appropriate to consider some of these.

Because mobility of elements in sediment is influenced by environmental conditions, it is important to select testing locations in which climatic conditions can be assumed to be relatively constant. In the Americas, such an assumption can be made for the archaeological record of the Holocene—the past 10,000 years. Comparable use of an area by previous human populations is a potential difficulty. Archaeological chemistry is in its infancy and there are few documented patterns of or predictions about the behavior of elements in previous human contexts.

Although controlling for general climatic conditions is possible, recent climatic changes such as the observed increase in acid precipitation may have immediate and perhaps significant effects on elemental content of the soil. Long-term effects are uncertain, but initial stimulation by increased acidity may give way to deficiencies of elements such as Ca, K, Mg, and P that are leached more rapidly. Magnesium and other elements are mobilized at low pH and leached from the soil. Metal toxicants and nutrients, because of the influence of hydrogen ions upon cation exchange and weathering, causes mobilization (*16*).

Because the archaeological record is time transgressive, questions should arise in the minds of researchers as to what elements have been lost, unknown, or changed and how these processes will affect accurate interpretation of data. Uncertainties are minimized if work is done at existing sites that are fully developed to the extent that the archaeological and historic record indicates a consistency of site conditions.

Acknowledgment

The work described in this paper was supported in part by the U.S. EPA Center of Excellence Grant for Hazardous Waste Research and by Louisiana State University, Baton Rouge.

References

(1) Sillen, A.; Kavanagh, M. *Yearbook of Physical Anthropology* **1982,** *26,* 67–90.
(2) Sillen, A. *Am. J. Phys. Anthropol.* **1981,** *56,* 131–37.
(3) Schoeninger M. *Am. J. Phys. Anthropol.* **1979,** *51,* 295–309.
(4) Parker, R. B.; Toots, H. *Geol. Soc. Am. Bull.* **1970,** *81,* 925–32.
(5) Toots, H.; Voorhies, H. R. *Science* **1965,** *149,* 854–55.
(6) Waldron, H. S. *J. Archaeol. Sci.* **1983,** *6,* 35–40.
(7) Wesson, G. et al. In *Archaeological Chemistry;* Carter, G. F., Ed.; Advances in Chemistry Series 171; American Chemical Society: Washington, D.C., 1978; pp. 99–108.
(8) Lambert, J. B. et al. *Archaeometry* **1984,** *26,* 131–38.
(9) Keeley, H.C.M.; Hudson, G. E.; Evans, J. *J. Archaeol. Sci.* **1977,** *4,* 19–24.
(10) Lambert, J. B. et al. In *Archaeological Chemistry;* Lambert, J. B., Ed.; Advances in Chemistry Series 205; American Chemical Society: Washington, D.C., 1983; pp. 97–113.
(11) Formica, S.; Thibodeaux, L. J. Presented at the American Chemical Society's International Chemical Congress of the Pa-

cific Basin Societies, Honolulu, 1984; paper 01F23.
(12) Thomas, J. M.S. Thesis, Louisiana State University, Baton Rouge, 1987.
(13) Thibodeaux, L. J.; Cheng, C. K. *Water Resour. Bull.* **1976,** *12*(2), 221–36.
(14) Lerman, A. *Geochemical Processes Water and Sediment Environment;* Wiley: New York, 1979; p. 81.
(15) Winograd, I. J. "Archaeology and Public Perception: A Transscientific Problem; Disposal of Toxic Wastes in the Unsaturated Zone."; Open File Report; U.S. Geological Survey: Denver, Colo., 1986.
(16) Committee on the Atmosphere and the Biosphere; In *Atmosphere/Biosphere Interactions: Towards a Better Understanding of the Ecological Consequences of Fossil Fuel Combustion;* National Academy Press: Washington, D.C., 1981; pp. 167–82.


Thibodeaux


Ramenofsky

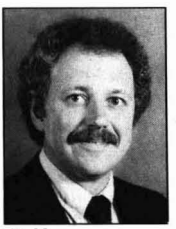
Field


Whitmer


Thomas

Louis J. Thibodeaux *is a professor of chemical engineering at Louisiana State University and director of the EPA-sponsored Center of Excellence in Hazardous Waste Research. His primary research and teaching interests are in the area of environmental chemodynamics.*

Ann F. Ramenofsky *is an assistant professor of archaeology at Louisiana State University. She received her Ph.D. in anthropology from the University of Washington in 1982 and joined the faculty of geography and anthropology in 1983. Her research interests include late prehistory of the eastern United States, disease diffusion at the contact horizon in North America, and the diagenesis of buried bones.*

Stephen P. Field *is an associate professor of civil engineering at Louisiana State University. He has been involved in several aspects of hazardous-waste management, including mechanisms in soil and treatment technology development and optimization. He currently serves on the Hazardous Waste Advisory Board for the state of Louisiana.*

Ann M. Whitmer *is a research associate in archaeology at Louisiana State University. She received her B.A. in sociology/anthropology in 1981 from Carleton College and her M.A. in anthropology from the University of Washington in 1987. Her research interests include the prehistory of the lower Mississippi Valley and the diagenesis of buried bone.*

Jacob Thomas *is a graduate student working toward his M.S. degree in chemical engineering at Louisiana State University, Baton Rouge, and has a bachelor of technology degree in chemical engineering from the Indian Institute of Technology, Kanpur, India. He is a member of the AIChE.*

Bob J. Miller, *recently deceased, was a professor of agronomy at LSU. He received a Ph.D. in agronomy in 1972 from the University of Tennessee. Miller joined the faculty at LSU in 1972. Bob Miller was a soil scientist of considerable reknown; his research areas included mineralogy, pedogenesis, and genesis of Quaternary Losses deposits in the lower Mississippi Valley.*

Modeling ozone concentrations

Urban- and regional-scale models are needed to develop emission control policies that reduce ozone levels

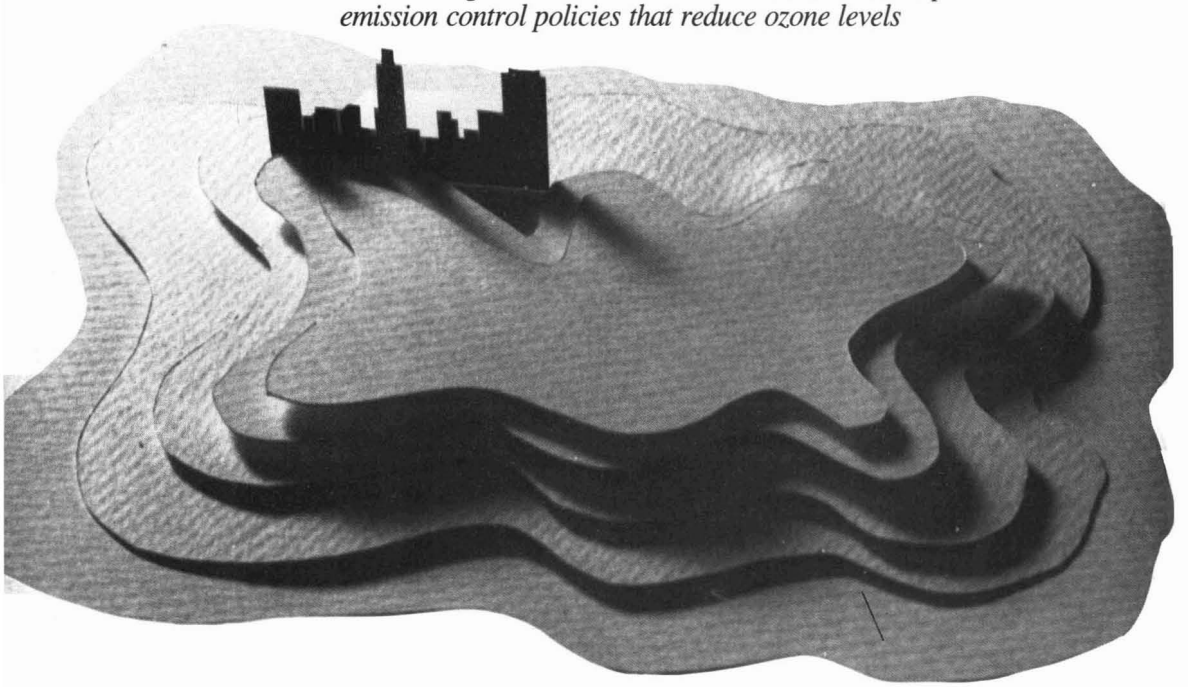

Kenneth L. Schere
Environmental Protection Agency
Research Triangle Park, N.C. 27711

Efforts to model ambient ozone (O_3) concentrations within urban areas have been under way for more than 15 years (*1–3*). Recorded events of O_3 and oxidant damage to materials and plants as well as its irritating effects on human tissues have been noted for an even longer period in areas affected by high ozone levels. During this time the realization arose that the urban O_3 problem often was a subcomponent of a larger, regional-scale ($\approx$ 1000 km) O_3 episode. The long-range transport of ozone between urban areas has become increasingly evident (*4–8*). As a result, model development programs to address the regional-scale O_3 issue began about 10 years ago and continue today.

Ozone not only affects health and welfare adversely in urban areas; it is becoming clear that O_3 damages crops and forest lands outside cities as well. Recent estimates of direct crop losses, based on the limited data available, suggest that about $3 billion would be lost annually if the United States experienced a seasonal daylight mean O_3 concentration of 60 ppb for seven hours each day (*9*). This value is within the range of frequently occurring daylight ozone concentrations in many agricultural areas of the United States.

The current primary National Ambient Air Quality Standard (NAAQS) for ozone, 120 ppb for one hour, is designed to protect human health. EPA is considering the issuance of a secondary standard to protect the nation's crops and forests from ozone damage. This standard is likely to specify a longer time period for estimating average ozone concentration, such as the 7-h seasonal daylight level. The cost of controlling pollution sources in order to bring areas that currently violate the ozone NAAQS into compliance is estimated to be in the billions of dollars. No estimates have yet been made of the control costs associated with a secondary ozone standard.

Only regional-scale air quality models for ozone can simulate concentrations over a sufficiently long time and wide area in a manner that is compatible with a secondary NAAQS standard. Such models are necessary components in the cost–benefit analysis that must be performed to assess the economic and social results of the emissions controls required to reduce ozone levels.

Meeting ozone reduction goals

Tropospheric ozone has been regulated since 1970, and nationwide levels have declined by about 10% between 1983 and 1984. Nevertheless, in the summer of 1986, EPA Administrator Lee Thomas announced that at least 28 metropolitan areas will have failed to meet the ozone concentration deadlines set for Dec. 31, 1987. By the end of 1987, this number turned out to exceed 50.

Technical issues

Determining wind flow patterns. Several technical problems, which are of minor significance in small-scale ozone models, must be considered for regional-scale ozone models. Foremost among them is the uncertainty in determining the correct wind flow pattern to use in the transport component of the model. The wind flow field may be obtained either by inference from meteorological observations or from the predictions of a meteorological model. The former method is more commonly

used to determine wind flows for air quality models.

The construction of a wind flow field often is a problem for urban-scale models as well as for regional models. In urban areas there typically is an inadequate number of meteorological monitors to determine a well-resolved wind field. Special studies, on occasion, have been conducted in urban areas in which the regular monitoring network is enhanced by additional meteorological monitors. The resulting network is useful for constructing a wind field. On the regional scale, however, the spatial extent of the modeling domain is too large to augment the monitoring network in the same manner.

Two types of wind measurements are needed to form a wind flow field for an air quality model: measurements made near the surface and measurements made aloft. Both are necessary to determine the characteristics of three-dimensional transport for the air quality model. In most regions of North America, the density of surface wind monitors is relatively high. Surface wind measurements, however, are affected greatly by their immediate environment, so their ability to represent air flow patterns in a model is limited in spatial extent. Upper air wind measurements are more difficult to obtain than wind measurements at the surface, but they are applicable over a larger spatial area because the highly localized frictional effects of the earth's surface no longer are significant. Upper air wind measurements are made twice a day at the network of monitoring stations shown in Figure 1.

Upper air monitoring stations typically are located 300–500 km apart. The number of these stations used in a wind field calculation for a regional ($\approx$1000 km) model domain therefore would vary between 4 and 12. Consequently, one upper air measurement station would determine the wind pattern over a square horizontal area 300 km on a side under the best circumstances, and 500 km on a side under the worst. Calculations based on measurements made at these stations assume an even spacing between them. By comparison, the typical spatial resolution required in a regional air quality model varies from 20 to 100 km.

In any attempt to determine a spatially gridded wind field pattern from upper air observations, an inherent uncertainty resulting from the 300–500-km distances between stations is unavoidable. The uncertainty in the trajectory of an air parcel, determined from this wind field, may grow with time as its distance from the origination point increases. In this context, it becomes clear that the accuracy of air quality predictions from a regional model is greatest at receptor locations that are near both meteorological stations and major sources of pollutant emissions. This predictability decreases with increasing distance from either the sources or the meteorological stations. In other words, the ability to attribute pollutant levels in remote regions to specific sources is inherently limited (*9*).

Lamb and Hati propose a method for generating an ensemble of possible wind fields that are applicable for use in regional-scale air quality models from a set of meteorological observations (*10*). This concept explicitly addresses the uncertainty inherent in the specification of atmospheric states. The application of this concept for regional air quality models takes them from a deterministic prediction mode to a probabilistic mode

FIGURE 1
North American upper air wind-monitoring stations

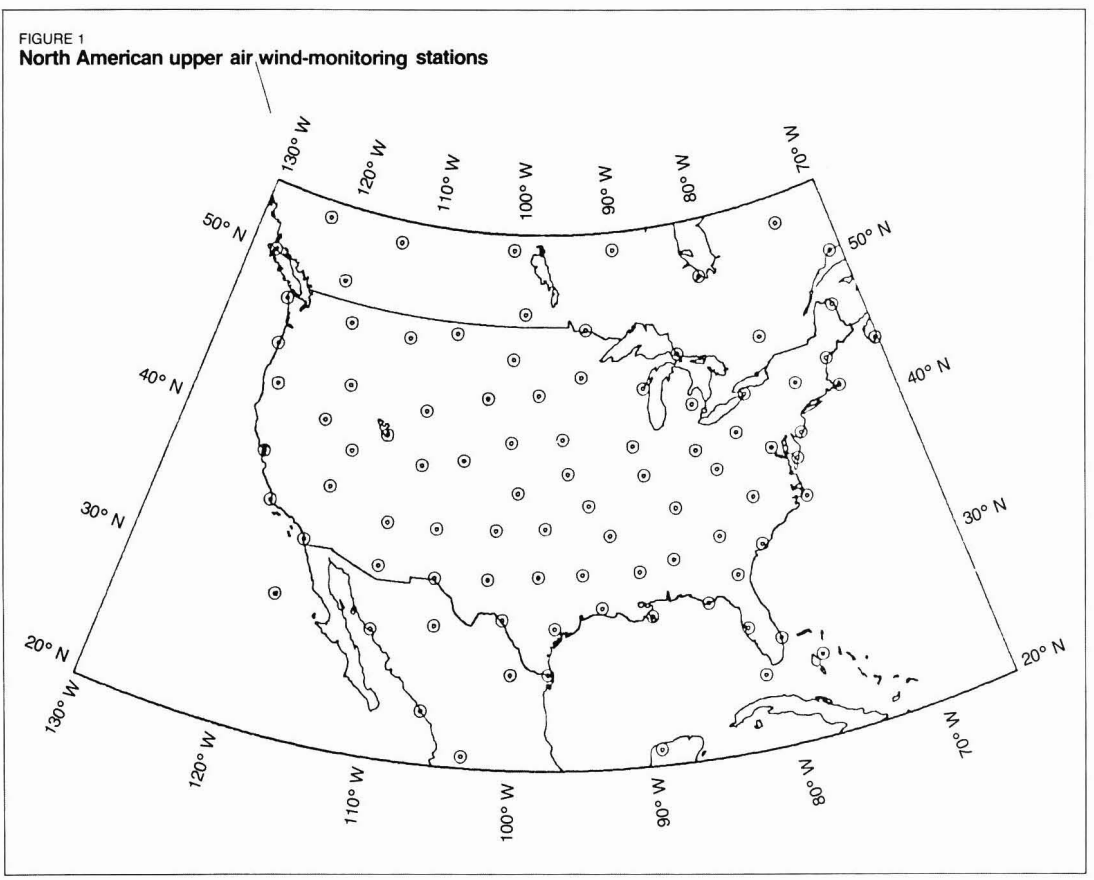

in which the prediction of the pollutant concentration at a receptor is in the form of an expected probability distribution. Lamb plans to test these ideas with the EPA Regional Oxidant Model (ROM) in the future (*11–13*).

Cloud venting. Another issue of continuing interest in the regional-scale modeling of ozone is the process of cloud "venting," or the vertical transport of mixed-layer material aloft into the free troposphere by cumulus clouds formed by convection (*14*). This issue is not as relevant to smaller scale models in which material lost through the top of the mixed layer does not become reentrained into the model domain during the simulation. In a regional-scale model, however, material that is vented above the mixed layer can be transported considerable distances downwind by the faster-moving air flow in the free troposphere. This material then can be reentrained into the mixed layer far downwind from the original source area the following day as the growing mixed layer incorporates the air aloft. This process occurs well within the time and space scales of a regional model simulation.

The mechanism of cloud venting is described conceptually by Ching (*14*). The scenario begins in the morning when the growing layer of well-mixed air above the surface becomes photochemically active and its concentrations of O_3 increase rapidly relative to ozone concentrations found aloft. This mixed layer of air quickly deepens, and cumulus clouds begin to appear when the layer rises to a height equal to or greater than the convective condensation level. The cloud material is derived primarily from the mixed layer, and the developing cloud layer adjusts for this mass input of mixed-layer air by an appropriate amount of subsidence.

The mixed-layer ozone is carried aloft in the convective cells, and a net upward transport is possible when the mixed layer contains higher ozone concentrations than the cloud layer above. The significance of cloud venting for ozone therefore should increase with time during the afternoon. It also is possible that other atmospheric constituents are lifted through the cloud venting process. Of these, formaldehyde might be of particular significance because of its reactive potential and its higher concentrations during the afternoon. Occasional episodes of tall-stack emissions entrained directly into a strong convective cell also provide a means of injecting reactive species directly into the cloud layer.

Recent field experience has provided evidence that confirms the existence of the cloud-venting process and the return flow from cloud layer to mixed layer. In one experiment, a mass of nontoxic fluorescent dye particles was released below and above cumulus clouds while an airborne lidar monitored their transport and dispersion. Observations showed that the dye released below a cloud was vented upward into the cloud; the dye released at or above the top of a cloud rapidly descended into the mixed layer (*15*). In another experiment, airborne lidar measurements of O_3 and aerosols showed that deep convection can produce pollutant-rich elevated "reservoir" layers, which are transported over long distances without surface interactions (*16*). The experimental results suggest that approximately 30% of the maximum concentration of ozone measured at the surface in Norfolk, Va., on July 31, 1981, was caused by reactions of precursors that originated from external sources more than 500 km upwind.

Biogenic vs. anthropogenic emissions. With respect to source emissions, there still is substantial uncertainty about the effect of naturally occurring (biogenic) organic emissions on rural ozone concentrations. This issue needs to be explored further with regional-scale photochemical air quality models. Biogenic organic species, mostly isoprene and several monoterpenes, are emitted by many types of forest trees and cultivated plants. A number of techniques are available to determine the flux of these chemical species from individual plants or forest groves (*17, 18*), although there is substantial variation among measurements.

The emissions of isoprene generally increase with increases in ambient temperature and light intensity, and the emissions of monoterpenes increase with temperature. Altshuller summarizes the experimental results that explore the effects of temperature and light intensity on these emissions (*19*). There obviously are seasonal and geographical differences between the biogenic organics emission rates; maximum emission rates are observed during the warmer summer months in the heavily forested eastern and southern sections of the United States.

Biogenic emissions that are significant as compared with anthropogenic organic emissions in a particular localized area would be most likely to occur in rural areas of the Southeast during the summer. When the rates of these emissions are integrated over a large regional area ($\approx 1000 \times 1000$ km), however, the biogenic component can easily be the larger. In a recent analysis that used a biogenic emissions inventory compiled for the northeastern United States EPA-ROM application, it was found that the integrated anthropogenic organic emissions rate over the modeling domain was 1.7×10^7 kg/day; the total biogenic organic emissions rate was 2.6×10^7 kg/day for a mid-summer day with clear skies (*20*). These figures encompass an emissions area of approximately 1 million km^2, and they include nonreactive as well as reactive compounds. If the nonreactive compounds are excluded, the ratio of biogenic emissions to anthropogenic emissions drops to 1.2:1.

Individual field programs designed to measure ambient concentrations of biogenic organic species have shown that isoprene and α-pinene are the species most often identified (*19*). Outside forest canopies, the average concentrations of these species usually are less than 10 parts per billion of carbon (ppbC), although maximum isoprene concentrations of 30–40 ppbC were reported in several studies.

Measured concentrations of biogenic organic species often are lower than those expected from the estimates based on biogenic emission inventories. One explanation for this discrepancy may be the highly reactive nature of isoprene and the monoterpenes. Isoprene can contribute as much as 50% of the overall reactivity of rural air, even though its concentration is as low as 6% of the ambient hydrocarbon level (*21*). These species are rapidly oxidized into a number of intermediate carbon-containing species, such as methyl vinyl ketone, methylglyoxal, and formaldehyde, which also are highly reactive.

Altshuller notes that when the concentration ratios of isoprene to propene in forested areas are compared with regional average emission ratios, propene measurements are higher than expected (*19*). Propene, however, is a reactive hydrocarbon of anthropogenic origin and should form reactive products almost as fast as the isoprene. In addition, the average transport distance of the propene to a sampling point in a forested area must be substantially larger than that for isoprene. Regional oxidant models should be capable of helping resolve the apparent contradictions in the measurements and emission inventories of reactive biogenic species.

Several chemical kinetic mechanisms for the atmospheric reactions of isoprene recently have been postulated (*21, 22*). They are available for inclusion in photochemical air quality simulation models for applications in which an isoprene emissions inventory exists.

In an urban-scale modeling study, Lurmann et al. have applied a photochemical trajectory model to the Tampa–St. Petersburg, Fla., area to assess the role of biogenic organic emissions on urban O_3 formation (*23*). Al-

FIGURE 2
VOC and NO_x emissions vs. source area and characteristic length scale[a]

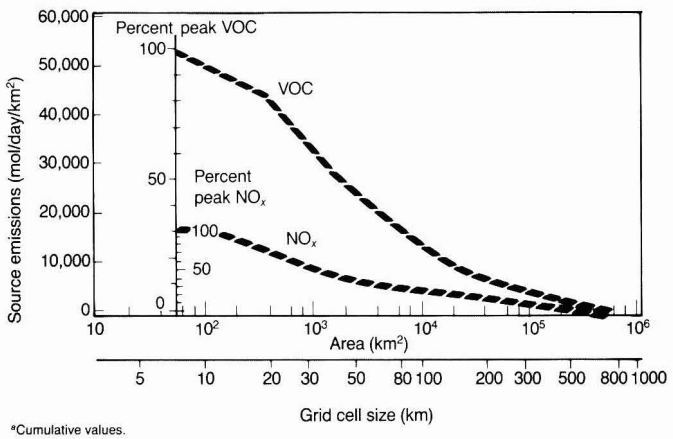

[a]Cumulative values.

though the biogenic and anthropogenic organic emission rates are estimated to be of comparable magnitude, the results of the study indicate that biogenic emissions contribute only 2–9% of the predicted maximum O_3 concentrations. The study also shows that this relatively small contribution is attributable to fast ozone–biogenic organic reactions that scavenge almost as much ozone as is produced by the biogenic organics in the urban environment.

On a regional scale, preliminary results from simulations of ozone transport in the northeastern United States with EPA's ROM model show noticeable impacts from biogenic emissions on ozone formation downwind of isolated major sources of nitrogen oxides (NO_x) in otherwise hydrocarbon-limited environments. The effect of biogenic emissions on ozone formation within most of the urban-source plumes in the ROM simulation were relatively small. Further studies of the effects of biogenic species in regional-scale applications are needed.

Major uncertainties also exist in the anthropogenic emission inventories used in regional models. Lamb explains that discrepancies between two recent emission inventories for the northeastern United States vary by a factor as large as 100 for emissions of NO_x in a given grid cell (*24*). Discrepancies between volatile organic carbon (VOC) emissions also are large. This noise in the emissions data can be larger than the changes in emissions that control strategies would cause.

This is a potential problem for regulators who use modeling scenarios as a partial basis for their decisions on emissions control measures, because the response of ozone concentrations to changes in VOC and NO_x emissions is a function of base emission levels. Therefore, if the estimated base emissions are erroneous, the simulated response of ozone concentrations to emission controls also will be erroneous. EPA and other groups responsible for compiling source emission inventories are working actively to reconcile discrepancies in the inventories and are producing more refined estimates of the true source strengths with each new generation of emission inventory.

The influence of stratospheric ozone. The intrusion of stratospheric ozone and its influence on concentrations of near-surface ozone is a frequently discussed issue that is beyond the range of investigation with regional air quality models. Generally, the upper boundary of the model domain is specified at a height varying from the top of the boundary layer (1–2 km above ground) to the mid-troposphere. Ozone concentrations above this level are specified as an upper boundary condition on the model and are determined by direct measurement (aircraft-based observations) or are inferred from ground observations.

Actually, large direct impacts of stratospheric ozone intrusions at ground level are unlikely. Analysis of the few published observations of high O_3 levels in stratospheric intrusions and of anomalously high O_3 at ground level attributed to stratospheric intrusions suggests that direct ground-level impacts may occur less than 1% of the time and usually are associated with ozone concentrations of 100 ppb or less (*25*). Regional models therefore will not conclusively quantify the near-surface impacts of stratospheric O_3.

Providing adequate spatial resolution. The final issue of regional ozone modeling encompasses the approximations made in solving the finite-difference analogs to the actual differential equations that describe over time the rates of changes in concentration of species that participate in chemical interactions in the model. This issue is important for most numerical air quality simulation models but has some special significance for regional-scale grid models. Modeling on this scale requires the model domain to cover a large horizontal area while holding the number of grid cells down to insure reasonable computation costs. This criterion is one factor that determines the spatial resolution achieved by the model; larger grid cells will provide coarse resolution and smaller cells will provide finer resolution.

Urban-scale ozone grid models typically use grid cells in a size range of 2–8 km to a side. This size generally is too small for regional models because an excessive number of grid cells would result. The problem, then, is to choose a grid cell size that will limit the overall number of cells and provide adequate spatial resolution.

How do we define adequate resolution in a regional ozone air quality model? We must be able to resolve the significant sources of emissions of ozone-forming species; otherwise, we risk diluting them into a large volume in which the model is likely to diminish their significance and underpredict the resulting O_3 concentrations.

Using the National Acid Precipitation Assessment Program emissions inventory (*24, 26*), Lamb has studied the issue of "scale length" of significant nationwide sources of VOC and NO_x emissions, the primary precursors of ozone in the northeastern United States. Following his analysis, let us rank the counties with the strongest emission fluxes (mol km^{-2} day^{-1}) in the study area from highest (No. 1) to lowest. Now let us define a cumulative emissions function, Q, that represents the area-weighted average of the individual county emissions from the greatest down to and including county No. N from our list:

$$Q = \sum_{i=1}^{N} Q(i)A(i) \Big/ \sum_{i=1}^{N} A(i)$$

where $A(i)$ is the area of county i. A plot of the cumulative emissions function, Q, vs. the cumulative area is shown in Figure 2 for both VOC and NO_x. The left edge of the upper curve corresponds to the highest VOC emissions source county, Q_{VOC} = 53,457 mol km^{-2} day^{-1} and A = 58.1 km^2. In order to define this strongest source,

we would need a model grid size of $A^{1/2}$, or 7.6 km. In other words, a model with grid size of 7.6 km would define 100% of the peak source strength.

If we follow the curves, we see that a grid size of 20 km would determine about 80% of the peak VOC and NO_x source strengths, provided that the strongest VOC and NO_x sources fall within the same grid cells. Likewise, a grid size of 50 km would resolve slightly less than 50% of the peak source strength. A model with grid cells of 500 km is essentially no better than one in which the entire domain is treated as a single cell. When a model is unable to resolve the strengths of the actual sources, errors will occur in the simulated concentrations of photochemical species. Recent applications of regional O_3 air quality models have used grid sizes from 18 to 100 km.

The method of numerical solution of chemical kinetics equations is another area in which approximations made to achieve a faster solution may produce errors in the model results. The kinetics modules of a photochemical air quality model typically consume 75–90% of the total model execution time and thus are prime candidates for efforts to achieve greater solution efficiency. Problems associated with solving the chemical equations arise because the time scales of the various reactions composing the kinetic mechanism span a range of several orders of magnitude. This makes it difficult to choose an optimum time increment for the solution. Such a set of reactions is characterized as "stiff."

Accurate numerical solvers based on the Gear method (*27*) usually are successful for stiff systems but consume large amounts of computer time and memory. This makes them inappropriate for use in large grid models of air quality simulation, although they may be tractable in trajectory or box models. The more common method of solution in grid models uses a more approximate method based on steady-state chemistry or "quasi-steady-states" that compares well with Gear-type solutions when all empirical parameters, such as the solution time increment, are optimally adjusted for accurate solutions over the range of expected ambient species concentrations (*28*). Outside the range of the optimally adjusted parameters, however, the solutions can degrade quickly.

Ozone measurement methods in current use

Several techniques for measuring ozone concentration have gained wide acceptance. EPA's standard reference method is the ozone–ethylene chemiluminescence method, by which a sample of ambient air that contains ozone is mixed with pure ethylene that flows at a slow, controlled rate. One product of the resulting reaction is formaldehyde in an excited state, which can be detected by a photomultiplier tube. This technique is ozone-specific and has a minimum detection limit of about 5 ppb and a response time of less than 30s. A number of commercially available instruments use this method.

A related technique, less commonly used, also is based on the chemiluminescence principle. With this method, ozone reacts with solid rhodamine B. Although this technique has a slightly longer response time, its minimum detection limit is 1 ppb.

Another technique is based on ultraviolet (UV) photometry. The degree of UV absorption is detected within a particular wavelength band in which ozone is absorbed. This technique is ozone-specific and has a response time of about 30 s and a minimum detection limit of about 5 ppb. It is used by some commercially available instruments and often serves as a calibration reference for chemiluminescence instruments.

Continuous ozone-monitoring instruments in current use are quite reliable. Performance specifications for the instruments show precision values within 10 ppb. In continuous field operation, the expected variability or error in a measurement may be 10–30%.

Most of the O_3 data available in the United States today from regular continuous-monitoring stations have been collected at urban or suburban sites; a typical urban area contains one to five monitors. Some of the larger metropolitan urban areas contain more monitoring sites. These data are compatible with the urban model simulation studies in which the measured O_3 concentrations are used to define initial or boundary conditions and to evaluate the models.

Although it is sufficient for most urban model application studies, the existing O_3 data base is far from ideal in terms of the number and spatial distribution of monitors in metropolitan areas. For regional-scale modeling, the existing network is clearly insufficient because only a few monitoring stations are located in rural and "regionally representative" locations away from the influence of urban emission sources. Ozone monitors sometimes are located in rural areas for a limited amount of time during special field studies in a given region.

Because of concerns about O_3 damage to crops and forests, additional monitors are being installed in rural and remote areas on a permanent basis. Even in the most optimistic of futures, however, it would be unrealistic to expect a dense network of O_3 monitors on a regional ($\approx$ 1000 km) scale. Nevertheless, an increase in the number of monitors and a better spatial distribution of these monitors in the ambient O_3 data base will make the use of these data in regional-scale modeling applications easier and more meaningful.

Regional models for ozone

The air quality simulation model attempts to provide a mathematical solution to the atmospheric diffusion equation for all species of interest. Generally, analytic solutions for the set of model equations are not available. Iterative numerical solutions to the finite-difference analogs of the original differential equations therefore are used. The terms in the model equations include those for three-dimensional transport and diffusion, pollutant sources and sinks, and chemical transformations. The framework of the model in which these equations are solved can vary from a three-dimensional Eulerian grid model to a moving trajectory model to the relatively simple box model. Hybrid formulations between the three types of models also are possible. In our discussion of regional ozone modeling, we limit ourselves to the grid models. Most of its concepts apply to the other model types, however, since their formulations essentially are subsets of the grid model formulation.

All grid models include representations of the advective transport terms. The transport considers the movement of mass as governed by the mean wind velocity. (In regional-scale O_3 models, mean quantities generally are averaged over a period of 1–3 h.) Models vary in the methods by which the gridded three-dimensional wind field is specified. The most common device is the use of an objective analysis technique to interpolate between observations of wind speed and direction (*29*). The interpolation technique sometimes is enhanced by mass-conservation principles to improve the results in areas of complex flow such as those with sea breeze circulations or mountain–valley systems (*30*).

In the most rigorous approach, a dy-

namic wind field model calculates the gridded winds based on a numerical solution of the equations of mass, momentum, energy, and moisture (*31*). Once the wind field is determined, various numerical solution techniques may be used to solve the advective transport equation (*32*). Each technique has its own behavioral characteristics; some prevent negative concentrations from being calculated and others preserve the peak concentration areas better. The magnitude of the gradients in the spatial patterns of predicted concentrations is determined, in part, by the choice of transport solution technique.

Turbulent diffusion is the process whereby mass is spread out and diluted based on the perturbations of the wind field from the mean flow. This part of the flow field is not resolved on the time or space scales of the model. Typically this component is modeled empirically by the K-theory, or gradient transfer theory approach. This theory assumes that the local concentration of mass will change with time as a function of the mean wind speed, the local concentration gradient in space, and a stability-dependent empirical diffusivity coefficient. This approach also is convenient for numerically solving the diffusion component along with the transport.

Other methods of treating turbulent diffusion in regional models are possible, including a more rigorous approach to specifying the turbulent fluctuations themselves. If this approach is used, it usually is confined to the vertical direction, where the diffusive effects are closer in scale to the mean transport and thus have a greater relative impact than in the horizontal direction.

Modeling the kinetics of the relevant atmospheric photochemistry is an integral part of all regional-scale ozone models. It is difficult to condense the hundreds of tropospheric photochemical reactions that involve NO_x, oxygen (O_x), and hydrocarbon (HC) species into a set that can be simulated efficiently within an air quality model. The techniques for accomplishing this are varied and continue to evolve.

Currently, there are three generally accepted techniques:

- the surrogate species technique, in which the reactions of a few hydrocarbon species represent the entire atmospheric mixture of hydrocarbons (for example, the Dodge mechanism [*33*]);
- the lumped molecule technique, in which one hydrocarbon species, sometimes a generalized species, serves as a surrogate for a group of similarly reacting species (for example, the Carter–Atkinson–Lurmann–Lloyd (CALL) mechanism [*34*]); and
- the lumped structure, or carbon-bond method, in which hydrocarbon groupings are based on structural units (for example, the CBM-IV mechanism [*35*]).

Chemical mechanisms applicable to regional O_3 modeling must include the slower reacting compounds because of the multiday nature of the model simulations and certain reactive biogenic hydrocarbon species that may become important in rural areas. These chemical aspects have been ignored in urban-scale ozone models because their scope is more limited in time and space.

Our understanding of atmospheric chemistry of the O_3-NO_x-HC cycle has improved greatly during the past 20 years. Uncertainties still exist, however, and are reflected in all of the contemporary literature on chemical mechanisms. First of all, some of the reaction rate constants are highly speculative. Also, for regional-scale modeling, the more significant uncertainties include those associated with nighttime NO_x chemistry, the fate of many slower-reacting organic species, and numerous heterogeneous processes involving aerosols that generally are neglected in the examination of chemical mechanisms for the production of ozone. The degree of error introduced into mechanism predictions from these uncertainties has not been quantified adequately.

Most ozone predictions based on current knowledge of the applicable mech-

TABLE 1
Comparison of two regional air quality simulation models[a]

	Regional Oxidant Model (ROM)	Regional Transport Model (RTM-III)
Model type	Regional ozone	Regional ozone
Developers	EPA Atmospheric Sciences Research Laboratory, Research Triangle Park, N.C. (Robert Lamb)	Systems Applications, Inc., San Rafael, Calif. (Mei-Kao Liu and Ralph Morris)
References	*11–13*	*36, 37*
Horizontal grid resolution	18.5-km grid cells (780 × 1100-km model domain)	Variable, 10–80-km grid cells (1800 × 2000-km model domain in eastern U.S. application)
Vertical grid resolution	Three layers extending to height of tops of cumulus clouds and one diagnostic surface layer	Three layers extending to 2000–6000 m above ground level and one diagnostic surface layer
Temporal resolution	1 hour	1–3 hours
Subgrid-scale features	Parameterized estimate of near-surface concentration variance of NO, NO_2, and O_3 within a grid cell, based on heterogeneous emissions distribution	Gaussian-type point source module with O_3–NO_x photostationary chemistry at receptor points or, optionally, reactive plume module for point sources
Horizontal transport	Winds interpolated from observations, except nighttime jet-layer winds, which are derived from hydrostatic model. "Probabilistic" generation of wind fields. Numerical advection by biquintic[b] polynomial scheme	Winds interpolated from observations or generated by dynamic wind model. Numerical advection by Flux-Corrected Transport method (SHASTA or multidimensional FCT)
Chemical kinetics	Carbon-bond IV (28 species, 70 reactions). No steady-state approximations made. All species advected	Carbon-bond IV (28 species, 70 reactions). Solution procedure uses local steady-state approximations. Fourteen species advected
Deposition	Dry deposition parameterized by empirical relationship with friction velocity, Obukhov length[c], and surface resistance	Dry deposition parameterized with aerodynamic resistance of the laminar layer and surface resistance
Cloud processes	Direct cumulus cloud mass flux from surface layer to cloud layer	Cloud mass flux parameterization planned for the future
Applications	Northeastern United States (NEROS region); southeastern United States	Eastern United States (SURE region); Midwest–Southeast United States; California Central Valley; western Europe (PHOXA)

[a] 3-dimensional grid type.
[b] 2-dimensional, fifth order.
[c] Obukhov length is a characteristic scale length based on stability of the lower atmosphere.

anisms are quite similar for the same set of operating conditions. Fractional changes of some key parameters, however, may cause dissimilar responses among these mechanisms. This aspect disturbs policy-makers, who base their decisions, in part, on the response of ozone production mechanisms to fractional changes in concentrations of precursor species. Further development and understanding of these mechanisms and of all important chemical processes are needed before these differences can be reconciled.

Sources and sinks of pollutants are another essential aspect of regional models. Mass is removed either chemically (through the chemical kinetic mechanism), by rainout and washout (usually not considered in models for O_3, but important factors in acid deposition models), or by deposition to the surface. The latter process usually is characterized by a "deposition velocity" for a chemical species that is empirically linked to the resistance of the atmosphere as well as the resistance of the underlying surface to the downward movement of the species near the surface.

Pollutants typically include NO_x, HC, and carbon monoxide (CO) species from distributed-area and large point sources. The area sources are specified as emission fluxes averaged over the cross-sectional area of each grid cell. Point source emissions are added to the appropriate grid cell after any buoyant plume rise is accounted for. Some models attempt to treat the point source plume separately while it is of a subgrid scale size. Treating the subgrid scale effects, in one form or another, is a common issue in regional models, where a single source or an urban area occupies only a portion of a single grid cell.

Table I compares the characteristics of two currently used grid models for regional-scale air pollution. They are designed exclusively for the prediction of ozone concentrations as well as for those of the other constituent species of photochemical smog. Three other regional models have been designed for the simulation of the acid deposition phenomenon—the Sulfur Transport Eulerian Model (*38–40*), the Regional Acid Deposition Model (*41–43*), and the Acid Deposition and Oxidant Model (*44*). All of the models are operational, although development continues on each.

Models for the rigorous treatment of acid deposition must include all of the physical processes that affect photochemical smog as well as many others that uniquely affect acid deposition, such as in-cloud physical processes, rainout, washout, wet deposition, aqueous-phase chemistry, and others. Because O_3, the hydroxyl radical (OH), and hydrogen peroxide (H_2O_2) represent important oxidizing pathways in the chemistry of acid deposition (*45*), these models must simulate their concentrations accurately and include the primary precursor species in their emission inventories. Thus regional ozone concentrations are derived, albeit as a by-product, from regional-scale models of acid deposition.

Certain factors, such as spatial scales, separate the two model types. The overall domains and grid sizes of acid deposition models tend to be larger than those for regional ozone and may be too coarse for proper resolution of high-concentration areas. On the other hand, acid deposition models have more vertical resolution than ozone models to account for the physical processes in clouds properly.

Applications of the regional air pollution models so far have centered on the eastern parts of the United States and North America where multiday, multicity pollution episodes are most common and for which comprehensive data bases have been collected. Other areas of application, however, are being planned or are in progress. Particular interest in regional models exists in Europe because of the large-scale pollution episodes that can develop there and cross political boundaries. The governments of West Germany and the Netherlands are sponsoring development and application projects using the Regional Transport Model (RTM-III) and the Acid Deposition and Oxidant Model (ADOM).

Figure 3 illustrates one of the primary benefits of the use of regional oxidant models: defining individual urban plumes within the model domain. In a test application of the first generation ROM, maximum predicted O_3 concentrations were contoured over an area downwind of the Detroit–Windsor metropolitan plume during the second day of simulation of a pollution episode in August 1979. (Only a limited portion of the ROM grid is shown.) Although the principal axis of the plume extended out over Lake Erie, predicted ozone concentrations agreed fairly well with the pattern of surface measurements shown. The shaded region in the figure corresponds to an area of aircraft monitoring on Aug. 4, 1979, when the O_3 measurements aloft (within the well-

FIGURE 3
Contours of predicted maximum ozone concentrations [a]

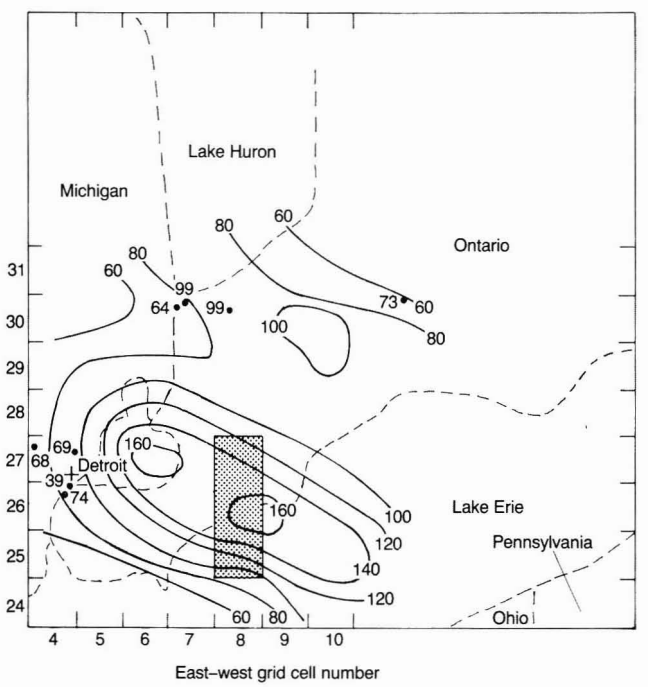

[a]From ROM for the Detroit metropolitan plume, Aug. 4, 1979. Points are maximum observed concentrations at monitoring stations. Shaded area indicates grid cells in which measurements of ozone taken from aircraft were above the regional background value and as high as 150 ppb.

mixed layer) were observed to be as high as 150 ppb close to the area in which a concentration of 160 ppb had been predicted (*46*).

Issues to be resolved

There is considerable interest in regional-scale air quality modeling for O_3, other photochemical oxidants, and acid deposition. This interest is fueled by members of the scientific community and by policy-makers who now recognize that large-scale episodes of air pollution can span many days and cross many political boundaries. Coordinated planning of optimum emission control strategies to reduce the pollutant burden must be organized around a comprehensive approach to the problem. Part of the process includes the use of both regional-scale and urban-scale air quality models. Urban-scale models alone cannot provide the link between source areas as effectively as regional models.

The challenge to air quality regulators is to integrate the use of regional O_3 models with the urban models in a way that allows interaction between the different spatial scales and makes best use of the data provided by each type of model. The coarser resolution of regional models helps define the broad spatial patterns of ozone and the directional movement of these patterns over time; the finer scale of the urban models better locates areas of high concentration within an airshed. Nesting an urban model within the structure of a regional model for particular cities is one way to provide a dynamic interaction between the spatial scales. Another approach would be to maintain the separate integrity of the models, but to allow the regional model to provide boundary conditions to the smaller scale model, using the models in an iterative manner to provide the link between the scales.

We have described the structural components of the more rigorous grid-type regional O_3 models and have discussed some of the issues that have yet to be resolved to achieve credible regional-scale simulations. Chief among these issues are the questions of the magnitude and photochemical effects of regional-scale biogenic organic emissions, the mass transfer from the lower to upper boundary layer by cloud fluxes, the lack of determinism in regional-scale wind fields, and perhaps most critically, the proper description of the subgrid-scale chemical and physical processes within the enormous volume of a regional grid cell. Further theoretical research and field experiments will help provide the knowledge necessary to resolve these outstanding issues of regional-scale air quality modeling.

Acknowledgments

Although the research described in this article has been supported by EPA, it has not been subjected to agency review. It therefore does not necessarily reflect the views of the agency, and no official endorsement should be inferred.

This article has been reviewed for suitability as an *ES&T* feature by Joseph Norbeck, Ford Motor Company, Dearborn, Mich. 48121; and by William B. Innes, Purad, Inc., Upland, Calif. 91786.

References

(1) Reynolds, S. D.; Roth, P. M.; Seinfeld, J. H. *Atmos. Environ.* **1973,** *7,* 1033–61.
(2) *Uses, Limitations and Technical Basis of Procedures for Quantifying Relationships Between Photochemical Oxidants and Precursors;* U.S. Environmental Protection Agency: Research Triangle Park, N.C., 1977; EPA-450/2-77-021a, PB278-142/5.
(3) McRae, G. J.; Goodin, W. R.; Seinfeld, J. H. *Atmos. Environ.* **1982,** *16,* 679–96.
(4) Cox, R. A. et al. *Nature* **1975,** *255, 118–21.*
(5) Wolff, G. T. et al. *Atmos. Environ.* **1977,** *11,* 797–802.
(6) Hov, O.; Hesstvedt, E.; Isaksen, I.S.A. *Nature* **1978,** *273,* 341–44.
(7) Wolff, G. T.; Lioy, P. J. *Environ. Sci. Technol.* **1980,** *14,* 1257–60.
(8) Shipley, S. T. et al. *Environ. Sci. Technol.* **1984,** *18,* 749–56.
(9) Lamb, R. G. *Atmos. Environ.* **1984,** *18,* 591–606.
(10) Lamb, R. G.; Hati, S. K. *J. Clim. Appl. Meteorol.* **1987,** *26,* 837–46.
(11) Lamb, R. G. *A Regional Scale (1000 km) Model of Photochemical Air Pollution;* Part 1, Theoretical Formulation; U.S. Environmental Protection Agency: Research Triangle Park, N.C., 1983; EPA-600/3-83-035, PB83-207688.
(12) Lamb, R. G. *A Regional Scale (1000 km) Model of Photochemical Air Pollution;* Part 2, Input Processor Network Design; U.S. Environmental Protection Agency: Research Triangle Park, N.C., 1984; EPA-600/3-84-085, PB84-232651.
(13) Lamb, R. G.; Laniak, G. F. *A Regional Scale (1000 km) Model of Photochemical Air Pollution;* Part 3, Tests of the Numerical Algorithms; U.S. Environmental Protection Agency: Research Triangle Park, N.C., 1985; EPA/600/3-85/037, PB85-203818.
(14) Ching, J.K.S.; Shipley, S. T.; Browell, E. V. *Atmos. Environ.* **1988,** *22,* 225–42.
(15) Uthe, E. E. et al. *Bull. Am. Meteorol. Soc.* **1985,** *66,* 1255–62.
(16) Shipley, S. T. et al. *Environ. Sci. Technol.* **1984,** *18,* 749–56.
(17) Lamb, B.; Westberg, H.; Allwine, G. *Atmos. Environ.* **1986,** *20,* 1–8.
(18) Isidorov, V. A.; Zenkevich, I. G.; Ioffe, B. V. *Atmos. Environ.* **1985,** *19,* 1–8.
(19) Altshuller, A. P. *Atmos. Environ.* **1983,** *17,* 2131–65.
(20) Novak, J. H.; Reagan, J. A. Presented at the 79th Annual Meeting of the Air Pollution Control Association, Minneapolis, 1986.
(21) Killus, J. P.; Whitten, G. Z. *Environ. Sci. Technol.* **1984,** *18,* 142–48.
(22) Brewer, D. A. et al. *Atmos. Environ.* **1984,** *18,* 2723–44.
(23) Lurmann, F. W. et al. *Atmos. Environ.* **1984,** *18,* 1133–43.
(24) Lamb, R. G. *Numerical Simulations of Photochemical Air Pollution in the Northeastern United States: ROM1 Applications;* U.S. Environmental Protection Agency: Research Triangle Park, N.C., 1986; EPA/600/3-86/038, PB86-219201.
(25) Viezee, W.; Johnson, W. B.; Singh, H. B. *Atmos. Environ.* **1983,** *17,* 1979–93.
(26) Toothman, D. A.; Yates, J. C.; Sabo, E. J. Status Report on the Development of the NAPAP Emission Inventory for the 1980 Base Year and Summary of Preliminary Data; U.S. Environmental Protection Agency: Research Triangle Park, N.C., 1984; EPA/600/7-84-091, PB85-167930.
(27) Gear, C. W. *Commun. ACM* **1971,** *14,* 176–79.
(28) Hesstvedt, E.; Hov, O.; Isaksen, I. S. *Int. J. Chem. Kinet.* **1978,** *10,* 971–94.
(29) Goodin, W. R.; McRae, G. J.; Seinfeld, J. H. *J. Appl. Meteorol.* **1980,** *19,* 98–108.
(30) Davis, C. J.; Bunker, S. S.; Mutschlecner, J. P. *J. Clim. Appl. Meteorol.* **1984,** *23,* 235–38.
(31) Anthes, R. A. *Mon. Weather Rev.* **1983,** *111,* 1306–35.
(32) Schere, K. L. *Atmos. Environ.* **1983,** *17,* 1897–1907.
(33) Dodge, M. C. *Combined Use of Modeling Techniques and Smog Chamber Data to Derive Ozone-Precursor Relationships;* U.S. Environmental Protection Agency: Research Triangle Park, N.C., 1977; EPA-600/3-77/001a, PB264-233/8.
(34) Lurmann, F. W.; Lloyd, A. C.; Atkinson, R. *J. Geophys. Res.* **1986,** *91,* 10905–36.
(35) Whitten, G. Z.; Gery, M. W. *Development of CBM-X Mechanisms for Urban and Regional AQSMs;* U.S. Environmental Protection Agency: Research Triangle Park, N.C., 1986 EPA-600/3-86-012, PB86-155033.
(36) Liu, M. K.; Morris, R. E.; Killus, J. P. *Atmos. Environ.* **1984,** *18,* 1145–61.
(37) Morris, R. E.; Stewart, D. A. Development of a Regional Oxidant Model and Application to National Parks in the Eastern United States, Part I; Systems Applications: San Rafael, Calif., 1987; SYSAPP-87/142.
(38) Carmichael, G. R.; Peters, L. K.; Kitada, T. *Atmos. Environ.* **1986,** *20,* 173–88.
(39) Carmichael, G. R.; Peters, L. K. *Atmos. Environ.* **1984,** *18,* 953–67.
(40) Carmichael, G. R.; Peters, L. K. *Atmos. Environ.* **1984,** *18,* 937–52.
(41) "The NCAR Eulerian Regional Acid Deposition Model"; National Center for Atmospheric Research: Boulder, Colo., 1985; ADMP-85-3.
(42) Chang, J. S. et al. "Preliminary Evaluation Studies with the Regional Acid Deposition Model (RADM)"; U.S. Environmental Protection Agency: Research Triangle Park, N.C., 1986; EPA/600/3-86/024, PB86-175692.
(43) Chang, J. S. et al. *J. Geophys. Res.* **1987,** *92,* 14681–700.
(44) Venkatram, A.; Karamchandani, P. *Environ. Sci. Technol.* **1986,** *20,* 1084–91.
(45) Calvert, J. G.; Stockwell, W. R. *Environ. Sci. Technol.* **1983,** *17,* 428–43.
(46) Schere, K. L. EPA Regional Oxidant Model: ROM1 Evaluation for 3-4 August 1979; U.S. Environmental Protection Agency: Research Triangle Park, N.C., 1986; EPA/600/3-86/032, PB86-215886.

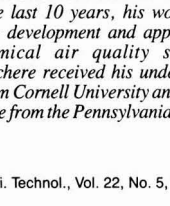

Kenneth L. Schere *is a research meteorologist at the Meteorology Division of EPA's Atmospheric Sciences Research Laboratory. During the last 10 years, his work has included the development and application of photochemical air quality simulation models. Schere received his undergraduate degree from Cornell University and his graduate degree from the Pennsylvania State University.*

"The book is rich in content and well written. It is difficult to resist the temptation of reading it all."

Dr. Evgeny Shustorovich
Eastman Kodak Company

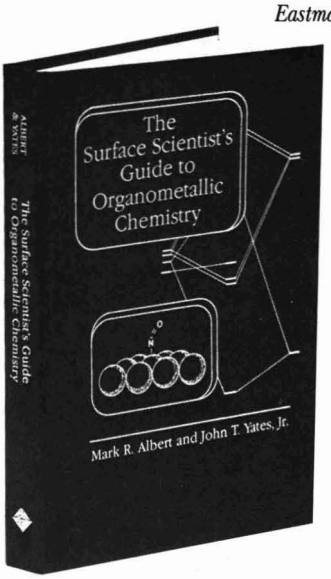

Surface Scientist's Guide to Organometallic Chemistry

"This book does an excellent job of systematizing available data in the surface science and organometallic literature in an understandable and readable manner."

Professor Cynthia Friend
Harvard University

"This is the most useful volume for those of us who work in the field of structural surface chemistry. More and more it appears that the cluster bonding is best to describe the nature of the surface chemical bond. This book describes the various cluster bonding possibilities starting with good sound organometallic chemical principles. The book is well written . . . broad, and most useful to those surface chemists who are interested in bonding and applications of bonding to a variety of macroscopic surface phenomena. I am delighted to have this book on my book shelf."

Professor Gabor A. Somorjai
University of California, Berkeley

Within the field of surface science, concepts from the fields of organometallic and coordination chemistry are becoming more important as a means of understanding chemisorption systems.

This valuable resource was written as a means of communicating to surface scientists the aspects of organometallic chemistry that are relevant to current surface science research. This book, divided into three sections, makes relevant organometallic chemistry issues understandable to the surface scientist. Specific topics covered include:

- **basic coordination chemistry**
- **coordination ligands**
- **bonding sites in clusters and their relationships to surface bonding sites**
- **application of orbital symmetry and orbital overlap to surface band structure calculations**

Surface Scientist's Guide to Organometallic Chemistry serves the dual purpose of being both a reference work and an overview of selected aspects of organometallic and coordination chemistry. Surface scientists whose backgrounds include physics, physical chemistry, and engineering will find this book an important addition to the literature of organometallic and coordination chemistry.

by Mark R. Albert and John T. Yates, Jr.

214 pages (1986) Clothbound
LC 87-25937 ISBN 0-8412-1003-9
US & Canada **$49.95**, Export **$59.95**

Order today! Mail the coupon below, or call **TOLL FREE 800-227-5558** and charge your credit card.

Order Form

Please send me:		Qty.	US & Can.	Export	Total
Surface Scientist's Guide to Organometallic Chemistry	OTB	____	$49.95	$59.95	____
				Total	____

☐ Payment Enclosed (make checks payable to ACS).
☐ Purchase Order Enclosed. P.O.# _____

Charge my ☐ VISA/MasterCard ☐ American Express ☐ Diners Club/Carte Blanche ☐ ACCESS ☐ Barclaycard

Account # _____

Expires _____ Interbank # _____ (MC/ACCESS)

Cardholder _____ Phone # _____

Signature _____

Name _____

Address _____

_____

City, State, Zip _____

ORDERS FROM INDIVIDUALS MUST BE PREPAID.
Prices subject to change without notice. Please allow 4-6 weeks for delivery. Foreign payment must be made in US currency by international money order, UNESCO coupons, or US bank draft. Order through your local bookseller or directly from ACS.

Mail this order form with your payment or purchase order to:
American Chemical Society, Distribution Office Dept. 241, P.O. Box 57136, West End Station, Washington, DC 20037

FY '89 budget request

Richard M. Dowd

The EPA budget submitted to Congress in February is effectively President Reagan's last budget. For that reason, it is timely to examine the administration's budgets and identify trends on environmental issues. Such a review reveals a dramatic shift in priorities from traditional pollution control programs and research to the Superfund program.

Before comparing budgets, however, a brief synopsis of the Fiscal Year (FY) 1989 budget is in order. The EPA budget totals $4.8 billion, which is a $650 million decline from 1988. The budget includes $1.6 billion for operating programs (air, water, drinking water, pesticides, solid and hazardous waste, toxics, radiation, and research and development); $1.7 billion for Superfund; and $1.5 billion for grants for sewage treatment plants.

Superfund continues its rapid growth in spending (up 13%), becoming the equivalent of the 800-pound gorilla at the EPA dinner table who can sit anywhere he wants. In FY '89, EPA intends to initiate design work at 75 sites and construction work at 50 sites. EPA's operational programs are also increased, but not as much (about 3%).

EPA plans to phase the construction grant program into state revolving funds by 1991. For FY '89 the program is to be reduced from $2.3 billion to $1.5 billion, with half going to a state revolving fund.

The agency's research and development program shows a 6% increase to $375 million. In addition, this year EPA has proposed a long-needed capital budget of about $19 million for refurbishing laboratories. There has been a considerable shift in priorities in the agency's budgets since FY '81.

Are priorities in order?

In particular, the growing impact of Superfund activities has been overwhelming. Superfund activities have grown from 5% of nongrant funds in FY '81 to about 50% in FY '89; this is an increase from $75 million in FY '81 to $1.7 billion in FY '89. Personnel has increased from 70 people to more than 2800.

Congress and the administration have expanded Superfund at the expense of pollution control programs. During the same period, the effort expended on the program areas of air and water pollution has been reduced; the amount of money spent on these programs is about 35% lower than for FY '81 (in constant 1981 dollars). Personnel has been reduced by about 12%.

This shift between air and water programs and Superfund raises questions about priorities. The reduction in air and water program budgets prevents the agency from keeping pace with the resistant character of air and water issues. Air and water pollution has not been eliminated (witness the debate over the revisions of the Clean Air Act). The tasks assigned to the air and water programs have grown more complicated because of increasing concern about toxic air and water pollution. At the same time, arguably, a disproportionate share of funds is being spent on Superfund—the increase this year of $200 million for initiation of work on a fraction of the 2000 Superfund sites is almost as large as the amount budgeted for the entire air program ($255 million).

Other decreases

Research budgets also have suffered a substantial reduction in the support and priority given. EPA will spend 25% less on research in constant dollars than was budgeted in FY '81. If new initiatives under investigation are subtracted, the reduction is closer to 50%. For example, only $170 million (in 1981 dollars) is available in 1989 to investigate those issues for which $358 million was appropriated in FY '81. In addition, EPA has a smaller core of scientists in R&D (down 15%), and R&D has lost ground with respect to other EPA programs. Fewer than 1 of every 8 nongrant dollars is spent on research today, compared with 1 out of 4 in FY '81.

The relative share of monies spent on various areas of research also reflects the shifting priorities on programs discussed above. In the first four years of the Reagan Administration, research on air and water averaged almost 40% of the research funds, with toxics and hazardous waste making up about 25%. In 1989 these percentages will be nearly reversed, with air and water slightly more than 25% of a relatively smaller effort.

The shift of priorities to Superfund has had a debilitating effect on research. The Superfund program has not supported the research base necessary for effective action. Superfund spends a ludicrously small amount on research (only 3% of the Superfund budgets during the last eight years, compared with 20% for air and water in the same period). Thus Superfund is pouring huge amounts of money into on-site cleanup in lieu of funding research that might mitigate those costs and ameliorate the problems.

The importance of the decline in research should not be underestimated. In my view, the fate of the research program is critical to the success EPA will have in meeting the challenges of the 1990s.

Richard M. Dowd, Ph.D., is president of R. M. Dowd & Company, scientific and environmental policy consultants in Washington, D.C.

0013-936X/88/0922-0497$01.50/0

Sources and Fates of Aquatic Pollutants. Ronald A. Hites and Steven J. Eisenreich, Eds. American Chemical Society, 1155 16th St., N.W., Washington, D.C. 20036. 1987. xiii + 558 pages. $99.95, cloth.

Reviewed by John W. Farrington, University of Massachusetts—Boston, Boston, Mass. 02125-3393.

Sources and Fates of Aquatic Pollutants is a useful collection of papers selected from a symposium sponsored by the American Chemical Society in September 1985. Its index is excellent and the format of its figures, tables, and type make the book easy to read.

The book's first three sections emphasize air and water processes, water column processes, and water sediment processes. A fourth section presents case studies.

Most of the chapters are reviews or extensive summaries and overviews that tie several published works together. The first chapter, "Methods of Estimating Solubilities of Hydrophobic Organic Compounds—Environmental Modeling Efforts," by Andren, Doucette, and Dickut, provides an easily readable synopsis of the state of the art. It is recommended for beginning graduate students and advanced undergraduate students and also is a useful refresher for those who have been pondering this issue for several years. My only difficulty with this chapter is that the influence of ionic strength and salinity on solubility is not discussed.

In Chapter 2, Bidleman and Foreman provide theoretical and pragmatic discussions on the vapor–particle partitioning of semivolatile organic compounds. They address polycyclic aromatic hydrocarbons (PAHs), polychlorinated biphenyls (PCBs), and chlorinated pesticides and provide examples from studies of urban and rural environments. This chapter would have been enhanced, however, by a deeper discussion of the value of studies involving individual congeners of PCBs, chlorinated boranes, and camphenes.

The chapters by Astle, et al. cover records of pollution in lake sediments. They do not, however, include benthic microfauna and irrigation processes in their models; this is a notable omission with regard to the study of many aquatic ecosystems.

Clouds and fog introduce numerous complications into the atmospheric chemistry of man-made pollutants. Waldeman and Hoffman discuss these complexities using nitrogen and sulfur species as examples. The combined theoretical treatment and field observations make this an excellent chapter on the subject.

The chapter by Arimoto and Duce provides an overview of the results of the Sea–Air Exchange (SEAREX) program that studied the transfer of trace elements. The data from remote and presumably more pristine areas furnish a basis for evaluating man-made inputs of trace elements to lakes via atmospheric transport. Moreover, the importance of these studies to past and present oceanic geochemical cycles is discussed briefly. The thorny problem of estimating dry deposition is treated in a reasonable, up-front manner.

In the section on water column processes, Murray lucidly presents a review of mechanisms controlling the distribution of trace elements in oceans and lakes. The comparison of first-order processes active in oceans and lakes is instructive, especially the discussions on the differences between advective and eddy-diffusive scales and the similarities between lakes and estuaries in terms of the importance of fluxes from sediments to water.

In the chapter on metal speciation in natural waters, Campbell and Tessier delve into the importance of pH and the ionic composition of water in the control of metal speciation. Their review documents the issue of metal–organic interactions in natural waters that still beclouds the full understanding of metal speciation.

Two chapters address acid deposition, an issue of great concern to the aquatic chemistry community as well as to the public. The chapter on ion budgets, by Lin, Schnoor, and Glass, focuses on a lake in Wisconsin. It is interesting because it illustrates the importance of coupling hydrologic models with chemically and microbially mediated element budgets. The chapter also reminds the reader of the difficulty in obtaining reliable estimates of seemingly simple data such as the volume of precipitation. The next chapter, by Brezonik, Baker, and Perry, offers a tutorial on the processes of in-lake alkalinity generation.

Elzerman and Coates open the section on water sediment processes with a superb chapter that reviews hydrophobic organic compounds on sediments. I was especially pleased to see the extensive credit given to the pioneering research of Sam Karickhoff in this area of aquatic chemistry.

In the next chapter, Eadie and Robbins present compelling information on the insights gained when measurements of hydrophobic organic contaminants are combined with measurements of radionuclides (e.g., from nuclear weapons tests). They may take pride in this chapter, which summarizes several years of painstaking work and is a substantial contribution to the type of aquatic research necessary to mitigate environmental quality damage.

Charles and Hites review methods for studying sediments to reconstruct the history of certain pollutants introduced into the environment. They discuss the general principles governing the usefulness of these methods and cite several studies on lead, mercury, PAHs, PCBs, and DDT.

Eisenreich begins the section on case studies with a chapter on PCBs in Lake Superior. In the three chapters that follow, Oliver discusses the fate of some chlorobenzenes in Lake Ontario; Armstrong and co-workers provide information on the cycles of hydrophobic organic compounds and nutrient elements in Crystal Lake; and Homond and colleagues discuss element cycling in wetlands.

Unfortunately, *Sources and Fates of Aquatic Pollutants* lacks a summary and an overview of the presentations in the book—an omission that detracts from the book's value. In addition, the book lacks chapters on two critical topics: the uptake, fate, and release of aquatic pollutants by biota and the routes of pollutants in aquatic ecosystems back to man.

These shortcomings aside, I find *Sources and Fates of Aquatic Pollutants* to be a valuable addition to the literature in environmental sciences. Several of the chapters are teaching-quality, primary references for graduate and undergraduate courses. I highly recommend the book to graduate students and to students entering aquatic chemistry from other disciplines in chemistry. It should be on the shelves of libraries at universities, industry and government laboratories, and especially consulting companies.

0013-936X/88/0922-0498$01.50/0

CLASSIFIED SECTION

The University of Tennessee—Knoxville announces a newly formed fully endowed chair in the Department of Civil Engineering. The holder of the Henry Goodrich Chair of Excellence in Environmental Engineering must be a person of demonstrated national prominence to complement the existing strengths within the department and the university. As wide a consideration of potential candidates as possible will be made, considering not only the present reputation and areas of scholarly inquiry, but also the likelihood of continued national prominence within the field. The individual must have an earned doctorate in engineering in a field relevant to environmental engineering; must have senior academic experience and, preferably, also industrial experience; must have an outstanding professional reputation as evidenced by refereed publications, external research grants, honors, and awards. The holder of the Chair must have the vision and commitment to increase the quality of the research and curricular programs of the department. While any area of waste management may be selected, preference will be given to those applicants with expertise related to biological and/or chemical treatment technologies and/or transport modeling. Individuals wishing to apply should send a detailed resume and references to:

Dr. Gregory D. Reed, Chairman
Chair of Excellence Search Committee
Department of Civil Engineering
University of Tennessee
Knoxville, TN 37996-2010
(615) 974-2503

Review of applications will begin on June 1, 1988 and the search will remain open until the position is filled. UTK is an EEO/AA/Title IX/Section 504 Employer.

ENVIRONMENTAL CHEMIST

Conestoga-Rovers & Associates, a progressive environmental consulting firm with offices in Niagara Falls, N.Y. and St. Paul, Mn., has an opening in their analytical/monitoring department for an environmental chemist. The successful candidate must have a minimum of two years of professional experience related to general environmental water chemistry, organic analysis, potable water treatment systems and standard QA/QC procedures with respect to analyses of environmental matrices.

The position will include responsibility for review of analytical data for technical quality and general support of the company's analytical department.

Salary will be commensurate with experience. Interested, qualified individuals are requested to send a complete resume to:

CRA
Conestoga-Rovers & Associates
7703 Niagara Falls Boulevard
Niagara Falls, New York 14304
Re: Environmental Chemist

ENVIRONMENTAL AND WATER RESOURCES ENGINEERING ASSISTANTSHIPS

Graduate assistantships and scholarships for M.S. and Ph.D. students are available in the ENVIRONMENTAL & WATER RESOURCES ENGINEERING PROGRAM at TEXAS A&M UNIVERSITY to support research and teaching activities related to hazardous waste, air and water quality, estuary and marine research, hydrology, hydraulics and other areas. For further information, contact **Dr. Bill Batchelor, Group Head, EWRE, Civil Engineering Dept., Texas A&M University, College Station, TX 77843.**

Opportunities in San Antonio

Diversity, expertise, technology, and an environment for professional success. These are the hallmarks of The MITRE Corporation. For over 25 years, MITRE has specialized in the design, development and delivery of superior C^3I and civilian systems engineering solutions to meet the most technically demanding requirements of our U.S. Government clients. MITRE has immediate openings at its San Antonio facility that provide the dynamic atmosphere of a small company supported by the resources of a major, 5,000-employee corporation.

Analytical Chemists/ Quality Assurance

We have 2 positions open for highly qualified individuals to help us develop and monitor quality assurance activities in a major environmental sampling and analysis program. Individuals will be responsible for developing QA/QC requirements and evaluating commercial testing laboratories' performance in meeting those requirements. Evaluations will be based on a review of data and documentation and on-site inspections of laboratory operations. Both positions require expertise in analytical chemistry, a working knowledge of QA/QC principles and practices, and hands-on experience with the instrumentation and methods used in environmental testing (e.g., AA, ICP, GC, GC/MS). Experience with EPA test methods is highly desirable. The first position requires an advanced degree in Analytical Chemistry, 10 years of analytical laboratory or quality assurance experience, and at least one year of experience in environmental laboratory supervision. The second position requires a BS in Chemistry with emphasis on analytical procedures plus at least 5 years of experience in the quantitative analysis of environmental samples under a comprehensive QA/QC program. Individuals must be willing to travel 10 to 12 weeks a year.

For consideration, please submit your resume to J.V. Goudarzi, The MITRE Corporation, 7525 Colshire Drive, McLean, VA 22102. U.S. Citizenship required. An Equal Opportunity/Affirmative Action Employer.

MITRE

CLASSIFIED ADVERTISING RATES

Rate based on number of insertions used within 12 months from date of first insertion and not on the number of inches used. Space in classified advertising cannot be combined for frequency with ROP advertising. Classified advertising accepted in inch multiples only.

Unit	1-T	3-T	6-T	12-T	24-T
1 inch	$100	$95	$90	$85	$80

(Check Classified Advertising Department for rates if advertisement is larger than 10″.)
SHIPPING INSTRUCTIONS: Send all material to

Environmental Science & Technology
Classified Advertising Department
500 Post Road East
P.O. Box 231
Westport, CT 06881
(203) 226-7131

CLASSIFIED SECTION

Environmental Engineers and Scientists

Environmental experience relevant to consulting required. M.S. with 1 to 3 years' experience in:

- Civil/Environmental Engineering
- Environmental Chemistry

Work is in the areas of:

- Computerized environmental databases
- Chemical data interpretation at hazardous waste sites

Strong quantitative as well as verbal skills and a thorough knowledge of computers are mandatory. Knowledge of CERCLA, RCRA or resource recovery issues is desirable.

Gradient Corporation specializes in chemical fate/transport studies, chemical data management/interpretation, human exposure studies and health risk assessments. Our clients are nationwide and represent a balance of public and private sectors.

Please send resumes to:

Gradient Corporation

44 Brattle Street, Cambridge, MA 02138

Buried Waste Specialist

EG&G Idaho, Inc., prime operating contractor for the Department of Energy's Idaho National Engineering Laboratory, has an immediate opening for a Buried Waste Specialist. The successful candidate will have recognized experience in conducting and managing research and development projects in the area of environmental restoration; detailed knowledge of environmental acts, rules and regulations which include EPA Region 10 regulations; knowledge of low level radiological waste regulations and methods used to handle, process and store this waste.

The Buried Waste Specialist will have a PhD. in the area of environmental science with a MS and undergraduate degree in related fields such as chemistry, geology, etc. The position involves conducting research into advanced state-of-the-art concepts in the area of environmental restoration; attending technical society meetings, writing and presenting papers; participating on national boards and panels that address environmental issues and being a panel member that prioritizes and funds for the project.

Idaho Falls is located in the heart of the country's most scenic recreational areas. If interested and qualified please submit resume, with salary history and references, in confidence to: **Employment Services, (Code TBD-44), EG&G Idaho, Inc., P.O. Box 1625, Idaho Falls, Idaho 83415.** Equal Opportunity Employer M/F/H/V.

EG&G Idaho, Inc.

ENVIRONMENTAL ENGINEER

Selected applicant will assume a project management role for investigation of hazardous waste sites and for research programs to assess and develop engineering technology for management of hazardous chemical wastes. Position will require marketing skills to develop new programs and supervisory skills to manage junior staff. Engineering studies will be coordinated with a large ongoing chemical analytical program. Ph.D., Chemical Engineering, Environmental Engineering. Minimum of three years experience in investigation and remedial action of hazardous waste sites. Experience with research for new engineering technology for clean-up of hazardous wastes desirable.

Southwest Research Institute is a nonprofit research and development organization with competitive salaries and a comprehensive benefit program, which includes health, dental, life and disability insurance; 100% tuition reimbursement; paid vacations and holidays, and pension plan.

Resumes should be forwarded to: C. J. Luna, Sr. Personnel Specialist, Southwest Research Institute, Personnel Department, #262, P.O. Drawer 28510, 6220 Culebra, San Antonio, TX 78284.

Equal Opportunity Employer M/F

Southwest Research Institute
San Antonio

ENVIRONMENTAL ENGINEERS AND SCIENTISTS—At E.C. Jordan, a subsidiary of C-E Environmental, Inc., we've built a national reputation in environmental engineering and hazardous waste management. With a unique multidisciplinary approach, our engineers and scientists provide total environmental management services to industrial, commercial and governmental clients. Our continued expansion has created a variety of opportunities at our Portland, ME headquarters and at our regional offices in Wakefield, MA; Tallahassee, FL; Washington, DC; Farmington Hills, MI; and Oakridge, TN for:

- **ENVIRONMENTAL/SOLID WASTE ENGINEERS**
- **CHEMICAL ENGINEERS**
- **GEOHYDROLOGISTS/HYDROGEOLOGISTS**
- **FATE & TRANSPORT SPECIALISTS**
- **FIELD GC OPERATORS/SCIENTISTS.**

The professionals we seek should have hazardous waste experience with particular emphasis on site contamination, and remedial action evaluation and design. We offer a competitive salary and an outstanding benefits package. For immediate consideration, send your resume with geographic preference and salary requirements, to: **Human Resources Department, E.C. Jordan, 261 Commercial Street, P.O. Box 7050 DTS, Portland, ME 04112.** EOE.

USE THE CLASSIFIED SECTION

ANNOUNCEMENT OF POSITION

Director for the Institute for Water Sciences

Western Michigan University invites applications for the directorship of its newly established Institute for Water Sciences. The Institute was created to coordinate research, instruction and public service programs in ground water and water sciences. The Director will administer the Institute and Water Quality Laboratory, facilitate interdisciplinary research, develop curricula and promote public service. The ability to relate to industry, government and the general public, and to work with departments currently engaged in water related activities is essential. The Institute is expected to be self-supporting within three to five years, thus, the ability to attract outside funding to support the Institute's research, training and public service activities is seen as a primary requisite for a successful director.

Applicants are expected to have previous experience in the water sciences and a successful record of acquiring grants. Ph.D. preferred. Salary competitive.

Closing date for receipt of application is May 31, 1988. Please send letters of application with resumes and/or inquiry to: **Dr. Donald E. Thompson, Assistant Vice President for Academic Affairs and Chief Research Officer, Research and Sponsored Programs, A-223 Ellsworth Hall, Western Michigan University, Kalamazoo, Michigan 49008-5162. Phone: (616) 383-1632** Western Michigan University is an equal opportunity/affirmative action employer.

COMPUTER ANALYST

Design, implement, construct micro-processor based intelligent computer subsystems using 803X, 805X, 8751, and 8086/8088 micro-processors for use in chemical analytical instruments (both hardware and software) to monitor environmental contamination. Development of analog and digital electronic sensors for field and laboratory use. Consult with scientists about their needs for certain instruments and evaluate performance of existing instruments with a view towards solving their problems. Development of software for chemical oriented applications on personal computers. Requirements are a M.S. in Electrical Engineering or equivalent. 40 Hrs. per week, 8 am to 5 pm, $27,000/year. Contact **Louisiana Office of Employment Security, 1991 Wooddale Blvd., Baton Rouge, Louisiana 70896. Job Order 656392.**

LABORATORY ENVIRONMENTALIST

Mobil Research and Development Corporation has an immediate opening for an Environmentalist at its Paulsboro Research Laboratory located in Paulsboro, New Jersey.

Position requires a B.S. in Engineering or Science, preferably Environmental Engineering or Environmental Science. A Master's Degree in either of these latter two disciplines is desired. Applicants should have 3-5 years of industrial environmental compliance experience and a working knowledge of all environmental laws.

The successful candidate will be primarily responsible to insure that the Paulsboro Research Laboratory operates in compliance with all environmental laws. Regular assigned duties include audits, inspections, advising management and working with Laboratory personnel to solve environmental problems. This position reports to the Laboratory's Supervisor of Environmental Matters.

Qualified applicants are requested to forward their resume, including salary requirements, to:

Mobil Research and Development Corporation

Paulsboro Research Laboratory
Billingsport Road
Paulsboro, NJ 08066

Attention: Environmental Manager

An Equal Opportunity Employer

professional consulting services directory

CONSULTING GROUND-WATER
GEOLOGISTS AND ENGINEERS

ROUX ASSOCIATES INC

ROUX 11 STEWART AVENUE
HUNTINGTON, NEW YORK 11743
516 673-7200

CHERRY HILL,	DANBURY,	CONCORD
NEW JERSEY	CONNECTICUT	CALIFORNIA
609 424-3993	203 798-6969	415 685-8742

CenrefLabs

BRIGHTON CO. (303) 659-0497
(800) 634-0497
LIBERAL, KS (316) 624-4292

ENVIRONMENTAL TESTING

Priority Pollutants • PCB's
RCRA Hazardous Waste Analyses
Drinking Water • Wastewater
Pesticides • Sludge • CLP
Engine Emmission Monitoring

THE CONSULTANT'S DIRECTORY

UNIT	Six Issues	Twelve Issues
1″ × 1 col.	$55	$50
1″ × 2 col.	110	100
1″ × 3 col.	160	140
2″ × 1 col.	110	100
2″ × 2 col.	200	180
4″ × 1 col.	200	180

ENVIRONMENTAL
SCIENCE & TECHNOLOGY
500 Post Road East
P.O. Box 231
Westport, CT 06880

NEi

COMPLETE ANALYTICAL SERVICES GC/MS CAPABILITIES

- ☐ Screening & Analysis of Industrial & Hazardous Waste.
- ☐ Superfund & RCRA Requirements.
- ☐ Sampling to EPA Protocols.
- ☐ Toxicity Studies.

(516) 625-5500
60 SEAVIEW BLVD., PORT WASHINGTON, NY 11050
NYTEST ENVIRONMENTAL INC.

SPECIALISTS IN AIR EMISSIONS TESTING

With over 16 years experience, Entropy is the proven expert in air emissions testing. Call today for cost effective solutions to your air testing needs.

P.O. Box 12291, Research Triangle Park, NC 27709
(919) 781-3550 Fax (919) 787-8442

ENTROPY

GERAGHTY & MILLER, INC.
Ground-Water Consultants

Our 30th Year

125 East Bethpage Road
Plainview, New York 11803
(516) 249-7600
Offices Located Nationwide

Aquatic Toxicity Consultants

- Aquatic Toxicity Monitoring
- EPA Phase One Aquatic Toxicity Characterization Procedures
- Routine Bioassay Monitoring

Samples Delivered Overnight by Special Carriers

Burlington Research, Inc.
615 Huffman Mill Rd., Box 2481, Burlington, NC 27215
919-584-5564

INDEX TO THE ADVERTISERS IN THIS ISSUE

Advertising Management for the American Chemical Society Publications

CENTCOM, LTD.

President
Thomas N. J. Koerwer

Executive Vice President **James A. Byrne**
Senior Vice President **Benjamin W. Jones**
Clay S. Holden, *Vice President*
Robert L. Voepel, *Vice President*
Joseph P. Stenza, *Production Director*

500 Post Road East
P.O. Box 231
Westport, Connecticut 06880
(Area Code 203) 226-7131
Telex No. 643310

ADVERTISING SALES MANAGER
Bruce Poorman

ADVERTISING PRODUCTION MANAGER
Jay S. Francis

SALES REPRESENTATIVES

Philadelphia, Pa. . . . Patricia O'Donnell, CENTCOM, LTD., GSB Building, Suite 405, 1 Belmont Ave., Bala Cynwyd, Pa. 19004 (Area Code 215) 667-9666

New York, N.Y. . . . Patricia O'Donnell, CENTCOM, LTD., 60 E. 42nd Street, New York 10165 (Area Code 212) 972-9660

Westport, Ct. . . . Edward M. Black, CENTCOM, LTD., 500 Post Road East, P.O. Box 231, Westport, Ct 06880 (Area Code 203) 226-7131

Cleveland, OH. . . . John Guyot, CENTCOM, LTD., 325 Front St., Berea, OH 44017 (Area Code 312) 234-1333

Chicago, Ill. . . . Michael J. Pak, CENTCOM, LTD., 540 Frontage Rd., Northfield, Ill 60093 (Area Code 312) 441-6383

Houston, Tx. . . . Michael J. Pak, CENTCOM, LTD., (Area Code 312) 441-6383

San Francisco, Ca. . . . Paul M. Butts, CENTCOM, LTD., Suite 1070, 2672 Bayshore Frontage Road, Mountainview, CA 94043. (Area Code 415) 969-4604

Los Angeles, Ca. . . . Clay S. Holden, CENTCOM, LTD., 3142 Pacific Coast Highway, Suite 200, Torrance, CA 90505 (Area Code 213) 325-1903

Boston, Ma. . . . Edward M. Black, CENTCOM, LTD., (Area Code 203) 226-7131

Atlanta, Ga. . . . Edward M. Black, CENTCOM, LTD., (Area Code 203) 226-7131

Denver, Co. . . . Paul M. Butts, CENTCOM, LTD., (Area Code 415) 969-4604

ES&T
RESEARCH

Linear Solvation Energy Relationships. 44. Parameter Estimation Rules That Allow Accurate Prediction of Octanol/Water Partition Coefficients and Other Solubility and Toxicity Properties of Polychlorinated Biphenyls and Polycyclic Aromatic Hydrocarbons

Mortimer J. Kamlet*

Advanced Technology and Research, Inc., 14900 Sweitzer Lane, Laurel, Maryland 20707

Ruth M. Doherty

Naval Surface Warfare Center, White Oak Laboratory, Silver Spring, Maryland 20910

Peter W. Carr

Department of Chemistry, University of Minnesota, Minneapolis, Minnesota 55455

Donald Mackay

Department of Chemical Engineering and Applied Chemistry, University of Toronto, Toronto, Canada M5S 1A4

Michael H. Abraham

Department of Chemistry, University of Surrey, Guildford, Surrey GU2 5XH, United Kingdom

Robert W. Taft

Department of Chemistry, University of California, Irvine, California 92717

■ Methods are presented for estimation of V_I (intrinsic molar volume), π^*, and β of polychlorinated biphenyls and polycyclic aromatic hydrocarbons. Taken with the equation

$$\log K_{ow} = 0.45 + 5.15V_I/100 - 1.29(\pi^* - 0.40\delta) - 3.60\beta$$

reported recently by Leahy, these parameter estimation rules allow prediction of log K_{ow} with a precision that is better than the usual reproducibility of the measurements between laboratories.

Introduction

The environmental fates of organic chemicals are largely determined by their partitioning tendencies between atmospheric, aqueous, and organic phases. These latter phases include natural organic matter present in soils and bottom sediments and dispersed in suspended sediments, as well as in living tissues. Lipid tissues, for example, in fish, are of particular concern since they are important dietary components. The most commonly used descriptor of aqueous/organic partitioning is the octanol/water partition coefficient K_{ow}. It has been linearly related to fish bioconcentration factors, to soil organic carbon partition coefficients, and to toxicities to a wide variety of aquatic and mammalian species. Indeed, an entire new field of quantitative structure/activity relationships (QSARs) in pharmacology and toxicology has been founded on Hansch-type correlations with log K_{ow}.

Of particular concern in this context are hydrocarbons (aliphatic, aromatic, and polyaromatic) and their halogenated derivatives. These chemicals are often persistent and toxic and display appreciable partitioning into organic media as a result of their low solubility, or correspondingly their large K_{ow} values. In view of the large number of possible chemical species, and the difficulty of experimental measurements, there is an incentive to develop a methodology for prediction of log K_{ow} values based only on a knowledge of chemical structures. Further, with the growth of computer-based data compilations and estimation procedures necessary to treat the large number of existing and new chemicals, there is a need for reliable correlation procedures for estimation of K_{ow}, solubility, and other properties. Further, and more important, a method that allows estimation of log K_{ow} in terms of fundamental physicochemical properties of the solutes, should also allow direct estimation of the types of toxicological properties usually correlated with log K_{ow} in terms of those same solute properties.

Lyman et al. (*1*) have summarized the methods that are commonly used for the estimation of K_{ow}. The foremost method in use is that of Hansch and Leo (*2*), who have developed a computerized fragment additivity method that is very accurate for many classes of compounds but is known to overestimate seriously K_{ow} for compounds with log K_{ow} greater than about 6 (*1*). Although this method and other fragment additivity methods for estimating solubilities (*3*) have the advantage of requiring only the

0013-936X/88/0922-0503$01.50/0

molecular structure as input, they do not reflect the relative magnitudes of the contribution of various types of solvent–solute interactions to K_{ow}.

A more recent contribution from Kaiser (*4*) provided equations of the form of eq 1 that can be used to estimate log K_{ow} for chlorosubstituted aromatic compounds in a series from the partition coefficient of the unsubstituted parent compound. This method is a substantial improvement over the fragment additivity method of Hansch and Leo for polychlorobiphenyls, polychloropolycyclic aromatic hydrocarbons, and many chlorinated heterocycles. Kaiser acknowledges the difficulty in obtaining good interlaboratory correlations for compounds of these types, which have large values of log K_{ow}, and restricts his correlations to data from a single laboratory for any given series of compounds. He also shows that the exponent b is a function of log K_{ow}^0.

$$\log K_{ow} = (n + 1)^b \log K_{ow}^0 \quad (1)$$

where n = number of chlorine atoms, and log K_{ow}^0 = log K_{ow} of the parent compound.

The main restrictions on Kaiser's method are that it requires a measured or accurately estimated value of log K_{ow} for the parent compound and is limited to families of chlorinated aromatic compounds. For those families to which it is applicable, it gives very good estimates of log K_{ow}.

In this paper we present a set of *parameter estimation rules* that, in combination with an equation recently reported by Leahy (*5*), allow facile and accurate estimation of octanol/water partition coefficients of large numbers of polychlorobenzenes, polychlorinated biphenyls, and polycyclic aromatic hydrocarbons of environmental interest.

In earlier papers of this series and in a number of recent review articles (*6–11*), we have shown that large numbers of properties (XYZ) that depend on solute–solvent interactions, including aqueous solubilities (*12–14*), octanol/water partition coefficients (*15*, *16*), and toxicities to *Photobacterium phosphoreum* (*17*) and the golden orfe fish (*18*), are well correlated in terms of a generalized linear solvation energy relationship (LSER) of simple and conceptually explicit form. This LSER includes terms that measure the endoergic cavity-forming process ($mV/100$), the usually exoergic balance between solute–solvent and solute–solute dipolarity/polarizability interactions [$s(\pi^* + d\delta)$], and exoergic effects of hydrogen-bonding interactions involving the solute as donor and the solvent as acceptor ($a\alpha$), or the solvent as donor and the solute as acceptor ($b\beta$). Accordingly, the general LSER that involves solute properties is given by eq 2.

$$XYZ = XYZ_o + mV_I/100 + s(\pi^* + d\delta) + a\alpha + b\beta \quad (2)$$

The V term in eq 2 is a measure of solute volume and has been either the liquid molar volume, $\bar{V}$, taken as the molecular weight divided by the solute liquid density, or the computer calculated (*5*) intrinsic molar volume, V_I. We now prefer V_I as the measure of the cavity term, as it allows the routine inclusion of solid solutes in the correlations. We use $V_I/100$ so that the parameters in eq 2 should cover roughly the same range, which makes easier the evaluation of the contributions of the various solute–solvent interactions to the XYZ property studied. The π^*, α, and β terms in eq 2 are the *solvatochromic parameters* that measure solute dipolarity/polarizability, hydrogen bond donor (HBD) acidity, and hydrogen-bond acceptor (HBA) basicity. The $d\delta$ term in eq 2 allows for variable dipolarity/polarizability blends in the solute–solvent interactions studied; δ = 0.00 for nonpolychlorinated aliphatic solutes, 0.50 for polychlorinated aliphatics, and 1.00 for aromatic solutes; d = near zero where polarizability contributions to the property studied are maximal and near −0.40 where polarizability contributions are minimal.

Measures of statistical goodness of fit to eq 2 have been better than has usually been the case for other type solubility, partition, and toxicological correlations involving solutes or toxicants of such widely diverse sorts. Thus, for correlation of aqueous solubilities of 105 liquid aliphatic non-HB, HBA, and weak HBD solutes in terms of $\bar{V}$, π^*, and β, we have reported (*13*) n = 105, r = 0.9954, and SD = 0.137. The corresponding correlation, using V_I in place of $\bar{V}$ for 115 solutes gave r = 0.9944 and SD = 0.153 (*14*). For 70 liquid and solid aromatic solutes, including PAHs with up to three fused rings, we obtained (*14*) r = 0.9917 and SD = 0.216. We shall show in a future paper that, through the use of the parameter estimation rules presented here, the latter correlation, which includes a term (mp −25) to convert "supercooled liquid" to solid solubilities (following Yalkowsky) (*19*), can be extended to include PAHs with up to six fused rings without deterioration in r (albeit with a somewhat larger SD).

Our correlation of octanol/water partition coefficients of liquid aliphatic and aromatic non-HB, HBA, and weak HBD solutes in terms of $\bar{V}$, $(\pi^* - 0.40\delta)$, and β was given by eq 3 (*16*). We took d to be −0.40 on the assumption

$$\log K_{ow} = 0.20 + 2.74\bar{V}/100 - 0.92(\pi^* - 0.40\delta) - 3.39\beta \quad (3)$$

$$n = 102,\ r = 0.989,\ \text{SD} = 0.17$$

that polarizability effects canceled out between phases. More recently, for essentially the same data set, and using V_I in lieu of $\bar{V}$, Leahy (*5*) reported eq 4, which shows

$$\log K_{ow} = 0.45 + 5.15V_I/100 - 1.29(\pi^* - 0.40\delta) - 3.60\beta \quad (4)$$

$$n = 103,\ r = 0.9915,\ \text{SD} = 0.16$$

slightly better statistical goodness of fit and, we believe, a somewhat "cleaner" dissection of log K_{ow} into the various solute–solvent interactions involved.

The major disadvantage of using the solvatochromic parameters to estimate any of these solubility-related properties is that the parameters are not universally available or predictable. Although they can be estimated fairly accurately for a large number of important compounds, there are gaps.

In the next section, we present simple methods for estimation of V_I, π^*, and β, which, in combination with eq 4, allow significantly more accurate prediction of octanol/water partition coefficients for PCBs, PAHs, and other compounds of environmental interest than has hitherto been possible.

Results and Discussion

Estimation of V_I. For large numbers of compounds, including many that are frequently encountered in environmental studies, simple group additivity methods allow estimation of V_I values that correspond quite closely to computer-calculated values reported by Leahy (*5*) and Pearlman (*20*) (Pearlman's molecular volumes need to be multiplied by Avogadro's number to obtain V_I). These group additivity methods are summarized as follows:

(a) For replacement of aromatic H by CH_3, or for introduction of CH_2 in side chain, add 9.8 to V_I.

(b) For replacement of aromatic H by Cl, add 9.0 to V_I.

(c) For replacement of aromatic H by Br, add 13.3 to V_I.

Table I. Prediction of Octanol/Water Partition Coefficients of Polychlorobenzenes

no.	compound	$V_I/100$	$\pi^* - 0.4$	β	log K_{ow}[a]	calcd by eq 4	diff
1	C_6H_5Cl	0.581	0.30	0.07	2.98	2.80	−0.18
2	1,2-$C_6H_4Cl_2$	0.671	0.40	0.03	3.38	3.28	−0.10
3	1,3-$C_6H_4Cl_2$	0.671	0.35	0.03	3.48	3.35	−0.13
4	1,4-$C_6H_4Cl_2$	0.671	0.25	0.03	3.38	3.48	+0.10
5	1,2,3-$C_6H_3Cl_3$	0.761	0.45	0	4.04	3.79	−0.25
6	1,2,4-$C_6H_3Cl_3$	0.761	0.35	0	3.98	3.92	−0.06
7	1,3,5-$C_6H_3Cl_3$	0.761	0.30	0	4.02	3.98	−0.04
8	1,2,3,4-$C_6H_2Cl_4$	0.851	0.40	0	4.55	4.32	−0.23
9	1,2,3,5-$C_6H_2Cl_4$	0.851	0.40	0	4.65	4.32	−0.33
10	1,2,4,5-$C_6H_2Cl_4$	0.851	0.30	0	4.51	4.44	−0.07
11	C_6HCl_5	0.941	0.35	0	5.03	4.84	−0.19
12	C_6Cl_6	1.031	0.30	0	5.47	5.37	−0.10

[a] Ref 26.

(d) For replacement of aromatic H by NO_2, add 14.0 to V_I.

(e) For addition of fused aromatic ring, add 6.55 per additional CH, e.g., add 26.2 for benzene to naphthalene, add 39.3 for naphthalene to pyrene.

(f) For addition of ring CH_2 to already rigid system (i.e., naphthalene to acenapthene, but not biphenyl to fluorene), add 8.15 per CH_2, e.g., add 16.3 for naphthalene to acenapthene.

(g) Use V_I value of 92.0 rather than Pearlman's 93.4 or Leahy's 89.5 for biphenyl. Use V_I = 96.0 for fluorene (which involves a smaller CH_2 increment relative to biphenyl than simple additivity would indicate).

Although the frequent user will find Leahy's or Pearlman's computer methods more convenient, these additivity methods are completely adequate for those who need to make only the occasional estimate. Uncertainties in the π^* and β estimates will most frequently lead to larger errors than the uncertainties in these V_I estimates.

Polychlorobenzenes. The following parameter estimation rules agree well with published values of π^* and β (*11*): β = 0.10 for benzene, 0.07 for chlorobenzene, 0.03 for all dichlorobenzenes, and 0.00 for trichloro and higher chlorinated benzenes; π^* = 0.59 for benzene, 0.70 for chlorobenzene, and 0.80 for 1,2-dichlorobenzene. For other polychlorobenzenes, add 0.05 to π^* if addition of chlorine atom leads to higher dipole moment; subtract 0.05 if it leads to a lower dipole moment. Thus, we have the following π^* values:

1,3-dichlorobenzene	0.75
1,4-dichlorobenzene	0.65
1,2,3-trichlorobenzene	0.85
1,2,4-trichlorobenzene	0.75
1,3,5-trichlorobenzene	0.70
1,2,3,4-tetrachlorobenzene	0.80
1,2,3,5-tetrachlorobenzene	0.80
1,2,4,5-tetrachlorobenzene	0.70
pentachlorobenzene	0.75
hexachlorobenzene	0.70

Using these parameter estimation rules and eq 4, we have calculated log K_{ow} values for all the polychlorobenzenes. These are compared in Table I with experimental results reported by Miller et al. (*21*). It is seen that agreement is quite good; the largest difference between experimental and calculated values is 0.33 log unit; the average difference is ± 0.15 log unit. Experimental log K_{ow} values are also compared with values calculated by eq 4 in the plot in Figure 1.

If one fits the data from Table I to an equation of the form of eq 1, one obtains values of 0.5143 for b and 1.984 for log K_{ow}^0. These values give calculated log K_{ow} values for the compounds in Table I that agree better with experimental data than those calculated by eq 4. The

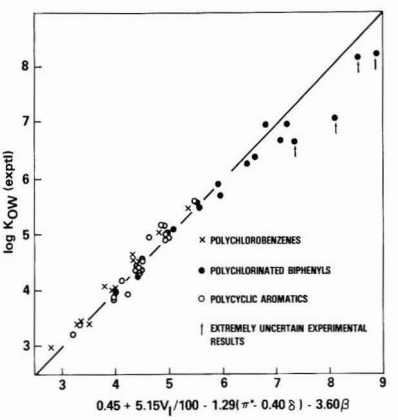

Figure 1. Comparison of experimental and calculated octanol/water partition coefficients.

standard deviation for the fit of Kaiser's equation to these data is 0.08, compared to 0.18 for those calculated by eq 4. The better fit may be due to the fact that the parameters b and log K_{ow}^0 were derived specifically for this class of compounds. However, because this is strictly an empirical relationship between log K_{ow} and the number of chlorine atoms in the molecule, the values are applicable only to the members of the class of chlorinated benzenes.

Polychlorinated Biphenyls (PCBs). We have found that the log K_{ow} values of the PCBs are reasonably closely predicted if the π^* and β values are calculated separately for each ring and the summations of ($\pi^* - 0.40$) and β values are used (i.e., subtract 0.80 from $\sum\pi^*$). A sample calculation for 2,2',4,5-tetrachlorobiphenyl (compound 8 of Table II) is as follows: for the monosubstituted ring, π^* = 0.70 and β = 0.07; for the trisubstituted ring, π^* = 0.75 and β = 0.00. Hence, $\sum\pi^* - 0.80 = 0.65$ and $\sum\beta = 0.07$.

Values of log K_{ow} calculated by eq 4 are compared in Table II and Figure 1 with "selected" experimental results reported by Shiu and Mackay (*22*) for biphenyl and 16 PCBs. It is seen that our calculations agree quite well with the experimental determinations for biphenyl and its mono- through hexachlorinated derivatives (compounds 1–13 of Table II); the average difference for these 13 compounds being ±0.14 log unit (which compares well with the SD of eq 4). For the higher PCBs, compounds 14, 16, and 17 of Table II, however, our calculated values are higher than the experimental values by 0.64–1.02 log units.

We think it significant that the reported experimental log K_{ow} values are essentially the same (6.9 ± 0.2) for the Cl_6, Cl_7, and Cl_8 derivatives and then increase by more than

Table II. Prediction of Octanol/Water Partition Coefficients of Some Polychlorinated Biphenyls[a]

no.	compound	$V_I/100$	$\sum\pi^* - 0.80$	$\sum\beta$	log K_{ow} exptl	log K_{ow} eq 4	diff	fragment additivity[b] calcd	diff
1	biphenyl	0.920	0.38	0.20	3.90	3.98	+0.08	3.99	+0.09
2	2-Cl	1.010	0.49	0.17	4.30	4.46	+0.16	4.70	+0.40
3	2,5-Cl_2	1.100	0.44	0.13	5.10	5.08	−0.02	5.30	+0.20
4	2,6-Cl_2	1.100	0.54	0.1	5.00	4.95	−0.05	5.31	+0.31
5	2,4,5-Cl_3	1.190	0.54	0.10	5.60	5.52	−0.08	6.15	+0.55
6	2,4,6-Cl_3	1.190	0.49	0.10	5.50	5.59	+0.09		
7	2,3,4,5-Cl_4	1.280	0.59	0.10	5.91	5.92	+0.01	6.74	+0.73
8	2,2′,4,5-Cl_4	1.280	0.65	0.07	5.73	5.95	+0.22		
9	2,3,4,5,6-Cl_5	1.370	0.54	0.10	6.30	6.45	+0.15	7.49	+1.19
10	2,2′,4,5,5′-Cl_5	1.370	0.60	0.03	6.40	6.62	+0.22	7.24	+0.84
11	2,2′,3,3′,6,6′-Cl_6	1.460	0.70	0	6.70	7.09	+0.37	6.51	−0.19
12	2,2′,3,3′,4,4′-Cl_6	1.460	0.90	0	7.00	6.81	−0.19	7.97	+0.97
13	2,2′,4,4′,6,6′-Cl_6	1.460	0.60	0	7.00	7.20	+0.20	8.18	+1.18
14	2,2′,3,3′,4,4′,6-Cl_7	1.550	0.85	0	6.70	7.34	+0.64		
15	2,2′,3,3′,5,5′,6,6′-Cl_8	1.640	0.60	0	7.10	8.12	+1.02	9.73	+1.63
16	2,2′,3,3′,4,5,5′,6,6′-Cl_9	1.730	0.65	0	8.16	8.52	+0.36	10.44	+2.26
17	Cl_{10}	1.820	0.70	0	8.26	8.92	+0.66	11.20	+2.94
	av, compounds 1–13						±0.14		±0.60
	av, all compounds						±0.27		±0.96

[a] Data are from ref 21 and 22 and are usually the selected values of Shiu and Mackay (*22*). Data are included only for compounds that appear in both references. [b] These are average calculated values from ref 22. The calculations are usually by the fragment additivity method of Recker (*24*) or Hansch and Leo (*2*).

1 log unit between Cl_8 and Cl_9. We believe that nature provides no reason for such discontinuities in simple partition properties and that they must therefore reflect experimental inaccuracies. We further believe that we have reached the "level of exhaustive fit", where the reliability of log K_{ow} predictions for the higher PCBs exceeds that of the measurements. [According to a definition by Wold and Sjostrom (*23*), the "level of exhaustive fit" is reached when the standard deviation of the calculation is better than the usual reproducibility of the experimental measurements between data sources.]

We have also included in Table II values of log K_{ow} calculated by the fragment additivity methods of Rekker (*24*) and Hansch and Leo (*2*). It is seen that there is a systematic trend wherein the latter values grow increasingly higher compared with our calculations and the experimental results as the sizes of the PCBs increase. It may also be noted that our standard deviations are about one-quarter as large as those for the fragment additivity calculations.

Application of eq 1 to the data for the polychlorinated biphenyls in Table II yields values of 0.3246 for b and 3.587 for log K_{ow}^0. For the first 13 compounds in Table II, eq 1 and 4 are equally good at estimating log K_{ow}. However Kaiser's method fits the data for the higher members of the series better than eq 4, which systematically overestimates log K_{ow} for the Cl_7 through Cl_{10} chlorinated biphenyls, although not as severely as the fragment additivity method (*24*). This may be due to a breakdown in the estimation of V_I for larger species. The fact that the exponent b is less than 1 for the polychlorinated benzenes and polychlorinated biphenyls indicates that the increment in log K_{ow} decreases with increasing number of chlorine atoms. A strictly additive method, such as that of McGowan and Abraham (*25*) used here, cannot take this into account. Although the correlation between the characteristic volume calculated by the method of McGowan (see Appendix) and computed intrinsic volumes has been shown to apply to compounds with large characteristic volumes (*25*), all of the compounds that are given as examples of the good correlation contain large numbers of hydrogen atoms (e.g., 1-octanol, pentamethylbenzene) and none contain chlorine. Of the 40 compounds used in deriving the relationship between characteristic volumes and intrinsic volumes, none had more than four chlorine atoms. Since the coefficient of V_I in eq 4 is the largest of all those in the equation, it is likely that an overestimation of V_I is responsible for the deviations at large log K_{ow} for polychlorinated compounds.

Polycyclic Aromatic Hydrocarbons (PAHs). Parameter estimation methods, which again are in accord with previously published solvatochromic parameters (*11*) and informed chemical intuition, are as follows. The estimation methods for β have already been used in the prediction of aqueous solubilities of PAHs with up to three fused rings (*14*) and will be shown in a future paper to be effective in predicting aqueous solubilities of PAHs with up to six fused rings.

(a) For naphthalene, $\pi^* = 0.70$ and $\beta = 0.15$. For each additional fused aromatic ring, add 0.10 to π^* and 0.05 to β, e.g., for naphthalene to dibenzanthracene, $\Delta\pi^* = 0.30$ and $\Delta\beta = 0.15$.

(b) For chloro PAH derivatives, use same increments and decrements as for the corresponding benzene derivatives.

(c) For alkyl PAH derivatives, also use same increments and decrements as for corresponding benzenes.

(d) For HBA substituents on PAH, start with correspondingly substituted benzene; add nothing to π^* or β for first fused ring; add 0.10 to π^* and 0.05 to β for additional fused rings. Thus, for nitrobenzene and nitronaphthalene, $\pi^* = 1.01$ and $\beta = 0.30$; for 1-nitroanthracene, $\pi^* = 1.11$ and $\beta = 0.35$.

In Table III and Figure 1 we have compared log K_{ow} values calculated from the above parameter estimation rules and eq 4 with experimental and calculated values reported by Miller and co-workers (*21*). Agreement with the 17 experimental values determined by the latter workers and four additional results from other sources is seen to be quite good; the average difference between the experimental and calculated results is ±0.12 log unit, and the greatest difference is 0.33 log unit. those knowledgeable about measurements of octanol/water partition coefficients above 4.0 would probably agree that such agreement is remarkable and probably fortuitous. They would also most likely agree that we are at the "level of

Table III. Prediction of Octanol/Water Partition Coefficients of Polycyclic Aromatic Hydrocarbons

no.	compound	$V_I/100$	$\pi^* - 0.4$	β	log K_{ow}[a]	calcd by eq 4	diff
1	naphthalene	0.753	0.30	0.15	3.35	3.40	+0.05
2	1-methylnaphthalene	0.851	0.26	0.16	3.87	3.92	+0.05
3	2-methylnaphthalene	0.851	0.26	0.16	3.86	3.92	+0.06
4	1,3-dimethylnaphthalene	0.949	0.22	0.17	4.42	4.44	+0.02
5	1,4-dimethylnaphthalene	0.949	0.22	0.17	4.37	4.44	+0.07
6	1,5-dimethylnaphthalene	0.949	0.22	0.17	4.38	4.44	+0.06
7	2,3-dimethylnaphthalene	0.949	0.22	0.17	4.40	4.44	+0.04
8	2,6-dimethylnaphthalene	0.949	0.22	0.17	4.31	4.44	+0.13
9	1-ethylnaphthalene	0.949	0.24	0.17	4.39	4.42	+0.03
10	1,4,5-trimethylnaphthalene	1.047	0.20	0.18	4.90	4.94	+0.04
11	fluorene	0.960	0.38[b]	0.22	4.18	4.11	−0.07
12	acenaphthene	0.916	0.26	0.17	3.92	4.22	+0.30
13	phenanthrene	1.015	0.40	0.20	4.57	4.44	−0.13
14	anthracene	1.015	0.40	0.20	4.54	4.44	−0.10
15	1-methylfluorene	1.058	0.34	0.23	4.97	4.63	−0.34
16	pyrene	1.156	0.50	0.25	5.18	4.85	−0.33
17	3,4-benzopyrene	1.418	0.60	0.30	5.98	5.89	−0.09
18	2-chlorophenanthrene	1.105	0.51	0.16	5.16[c]	4.91	−0.25
19	benz[*a*]anthracene	1.277	0.50	0.25	5.61[c]	5.48	−0.13
20	2-methylphenanthrene	1.113	0.36	0.21	4.86[c]	4.96	−0.10
21	1-nitronaphthalene	0.893	0.61	0.30	3.19[d]	3.18	−0.01
22	9-methylanthracene	1.113	0.36	0.21	(5.07)[e]	4.96	(−0.11)
23	9,10-dimethylanthracene	1.211	0.32	0.22	(5.25)[e]	5.48	(+0.23)
24	1,2,5,6-dibenzanthracene	1.539	0.60	0.30	(7.19)[e]	6.52	(−0.67)
25	2,3-benzanthracene	1.277	0.50	0.25	(5.90)[e]	5.48	(−0.42)
26	benzo[*ghi*]perylene	1.547	0.70	0.35	(7.19)[e]	6.25	(−0.84)

[a] From ref 21 unless otherwise indicated. [b] $\sum\pi^* - 0.8$ and $\sum\beta$. [c] Ref 31. [d] Ref 2. [e] These are calculated values reported by Miller and co-workers (*21*).

exhaustive fit" with the log K_{ow} calculations for the higher PAHs.

The results for compounds 22–26 of Table III provide a comparison of our linear solvation energy relationship with calculations by fragment additivity. As with the PCBs, the latter predict increasingly higher log K_{ow} value than our calculations as the sizes of the PAHs increase.

Correlations of HPLC Data. In addition to predictions of octanol/water partition coefficients and aqueous solubilities, these new parameters estimation methods allow correlations by eq 2 of large numbers of other type solubility properties, as well as toxicological QSARs. As an example, Sarna et al. (*26*) have reported HPLC retention times for a data set that included many polychlorinated benzenes and biphenyls. The mobile phase was 85/15 methanol/water at a flow rate of 1.0 mL/min; stationary phases included μBondapak C_{18} (Waters Scientific) and LiChrosorb RP-18 (BDH/Merck). The data are assembled in Table IV; the correlations are given by eq 5 and 6. The signs and relative magnitudes of the

μBondapak C_{18}

$$\log t_R' = -(0.165 \pm 0.054) + (1.166 \pm 0.066)V_I/100 - (0.326 \pm 0.065)\pi^* - (0.869 \pm 0.189)\beta \quad (5)$$

$$n = 23,\ r = 0.986,\ \mathrm{SD} = 0.070$$

LiChrosorb RP-18

$$\log t_R' = -(0.141 \pm 0.064) + (1.522 \pm 0.076)V_I/100 - (0.471 \pm 0.075)\pi^* - (0.705 \pm 0.224)\beta \quad (6)$$

$$n = 23,\ r = 0.987,\ \mathrm{SD} = 0.083$$

coefficients of the independent variables are similar to those we have reported in other correlations of HPLC data with the solvatochromic parameters.

Another example involves an HPLC data set reported by Jinno and Kawasaki (*27, 28*) that contained a large number of PAHs. The column material was Jasco FineSIL C-18 (10 μm), and the mobile phases were 65/35 acetonitrile/water and 75/25 methanol/water. The correlations are given by eq 7 and 8. Experimental log capacity factors are compared with calculated values in Table V.

65/35 CH_3CN/H_2O

$$\log k' = -(0.49 \pm 0.03) + (1.207 \pm 0.026)V_I/100 - (0.110 \pm 0.038)\pi^* - (0.764 \pm 0.085)\beta \quad (7)$$

$$n = 32,\ r = 0.9943,\ \mathrm{SD} = 0.038$$

75/25 $MeOH/H_2O$

$$\log k' = -(0.76 \pm 0.03) + (1.596 \pm 0.034)V_I/100 - (0.135 \pm 0.051)\pi^* - (0.783 \pm 0.034)\beta \quad (8)$$

$$n = 32,\ r = 0.9943,\ \mathrm{SD} = 0.049$$

There are dozens of HPLC data sets in the literature that can similarly be correlated by the use of eq 2, earlier published solvatochromic parameters (*11*), and the parameter estimation rules presented here. The precision of the correlations is usually like that for eq 7 and 8, and the coefficients of the independent variables always have the same signs and relative magnitudes as in eq 5–8.

Appendix

Estimation of V_I by McGowan's Method. Another simple method of estimating V_I is via the characteristic volumes, V_x, of McGowan (*29, 30*). These are calculated through an atomic additive scheme as follows, in $cm^3\ mol^{-1}$: C = 16.35, H = 8.71, O = 12.43, N = 14.39, Cl = 20.95, and Br = 26.21; subtract 6.56 for each bond, no matter whether single, double, or triple. Then V_I is obtained through a correlation established by Abraham and McGowan (*25*):

$$V_I = 0.597 + 0.6823V_x \quad (9)$$

$$n = 209,\ r = 0.9988,\ \mathrm{SD} = 1.2\ cm^3\ mol^{-1}$$

As examples chosen at random, we find the following: for hexachlorobenzene, V_x = 145.1, V_I (calcd) = 99.6, and V_I (Table I) = 103.1; for biphenyl, V_x = 132.4, V_I (calcd) = 91.0 and V_I (Table II) = 92.0; for decachlorobiphenyl,

Table IV. Correlation of HPLC Retention Times, Solvent 85/15 Methanol/Water[a]

no.	compound	$V_I/100$	π^*	β	log t_R' Waters	log t_R' eq 5	log t_R' BDH	log t_R' eq 6[b]
1	benzene	0.491	0.59	0.10	0.18	0.13	0.28	0.26
2	toluene	0.591	0.55	0.11	0.25	0.25	0.39	0.42
3	bromobenzene	0.624	0.79	0.06	0.27	0.25	0.41	0.39
4	ethylbenzene	0.671	0.53	0.12	0.32	0.34	0.47	0.55
5	1,2,3-$C_6H_3(CH_3)_3$	0.769	0.47	0.13	0.40	0.47	0.61	0.72*
6	biphenyl	0.920	1.18	0.20	0.38	0.35	0.59	0.56
7	2-Cl	1.010	1.29	0.17	0.42	0.44	0.61	0.62
8	2,4-Cl_2	1.100	1.34	0.13	0.58	0.57	0.82	0.81
9	2,4,5-Cl_3	1.190	1.34	0.10	0.74	0.70	1.03	0.97
10	2,3,4,5-Cl_4	1.280	1.39	0.10	0.89	0.79*	1.21	1.08*
11	2,2′4,5,5′-Cl_5	1.370	1.40	0.03	0.84	0.95*	1.13	1.26*
12	2,2′,4,4′,5,5′-Cl_6	1.460	1.50	0.00	1.00	1.05	1.32	1.38
13	2,2′,3,3′,4,5-Cl_6	1.460	1.60	0.00	0.96	1.02	1.33	1.33
14	2,2′,3,4,5,5′,6-Cl_7	1.550	1.45	0.00	1.05	1.17*	1.38	1.54*
15	2,2′,3,3′,4,4′,5,5′-Cl_8	1.640	1.60	0.00	1.29	1.23	1.66	1.60
16	2,2′,3,3′,4,4′,5,5′,6-Cl_9	1.730	1.45	0.00	1.39	1.38	1.76	1.81
17	Cl_{10}	1.820	1.50	0.00	1.57	1.47*	1.99	1.92
18	1-chloronaphthalene	0.843	0.80	0.11	0.42	0.46	0.65	0.69
19	20-methylcholanthrene	1.538	0.80	0.31	1.08	1.10	1.63	1.61
20	1,2,4,5-tetrabromobenzene	1.023	0.80	0.00	0.68	0.77*	1.00	1.04
21	1,2,3,4-tetrachlorobenzene	0.851	0.80	0.00	0.56	0.57	0.81	0.78
22	pentachlorobenzene	0.941	0.75	0.00	0.74	0.69	1.06	0.94*
23	hexachlorobenzene	1.031	0.70	0.00	0.93	0.82	1.24	1.11*

[a] Ref 26. [b] * indicates difference by more than one standard deviation.

Table V. Correlation of HPLC log k' Values on C_{18} Column[a]

no.	solute	$V_I/100$	π^*	β	log k' 65/35 CH_3CN/H_2O exptl	log k' 65/35 CH_3CN/H_2O eq 7[b]	log k' 75/25 $MeOH/H_2O$ exptl	log k' 75/25 $MeOH/H_2O$ eq 8[b]
1	benzene	0.491	0.59	0.10	−0.01	−0.04	−0.09	−0.13
2	toluene	0.591	0.55	0.11	0.09	0.07	0.04	0.03
3	ethylbenzene	0.671	0.53	0.12	0.18	0.17	0.15	0.15
4	*o*-xylene	0.671	0.51	0.12	0.21	0.17*	0.17	0.15
5	*m*-xylene	0.671	0.51	0.12	0.20	0.17	0.19	0.15
6	*n*-propylbenzene	0.768	0.51	0.12	0.30	0.28	0.29	0.30
7	isopropylbenzene	0.768	0.51	0.12	0.27	0.28	0.26	0.30
8	1,2,4-trimethylbenzene	0.768	0.47	0.13	0.30	0.28	0.35	0.30*
9	*n*-butylbenzene	0.861	0.49	0.12	0.43	0.41	0.44	0.47
10	1,2,4,5-$C_6H_2(CH_3)_4$	0.867	0.43	0.14	0.41	0.40	0.48	0.46
11	pentamethylbenzene	0.965	0.39	0.15	0.49	0.51	0.62	0.61
12	hexamethylbenzene	1.063	0.35	0.16	0.58	0.63*	0.75	0.77
13	benzaldehyde	0.606	0.92	0.44	−0.17	−0.20	−0.22	−0.25
14	benzonitrile	0.590	0.90	0.37	−0.13	−0.16	−0.23	−0.22
15	nitrobenzene	0.631	1.01	0.30	−0.08	−0.08	−0.11	−0.13
16	acetophenone	0.690	0.90	0.49	−0.14	−0.13	−0.17	−0.15
17	methyl benzoate	0.736	0.76	0.39	−0.04	0.01*	−0.06	0.02*
18	anisole	0.630	0.73	0.32[c]	−0.05	−0.06	−0.05	−0.10
19	*o*-nitrotoluene	0.729	0.97	0.31	0.00	0.04*	−0.04	0.03*
20	naphthalene	0.753	0.70	0.15	0.19	0.22	0.19	0.23
21	anthracene	1.015	0.80	0.20	0.47	0.49	0.57	0.59
22	phenanthrene	1.015	0.80	0.20	0.44	0.49*	0.53	0.59*
23	pyrene	1.156	0.90	0.25	0.61	0.61	0.75	0.76
24	naphthacene	1.277	0.90	0.25	0.82	0.75*	1.06	0.95**
25	chrysene	1.277	0.90	0.25	0.74	0.75	0.94	0.95
26	triphenylene	1.277	0.90	0.25	0.70	0.75*	0.88	0.95*
27	benz[*a*]anthracene	1.277	0.90	0.25	0.74	0.75	0.96	0.95
28	perylene	1.415	1.00	0.30	0.92	0.87*	1.07	1.12*
29	benzo[*a*]pyrene	1.418	1.00	0.30	0.96	0.87**	1.23	1.12**
30	acenaphthene	0.916	0.66	0.17	0.35	0.42*	0.44	0.49*
31	benzo[*b*]fluorene	1.224	1.28	0.27	0.66	0.64	0.88	0.81*
32	dibenz[*a*,*c*]anthracene	1.539	1.00	0.30	1.02	1.02	1.35	1.32
33	biphenyl	0.920	1.18	0.20	0.29	0.33	0.33	0.39
34	fluorene	0.960	1.18	0.22	0.36	0.36	0.46	0.43

[a] Data of Jinno and Kawasaki (*27*, *28*). [b] * indicates a difference of more than one standard deviation, ** more than two standard deviations. [c] Summation of hydrogen-bonding effects on oxygen and on ring.

V_x = 254.8, V_I (calcd) = 174.5, and V_I (Table II) = 182.0; for triphenylene, V_x = 182.3, V_I (calcd) = 125.0, and V_I (Table V) = 127.7. Use of V_I (calcd) in eq 4–8 instead of V_I (ref 5) would not lead to significant differences for most compounds. However, for compounds such as the decachlorobiphenyl, the difference in the values of V_I calculated by Leahy's method and Abraham and McGowan's method leads to an overestimation of log K_{ow} of 5.15*(182.0 –

174.5)/100 = 0.39 log unit, which is more than half the deviation shown in Table II.

Registry No. C_6H_5Cl, 108-90-7; 1,2-$C_6H_4Cl_2$, 95-50-1; 1,3-$C_6H_4Cl_2$, 541-73-1; 1,4-$C_6H_4Cl_2$, 106-46-7; 1,2,3-$C_6H_3Cl_3$, 87-61-6; 1,2,4-$C_6H_3Cl_3$, 120-82-1; 1,3,5-$C_6H_3Cl_3$, 108-70-3; 1,2,3,4-$C_6H_2Cl_4$, 634-66-2; 1,2,3,5-$C_6H_2Cl_4$, 634-90-2; 1,2,4,5-$C_6H_2Cl_4$, 95-94-3; C_6HCl_5, 608-93-5; C_6Cl_6, 118-74-1; $HO(CH_2)_7CH_3$, 111-87-5; H_2O, 7732-18-5; $C_6H_5C_6H_5$, 92-52-4; 2-$ClC_6H_4C_6H_5$, 2051-60-7; 2,5-$Cl_2C_6H_3C_6H_5$, 34883-39-1; 2,6-$Cl_2C_6H_3C_6H_5$, 33146-45-1; 2,4,5-$Cl_3C_6H_2C_6H_5$, 15862-07-4; 2,4,6-$Cl_3C_6H_2C_6H_5$, 35693-92-6; 2,3,4,5-$Cl_4C_6HC_6H_5$, 33284-53-6; 2,2′,4,5-$Cl_3C_6H_2C_6H_4Cl$, 70362-47-9; 2,3,4,5,6-$Cl_5C_6C_6H_5$, 18259-05-7; 2,2′,4,5,5′-$Cl_3C_6H_2C_6H_3Cl_2$, 37680-73-2; 2,2′,3,3′,6,6′-$Cl_3C_6H_2C_6H_2Cl_3$, 38411-22-2; 2,2′,3,3′,4,4′-$Cl_3C_6H_2C_6H_2Cl_3$, 38380-07-3; 2,2′,4,4′,6,6′-$Cl_3C_6H_2C_6H_2Cl_3$, 33979-03-2; 2,2′,3,3′,4,4′,6-$Cl_4C_6HC_6H_2Cl_3$, 52663-71-5; 2,2′,3,3′,5,5′,6,6′-$Cl_4C_6HC_6HCl_4$, 2136-99-4; 2,2′,3,3′,4,5,5′,6,6′-$Cl_5C_6C_6C_6HCl_4$, 52663-77-1; $C_6Cl_5C_6Cl_5$, 2051-24-3; C_6H_6, 71-43-2; $C_6H_5CH_3$, 108-88-3; C_6H_5Br, 108-86-1; $C_6H_5CH_2CH_3$, 100-41-4; 1,2,3-$C_6H_3(CH_3)_3$, 526-73-8; 2,4-$Cl_2C_6H_3C_6H_5$, 33284-50-3; 2,2′,4,4′,5,5′-$Cl_3C_6H_2C_6H_2Cl_3$, 35065-27-1; 2,2′,3,3′,4,5-$Cl_4C_6HC_6H_3Cl_2$, 55215-18-4; 2,2′,3,4,5,5′,6-$Cl_5C_6C_6H_3Cl_2$, 52712-05-7; 2,2′,3,3′,4,4′,5,5′-$Cl_4C_6HC_6HCl_4$, 35694-08-7; 2,2′,3,3′,4,4′,5,5′,6-$C_6Cl_5C_6HCl_4$, 40186-72-9; naphthalene, 91-20-3; 1-methylnaphthalene, 90-12-0; 2-methylnaphthalene, 91-57-6; 1,3-dimethylnaphthalene, 575-41-7; 1,4-dimethylnaphthalene, 571-58-4; 1,5-dimethylnaphthalene, 571-61-9; 2,3-dimethylnaphthalene, 581-40-8; 2,6-dimethylnaphthalene, 581-42-0; 1-ethylnaphthalene, 1127-76-0; 1,4,5-trimethylnaphthalene, 2131-41-1; fluorene, 86-73-7; acenaphthene, 83-32-9; phenanthrene, 85-01-8; anthracene, 120-12-7; 1-methylfluorene, 1730-37-6; pyrene, 129-00-0; 3,4-benzopyrene, 50-32-8; 2-chlorophenanthrene, 24423-11-8; benz[*a*]anthracene, 56-55-3; 2-methylphenanthrene, 2531-84-2; 1-nitronaphthalene, 86-57-7; 9-methylanthracene, 779-02-2; 9,10-dimethylanthracene, 781-43-1; 1,2,5,6-dibenzanthracene, 53-70-3; 2,3-benzanthracene, 92-24-0; benzo[*ghi*]perylene, 191-24-2; 1-chloronaphthalene, 90-13-1; 20-methylcholanthrene, 56-49-5; 1,2,4,5-tetrabromobenzene, 636-28-2; *o*-xylene, 95-47-6; *m*-xylene, 108-38-3; *n*-propylbenzene, 103-65-1; isopropylbenzene, 98-82-8; 1,2,4-trimethylbenzene, 95-63-6; *n*-butylbenzene, 104-51-8; 1,2,4,5-tetramethylbenzene, 95-93-2; pentamethylbenzene, 700-12-9; hexamethylbenzene, 87-85-4; benzaldehyde, 100-52-7; benzonitrile, 100-47-0; nitrobenzene, 98-95-3; acetophenone, 98-86-1; methyl benzoate, 93-58-3; anisole, 100-66-3; *o*-nitrotoluene, 88-72-2; naphthacene, 92-24-0; chrysene, 218-01-9; triphenylene, 217-59-4; perylene, 198-55-0; benzo[*a*]pyrene, 50-32-8; benzo[*b*]fluorene, 30777-19-6; dibenz[*a*,*c*]anthracene, 215-58-7.

Literature Cited

(1) Lyman, W. J.; Reehl, W. F.; Rosenblatt, D. H. *Handbook of Chemical Property Estimation Methods*; McGraw-Hill: New York, 1982.

(2) Hansch, C.; Leo, A. *Substituent Constants for Correlations Analysis in Chemistry and Biology*; Wiley-Interscience: New York, 1979.

(3) Tsonopoulos, C.; Prausnitz, J. M. *Ind. Eng. Chem. Fundam.* **1971**, *10*, 593.

(4) Kaiser, K. L. E. *Chemosphere* **1983**, *12*, 1159.

(5) Leahy, D. *J. Pharm. Sci.* **1986**, *75*, 629.

(6) Kamlet, M. J.; Doherty, R. M.; Abboud, J.-L. M.; Abraham, M. H.; Taft, R. W. *CHEMTECH* **1986**, *16*, 566.

(7) Taft, R. W.; Abboud, J.-L. M.; Kamlet, M. J.; Abraham, M. H. *J. Solution Chem.* **1985**, *14*, 153.

(8) Kamlet, M. J.; Taft, R. W. *Acta Chem. Scand., Ser. B* **1985**, *B39*, 611.

(9) Kamlet, M. J.; Abboud, J.-L. M.; Taft, R. W. *Prog. Phys. Org. Chem.* **1981**, *13*, 485.

(10) Abraham, M. H.; Doherty, R. M.; Kamlet, M. J.; Taft, R. W. *Chem. Br.* **1986**, *22*, 551.

(11) Kamlet, M. J.; Abboud, J.-L. M.; Abraham, M. H.; Taft, R. W. *J. Org. Chem.* **1983**, *48*, 2877.

(12) Taft, R. W.; Abraham, M. H.; Doherty, R. M.; Kamlet, M. J. *Nature (London)* **1985**, *313*, 384.

(13) Kamlet, M. J.; Doherty, R. M.; Abboud, J.-L. M.; Abraham, M. H.; Taft, R. W. *J. Pharm. Sci.* **1986**, *75*, 336.

(14) Kamlet, M. J.; Doherty, R. M.; Abraham, M. H.; Carr, P. W.; Doherty, R. F.; Taft, R. W. *J. Phys. Chem.* **1987**, *91*, 1996.

(15) Kamlet, M. J.; Abraham, M. H.; Doherty, R. M.; Taft, R. W. *J. Am. Chem. Soc.* **1984**, *106*, 464.

(16) Taft, R. W.; Abraham, M. H.; Famini, G. R.; Doherty, R. M.; Kamlet, M. J. *J. Pharm. Sci.* **1985**, *74*, 807.

(17) Kamlet, M. J.; Doherty, R. M.; Veith, G. D.; Taft, R. W.; Abraham, M. H. *Environ. Sci. Technol.* **1986**, *20*, 690.

(18) Kamlet, M. J.; Doherty, R. M.; Abraham, M. H.; Veith, G. D.; Abraham, D. J.; Taft, R. W. *Environ. Sci. Technol.* **1987**, *21*, 149.

(19) Yalkowsky, S. H.; Valvani, S. C. *J. Pharm. Sci.* **1980**, *69*, 602.

(20) Pearlman, R. S. In *Partition Coefficient Determination and Estimation*: Dunn, W. J., Block, J. H., Pearlman, R. S., Eds.; Pergamon: New York, 1986; p 3.

(21) Miller, M. M.; Wasik, S. P.; Huang, G.-L.; Shiu, W.-Y.; Mackay, D. *Environ. Sci. Technol.* **1985**, *19*, 522.

(22) Shiu, W.-Y.; Mackay, D. *J. Phys. Chem. Ref. Data* **1986**, *15*, 911.

(23) Wold, S.; Sjostrom, M. *Acta Chem. Scand., Ser. B* **1986**, *B40*, 270.

(24) Rekker, R. F. *The Hydrophobic Fragment Constant*; Elsevier: New York, 1977.

(25) Abraham, M. H.; McGowan, J. C. *Chromatographia* **1987**, *23*, 243.

(26) Sarna, L. P.; Hodge, P. E.; Webster, G. R. B. *Chemosphere* **1984**, *13*, 975.

(27) Jinno, K.; Kawasaki, K. *Chromatographia* **1984**, *18*, 211.

(28) Jinno, K.; Kawasaki, K. *J. Chromatogr.* **1984**, *316*, 1.

(29) McGowan, J. C. *J. Appl. Chem. Biotechnol.* **1978**, *28*, 599.

(30) McGowan, J. C. *J. Chem. Technol. Biotechnol.* **1984**, *34A*, 38.

(31) Mackay, D. *Environ. Sci. Technol.* **1982**, *16*, 274.

Received for review February 5, 1987. Accepted November 20, 1987.

Environ. Sci. Technol. 1988, 22, 510–516

Chernobyl Radionuclides in the Environment: Tracers for the Tight Coupling of Atmospheric, Terrestrial, and Aquatic Geochemical Processes

Peter H. Santschi,* Silvia Bollhalder, Klaus Farrenkothen, Alfred Lueck, Stefan Zingg, and Michael Sturm

EAWAG, Swiss Federal Institute of Water Resources and Water Pollution Control, CH-8600 Duebendorf, Switzerland

■ Observations of the temporal trend in concentrations of Chernobyl radionuclides in atmospheric, terrestrial, and aquatic reservoirs near Dübendorf (Zurich) aided in quantifying fluxes and transfer velocities from one reservoir to another. Radionuclide dry and wet deposition rates and velocities from the atmosphere, washout from the catchment basins into surface waters, and deposition rates and mechanisms in lakes were determined. The results from these studies were compared to those from earlier observations on the fate of the radionuclides released by bomb tests, from reactor accidents, and from the purposeful tracer experiments in lakes. The results from our observations indicate the extent to which the Chernobyl radionuclides trace the movement of other atmospheric trace contaminants in the environment.

Introduction

Radioactive fallout from the burning Chernobyl reactor was measured during May and June 1986 all over the northern hemisphere, even though, at times, activities were at extremely low levels. The attention given in each country to the radioactivity measurements as a basis for estimating dose rates to man, and the relative ease of measurement of radionuclides, allowed scientists to follow the pathways of the radioactive cloud around the world. The accidental release of radioactivity provided a striking demonstration of the fact that trace contaminants, radioactive and nonradioactive, can be transported within days from one country to another via the atmospheric and aquatic conveyor belts. The radioactive fallout from the reactor accident in Chernobyl provided a pulsed release to the environment; this pulse presented a good opportunity to study transport processes in atmospheric, terrestrial, and aquatic reservoirs, as pulse inputs of radionuclides to the environment can be used to study physical (e.g., ^{3}H) (*1*), chemical (e.g., ^{54}Mn) (*2*), biological (e.g., ^{14}C) (*3*), and hydrological (e.g., ^{3}H) (*4*, *5*) processes operating in a particular system. Understandably, most of the attention was given to the dose rate aspect of the accident, i.e., the transfer of Chernobyl radionuclides to man, and relatively little to the geochemical behavior of the nuclides.

The purpose of this article is threefold: (1) to demonstrate, by use of selected radionuclides from the Chernobyl fallout as tracers, the tight coupling by the movement of water of the atmospheric, terrestrial, and aquatic reservoirs in the Zürich area; (2) to show which processes influence the rates of migration of radionuclides in the environment and transfer to man (Figure 1); (3) to indicate the extent to which the information on the Chernobyl radionuclide pulse agrees with what had been learned from previous studies of bomb fallout nuclides, from releases from previous reactor accidents, and from purposeful tracer experiments in lakes. While some of the radioactivity measurements reported here were also made by a number of other groups, the radionuclide mobility studies in atmospheric and aquatic systems reported here are unique.

*Address correspondence to this author at the Department of Marine Sciences, Texas A&M University at Galveston, P.O. Box 1675, Galveston, TX 77553-1675.

Methods

The γ-ray-emitting Chernobyl radionuclides were determined on solid-state detectors [Ge-(Li) and high-purity Ge] in samples from surface waters [Rhine River, Glatt River, Chriesbach (creek), Lake Zürich; several times a week during early May], drinking waters and groundwaters (near Dübendorf, a few times in May), sewage treatment plants (Zürich, Fällanden), air filters (Dübendorf, daily), total precipitation (Dübendorf, of every single rain event as well as the integral over the fallout period from April 29 to May 22), dry fallout (Dübendorf, 3 times during period April 30 to May 12), water and sedimenting particles from Lake Zürich caught in sediment traps (located at 50- and 130-m depth at the deepest point of the lake, sampled at 21-day intervals), fish (various lakes), grass (Dübendorf), milk (Dübendorf, Volketswil), and vegetables (northern Switzerland). The locations of the sampling stations are given in Figure 2. Results from measurements of milk and grass will not be reported here but can be found elsewhere (*6*). Detector geometries were calibrated with standards of the appropriate radionuclide (NEN, Amersham Co.) in order to circumvent summation corrections. For the calculations of fluxes, all concentrations were decay-corrected to May 1, 1986, and corrected for decay during the time of collection. Furthermore, in selected samples of each kind, β-ray-emitting ^{90}Sr and ^{89}Sr activities were determined according to ref 7.

The deposition rate was measured in special collectors for total precipitation and for dry deposition, either on consecutive days or as the total over the fallout period. Dry fallout was collected in pans filled with a thin layer of distilled water, open to the atmosphere only during times of no precipitation (*8*). Because surface water concentrations of ^{137}Cs soon became unmeasurably small with direct-counting techniques on 1-L samples, ^{137}Cs had to be preconcentrated from 1 to 30 L by ion exchange before measurement (*9*).

Chemical Form of the Nuclides in the Environment

The composition of radionuclides found in the radioactive Chernobyl cloud in Switzerland was determined by the following factors (Figure 1): (a) the asymmetrical fission yield of ^{235}U, which favors nuclides with neutron numbers near the "magic" numbers 50 and 82; (b) the relative volatility of the elements or their oxides at 1500 °C, the burning temperature of the reactor graphite (*10*); (c) fractionation and deposition processes in air.

On the basis of thermodynamic reasoning, the following chemical forms or oxidation states of selected Chernobyl radionuclides are likely: Cs^{+}, Ba^{2+}, La(III), Ce(IV), Nb(V), MoO_4^{2-}, TcO_4^{-}, and $HTeO_4^{-}$. For ^{131}I and ^{103}Ru, for which it is also possible to postulate metastable forms, the following species or oxidation states are possible: Ru(VI) as RuO_4^{2-} (*11*, *12*), Ru(III) as $RuNO^{3+}$ (*11*, *12*), and iodine as I_2, CH_3I, I^{-}, and IO_3^{-} (e.g., ref 13). The speciation of the radionuclides was partially established in the burning reactor by chemical and physical conditions which allowed

0013-936X/88/0922-0510$01.50/0

Table I. Deposition Rates and Deposition Velocities of Chernobyl Radionuclides in the Dübendorf Area

nuclide	half-life, days	deposition rate, r_D, kBq/m² (29.4.86 to 22.5.86)	deposition velocities, V_D, cm/s: total deposition, 30.4.86 (12 h)	total deposition, 30.4.86 to 8.5.86 (9 days)	dry deposition, days with fog and dew (30.4.86 to 2.5.86)	dry deposition, days without fog and dew (2.5.86 to 12.5.86)
^{134}Cs	7×10^2	2	3.4	0.5	0.13	0.024
^{137}Cs	1.1×10^4	4	3.4	0.5	0.13	0.024
^{103}Ru	40	4	2.8	0.4	0.10	0.024
^{131}I	8	20	3.0	0.4	0.21	0.080
^{132}Te (^{132}I)	3	18				
^{99}Mo (^{99m}Tc)	3	5.6				
^{90}Sr	10^4	0.03	~6.0[a]	0.7[a]		
^{89}Sr	50	0.63	~6.5[a]	0.7[a]		

[a] These values were calculated from $^{90}Sr/^{137}Cs$ activity ratios in selected air filter and precipitation samples. For further explanations, see text.

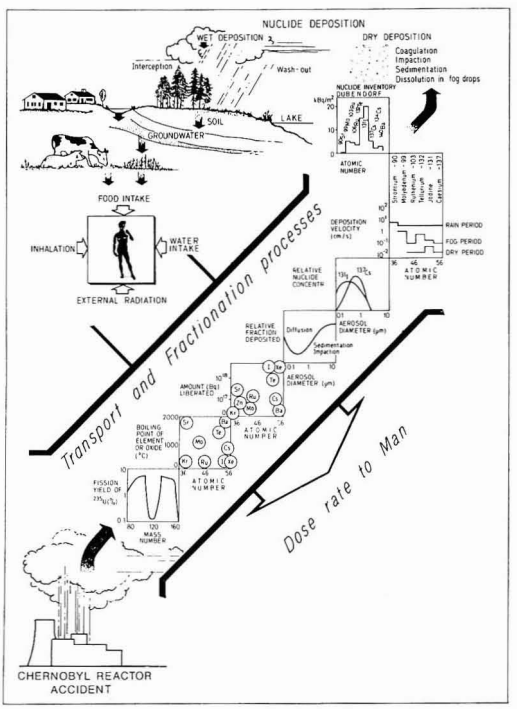

Figure 1. Release, transport, fractionation, deposition, and dose to man of Chernobyl radionuclides.

the production of the volatile species I_2 and RuO_4.

The proposed species or oxidation states are consistent with (1) the observed behavior of the Chernobyl radionuclides in extractions by ion-exchange and activated charcoal columns and by precipitation reactions (*14*) and (2) the observed nuclide mobility in the environment: uptake by and washout from soils and plants and groundwater infiltration behavior.

Results and Discussion

Washout of the Atmosphere by Rain, Fog, and Dew as the Determining Factor in the Deposition of the Chernobyl Radionuclides. The concentrations of selected radionuclides collected in Dübendorf in air filters (Figure 3) were similar to those in the rest of Switzerland (see ref 15), France, and Germany and only a little less than those measured in Sweden (*16*). The deposition rates

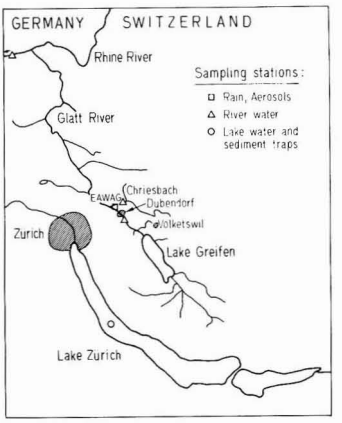

Figure 2. Map of the Zürich area in northern Switzerland, with locations of sampling stations.

were, however, very different in different parts of Switzerland and in Western Europe. This was mainly caused by the unequal rainfall during the transit of the radioactive cloud. Nuclide deposition in Switzerland was particularly high near Lake Constance and in southern parts of the Canton of Tessin (e.g., over Lake Lugano). For example, while ^{137}Cs deposition over central Switzerland was generally ≤ 3 kBq/m², it reached values of 12–20 kBq/m² over Lake Constance and 20–30 kBq/m² over Lake Lugano (*17*). The high efficiency of water droplets in rain and fog in transfering contaminants in the air to the ground is demonstrated by our measurements.

Table I shows the deposition rates and deposition velocities of selected radionuclides during periods of rainfall, fog, and dry weather calculated from the respective activities in our atmospheric collectors. Deposition rates evaluated from activities in rain collectors of different geometries and from maximum activities in grass samples generally agreed to within 20%. These measurements demonstrate the high deposition efficiency of rain events. These events accounted for 70–80% of the total deposition for $^{137,134}Cs$, $^{103,106}Ru$, ^{131}I, and ^{132}Te, while the dry fallout, which was measured separately, only accounted for 20–25%. Furthermore, by calculation of the ratio of the measured deposition rate (r_D) to the time-averaged air concentration (c_{air}) during that time interval (Δt), deposition velocities (V_D) for the different radionuclides could be calculated:

$$V_D = r_D/c_{air}\Delta t \text{ (cm/s)}$$

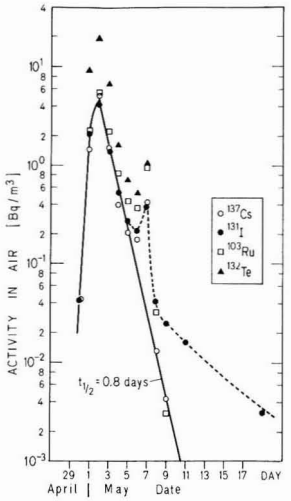

Figure 3. Radionuclide activities in air filter samples in Dübendorf collected with a high-volume sampler at a 960 m^3 d^{-1} flow rate (NABEL station).

The calculation of these deposition velocities is particularly important as they can serve as estimates for the deposition velocities of other contaminants in the air under similar atmospheric conditions. These calculations showed that the rain events of April 30, 1986, which lasted intermittently over a period of 12 h, washed out the nuclides in the air at a velocity of about 3–6 cm/s during the events. The average deposition velocity during the 9-day time period, accounting for 90% of the nuclide deposition, was, however, only 0.4–0.7 cm/s. This is due to the much smaller deposition velocities produced during dry weather periods. Nonetheless, during fog periods, deposition velocities increased by about fivefold as compared with those during dry weather.

The calculated deposition velocities are of the same order of magnitude as those estimated during the 1950s for the fission products of bomb fallout (*18*) and for the nuclides from the reactor accident of Windscale in England in 1957 (*13*). In the latter case, overall deposition velocities ranged between 0.1 and 0.3 cm/s, depending on the nuclide (*13*). The deposition velocities calculated here for Chernobyl radionuclides during different weather conditions are, however, more detailed than those reported before.

The average scavenging ratio by rain droplets, S (*19*), was calculated from

$$S = \rho c_{rain}/c_{air}$$

with ρ = density of air of 1.2 kg/m^3 and c_{rain} (Bq/kg) and c_{air} (Bq/m^3) = the concentrations in rainwater and air, respectively. The different nuclides scavenged during the rain event on April 30, 1986, all had an S value of 400 (*20*). It is close to the value expected for continental aerosols of an average diameter of 0.5–1 μm (*19*, *21*, *22*). Indeed, the Chernobyl radionuclides were attached to aerosols of such a size (*23*, *24*). This agreement should allow the calculation of deposition rates for other atmospheric trace contaminants which are associated with aerosols of similar sizes and which can, consequently, be transported over distances of hundreds to thousands of kilometers.

Radionuclides in Drinking Waters and Groundwaters in Switzerland. The highest concentration of ^{131}I measured in rainwater was about 10^4 Bq/L and that of ^{137}Cs about 500 Bq/L. These concentrations can be compared to maximum permissible concentrations for continuous consumption of these radionuclides in drinking water, of 2×10^3 and 10^4 Bq/L, respectively. Even though the highest concentrations measured for samples of cistern water used as the drinking water supply were of the same order of magnitude as those in rain samples containing most of the Chernobyl fallout, their average concentrations were considerably lower. However, the Chernobyl radionuclides were generally not measurable in drinking waters and groundwaters. One known exception is from the site of infiltration of the Glatt River into groundwater (*25*), where the groundwater was sampled very close (i.e., a few meters) to the river. Measurable activities of ^{103}Ru, ^{131}I, ^{132}Te, and ^{137}Cs (one data point only) were reported for the first 2 weeks after nuclide deposition. Another exception is from the Karstic region of southern Switzerland (*26*) where total γ activities in drinking waters from spring water were measurable during the month of May 1986, with activity levels of 1–2 Bq/L. Furthermore, drinking water taken from a 25–40-m depth in Lake Lugano during the month of September 1986 showed ^{137}Cs + ^{134}Cs activities of 0.3–0.5 Bq/L (*26*), in agreement with our lake water profiles (*27*).

Washout of Soils as Additional Input to Surface Waters. An important question asked is how much of the activity deposited onto catchment basins would be quickly lost via surface runoff. Even though many measurements were carried out to demonstrate that Chernobyl radionuclides were initially lost from grass at rates equivalent to 1–2 weeks of residence time, very few studies exist which followed the movement of the deposited activity from soils to surface waters. None have, however, attempted so far to quantify the rate and extent of this initially rapid leaching process. In this section such a process is quantified from measurements of radionuclide activities in surface waters soon after deposition.

Because ^{137}Cs concentrations in surface waters were relatively constant during that time, nuclide to ^{137}Cs ratios can be taken as indicative of the relative nuclide mobility with respect to ^{137}Cs in soils. The concentrations of ^{137}Cs in various surface waters of northern Switzerland are shown in Figure 4a, and the activity ratios of selected radionuclides, normalized to $^{137}Cs^+$ and corrected for radioactive decay, are shown in Figure 4b. $^{137}Cs^+$ concentrations in various rivers remained high during the first week after the fallout, and only after that they decreased to small values. Other Chernobyl radionuclides in the stream Chriesbach, located next to the EAWAG in Dübendorf, showed very high concentrations only during the first few days after deposition and quickly decreased to unmeasurably small values within 1 week during which ^{137}Cs activities remained approximately constant. Nuclide (^{131}I, ^{132}Te, and ^{103}Ru) to ^{137}Cs ratios in the Chriesbach on May 1, 1986, were much higher (by a factor of 4–5) than those in rainwater and air samples (Figure 4c), presumably because these nuclides were washed out of the catchment basin, most likely as neutral or anionic species. Due to the low adsorbability of anionic and neutral low molecular weight species on many particle surfaces, such species can be expected to be extremely mobile in the environment. For example, it is understandable then that anionic species of ^{131}I and ^{103}Ru, e.g., I^-, IO_3^-, and RuO_4^{2-}, were washed off soils and vegetation, infiltrated into test wells near the Glatt River (*25*), and able to penetrate the surfaces of leaves and pine needles (*28*). Increased mobility of anionic Ru nuclides was also observed in groundwater from the atomic bomb test sites in Nevada (*29*). However, $^{137}Cs^+$, a cation and partially deposited as insoluble particles

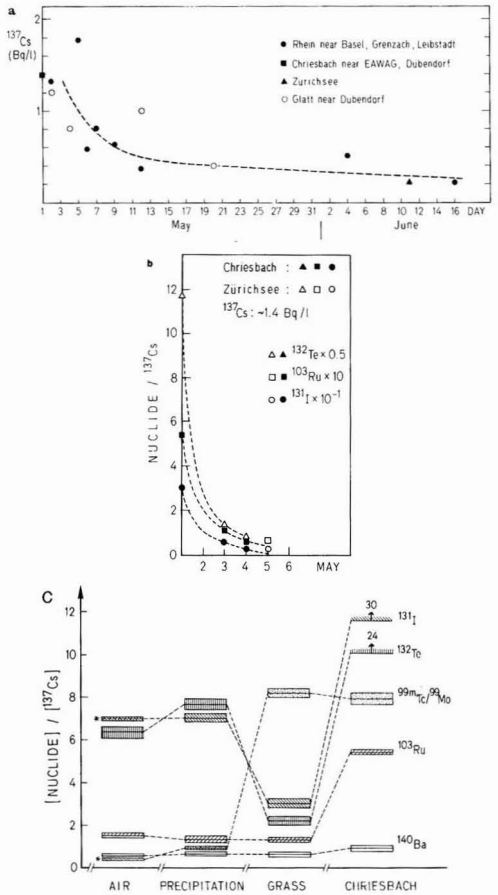

Figure 4. (a) ^{137}Cs in surface waters from northern Switzerland. The data are taken from ref 25 and 27. (b) Nuclide to ^{137}Cs ratios in the stream Chriesbach, next to EAWAG, and in Lake Zürich. (c) Nuclide to ^{137}Cs ratios on May 1, 1986, in Dübendorf compared for air, total precipitation, grass samples, and the Chriesbach.

(possibly as fine reactor debris), was much better retained by the soil.

Panels a and b of Figure 4 show qualitatively that mobile anionic and neutral species of these nuclides must have existed only during the first few days after the fallout. The subsequent very low concentration of these nuclides (i.e., ^{131}I, ^{132}Te, and ^{103}Ru) indicates that they must then have been immobilized in the soil after a few days to a much larger degree than was ^{137}Cs. Assuming a realistic value of the surface runoff during that time of about 0.2–0.3 cm^3 cm^{-2} day^{-1} and typical deposition rates as described previously (Table I), the fraction of the drainage basin of the stream Chriesbach with a very low retention capacity and concomitant short nuclide residence times of days to weeks can be determined. Such areas correspond in general to terrain covered with concrete such as streets and houses, but also to rocky grounds and rivers. For ^{137}Cs, this fraction can be calculated to be on the order of 1% and for the more mobile nuclides (^{131}I, ^{132}Te, and ^{103}Ru) to be about 5–10%. Similar values can be calculated for ^{137}Cs, ^{131}I, and ^{103}Ru in the drainage basin of the upper Danube River in Schäfstall in southern Germany from measurements of ^{137}Cs concentrations in the Danube River (*30*) and the published deposition rates of ^{137}Cs in selected places

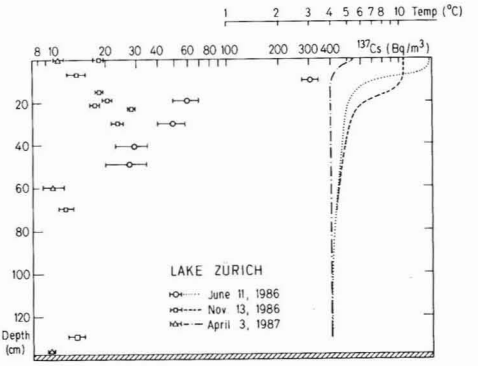

Figure 5. Vertical ^{137}Cs concentration profiles in Lake Zürich on June 11, 1986, November 13, 1986, and April 3, 1987. Corresponding inventories in the lake during those times, assuming horizontal homogeneity, amounted to 3.8, 0.9, and 0.5 kBq/m^2, or about 90%, 25%, and 12% of the assumed total deposition rate. Note that a significant fraction of the ^{137}Cs inventory in 1986 was moved below the position of the thermocline, which was centered at 7.5 and 15 m on June 11 and November 13, respectively.

in its drainage basin (*31*). If we, furthermore, assume ^{131}I/^{137}Cs and ^{103}Ru/^{137}Cs ratios in the activity deposited to the drainage basin of the Danube River to be similar to those we measured in Dübendorf and a surface runoff similar to that which we estimated before for northern Switzerland, we obtain again 1% for ^{137}Cs and 4% for ^{131}I and ^{103}Ru. These results agree also, within the errors, with those of previous studies using naturally occurring radionuclides (*32*) or those from bomb fallout (*33*). These latter studies determined this fraction of a catchment basin to be on the order of 1% for nuclides such as ^{137}Cs$^+$ and ^{7}Be^{2+}, which are relatively strongly sorbed onto soil particles, and about 10% for nuclides such as ^{90}Sr^{2+}, which are sorbed onto soils to a lesser degree. A similar behavior after deposition to catchment basins can, of course, be expected for other atmospherically delivered trace contaminants. The fraction of these radionuclides left after the initial rapid washout would, however, be residing in the soil for a very long time, i.e., about 10^3 years (*32*, *33*), without considering radioactive decay.

Direct Deposition of Chernobyl Radionuclides into Surface Waters. For medium-range and long-term studies, only ^{137}Cs (half-life of 30 years) and ^{103,106}Ru (half-life of 40 and 369 days, respectively) have to be considered. Because of the long residence time of water in lakes, which is often 1 year and longer, and the relatively small contributions from drainage basins to lakes for the long-lived ^{137}Cs, we can assume that lake nuclide inventories reflect the direct atmospheric fallout to the lake area only. Since horizontal mixing in lakes is fast compared to vertical mixing, horizontal gradients should be small, and one profile can be taken as representative for a whole lake. Vertical concentration profiles can therefore be indicative of mixing and elimination processes within a lake.

The ^{137}Cs inventory in Lake Zürich on June 11, 1986, calculated from a vertical concentration profile, was 3.8 kBq/m^2 (Figure 5). This is close to the atmospheric fallout measured in Dübendorf (Table I). At all depths sampled, the concentrations of ^{137}Cs decreased, however, by a factor of 5–10 in the following 5–10 months (Figure 5), indicating efficient removal mechanisms for ^{137}Cs.

A ^{137}Cs profile from Lake Lugano resulted in a ^{137}Cs inventory of 20 kBq/m^2 on September 9, 1986 (*27*). Here, too, this inventory agrees fairly closely with measurements of its deposition rate in southern Tessin of 21–26 kBq/m^2

(*17*). In both lakes, however, ^{137}Cs had been mixed below the actual position of the thermocline at the time of the measurement.

Accumulation and Elimination Processes in Lakes. Radionuclides in lakes are taken up by particles freshly produced in the lake (plankton and $CaCO_3$) and by those washed into the lake from drainage basins (composed mostly of clay minerals). Over a time scale of months, these radionuclides are transported to the sediments by the downward conveyor belt of particles. For example, the bioconcentration factor of $^{137}Cs^+$ on sinking plankton debris of Lake Zürich was about (3–4) × 10^4 cm^3/g dry weight. This means that the fraction of $^{137}Cs^+$ in the water, associated with suspended particles, was only a few percent. An important route for eliminating more soluble nuclides such as $^{137}Cs^+$ is also the direct adsorption onto surface sediments in shallow parts of a lake (*34*). One aim of ongoing studies is to differentiate between these two pathways.

Longer lived nuclides can be accumulated by fish via food (plankton, periphyton) and water. The bioconcentration factor for ^{137}Cs in selected fish (=activity in fish/activity in water) of about 2 × 10^3 cm^3/g wet weight (*27*) is similar to that of plankton and is mostly gained by the $^{137}Cs^+$ taken up by fish through intake of plankton (*35*). This behavior of $^{137}Cs^+$ agrees with that of other radioactive trace elements released by reactors and through atomic bomb testing, which are not magnified in the food chain.

^{137}Cs concentration in water from Lake Zürich was not measured before the Chernobyl fallout reached it, but concentrations must have been similar to those of other lakes of the 40–50° N latitude belt, i.e., 10^{-2}–10^{-3} Bq/L (*36–38*). After the Chernobyl fallout event, ^{137}Cs concentrations rose over 2 orders of magnitude, with a contribution of ^{134}Cs of about 55% of the ^{137}Cs value. ^{134}Cs did not exist in the natural environment before the Chernobyl fallout anymore except from regular discharges of nuclear reactors, as the ^{134}Cs from atomic bomb tests had decayed away. ^{137}Cs concentrations in sedimenting particles from Lake Zürich rose during that time from 3 × 10^{-2} to 5–8 Bq/g.

The pulse-like shape of the ^{137}Cs and ^{103}Ru flux out of the lake (Figure 6a shows that the largest ^{137}Cs and ^{103}Ru flux occurred during the first 3 weeks after the fallout) could indicate that about 10–20% of ^{137}Cs probably reached the lake in insoluble aerosol particles (possibly as fine debris from the reactor fuel), in agreement with our filtration results of rainwater (*27*). This pattern of decreasing ^{137}Cs fluxes, which was also observed elsewhere in European waters (*39–41*), was not produced by decreasing sedimentation rates as these rates either increased during the summer months or remained the same. Figure 6b indicates that the fraction of ^{137}Cs which was vertically transported out of the lake water to the lower laying sediments was 20% of the total inventory during the first 2 months, and only another 5–10% during the following 3 months. Comparison of ^{137}Cs fluxes in traps from 50- and 130-m depth in Lake Zurich (Figure 6a) allowed the calculation of particle settling velocities of 15 m/day and time scales for particles advected into the lower traps from the horizontal boundaries of 1–3 months (*42*).

During the same time, all other nuclides disappeared from the lake water, either due to radioactive decay or due to faster removal rates. For example, 80% of the total inventory of ^{103}Ru was vertically transported out of the lake within the first 2 months, and another 10% during the following 3 months, stressing the strong particle affinity

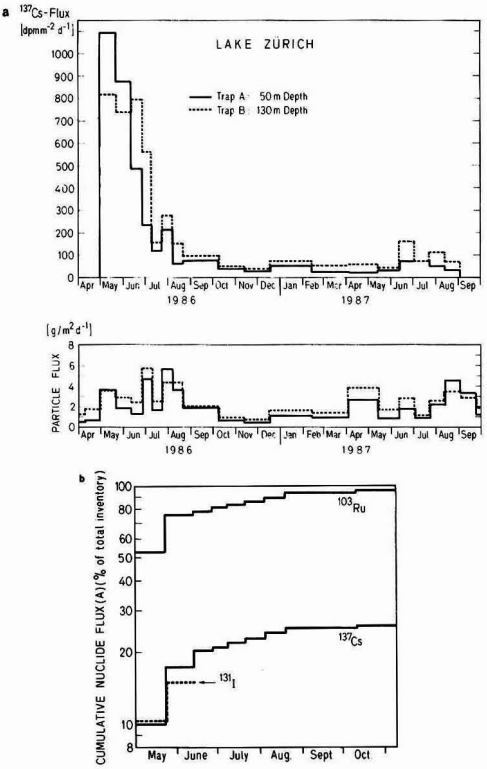

Figure 6. (a) ^{137}Cs and particle fluxes are compared for 50- (trap A) and 130-m depth (trap B) in Lake Zürich after May 1, 1986. (b) Cumulative nuclide fluxes at 50-m depth (trap A) show almost complete removal of ^{103}Ru by sinking particles during that time but incomplete removal by that pathway for ^{137}Cs (and ^{131}I). A boundary input of ^{137}Cs is suggested by the increased importance of the ^{137}Cs flux at 130-m depth, exceeding that measured at 50 m after 1–2 months. The presence of anoxic bottom water below 130-m depth during that time would argue strongly against the resuspension of underlying bottom sediments.

of Ru in lakes. Plankton in lakes and oceans concentrates Ru to a much greater extent than Cs; concentration factors are 2 × 10^5 (*43*). Such a behavior contrasts with that of Ru in soils and surface waters during the first few days after the fallout and most likely points to a reductive uptake of Ru (from VI to III or IV) by the plankton. The speciation in biological systems of trace elements with multiple oxidation states is characterized by the tendency of these systems to reduce trace element valence after adsorption to surfaces (e.g., reviewed in ref 44).

Removal fluxes of radionuclides by vertically settling particles should be compared to lake inventories calculated from their vertical profiles. For ^{137}Cs, for which this comparison is possible, the agreement between these two measurements is poor. While we would predict for the month of November 1986, from the measurement of vertical fluxes, an inventory in the lake of 75% of the initial value, we measured during that time a ^{137}Cs concentration profile which gives the equivalent of only 25% of the initial inventory (i.e., 1 instead of 4.2 kBq/m^2). Because these sediment traps collect 100 ± 20% of the measured atmospheric flux of ^{210}Pb (unpublished data), we interpret this apparent disagreement to indicate the importance of the direct sorption onto surface sediments as the primary removal mechanism for ^{137}Cs, in agreement with experi-

mental evidence from purposeful tracer studies in enclosures and whole lakes (*34*) and interpretations of bomb fallout records in lake sediments (*36, 37*). Net loss of ^{137}Cs to the outflow of the lake (i.e., inflow − outflow) is not known but can be estimated to be of minor importance (i.e., ≤20% of the atmospheric deposition rate). As the lake receives its water from two other lakes (i.e., upper Lake Zurich and Lake Walen) exhibiting similar elimination processes and with almost identical atmospheric inputs (*17*), it can be assumed that ^{137}Cs concentrations in the outflowing water are similar to those in the inflowing water during the stratified conditions of Summer 1986.

Because of their ultralow concentrations in the environment (i.e., $\leq 10^{-15}$ M), the fate and extent of accumulation in biological systems of some of these radioactive trace elements are determined by the concentration of the stable element or of a stable homologue (e.g., K^+ for $^{137}Cs^+$ and Ca^{2+} for $^{90}Sr^{2+}$). As both K^+ and Ca^{2+} concentrations are similar in most Swiss lakes, bioaccumulation factors in fish and other aquatic organisms should also be similar. Indeed, ^{137}Cs concentrations in fish from different lakes in Switzerland (*27*) were, during the summer months, approximately proportional to the deposition rate from the atmosphere, as this determined the values of the prevalent concentrations in the lake water and sediments. No differences between herbivores and carnivores, or between fish with pelagic and littoral habitat, were discernible during 1986, because of very large variability in ^{137}Cs concentrations of all species (*27*). However, the relatively uniform average concentrations of ^{137}Cs in different fish species from a single lake probably are the consequence of the uniform tagging of their food sources, i.e., suspended and sinking particles, shallow surface sediments, and periphyton, with ^{137}Cs. As the residence time of ^{137}Cs in fish (i.e., the inverse of its excretion rate) is about 300–500 days (*35*), ^{137}Cs concentrations in fish are indeed only decreasing slowly.

Conclusions

The processes which influenced the mobility of Chernobyl radionuclides in air, soil, and aquatic reservoirs were investigated. Results were compared to what has been learned from studies of the A bomb fallout radionuclides, those resulting from earlier accidents of nuclear installations, and those from purposeful tracer experiments in lakes. On the basis of these results, we conclude the following:

(1) Radionuclides deposited in the Zurich area were estimated to be 80% from wet deposition and about 20% from dry deposition. Transfer velocities were calculated from a comparison of total deposition rates measured in open pans and in wet collectors of dry deposition, open during dry weather, and air concentrations during the same time interval. Deposition velocities for different radionuclides were lowest during dry weather (0.024–0.08 cm/s), intermediate during fog conditions (0.1–0.2 cm/s), and highest during rain events (3 cm/s). Scavenging ratios of 400 could be calculated for different radionuclides from air and rain concentrations, in agreement with what is expected for continental aerosols of an average diameter of 0.5–1 μm.

(2) Radionuclides in anionic and molecular forms (i.e., ^{131}I, ^{103}Ru, and ^{132}Te) were washed from soils to surface waters only during the first few weeks after deposition. During that time, it was calculated that about 1% of the $^{134,137}Cs$ and about 4–10% of the I, Te, and Ru nuclides, deposited onto the catchment basins in northern Switzerland and southern Germany, were leached into surface waters.

(3) In Lake Zurich, about 20% of the $^{134,137}Cs$ and ^{131}I and about 80% of the ^{103}Ru were rapidly removed by settling particles within the first 2 months after deposition as determined from sediment trap measurements. This observation of fast removal of ^{103}Ru in lakes seems to contradict the initial observations of high mobility and correspondingly low adsorbability of this isotope in atmospheric and soil reservoirs and instead suggests a reductive uptake of Ru [i.e., reduction of adsorbed Ru(VI) to Ru(III,IV)] by plankton. Vertical fluxes of $^{134,137}Cs$ decreased during the rest of the summer of 1986, despite the fact that sedimentation rates remained at similar or higher levels during that time. A comparison of vertical profiles of ^{137}Cs, taken in June and November of 1986 in Lake Zurich, indicates that about 75% of the $^{134,137}Cs$ had been already eliminated from the lake by November, despite the fact that sediment trap fluxes indicated total vertical removal fluxes by that time amounting to only about 25% of the total (but amounting to 95% for ^{103}Ru). Direct sorption onto shallow surface sediments is suspected as an important removal mechanism for ^{137}Cs in lakes. Such a mechanism needs to be tested further by detailed sedimentological investigations.

(4) Further studies are needed to follow the fate of $^{134,137}Cs$, derived from Chernobyl fallout, in surface waters and sediments. Sediment resuspension, focusing, or other redistribution processes of Cs isotopes can be closely studied over the next decade. Furthermore, other potential remobilization processes for Cs isotopes, e.g., those that might occur during temporal anoxia (*45*), should be further investigated.

(5) Our observations on deposition velocities in atmospheric, soil, and aquatic reservoirs were consistent with what had been learned from earlier observations of radionuclide behavior of fallout from atomic weapons tests and nuclear accidents and from purposeful tracer experiments in enclosures and whole lakes. However, the Chernobyl fallout radionuclides provided a far better picture of the tight coupling of the atmospheric, terrestrial, and aquatic geochemical processes.

(6) The results from studies of the movement of the Chernobyl radionuclides in atmospheric, terrestrial, and aquatic environments should be highly relevant to our understanding of the transport behavior of other atmospheric trace contaminants in the environment.

Acknowledgments

We thank R. Gehrig (EMPA) for the air filter samples and J. Zobrist (EAWAG) for the dry fallout samples. We acknowledge the critical comments by B. Honeyman and two anonymous reviewers.

Registry No. ^{134}Cs, 13967-70-9; ^{137}Cs, 10045-97-3; ^{103}Ru, 13968-53-1; ^{131}I, 10043-66-0; ^{132}Te, 14234-28-7; ^{132}I, 14683-16-0; ^{99}Mo, 14119-15-4; ^{99}Tc, 14133-76-7; ^{90}Sr, 10098-97-2; ^{89}Sr, 14158-27-1.

Literature Cited

(1) Li, Y.-H.; Peng, T.-H.; Broecker, W. S.; Ostlund, H. G. *Tellus, Ser. B* **1984**, *36B*, 212–217.
(2) Hesslein, R. H.; Broecker, W. S.; Schindler, D. W. *Can. J. Fish. Aquat. Sci.* **1980**, *37*, 378–386.
(3) Hesslein, R. H.; Broecker, W. S.; Quay, P. O.; Schindler, D. W. *Can. J. Fish. Aquat. Sci.* **1980**, *37*, 454–463.
(4) Höhn, E.; Santschi, P. H. *Water Resour. Res.* **1987**, *23*(*4*), 633–640.
(5) Santschi, P. H.; Hoehn, E.; Lueck, A.; Farrenkothen, K. *Environ. Sci. Technol.* **1987**, *21*, 909–916.
(6) Santschi, P. H.; Bollhalder, S.; Farrenkothen, K.; Lueck, A.; Weber, C.; Zingg, S. In Proceedings of the Symposium

"Radioaktivitätsmessungen in der Schweiz nach Tschernobyl und ihre wissenschaftliche Interpretation", 1987, Bern; Bundesamt für Gesundheitswesen: Bern, Switzerland, 1987; pp 467–476.
(7) Goldin, A. S.; Velten, R. J.; Frishkorn, W. *Determination of Radioactive Strontium*; National Meeting of the American Chemical Society, Chicago, IL, 1958; American Chemical Society: Washington, DC, 1958; abstr.
(8) Dasch, J. M. *Environ. Sci. Technol.* **1985**, *19*, 721–725.
(9) Mann, D. R.; Casso, S. A. *Mar. Chem.* **1984**, *14*, 307–318.
(10) Seifritz, W. *Neue Zürcher Zeitung* **1986**, *193/5*, Aug 22.
(11) Burns, R. G. In *Radioactive Wastes*; Collins, J. C., Ed.; Wiley: New York, 1960; pp 113–140.
(12) National Academy of Sciences Report; *Platinum Group Metals*; Publishing Office of the National Academy of Science: Washington, DC, 1977; 232 p.
(13) Stewart, N. G.; Crooks, R. N. *Nature (London)* **1958**, *4636*, 627–628.
(14) Santschi, P. H.; Bollhalder, S.; Farrenkothen, K.; Hermann, A.; Lueck, A.; Schüpbach, M. R.; Weber, C. In Proceedings of the Symposium "Radioaktivitätsmessungen in der Schweiz nach Tschernobyl und ihre wissenschaftliche Interpretation", 1987, Bern; Bundesamt für Gesundheitswesen: Bern, Switzerland, 1987; pp 132–141.
(15) Völkle, H.; Murith, C.; Surbeck, H.; Nowak, St.; Baeriswyl, L.; Ferreri, G.; Gobet, M.; Gurtner, A.; Ribordy, L.; Wicht, F.; Santschi, P. H.; Farrenkothen, K.; Lueck, A.; Bollhalder, S.; Weber, C. In Proceedings of the Symposium "Radioaktivitätsmessungen in der Schweiz nach Tschernobyl und ihre wissenschaftliche Interpretation", 1987, Bern; Bundesamt für Gesundheitswesen: Bern, Switzerland, 1987; pp 72–83.
(16) Devell, L.; Tovedal, H.; Bergström, U.; Appelgren, A.; Chrysler, J.; Anderson, L. *Nature (London)* **1986**, *321*, 192–193.
(17) Czarnecki, J.; Cartier, F.; Honegger, P.; Zurkinden, A. In Proceedings of the Symposium "Radioaktivitätsmessungen in der Schweiz nach Tschernobyl und ihre wissenschaftliche Interpretation", 1987, Bern; Bundesamt für Gesundheitswesen: Bern, Switzerland, 1987; 93–109.
(18) Wiffen (1958) cited in *Radioactive Wastes*; Collins, J. C., Ed.; Wiley: New York, 1958; pp 200–221.
(19) Buat-Menard, P.; Duce, R. A. *Nature (London)* **1986**, *321*, 508–509.
(20) Santschi, P. H.; Bollhalder, S.; Farrenkothen, K.; Lueck, A.; Weber, C.; Zingg, S. In Proceedings of the Symposium "Radioaktivitätsmessungen in der Schweiz nach Tschernobyl und ihre wissenschaftliche Interpretation", 1987, Bern; Bundesamt für Gesundheitswesen: Bern, Switzerland, 1987; pp 176–187.
(21) Scott, B. C. *Atmospheric Pollutants in Natural Waters*; Eigenreich, S. J., Ed.; Ann Arbor Science: Stoneham, MA, 1981; pp 3–21.
(22) Duce, R. A.; Arimoto, R.; Ray, B. J.; Uuni, C. K.; Horden, P. J. *J. Geophys. Res., C: Oceans Atmos.* **1983**, *88*, 5321–5342.
(23) Jost, D. T.; Gäggeler, H. W.; Baltensperger, U.; Zinder, B.; Haller, P. *Nature (London)* **1986**, *324*, 22–23.
(24) Nyffeler, U. P.; Galli, B.; Bürki, P.; Krähenbühl, L. In Proceedings of the Symposium "Radioaktivitätsmessungen in der Schweiz nach Tschernobyl und ihre wissenschaftliche Interpretation", 1987, Bern; Bundesamt für Gesundheitswesen: Bern, Switzerland, 1987; pp 121–131.
(25) Waber, U.; Krähenbühl, U.; von Gunten, H. R. In Proceedings of the Symposium "Radioaktivitätsmessungen in der Schweiz nach Tschernobyl und ihre wissenschaftliche Interpretation", 1987, Bern; Bundesamt für Gesundheitswesen: Bern, Switzerland, 1987; pp 271–283.
(26) Massarotti, A. *Gas, Wasser Abwasser* **1986**, *66(12)*, 827–832.
(27) Santschi, P. H.; Bollhalder, S.; Camani, M.; Farrenkothen, K.; Goerlich, W.; Haesler, S.; Heiz, H.; Lueck, A.; Schuler, Ch.; Sturm, M.; Völkle, H.; Weber, C.; Zingg, S. In Proceedings of the Symposium "Radioaktivitätsmessungen in der Schweiz nach Tschernobyl und ihre wissenschaftliche Interpretation", 1987, Bern; Bundesamt für Gesundheitswesen: Bern, Switzerland, 1987; pp 323–338.
(28) Wyttenbach, A.; Tobler, L.; Bajo, S. In Proceedings of the Symposium "Radioaktivitätsmessungen in der Schweiz nach Tschernobyl und ihre wissenschaftliche Interpretation", 1987, Bern; Bundesamt für Gesundheitswesen: Bern, Switzerland, 1987; pp 495–504.
(29) Coles, D. G.; Ramspott, L. D. *Science (Washington, D.C.)* **1982**, *215*, 1235–1237.
(30) Friedmann, L.; Amann, W.; Lux, D. *GWF, Gas- Wasserfach: Wasser/Abwasser* **1986**, *127(H.12)*, 604–613.
(31) Herzog, T. *Haustech., Bauphys., Umwelttech. Gesund.-Ing.* **1986**, *107(H.5)*, S28/290-338/300.
(32) Dominik, J.; Burrus, D.; Vernet, J.-P. *Earth Planet. Sci. Lett.* **1987**, *84*, 165–180.
(33) Linsley, G. S.; Haywood, S. M.; Dionan, J. In Proceedings of the Symposium "Environmental Migration of Long-lived Radionuclides", Knoxville, TN, 27–31 July 1981; IAEA: Vienna, 1982; pp 615–643.
(34) Santschi, P. H.; Nyffeler, U. P.; Anderson, R. F.; Schiff, S. L.; O'Hara, P. *Can. J. Fish. Aquat. Sci.* **1986**, *43(1)*, 60–77.
(35) Thomann, R. V. *Can. J. Fish. Aquat. Sci.* **1981**, *38*, 280.
(36) Edgington, D. N.; Robbins, J. A. In Proceedings of the Symposium "Impacts of Nuclear Releases into the Aquatic Environment", Otaniemi, Finland, 1975; IAEA: Vienna, 1975; IAEA-SM-198/40, pp 245–260.
(37) Brunskill, G. J.; Ludlam, S. D.; Peng, T.-H. *Chem. Geol.* **1984**, *44(1/3)*, 101–118.
(38) Wahlgren, M. A.; Nelson, D. M. *Verh.-Int. Ver. Theor. Angew. Limnol.* **1975**, *19*, 317–322.
(39) Fowler, S. W.; Buat-Menard, P.; Yokoyama, Y.; Ballastra, S.; Holm, E.; Nguyen, H. V. *Nature (London)* **1987**, *329*, 56–58.
(40) Buesseler, K. O.; Livingston, H. D.; Honjo, S.; Hay, B. J.; Manganini, S. J.; Degens, E.; Ittekkot, V.; Iedar, E.; Konuk, T. *Nature (London)* **1987**, *329*, 825–828.
(41) Kempe, S.; Nies, H. Nature (*London*) **1987**, *329*, 828–831.
(42) Santschi, P. H. *Hydrobiologia*, in press.
(43) Lowman, F. G.; Rice, T. R.; Richards, F. A. In *Radioactivity in the Marine Environment*; National Academy of Sciences: Washington, DC, 1971; pp 161–199.
(44) Santschi, P. H. *Limnol. Oceanogr.*, in press.
(45) Evans, D. W.; Alberts, J. J.; Clark, R. A. *Geochim. Cosmochim. Acta* **1983**, *47*, 1041–1050.

Received for review July 7, 1987. Accepted November 20, 1987.

Environ. Sci. Technol. 1988, 22, 517–522

Atmospheric Speciation and Wet Deposition of Alkyllead Compounds

Andrew G. Allen, Miroslav Radojevic,† and Roy M. Harrison*

Institute of Aerosol Science, Department of Chemistry, University of Essex, Colchester CO4 3SQ, Essex, U.K.

■ Concentrations of individual tetra-, tri-, and dialkyllead compounds have been measured in the gas phase and in aerosol and rainwater samples at two sites in eastern England and at one site in western Ireland. The results show a predominance of gas-phase over aerosol-associated species in the air at all sites, and in general a greater abundance of tetraalkyllead than trialkyllead. Washout factors for total alkyllead are lower than for inorganic lead and correlate highly between adjacent urban and semirural sites.

Introduction

Alkyllead compounds resulting from the use of tetraalkyllead (R_4Pb) as a gasoline additive have been determined in a variety of environmental samples, including air, water, sediment, and fish (*1*). The major anthropogenic source involves the release of volatile R_4Pb species into the atmosphere. About 1% of the organolead content of gasoline is emitted into the atmosphere via the exhaust unchanged, and further emissions include evaporative losses of fuel from fuel tanks and carburetors, evaporation at gasoline stations, and accidental spillages of gasoline as well as other minor sources that involve the use of leaded gasoline (e.g., chain saws, lawnmowers, and motor boats). A possible environmental source involving alkylation of inorganic lead is also suspected (*2*). In the environment, R_4Pb compounds decompose eventually to inorganic lead via trialkyllead (R_3Pb^+) and dialkyllead (R_2Pb^{2+}) species as intermediates. The mechanisms of decomposition and alkylation reactions are still not fully understood and some of these may be biologically mediated. Environmental pathways of organic lead have recently been reviewed (*1*), and atmospheric transformations play a prominent role in the biogeochemical cycle of organic lead.

The primary pollutant R_4Pb species may decompose in the atmosphere to produce vapor-phase R_3Pb^+ and R_2Pb^{2+} species and inorganic lead aerosol, the dominant mechanism being reaction with hydroxyl OH radical (*3*). R_3Pb^+ compounds also react with OH radical, but the reaction rates are slower than for the R_4Pb – OH reaction, resulting in longer atmospheric lifetimes of R_3Pb^+ (*4*). R_4Pb, R_3Pb^+, and R_2Pb^{2+} compounds may be scavenged in cloud and raindrops or may react with atmospheric aerosols. Recent measurements of alkyllead compounds in rainwater suggest that wet deposition processes (rainout/washout) may be an important removal mechanism of these pollutants from the atmosphere and a source of these species in surface waters (*5–8*). Alkyllead species released into the atmosphere may therefore enter into other environmental reservoirs via the hydrological cycle and have been identified at very low levels in potable water (*9*). Damage to German forests has recently been attributed to R_3Pb^+ compounds in rainwater (*10*), but high concentrations measured in the latter study with a nonspecific biochemical technique have been disputed on the basis of measurements made by using species-specific gas chromatography/atomic absorption spectroscopy (GC/AAS) (*7*).

GC/AAS techniques have been applied in the determination of alkyllead compounds in air, atmospheric aerosol, and rainwater (*5, 6, 8, 11–14*) in an attempt to improve our understanding of the atmospheric cycle of organic lead. R_4Pb compounds in air and R_4Pb, R_3Pb^+, and R_2Pb^{2+} species in atmospheric aerosol have been determined at urban and rural sites (*13*), and concentrations of vapor-phase R_3Pb^+ and R_2Pb^{2+} compounds have been inferred by difference from total vapor-phase concentrations measured with a nonspecific extraction/graphite furnace atomic absorption spectroscopy (GFAAS) technique. Recently, a GC/AAS technique for gas-phase R_3Pb^+ and R_2Pb^{2+} compounds has been developed and successfully applied to atmospheric samples (*14*).

Here we report simultaneous measurements of R_4Pb, R_3Pb^+, and R_2Pb^{2+} compounds in the atmospheric gaseous and aerosol phases and in bulk deposition. Measurements were carried out simultaneously at an urban and a semirural site, and at a remote rural site on the west coast of Ireland for a brief period. In addition to the quantitative physicochemical speciation study of alkyllead in the atmosphere at these sites, data on the deposition of these species were also obtained.

Experimental Section

Alkyllead compounds in the gas phase, atmospheric aerosol, and bulk deposition were determined at urban (Colchester, U.K.) and semirural (Essex University, U.K.) sites and at a rural site, distant from major anthropogenic sources, on the west coast of Ireland (Adrigole, Republic of Ireland). A map of the U.K. and Ireland showing the location of the sampling sites is shown in Figure 1. Samplers were placed on the roofs of Colchester and Essex University libraries, both of which were the highest buildings in the locality. These sites were separated by a distance of 3.6 km. At the rural site, samples were collected in an open field with no major obstructions in the vicinity.

Gas-phase R_4Pb compounds were sampled at 100 mL min^{-1} with stainless steel tubes (3.25 in. long × 0.2 in. i.d.) packed with Poropak Q. A filter for removing atmospheric ozone, consisting of a piece of Teflon tubing (2 in. long × 0.2 in. i.d.) packed with 0.25 g of iron(II) sulfate crystals, was attached to the upstream end of the sampling tube, and a 0.45-μm filter was placed upstream of this in order to remove atmospheric aerosol. A GN Instruments two-stage concentrator was used to thermally desorb R_4Pb compounds into the GC/AAS system. The sampling tube was heated to 150 °C with the carrier gas flowing through at a rate of 140 mL min^{-1}, and the R_4Pb species were transferred into a glass-lined stainless steel U tube packed with 0.05 g of ground glass (250/500 μm), which was found to perform better than several other packings that were tested. This U tube was kept at liquid nitrogen temperature during the transfer. After completion of this procedure, the tube was flash-heated to 140 °C, and the R_4Pb compounds were swept into the GC/AAS system for analysis. Prior to sampling, each tube was thermally cleaned by flushing with helium for 10 min at 170 °C. A breakthrough volume of 800 L at 20 °C was found for this

†Present address: Department of Chemistry, UMIST, Manchester, U.K.

0013-936X/88/0922-0517$01.50/0

Table I. Detection Limits and Recoveries for Alkyllead Compounds in Environmental Samples Using the GC/AAS Method Employed in This Study

	air (vapor)[a]		aerosol[a]		rainwater	
compd	det lim, ng of Pb m^{-3}	recovery, %	det lim,[a] pg of Pb m^{-3}	recovery, %	det lim,[b] ng of Pb L^{-1}	recovery, %
Me_4Pb	0.14	78	0.19	93	0.2	60
Me_3EtPb	0.14	73	0.13	93	0.1	60
Me_2Et_2Pb	0.28	76	0.22	93	0.2	60
$MeEt_3Pb$	0.49	56	0.30	93	0.3	60
Et_4Pb	0.83	53	0.30	93	0.3	60
Me_3Pb^+	0.34	78	0.27	89	0.3	102
Et_3Pb^+	0.76	70	0.54	100	0.6	100
Me_2Pb^{2+}	0.53	66	0.32	101	0.4	98
Et_2Pb^{2+}	1.96	46	0.86	104	1.0	102

[a] Based on 24-h sample. [b] Based on 1-L sample.

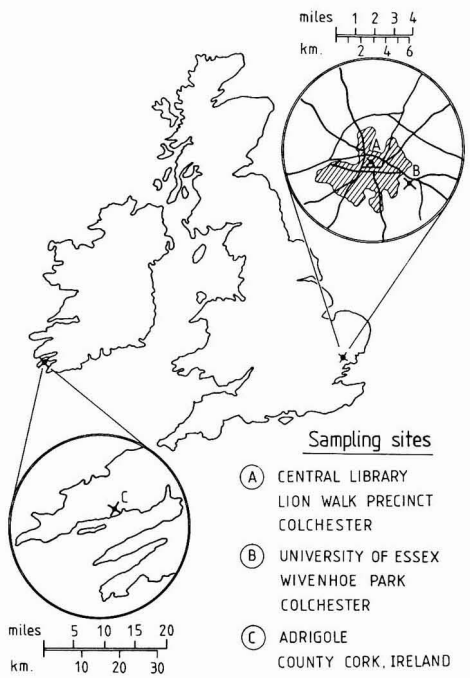

Figure 1. Map indicating locations.

sampling method by extrapolation from elevated-temperature measurements made in the laboratory and was confirmed by parallel sampling of the atmosphere over a set-time interval with absorption tubes pumped at differing flow rates. The technique employed for vapor-phase R_4Pb compounds is similar to that originally described by Hewitt and Harrison (*11*), who reported a collection efficiency of 100% and a breakthrough volume of 89 L on the basis of very conservative assumptions.

Gas-phase trialkyllead and dialkyllead compounds were sampled by bubbling filtered (0.45 μm) air at 1 L min^{-1} into two bubblers in series, each containing 80 mL of Milli-Q purified water. After sampling was complete, the contents of the two bubblers were combined, transferred into a glass bottle, and extracted into *n*-hexane in the presence of NaCl and sodium diethyldithiocarbamate (NaDDTC). Further details of this method have recently been published (*14*). Atmospheric aerosols were sampled at 1 m^3 min^{-1} onto GF/A filter papers in a standard Hi-Vol sampler. After sample collection, the filter papers were rolled up, placed inside glass tubes together with 30 mL of Milli-Q water, and extracted into *n*-hexane after addition of NaCl and NaDDTC in a manner reported previously (*12*, *13*). Rainwater samples were collected with glass bulk "funnel in bottle" samplers, which were left in the field until a sufficient sample was collected to enable analysis. These samplers also collect dry-deposited alkyllead vapors and aerosols in addition to the wet-deposited species. Sampling bottles were kept in the dark in the field so as to minimize any photochemical decomposition. In the laboratory, samples were extracted into *n*-hexane in the presence of NaCl and NaDDTC. Extraction was carried out in the sampling bottles because of possible adsorption of R_4Pb compounds onto the walls of glass vessels (*12*), and samples were not filtered because of the possible adsorption of these species on suspended particles (*15*).

Solvent extracts of atmospheric aerosols, rainwater, and vapor-phase trialkyl- and dialkyllead species were separated and alkylated by the addition of propyl magnesium chloride in diethyl ether so as to convert R_3Pb^+ and R_2Pb^{2+} to the more volatile R_4Pb form suitable for GC/AAS analysis. Details of the propylation technique have been given elsewhere (*16*). It was also possible to further concentrate the extracts prior to analysis by purging with N_2 (*16*), and this was particularly useful when analyzing samples from less polluted sites. The GC/AAS system, consisting of a specialized silica furnace detector cell that was electrothermally heated, has been outlined in a separate publication (*16*), and identical instrumentation, operating conditions, and methods of analysis were employed in this work. Typical detection limits and recovery efficiencies for the individual alkyllead compounds are given in Table I. Correction factors for incomplete recoveries have been used in calculating the environmental concentrations reported in this paper. Repeatabilities between duplicate environmental samples were typically on the order of 7–15% relative standard deviation (rsd) dependent upon compound and concentration. Inorganic lead was determined by extracting the 0.45-μm filter placed upstream of the vapor-phase ionic alkyllead sampling device into nitric acid and analyzing by graphite furnace atomic absorption spectrometry (GFAAS). Inorganic lead in rainwater was determined by GFAAS after filtering the solution through a 0.45-μm filter to remove the large particulate fraction. Detection limits for alkyllead species in the rural samples were lower than those in urban and semirural samples because of greater sample volumes and/or greater concentration of the extract. Deuterium arc background correction was always employed when analyzing environmental samples.

Where results are reported for total alkyllead, these have been calculated assuming compounds below the analytical

Table II. Results of Measurements of Atmospheric Alkyllead Compounds at the Urban Site (Colchester, U.K.) 7 January to 19 February 1986

	gas		aerosol	
compd	concn range, ng of Pb m^{-3}	no. of samples with alkyllead compd detectable[b]	concn range, pg of Pb m^{-3}	no. of samples with alkyllead compd detectable[b]
Me_4Pb	0.7–10.9	24	<0.06	0
Me_3EtPb	<0.14–2.6	9	<0.04	0
Me_2Et_2Pb	<0.28–1.6	2	<0.07	0
$MeEt_3Pb$	<0.49–3.3	3	<0.10	0
Et_4Pb	<0.83–6.6	5	<0.10	0
Me_3Pb^+	<0.11–19.8	8	<0.09–2.3	4
Me_2EtPb^+	<0.16–1.2	1	<0.12–0.2	1
$MeEt_2Pb^+$	<0.20	0	<0.15–0.3	1
Et_3Pb^+	<0.25–1.1	1	<0.18–2.6	4
Me_2Pb^{2+}	<0.18–2.6	7	<0.11–1.1	5
Et_2Pb^{2+}	<0.65–5.1	3	<0.29–23.7	12
RPb^{3+} [c]	<0.65–1.0	1	<0.29–9.5	12
total alkyl lead[a]	0.7–35.9	24	0.31–35.8	14
inorganic lead			45 000–768 000	
alkyl/inorganic Pb, %	1.3–26.9		10^{-4}–0.03	

[a] Minimum and maximum of measured concentrations (values less than detection limit taken as zero). [b] Total number of samples analyzed = 24. [c] Tentative assignment, see text.

Table III. Results of Measurements of Atmospheric Alkyllead Compounds at the Semirural Site (Essex University, U.K.) 7 January to 19 February 1986.

	gas		aerosol	
compd	concn range, ng of Pb m^{-3}	no. of samples with alkyllead compd detectable[b]	concn range, pg of Pb m^{-3}	no. of samples with alkyllead compd detectable[b]
Me_4Pb	<0.14–11.0	23	<0.06–1.3	1
Me_3EtPb	<0.14–1.7	3	<0.04	0
Me_2Et_2Pb	<0.28	0	<0.07	0
$MeEt_3Pb$	<0.49–1.2	1	<0.10	0
Et_4Pb	<0.83–5.0	2	<0.10–0.4	2
Me_3Pb^+	<0.11–2.1	5	<0.09–2.0	5
Me_2EtPb^+	<0.16	0	<0.12–0.5	1
$MeEt_2Pb^+$	<0.20	0	<0.15–0.2	1
Et_3Pb^+	<0.25–2.6	2	<0.18–0.4	2
Me_2Pb^{2+}	<0.18–0.6	1	<0.11–0.5	4
Et_2Pb^{2+}	<0.65–1.0	2	<0.29–15.6	6
RPb^{3+} [c]	<0.65	0	<0.29–4.6	12
total alkyl lead[a]	0.4–11.0	23	0.5–19.4	14
inorganic lead			<13 000–397 000	
alkyl/inorganic Pb, %	0.6–>20		5×10^{-4}–0.06	

[a] Minimum and maximum of measured concentrations (values less than detection limit taken as zero). [b] Total number of samples analyzed = 24. [c] Tentative assignment, see text.

detection limit to have a concentration of zero.

Results and Discussion

Atmospheric Concentrations and Speciation. The results of the analysis for the urban and semirural sites in the U.K. are given in Tables II and III in terms of the range of observed concentrations and the number of occurrences of each alkyllead species in the gas and aerosol phases. It is apparent that Me_4Pb is the predominant gas-phase species at both sites, being observed in all the samples collected with the exception of one semirural sample. Occasionally other R_4Pb compounds and ionic alkyllead species (R_3Pb^+ and R_2Pb^{2+}) were observed. R_4Pb compounds were generally not found in atmospheric aerosol, although the less volatile ionic alkyllead compounds were observed in many of the aerosol samples. The form of occurrence of alkyllead compounds in the atmosphere at these sites appears to be related to their volatility. In general, the number of occurrences in the gas phase decreases with decreasing volatility of compound, while in the aerosol the number of observations increases with decreasing volatility of species. Aerosol-associated alkyllead represent only a minor fraction of organic lead in the atmosphere, being present generally at levels 3 orders of magnitude lower than the concentration of vapor-phase alkyllead. Particulate matter therefore seems to play a minor role in the atmospheric cycle of organic lead. These conclusions are in accord with those drawn in a similar comparative study at an urban and rural site in northwestern England (*13*).

The relation between gas-phase alkyllead and inorganic lead aerosol at the urban site is shown in Figure 2. This shows a rather close relationship between the two variables, indicative of a common source in vehicular emissions. A best fit line (Figure 2) ignoring two outlier points indicates an intercept of ca. 50 ng m^{-3} inorganic lead, perhaps corresponding to wind-blown street dust or industrially derived lead, and a gradient corresponding to alkyllead comprising 10% of total (inorganic plus alkyl) lead. The latter figure is consistent with earlier data from urban sites obtained with techniques that measure total alkyllead (*1*). A plot of the same variables from the semirural site was

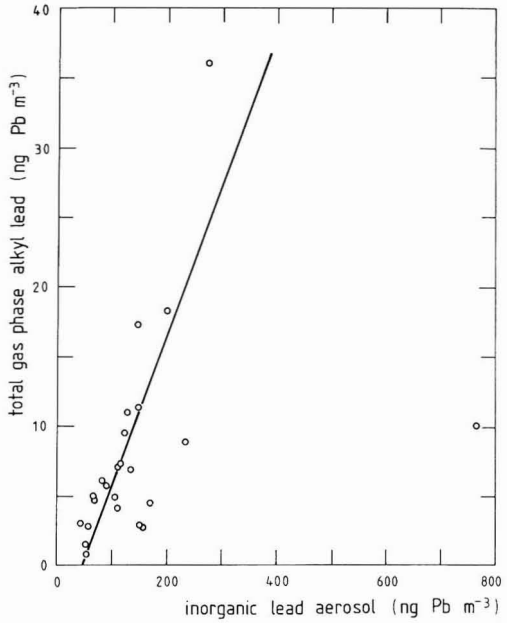

Figure 2. Total gas-phase alkyllead plot against inorganic lead aerosol at the urban (Colchester) site.

far more scattered ($r^2 = 0.32$), indicating advection of air masses of differing origins, travel time from major sources, and thus composition to this site.

A comparison of gas-phase total alkyllead at the two sites appeared to show some slight relationship and a ratio of concentrations of urban:semirural of ca. 2.4. The plot was, however, very scattered ($r^2 = 0.48$), and no direct relationship between the sites would be expected or was found. The inorganic lead data from the two sites plotted against one another showed even greater scatter.

In air samples collected at Adrigole, a remote site on the west coast of Ireland, tetraalkyllead compounds were generally below the detection limits (16–81 pg m^{-3} gas phase and 0.01–0.03 pg m^{-3} aerosol phase for individual compounds). Three out of eight gas-phase samples showed measurable Me_4Pb (up to 590 pg m^{-3}), and one had measureable Et_4Pb (1.05 ng m^{-3}). In no case was tetraalkyllead detected in the aerosol. Trialkyllead was consistently below the gas-phase detection limits (0.10–0.22 ng m^{-3} for individual compounds) and was detected only once in the aerosol (detection limits 0.03–0.05 pg m^{-3}) as trimethyllead (0.11 pg m^{-3}). Dimethyllead was consistently below detection limits in both gas phase (<0.15 ng m^{-3}) and aerosol (<0.03 pg m^{-3}). Diethyllead, however, was detected at concentrations up to 1.1 ng m^{-3} in the gas phase (three samples out of eight) and at concentrations from 0.12 to 0.31 pg m^{-3} in all three aerosol samples. An analytical peak apparently corresponding to monoalkyllead, RPb^{3+}, occurred in one gas-phase sample (1.7 ng m^{-3}) and two aerosol samples (up to 0.25 pg m^{-3}).

Alkyllead compounds were observed in sediment from a nearby beach (*17*), and the production of R_3Pb^+, R_2Pb^{2+}, and what may be RPb^{3+} compounds by sea algae has recently been investigated (*18*). The existence of monoalkyllead, RPb^{3+}, in the environment is highly improbable due to its known instability, and the apparent existence of these species in the analysis is very likely due to an analytical artifact (*19*). If so, it arises from rearrangement of other species (probably trialkyllead) during the analysis. It has been included in the estimation of total alkyllead in this study and any underestimation of concentrations because of its formation is likely to be small (*19*).

The presence of volatile R_4Pb compounds in the atmosphere is well established, and concentrations reported at a variety of sites have been reviewed (*1*, *20–22*). Me_3Pb^+ has been previously reported in the atmospheric gas phase (*23*), and in this study the presence of other R_3Pb^+ species has been noted. Vapor-phase R_3Pb^+ compounds may result from gas-phase decomposition of R_4Pb species (*4*) or direct vehicular emissions (*22*). The presence of R_3Pb^+ species containing mixed alkyl groups (Me_2EtPb^+ and $MeEt_2Pb^+$) was observed in some gas-phase and aerosol samples in this study. It may be assumed that these species result from the atmospheric decomposition of mixed methyl–ethyl containing R_4Pb compounds (Me_3EtPb, Me_2Et_2Pb, and $MeEt_3Pb$) by analogy with Me_4Pb and Et_4Pb species. Vapor-phase R_3Pb^+ compounds also decompose in the atmosphere by reaction with OH radicals, but the reaction rate is considerably slower than for R_4Pb. Half-lives of 126 h for Me_3Pb^+, 34 h for Et_3Pb^+, 41 h for Me_4Pb, and 8 h for Et_4Pb were recently predicted for reaction with OH radical in the atmosphere (*4*). These values suggest that R_3Pb^+ compounds, in particular Me_3Pb^+, may be advected to areas distant from vehicular sources, as they form from R_4Pb in the atmosphere. Alkyllead compounds may be adsorbed on the surfaces of atmospheric particles where decomposition may proceed (*3*), but as was already pointed out, aerosol forms play only a minor role in the atmospheric cycle of organic lead.

Deposition. The term "bulk deposition" was chosen to describe the samples because in addition to alkyllead compounds in rainwater, dry deposition of alkyllead vapor and aerosols may also contribute to the measurements.

Bulk collectors have been very widely used in deposition surveys and hence the data will be comparable with those from many other studies (e.g., ref 24 and 25). The contribution of dry deposition of aerosol alkyllead to total alkyllead deposition is likely to be very small, due to the low abundance of alkyllead in the aerosol. The vapor-phase component of deposition to the collector cannot be estimated, but some adsorptive collection is possible. This would lead to an overestimation of alkyllead deposition but is likely to be small or insignificant in this work since the ratios of alkyllead concentrations in air and in deposition at the urban and rural sites differ substantially.

Alkyllead compounds were identified in all the bulk deposition samples collected in this study, and the results of the analysis are given in Table IV. Simultaneous measurements were made at the urban and semirural sites. No R_4Pb species were found in any of these deposition samples, and this may be due to their rapid decomposition in rainwater. R_4Pb compounds are completely converted to the more stable R_3Pb^+ forms within 48 h unless special measures are taken to preserve them in collected samples (*6*). R_3Pb^+, R_2Pb^{2+}, and what appear to be RPb^{3+} species were identified in the deposition samples, and these compounds were also reported in bulk-deposition samples recently by another group of workers (*8*). Ionic alkyllead species are very stable in collected samples stored in the dark (*6*). The concentrations of organic lead measured in snow are similar to those found in rainwater as shown in Table VI and in a previous study (*8*). The ratios of total alkyllead to inorganic lead are also given in Table IV indicating that organic lead is only a minor component. In a recent study of rainwater samples collected in West Germany, it was reported that Et_3Pb^+ accounted in some cases for >50% of the total lead, and it was proposed that

Table IV. Alkyllead Compounds and Inorganic Lead in Bulk Deposition

date	site	ng of Pb L^{-1}								inorganic lead	alkyl/ inorganic, %
		R_4Pb[b]	Me_3Pb^+	Me_2EtPb^+	$MeEt_2Pb^+$	Et_3Pb^+	Me_2Pb^{2+}	Et_2Pb^{2+}	RPb^{3+}[f]		
7–8.1.86	urban	–[c]	8.6	–	–	40.4	–	14.3	7.8	18000	0.4
	semirural	–	10.4	4.4	–	46.0	5.1	16.8	2.2	16000	0.5
8–21.1.86	urban	–	41.2	–	–	68.7	–	164	164	NA[e]	NA
	semirural	–	47.6	–	–	63.5	–	127	127	2000	18.2
21–28.1.86	urban	–	14.1	5.0	–	22.2	5.0	20.8	28.7	24000	0.4
	semirural	–	15.5	5.9	–	28.4	5.9	17.7	17.7	3000	3.0
28.1–3.2.86	urban	–	56.5	–	–	67.8	22.6	67.8	33.9	51000	0.5
	semirural	–	39.3	–	–	65.6	19.7	59.0	32.8	63000	0.3
7.2.86	urban (snow)	–	111.1	–	–	55.5	–	119	39.7	116000	0.3
	semirural (snow)	–	20.0	–	–	10.0	–	20.0	30.0	22000	0.4
9–11.3.86	rural[d]	–	0.68	–	–	–	1.24	3.41	6.70	–	>0.9
11–12.3.86	rural[d]	–	0.92	0.84	0.84	0.28	–	1.40	2.80	–	>0.5
12–15.3.86	rural[d]	–	0.23	–	–	–	–	0.60	2.03	–	>0.2
15–16.3.86	rural[d]	–	2.04	–	–	–	4.96	2.17	3.72	–	>1.0
dl[d]	rural	0.02–0.06	0.06	0.08	0.10	0.12	0.08	0.20	0.20	1280	

[a] Urban, Colchester, U.K.; semirural, Essex University, U.K.; rural, Adrigole, Republic of Ireland. [b] Me_4Pb, Me_3EtPb, Me_2Et_2Pb, $MeEt_3Pb$, and Et_4Pb. [c] Below detection limits. [d] Detection limits for urban and semirural samples are the same as those cited in Table II. [e] NA = not available. [f] Tentative assignment, see text.

Table V. Deposition Rates of Alkyllead and Inorganic Lead

site	deposition rate, ng of Pb cm^{-2} $month^{-1}$ [a]	
	alkyllead	inorganic lead
urban	1.1	217
semirural	0.7	98.7

[a] Average of measurements in the period 7 January to 3 February 1986.

alkyllead species in deposition may be responsible for the observed damage to forests (*10*). The authors, however, employed a nonspecific biochemical technique, and their results have been disputed (*7*). Ionic alkyllead compounds observed in the deposition samples may result from washout and rainout of water-soluble gas-phase R_3Pb^+ and R_2Pb^{2+}, scavenging of atmospheric aerosols containing alkyllead species, and the aqueous decomposition in rainwater of scavenged R_4Pb species (*6*). The same ionic alkyllead species were also found in deposition collected at the remote rural site on the west coast of Ireland although the concentrations were considerably lower than those measured in the U.K. deposition.

Deposition rates estimated for the urban and semirural sites are compared in Table V. Washout factors for total alkyllead and inorganic lead were evaluated for the two sites, and the results appear in Table VI. Since earlier work had shown rapid conversion of tetraalkyllead in freshly collected rainwater (*5*, *6*), it was not possible to calculate washout factors for individual alkyllead compounds, and thus a single value for total alkyllead is presented for each sampling period. This value should be useful in predicting total alkyllead behavior but does not assist the comprehension of the behavior of individual species. In line with other studies (*24*, *25*), washout factors are very variable, although the values for inorganic lead agree well with those from an earlier study in northwestern England (*24*), which reported a range of 53–830 and a mean of 320 for lead. The generally lower values of washout factor for alkyllead than for inorganic lead are indicative of less efficient scavenging of the former species. It is quite possible, however, that the water-soluble trialkyllead compounds make up a disproportionate component of the scavenged alkyllead relative to the far less soluble tetraalkyllead species. It should be noted that the washout factors have been calculated from samples collected over

Table VI. Values of Washout Factor, *W*, for Total Alkyllead and Inorganic Lead at an Urban and Semirural Site

date, 1986	washout factor, W[a]			
	urban		semirural	
	alkyllead	inorganic lead	alkyllead	inorganic lead
7–8.1	12	187	30	141
8–21.1	51		104	24
21–28.1	8	93	33	47
28.1–3.2	79	633	99	1141
mean	38	304	66	338

[a] W = lead in rainwater, ng of Pb kg^{-1}/lead in air, ng of Pb kg^{-1}. 1 m^3 of air = 1.226 kg at 15 °C, 1 atm.

several days, and thus represent a composite of different air masses and include periods during which no rain fell but air-sample collection continued. Because of this fact and the use of total deposition samplers, the washout factors must be treated with some caution as they are not strictly comparable with data collected over short-time intervals using wet-only collectors. They are, however, comparable with many other data sets that have been collected in a similar manner (e.g., ref 24) and provide a time-averaged representation of alkyllead behavior. They also serve to provide a useful comparison of the behavior of alkyllead and inorganic lead.

Total alkyllead deposition fluxes for the urban and semirural sites are plotted against one another in Figure 3. These are very highly correlated and show a ratio of approximately 1.45 in favor of the urban site, far lower than the ratio of gas-phase alkyllead concentrations, confirming the minor importance of dry deposition to the collector. This behavior is indicative of the major proportion of alkyllead scavenging taking place at a considerable altitude, such that intersite differences are minimized on a small geographic scale.

Conclusions

Total alkyllead correlates strongly with inorganic lead at the urban site, indicating a common vehicular source. At a semirural site 3.6 km distant, the correlation is far weaker, suggesting the influence of air masses of differing origins in which sink processes have removed alkyllead and

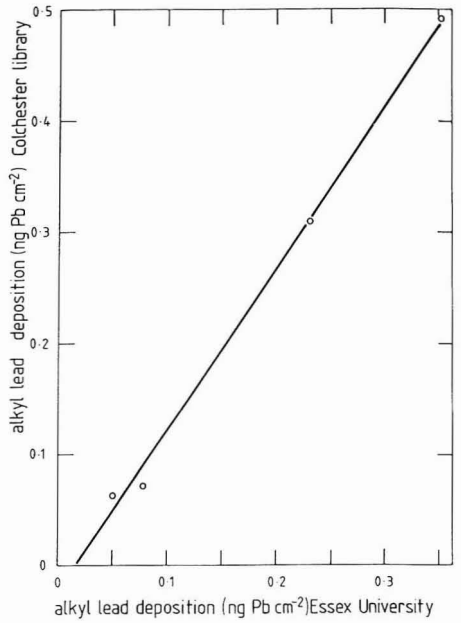

Figure 3. Plot of total alkyllead deposition during each sampling interval at urban (Colchester) and semirural (University) sites.

inorganic lead at different rates. Concentrations of alkyllead at the remote Adrigole site on the west coast of Ireland are mostly below the detection limit of the analytical procedure.

Washout of total alkyllead is less efficient than for inorganic lead. This is probably due to the predominant occurrence of alkyllead as gas-phase tetraalkyllead, which leads to less effective scavenging than for aerosol inorganic lead. If alkyllead is indeed removed from the atmosphere more slowly than inorganic lead (assuming inefficient dry deposition), the elevated ratios of total alkyllead to inorganic lead in maritime air relative to those typical of continental air (*26*) may arise partly as a result of this influence, although the generally lower rainfall at sea than over land would have a contrary influence.

Registry No. Me_4Pb, 75-74-1; Me_3EtPb, 1762-26-1; Me_2Et_2Pb, 1762-27-2; $MeEt_3Pb$, 1762-28-3; Et_4Pb, 78-00-2; Me_3Pb^+, 14570-16-2; Me_2EtPb^+, 103730-90-1; $MeEt_2Pb^+$, 105956-70-5; Et_3Pb^+, 14570-15-1; Me_2Pb^{2+}, 21774-13-0; Et_2Pb^{2+}, 24952-65-6; Pb, 7439-92-1.

Literature Cited

(1) Radojević, M.; Harrison, R. M. *Sci. Total Environ.* **1987**, *59*, 157–180.
(2) Harrison, R. M.; Laxen, D. P. H. *Nature (London)* **1978**, *275*, 730–740.
(3) Harrison, R. M.; Laxen, D. P. H. *Environ. Sci. Technol.* **1978**, *12*, 1384–1392.
(4) Hewitt, C. N.; Harrison, R. M. *Environ. Sci. Technol.* **1986**, *20*, 797–802.
(5) Harrison, R. M.; Radojević, M.; Wilson, S. J. *Sci. Total Environ.* **1986**, *50*, 129–137.
(6) Radojević, M.; Harrison, R. M. *Atmos. Environ.* **1987**, *21*, 2403–2411.
(7) Unsworth, M. H.; Harrison, R. M. *Nature (London)* **1985**, *317*, 674.
(8) Van Cleuvenbergen, R. J. A.; Chakraborti, D.; Adams, F. C. *Environ. Sci. Technol.* **1986**, *20*, 589–593.
(9) Radojević, M.; Harrison, R. M. *Environ. Technol. Lett.* **1986**, *7*, 519–524.
(10) Faulstich, H.; Stournaras, C. *Nature (London)* **1985**, *314*, 714–715.
(11) Hewitt, C. N.; Harrison, R. M. *Anal. Chim. Acta* **1985**, *167*, 277–287.
(12) Harrison, R. M.; Radojević, M. *Environ. Technol. Lett.* **1985**, *6*, 129–136.
(13) Harrison, R. M.; Radojević, M.; Hewitt, C. N. *Sci. Total Environ.* **1985**, *44*, 235–244.
(14) Hewitt, C. N.; Harrison, R. M.; Radojević, M. *Anal. Chim. Acta* **1986**, *188*, 229–238.
(15) Potter, H. R.; Jarvie, A. W. P.; Markall, R. N. *Water Pollut. Control (Maidstone, Engl.)* **1977**, *76*, 123–128.
(16) Radojević, M.; Allen, A.; Rapsomanikis, S.; Harrison, R. M. *Anal. Chem.* **1986**, *58*, 658–661.
(17) Radojević, M.; Harrison, R. M. *Environ. Technol. Lett.* **1986**, *7*, 525–530.
(18) Radojević, M.; Allen, A.; Harrison, R. M. University of Essex, unpublished data, 1985.
(19) Van Cleuvenbergen, R. J. A.; Chakraborti, D.; Adams, F. C. *Anal. Chim. Acta* **1986**, *182*, 239–244.
(20) Harrison, R. M.; Perry, R. *Atmos. Environ.* **1977**, *11*, 847–852.
(21) De Jonghe, W. R. A.; Adams, F. C. *Talanta* **1982**, *29*, 1057–1067.
(22) Nielsen, T. In *Biological Effects of Organolead Compounds*; CRC: Boca Raton, Fl, 1984; pp 43–62.
(23) Hewitt, C. N.; Harrison, R. M. *Proceedings of the International Conference on Heavy Metals in the Environment*; C.E.P. Consultants: Edinburgh, 1985; pp 171–173.
(24) Harrison, R. M.; Williams, C. R. *Atmos. Environ.* **1982**, *16*, 2669–2681.
(25) Cawse, P. A. *U.K. Atomic Energy Authority Report AERE-R9164*; HMSO: London, 1978.
(26) Hewitt, C. N.; Harrison, R. M. *Environ. Sci. Technol.* **1987**, *21*, 260–266.

Received for review February 24, 1987. Accepted October 6, 1987.

Environ. Sci. Technol. 1988, 22, 523–526

Nature and Properties of Some Chlorinated, Lipophilic, Organic Compounds in Spent Liquors from Pulp Bleaching. 1. Liquors from Conventional Bleaching of Softwood Kraft Pulp†

A. Bruce McKague,* Marie-Claude Kolar, and Knut P. Kringstad

STFI (Swedish Pulp and Paper Research Institute), Box 5604, S-114 86 Stockholm, Sweden

■ A sample of spent chlorination liquor from the bleaching of softwood kraft pulp was fractionated to isolate the chlorinated lipophilic compounds. These were investigated by gas chromatography and gas chromatography/mass spectrometry, and a number were identified as chlorinated diones and enol lactones. The compounds were found to be weakly mutagenic and to have limited potential for bioaccumulation. Quantities ranged from <1 to 72 g/ton of pulp. At pH 7 and room temperature, these compounds were found to be relatively unstable and to decompose.

Introduction

During the conventional bleaching of chemical pulps, between 45 and 90 kg of organic material/ton of pulp is dissolved in the bleaching liquors (*1*). Much of the dissolved material is chlorinated, and in the case of softwood kraft pulp, about 5 kg of organically bound chlorine/ton of pulp is produced (*1*). As a result of studies performed in recent years, more information is now available on the composition and biological effects of spent bleach liquors (*1–3*). Thus, it is known that such liquors exert weak acute toxic and genotoxic effects (Ames test) and that several compounds which are responsible for such effects have been identified. Most of the toxic compounds are chemically rather unstable and biodegradable.

However, one area that needs further investigation concerns the existence and properties of lipophilic compounds in spent bleach liquors. This subject is of importance from an environmental point of view since such compounds have the potential for bioaccumulation in aquatic organisms and in food chains.

Previous investigations have shown that chlorinated phenols, catechols, and guaiacols originating from pulp bleaching accumulated in fish living in the vicinity of pulp mill outlets (*4*, *5*) and dichloromethyl methyl sulfone, a compound often present in spent bleach liquors, have been found in fish and mussels (*6*). Recently, new chromatographic methods have been developed to evaluate the lipophilic character of organic compounds (*7–9*). Reverse-phase thin-layer chromatography (RPTLC) has been found to be a rapid method for estimating P values, indicators of lipophilicity. This paper presents initial results arising from the incorporation of the RPTLC technique into systematic investigations aimed at identifying and characterizing additional chlorinated lipophilic compounds present in spent bleach liquors.

Experimental Section

Spent Chlorination Liquor. An industrially prepared unbleached softwood kraft pulp having a κ number of 37.7 was used to prepare the spent chlorination liquor. The κ number is a measure of the lignin content of pulp, higher numbers indicating greater amounts of lignin. The pulp was atypical of pulps produced in most mills in Sweden that now employ oxygen prebleaching to reduce the κ number prior to bleaching with chlorine. The pulp was bleached at 3.5% pulp consistency at room temperature with 7.5% chlorine charge on pulp for 1 h and then filtered to give the liquor having a pH of 1.5.

Isolation and Identification of Lipophilic Compounds. The liquor was extracted with hexane (3 × 100 mL). The extracts were combined, washed with saturated NaCl solution (50 mL) and water (50 mL), and dried with anhydrous magnesium sulfate. The solvent volume was reduced to 0.2–0.3 mL. Quantification of lipophilic compounds was done on the hexane concentrate by gas chromatography/mass spectrometry (GC/MS) with anthracene as the internal standard according to the conditions described below. The concentrated hexane extract above was applied to a RPTLC plate (10 cm × 10 cm) and developed with acetone/H_2O (80:20). The portion of the plate containing material with R_f < benzophenone was recovered and extracted with hexane. The extract was concentrated and analyzed initially by gas chromatography/electron capture detection (GC/ECD) with a 30-m fused-silica capillary OV 101 column. Temperature was held at 170 °C for 4 min and then programmed to 270 °C at 10 deg/min. The extract was also analyzed by GC/MS with a Finnigan TSQ-46C mass spectrometer system. Splitless injections were made with a J&W Scientific (Cordova, CA) fused-silica capillary column, 30 m × 0.245 mm i.d. Temperature was programmed from 50 to 270 °C.

The recovered RPTLC material was further fractionated on SiO_2 (0.5 g), eluting with 2.5-mL fractions of hexane/CH_2Cl_2 (9:1), hexane/CH_2Cl_2 (4:1), hexane/CH_2Cl_2 (1:1), CH_2Cl_2, CH_2Cl_2/methanol (9:1), and methanol. Fractions were concentrated with N_2 and analyzed by GC/ECD and GC/MS as described above. Retention times of chlorinated enol lactones were confirmed by mixed injections with standards prepared as described below.

Chemical Standards. Perchlorocyclopentene-1,3-dione (**1**) was obtained commercially from K & K Laboratories, Plainview, NY, and recrystallized from hexane.

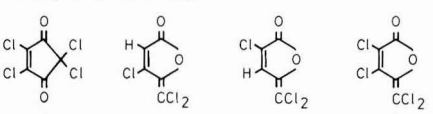

1 **2a** **2b** **3**

The trichloro enol lactone **2a** was prepared by adding a 3.5 mole ratio of Cl_2 buffered to pH 7 with phosphate buffer to a stirred solution of aqueous resorcinol (*10*). After being stirred overnight at pH 6.5–7.0, the mixture was acidified with HCl and extracted with ether. The extract was washed with saturated NaCl and water and then dried with anhydrous $MgSO_4$. The brown oil obtained after evaporation of the ether was fractionated on SiO_2. Residual resorcinol was eluted with hexane/ether (1:1) and the product with the same solvent and ether. The product was heated in a bath at 130 °C for 30 min and, after cooling, extracted with ether. The ether was evaporated

† This paper is based on a paper presented at the Fourth International Symposium on Wood and Pulping Chemistry, Paris, France, April 1987.

0013-936X/88/0922-0523$01.50/0

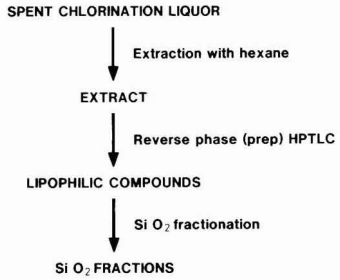

Figure 1. Scheme for concentration and identification of lipophilic compounds.

and the product purified on SiO_2 by elution with hexane/CH_2Cl_2 (4:1). Crystallization from ether/hexane gave pale yellow crystals, approximately 200 mg from 4.4 g of resorcinol, mp 67–68.5 °C, having identical spectral properties to those reported for a chlorination product of resorcinol (*10*). ^{13}C NMR ($CDCl_3$) δ: 113.9 (C5), 119.8 (C3), 143.5 (C4 or C6), 145.5 (C4 or C6), 162.6 (C2).

The trichloro enol lactone **2b** was prepared by chlorination of softwood kraft lignin that had been precipitated from a partly evaporated industrial kraft black liquor by addition of dilute sulfuric acid at 80 °C to pH 9.5. Chlorine water (2.9 L, containing 18.8 g, 0.265 mol of Cl_2) was added to a stirred suspension of 10 g of the lignin in 2.5 L of water in an amber bottle. After being stirred 1 h at pH 1.5, the liquor was allowed to settle for 2 h. The clear supernatant was transferred to a separatory funnel and extracted with hexane (3 × 100 mL). The extracts from five chlorinations were combined, washed with saturated NaCl (100 mL), and concentrated to 0.5 mL. Fractionation on 4 g of SiO_2 and elution with hexane/CH_2Cl_2 (4:1) gave 0.25 mg of pure lactone, mp 98–99 °C, as colorless needles. UV (hexane) λ_{max} 305 nm; ^1H NMR ($CDCl_3$) δ 7.62 (s). MS (70 eV), *m/z* (rel intensity, %): 202 (35) ($M^+ + 4$), 200 (90) ($M^+ + 2$), 198 (100) (M^+), 170 (15), 142 (10), 110 (15). A total synthesis of this enol lactone has also been completed recently and will be described in a separate publication.

The tetrachloro enol lactone **3** was prepared from 3,4-dichloro-5-(dichloromethyl)-5-hydroxy-2-furanone by treatment with 20% oleum as described in the literature (*11*). Spectral properties agreed with reported values. ^{13}C NMR ($CDCl_3$) δ: 114.9 (C5), 124.6 (C3), 139.4 (C4 or C6), 141.6 (C4 or C6), 159.2 (C2). MS (70 eV), *m/z* (rel intensity, %): 236 (50) ($M^+ + 4$), 234 (100) ($M^+ + 2$), 232 (75) (M^+), 180 (25), 178 (60), 176 (50), 143 (25), 141 (25), 112 (20), 110 (35), 87 (50).

Mutagenicity Tests. Ether solutions (20 μL/plate) of the synthesized compounds were tested for mutagenicity by using the Ames test (*12*).

Salmonella typhimurium TA 100 and TA 98 were used without metabolic activation. All test values reported are mean values of six plates. Quercetin dihydrate (Fluka AG) was used as a positive control for the two strains.

Determination of the Bioaccumulation Potential. The determination of the bioaccumulation potential was carried out by the method based on RPTLC giving $R_M°$ (*7–9*).

Stability Tests. An ether solution (1 mL) containing 5 mg of each of the compounds **1**, **2a**, **2b**, and **3** was added to a mixture of H_2O (400 mL) and pH 7 phosphate buffer (100 mL). The resultant solution was stirred at room temperature at pH 6.5–7.0, and aliquots (100 mL) were removed periodically for analysis. Naphthalene (0.2 mg) was added to each aliquot as an internal standard, and the aliquot was extracted with ether, washed once with H_2O,

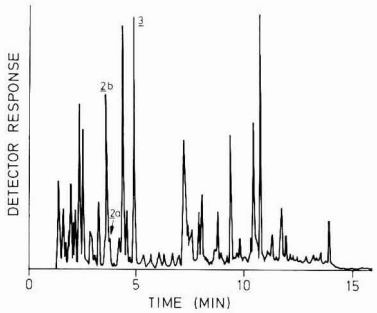

Figure 2. GC/ECD chromatogram of extract containing lipophilic compounds.

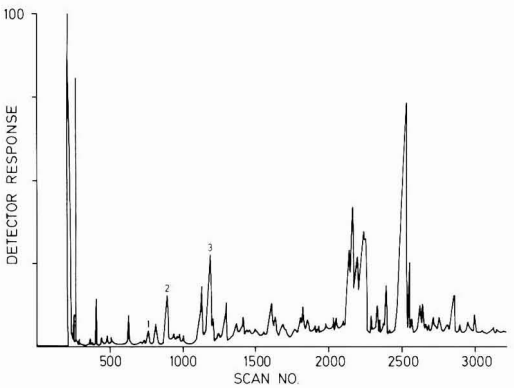

Figure 3. GC/MS of extract containing lipophilic compounds.

and dried. After concentration to 1 mL, the extract was analyzed by GC at 130 °C.

Results and Discussion

Basically, a three-step procedure was used for the concentration and identification of lipophilic compounds in the liquor (Figure 1). Extraction with hexane was used as a preliminary step to separate nonpolar material from the large number of more polar compounds present. Further concentration of the lipophilic material by RPTLC gave material of equal or greater lipophilicity than benzophenone, $R_M°$ value 3.18 (*13*). After concentration of the extract, it was analyzed by gas chromatography/mass spectrometry. Further fractionation on SiO_2 was intended to be optional, depending on the complexity of the extract from RPTLC, and was to provide fractions containing fewer components.

Preliminary analysis by GC/ECD of material recovered by RPTLC showed the presence of a number of chlorinated compounds (Figure 2). Molecular ion isotope and fragmentation patterns indicated that the recovered material contained at least 20 chlorinated compounds. Three of these (peaks 1–3, Figure 3) gave mass spectra suggestive of cyclopentenediones (*14*). Two of these had a molecular weight of 232 and contained 4 chlorine atoms (peaks 1 and 3), and one had a molecular weight of 198 and contained 3 chlorine atoms (peak 2).

Cyclopentenediones have previously been reported in spent chlorination liquor (*14*, *15*) and 3,5,5-trichlorocyclopentene-1,2-dione has been identified as the most likely structure for a product of the chlorination of humic acid (*16*) and resorcinol (*10*). Also perchlorocyclopentene-1,3-dione has been identified in spent chlorination liquor and is formed in the chlorination of kraft lignin,

Table I. Quantities of Perchlorocyclopentene-1,3-dione (1) and Enol Lactones 2a, 2b, and 3 Produced in the Chlorination of a Softwood Kraft Pulp

compound	g/metric ton of pulp
1	72
2a	0.8
2b	4.9
3	0.3

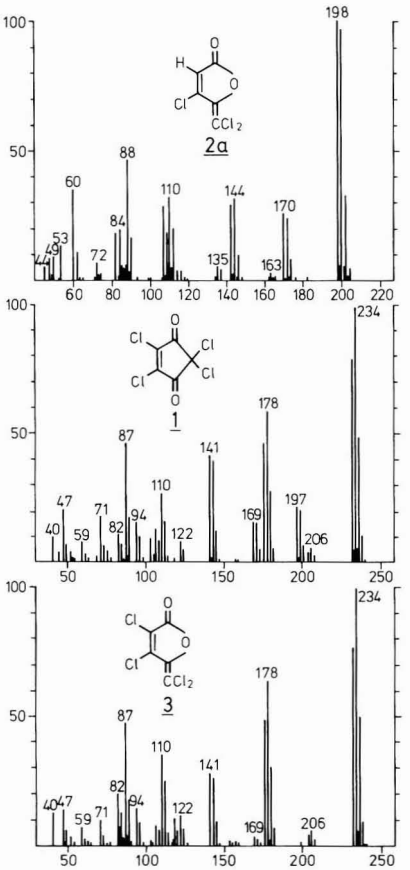

Figure 4. Mass spectra of enol lactones **2a** and **3** and perchlorocyclopentene-1,3-dione (**1**).

tetrachlorocatechol, and tetrachloro-σ-benzoquinone (*17*). Peak 1 in the total ion chromatogram in Figure 3 was identified as **1** by comparison of the retention time and mass spectrum with the standard. Although **1** is less lipophilic than benzophenone, complete separation from more lipophilic material by RPTLC was difficult since a large amount of this compound is present (see Table I).

When the material recovered from RPTLC was fractionated on SiO_2, the components representing peaks 2 and 3 (Figure 3) eluted with hexane/CH_2Cl_2 (4:1 and 1:1). Peak 2 was found to be a mixture of two components, a major and a minor, that both gave the same trichlorocyclopentenedione-type mass spectra. For final identifications and for characterizations of chemical properties and biological effects, methods available from the literature were used to synthesize some of the possible compounds present.

Chlorination of resorcinol with a 3.5 mole ratio of chlorine at pH 7 gave a product whose mass spectrum (Figure 4) was the same as that of either component of peak 2. Carbonyl absorption was present in the infrared spectrum at 1780 cm^{-1}. The UV maximum in hexane or methanol occurred at 295 nm, and the ^{13}C NMR revealed that the compound contained only one carbonyl group. No signal was present in the ^{13}C NMR in the region of 70–90 ppm where expected for a carbon bearing 2 chlorine atoms adjacent a carbonyl group (*18*). A single proton was present at 6.39 ppm in the ^{1}H NMR. Altogether, these observations and comparison with spectral data from other compounds in this study indicated that the product from resorcinol was the previously unreported enol lactone **2a**. This was identical with the minor of the two components of peak 2.

The spectral data of the major component of peak 2 were consistent with those of the enol lactone **2b**, isomeric with **2a**. A small amount of **2b** was initially obtained by the chlorination of kraft lignin, and subsequently larger amounts were obtained by a total synthesis to be described later.

The compound responsible for peak 3 (Figure 3) was identified as the enol lactone **3** by comparison with synthetic material. Thus, all three compounds in the SiO_2 fraction giving cyclopentenedione-type spectra were enol lactones. The similarity in the mass spectra of isomeric compounds of this type is illustrated by the spectra of perchlorocyclopentene-1,3-dione and the enol lactone **3** (Figure 4).

The enol lactones in spent chlorination lignin probably originate from chlorinated cyclopentene-1,3-diones. Recently, the hydroxy lactone **4** was identified in spent chlorination liquor (*19*). This compound is formed (*19*) by hydrolysis of perchlorocyclopentene-1,3-dione (**1**), a constituent of fresh spent chlorination liquor (*17*), and undergoes dehydration to the enol lactone **3** with acid (*11*). Analogous reactions of 2,2,4-trichlorocyclopentene-1,3-dione (**5**) can yield both the trichloro enol lactones **2a** and

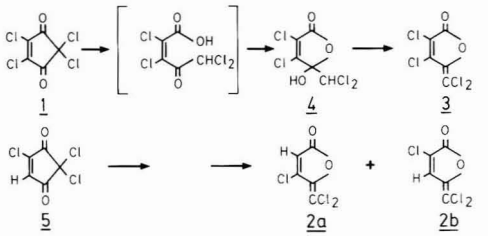

2b, and this reaction sequence has been incorporated into the total synthesis of **2b** to be reported later. A different mechanism is required to explain the formation of enol lactone **2a** from resorcinol.

Quantities of Enol Lactones. The quantities of the enol lactones **2a**, **2b**, and **3** formed in the chlorination of a softwood kraft pulp were measured by GC/MS analysis of hexane extracts of the spent chlorination liquor. A pulp with κ number 33 was used in these experiments. Results are shown in Table I. The quantity of perchlorocyclopentene-1,3-dione (**1**) formed is also shown for comparison, since this compound is probably the precursor of the furanone **4** and the enol lactone **3**. As can be seen, the quantities in the enol lactones are of the same order of magnitude as many of the chlorinated phenols or catechols normally found in spent chlorination liquor.

Mutagenicity and Potential for Bioaccumulation. An investigation of the lipophilic and mutagenic properties of compounds **2a**, **2b**, and **3** was carried out. The results (Table II) show that the compounds have weak potentials

Table II. Potential for Bioaccumulation and Mutagenicity of the Enol Lactones 2a, 2b, and 3

compd	$R_M°$ (log P_{ow}) value	net revertants/nmol of TA 100	net revertants/nmol of TA 98
2a	2.61	26	2
2b	2.58	25	*a*
3	3.42	36	*a*

[a] No significant mutagenic activity could be observed.

for bioaccumulation. Also, they show some mutagenic activity when tested with *Salmonella typhimurium* TA 100. Compared to other previously identified compounds of spent bleach liquors, these activities are similar to those of chloroacetones (*20*) but less than the activities of 2-chloropropenal (*21*) and 3-chloro-4-(dichloromethyl)-5-hydroxy-2(5*H*)-furanone (*22*). Enol lactone **2a** also showed mutagenic activity when tested with strain TA 98.

Chemical Stability. Perchlorocyclopentene-1,3-dione (**1**) disappeared from an aqueous solution at pH 7 in 1 h. This compound is known to be converted to the hydroxy lactone **4** under these conditions (*19*). Over 90% of the lactones **2b** and **3** had disappeared in 10 h and 100% in 24 h. However, after 24 h, 36% of the lactone **2a** was still present, and this compound did not disappear completely even after 48 h. The difference in stabilities of the lactones **2a**, **2b**, and **3** is interesting and suggests that the lactone **2a**, although found in smaller amounts than the isomer **2b** in this paper, may be more important from an environmental point of view.

Other Lipophilic Compounds. As mentioned earlier, GC/MS showed the presence of least 20 chlorinated lipophilic compounds in the spent bleach liquor investigated. This paper described the identification, synthesis, and evaluation of the properties of four of these compounds. Similar investigations to characterize the other compounds are in progress in this laboratory.

Conclusions

Spent liquors from the chlorination of softwood kraft pulp contain a number of chlorinated compounds with a potential for bioaccumulation. Identification and synthesis have shown that some of these are chlorinated enol lactones and diones. These show weak mutagenicity but are chemically unstable and decompose under receiving water conditions.

Acknowledgments

We received many valuable suggestions from Lars M. Strömberg during the course of the work. GC/MS work was done by Pierre Ljungquist.

Registry No. **1**, 15743-13-2; **2a**, 112654-67-8; **2b**, 112654-68-9; **3**, 31555-54-1.

Literature Cited

(1) Kringstad, K. P.; Lindström, K. *Environ. Sci. Technol.* **1984**, *18*, 236A.
(2) Lindström, K.; Nordin, J.; Österberg, F. In *Advances in the Identification and Analysis of Organic Pollutants in Water*; Keith, L., Ed.; Ann Arbor Science: Ann Arbor, MI, 1981; p 1039.
(3) Annergren, G.; Kringstad, K. P.; Lehtinen, K.-J. Presented at EUCEPA Symposium on Environmental Protection in the 90's, Helsinki, Finland, May 1984.
(4) Landner, L.; Lindström, K.; Karlsson, M.; Nordin, J.; Sörensen, L. *Bull. Environ. Contam. Toxicol.* **1977**, *18*, 663.
(5) "Environmentally Harmonized Production of Bleached Pulp" final report; The Swedish Forestry Industries Water and Air Pollution Research Foundation: Stockholm, Sweden, 1982.
(6) Lindström, K.; Schubert, R. *HRC CC, J. High Resolut. Chromatogr. Chromatogr. Commun.* **1984**, *7*, 68.
(7) Renberg, L. O.; Sundström, S. G.; Rosén-Olofsson, A.-C. *Toxicol. Environ. Chem.* **1985**, *10*, 333.
(8) Butte, W.; Fooker, C.; Klussman, R.; Schuller, D. *J. Chromatogr.* **1984**, *214*, 59.
(9) Kringstad, K. P.; de Sousa, F.; Strömberg, L. M. *Environ. Sci. Technol.* **1984**, *18*, 200.
(10) Boyce, S. D.; Hornig, J. F. *Environ. Sci. Technol.* **1983**, *17*, 202.
(11) Roedig, A.; Märkl, G. *Justus Liebigs Ann. Chem.* **1960**, *636*, 1.
(12) Maron, D. M.; Ames, B. N. *Mutat. Res.* **1983**, *113*, 173.
(13) Leo, A.; Hansch, C.; Elkins, D. *Chem. Rev.* **1971**, *71*, 525.
(14) Kringstad, K. P.; Ljungquist, P. O.; de Sousa, F.; Strömberg, L. M. *Environ. Sci. Technol.* **1981**, *15*, 562.
(15) Carlberg, G. E.; Drangsholt, H.; Gjös, N. *Sci. Total Environ.* **1986**, *48*, 157.
(16) Christman, R. F.; Johnsson, J. D.; Hass, J. R.; Pfaender, F. K.; Liao, W. T.; Norwood, D. L.; Alexander, H. T. In *Water Chlorination: Environmental Impact and Health Effects*; Jolley, R. L., Ed.; Ann Arbor Science: Ann Arbor, MI, 1978; Vol. 2, p 15.
(17) McKague, A. B.; de Sousa, F.; Strömberg, L. M.; Kringstad, K. P. *Holzforschung* **1987**, *41*, 191.
(18) Hawks, G. E.; Smith, R. A.; Roberts, J. D. *J. Org. Chem.* **1974**, *39*, 1276.
(19) Strömberg, L. M.; de Sousa, F.; Ljungquist, P.; McKague, B.; Kringstad, K. P. *Environ. Sci. Technol.* **1987**, *21*, 754.
(20) Bull, R. J.; Robinson, M. In *Water Chlorination: Environmental Impact and Health Effects*; Jolley, R. L., Ed.; Lewis: Chelsea, MI, 1985; Vol. 5, p 221.
(21) Kringstad, K. P.; Ljungquist, P. O.; de Sousa, F.; Strömberg, L. M. In *Water Chlorination: Environmental Impact and Health Effects*; Jolley, R. L., et al.; Eds.; Ann Arbor Science: Ann Arbor, MI, 1983; Vol. 4, p 1311.
(22) Holmbom, B. R.; Voss, R. H.; Mortimer, R. D.; Wong, A. *Environ. Sci. Technol.* **1984**, *18*, 333.

Received for review May 11, 1987. Accepted November 4, 1987. This investigation received support from the Environmental Research Foundation of the Swedish Pulp and Paper Association, Project "Environment 90—project 1—Bleaching Effluents".

Environ. Sci. Technol. 1988, 22, 527-531

Rainwater Analysis: A Comparison between Proton-Induced X-ray Emission and Graphite Furnace Atomic Absorption Spectroscopy†

Hans-Christen Hansson,*,‡,§ Ann-Kristin P. Ekholm,‡ and Howard B. Ross§

Department of Nuclear Physics, University of Lund, Sölveg. 14, S-22 362 Lund, Sweden, and Department of Meteorology, University of Stockholm Arrhenius Laboratory, S-106 91 Stockholm, Sweden

■ Rainwater was collected and analyzed for trace metals by graphite furnace atomic absorption spectroscopy (GFAAS) and proton-induced X-ray emission (PIXE). For the PIXE analysis, a nonselective preconcentration technique was used to dry the samples onto polystyrene films. Good agreement was found in the concentrations for the elements determined in common (Cu, Fe, Mn, Pb, and Zn), even though the PIXE analysis had some problems with sample contamination. An advantage of the PIXE analysis is that 26 elements can be determined simultaneously. The elements P, S, K, Ca, V, Mn, Fe, Ni, Zn, As, Br, and Pb had concentrations significantly higher than the chemical blank and detection limits and thus could be routinely analyzed by PIXE. The technique is promising for the other elements Ti, Cr, Co, Cu, Ga, Ge, Se, Rb, and Sr because considerable improvements in detection limits can be achieved by lowering the content of the blank and by increasing the analysis time.

Introduction

With the advent of industrialization, the atmosphere, via wet and dry deposition, has become a major source of trace metals to ecosystems in and around industrial areas. Trace metals such as Cd, Hg, As, and Pb, which are highly toxic even at low levels, are known to be accumulating in the biosphere and are to a great extent cycled through the environment by atmospheric transport (*1–5*). In addition, Cd and Pb even have been investigated as possible causes of forest decline in Europe and the United States (*6*). Around anthropogenic point sources such as smelters, atmospheric deposition of Cr, Cu, Ni, and Zn has led to adverse affects to forest ecosystems (*7, 8*). It is primarily for these toxicological reasons that interest has grown in monitoring trace metal concentrations in atmospheric precipitation.

By far the most popular instrumental method for determining trace metals in atmospheric precipitation and even other natural water samples is graphite furnace atomic absorption spectroscopy (GFAAS) (*9*). Many trace metals in atmospheric precipitation can be analyzed without preconcentration. With the advent of computer-controlled autosamplers, preconcentration is even less of a problem and can now be performed directly in the furnace. This saves much time. Still, the major drawback with most commercial GFAAS instruments is that only one element at a time can be analyzed.

Another spectroscopic technique, inductively coupled plasma (ICP), is multielement but sensitivities are generally too low for natural water sample determinations (*10*). Therefore, samples may need to be preconcentrated. Recent advances in the interfacing of mass spectrometers with ICP and graphite furnaces offer promising multielemental techniques with very low detection limits (*11, 12*). However, commercial availability of such instrumentation is in its infancy.

Techniques such as X-ray fluorescence, instrumental neutron activation analysis (INAA), and proton-induced X-ray emission (PIXE) can simultaneously determine a large number of trace metals in a single analysis. These techniques have been used extensively in determining trace metal concentrations in atmospheric aerosol samples (*13–20*). INAA has also been used to determine trace metal concentrations in natural water samples; the analysis, however, requires preconcentration of the sample onto a solid substrate such as activated carbon or filter paper (*21–23*).

In PIXE analysis as well as with INAA, one can not directly analyze water samples but must first preconcentrate the sample onto a solid substrate (*24*). Recently, we reported a nonselective preconcentration technique for PIXE analysis of water samples, which is simple and quick (*25*). The liquid is forced through a nebulizer and pressurized air into a dry clean airstream where the droplets evaporate. The solid residual aerosol is collected by an impactor on a thin polystyrene film. The film is then analyzed by PIXE. This technique is similar to the one used by Kellogg et al. (*26*) for the analysis of solutions with X-ray fluorescence analysis. In this paper, we report a comparison between GFAAS and PIXE using this preconcentration technique for the analysis of rainwater. The two laboratories involved in this study have much experience and expertise in the analytical methods they use respectively.

Experimental Section

In October 1984, monthly precipitation samples for trace metal analysis were collected at four sites in Sweden (Figure 1) as part of the SNV–PMK (The National Swedish Environmental Protection Board–Environmental Monitoring Program). At each site there were five acid-washed rain collectors. Rain collectors were of funnel and bottle type and are constructed out of conventional polyethylene. They were placed 1 m from the ground and in open fields, at least 10 m from the nearest tree. The maximum distance between collectors did not exceed 40 m. Sampling locations were at least 500 m from the nearest road and 200 m from the nearest building (*27–29*).

For GFAAS analysis, the samples arrived at the University of Stockholm Rain Chemistry Laboratory and were acidified to pH ≈1.0 with concentrated HNO_3 (supra-pur, Merck A.G.) to prevent adsorption onto the container walls. Cd, Cu, Fe, Mn, Pb, and Zn were then determined by GFAAS. A detailed description of collection and analytical methodologies to avoid sample contaminations is given by Ross (*27–29*).

For PIXE analysis, 50 mL of the samples was poured into ultraclean conventional polyethylene bottles in a metal-free clean room. Previous studies indicate that these bottles do not appreciably effect metal concentrations. Samples were then sealed in two plastic bags and sent to

† This paper is Contribution No. 573 from the University of Stockholm Arrhenius Laboratory.

‡ University of Lund.

§ University of Stockholm Arrhenius Laboratory.

0013-936X/88/0922-0527$01.50/0

Table I. Arithmetic Mean Trace Metal Concentrations ($\mu g\ L^{-1}$) for Each Sampling Site and Associated Standard Deviations Determined with GFAAS[a]

	sampling site			
	Aspvreten	Arup	Bredkälen	Liehittäjä
Mn	3.8 ± 0.5	5.4 ± 1.6	1.3 ± 0.2	1.8 ± 0.2
Fe	19 ± <1	21 ± 1.6	8.4 ± 0.4	11 ± <1
Cu	0.65 ± 0.05	1.3 ± 0.5[b]	0.20 ± 0.05	0.46 ± 0.06
Zn	11 ± <1	14 ± 1	3.6 ± 0.4	6.0 ± 0.5[c]
Cd	0.099 ± 0.002	0.097 ± 0.002	0.031 ± 0.010	0.039 ± 0.003
Pb	5.5 ± 0.1	6.6 ± 0.2	3.0 ± 0.2	3.0 ± 0.42

[a] Number of samples taken into the mean value is 5 unless otherwise noted. [b] $n = 3$. [c] $n = 4$.

the PIXE laboratory of the University of Lund. There the samples were spiked with yttrium, an internal standard to compensate for unquantified losses in the spray drying system. Three replicates (10 mL each) were preconcentrated onto polystyrene films by the spray-drying system (Figure 2) and then analyzed with PIXE. To avoid the contamination problems reported in the first report, crucial parts such as the impaction nozzle were manufactured of Teflon instead of brass (*25*).

Results and Discussion

GFAAS Analysis. The precision and accuracy of trace metal analysis with GFAAS has been estimated previously (*27*). Precision is about 5%, while estimates of accuracy are ±20%. Mean trace metal concentrations for each sampling site determined by GFAAS and the associated uncertainties are given in Table I.

PIXE Analysis. In the preconcentration step for the PIXE analysis, yttrium is used as the internal standard because of its extremely low abundance, if any, in rainwater. The recovery of yttrium gives the efficiency of the spray-drying system. Typical efficiencies are on the order of 25–40%. When the spray droplets are injected with high speed (≈100 m/s) into the drying tower, the resulting turbulent airstream causes some of the droplets to stick

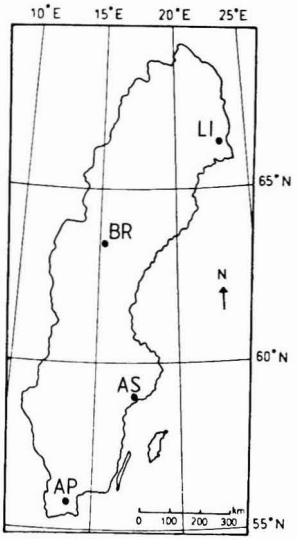

Figure 1. Location in Sweden where atmospheric precipitation was collected. Station code: AP = Arup; AS = Aspvreten; BR = Bredkälen; LI = Liehittäjä.

to the wall and thus lowers the collection efficiencies. Other losses may result from bounce off from the impaction surface. If the water contains a very low amount of dissolved salt, then a significant portion of the dry aerosol is associated with particles having a diameter below the cut-off diameter of the impactor. This effect is clearly seen when blanks are analyzed.

For the PIXE technique, 26 elements have been detected. Mean trace metal concentrations for each sampling site and associated uncertainties are given in Table II. It should be noted that Cl concentrations are probably erroneous, because Cl evaporates as HCl during the drying procedure and thus significant losses may have occurred.

Table II. Arithmetic Mean Trace Metal Concentrations and Associated Uncertainties (Standard Deviation) ($\mu g\ L^{-1}$) for Each Sampling Site Determined with PIXE

	sampling site							
	Aspvreten	n^a	Arup	n^a	Bredkälen	n^a	Liehittäjä	n^a
Si	11 ± 3	15	11 ± 7	13*	7.9 ± 5.4	13	22 ± 3	8*
P	45 ± 8	15	32 ± 4.8	15	19 ± 3.8	15	31 ± 3	15
S	990 ± 70	15	1000 ± 130	15	600 ± 120	15	910 ± 80	15
Cl	3.0 ± 0.8	6*	4.3 ± 1.8	11*	2.1 ± 0.4	8*	1.5 ± 0.34	8*
K	90 ± 10	15	90 ± 13	15	26 ± 7	15	56 ± 22	15
Ca	160 ± 10	15	170 ± 30	15	48 ± 8	15	86 ± 36	15
Ti	0.58 ± 0.16	15	0.99 ± 0.37	15	0.45 ± 0.31	15	0.77 ± 0.54	15
V	1.0 ± 0.01	15	1.5 ± 0.3	15	0.50 ± 0.08	15	1.2 ± 0.1	14*
Cr	0.18 ± 0.13	10	0.19 ± 0.1	12*	0.071 ± 0.01	11*	0.14 ± 0.03	7*
Mn	3.4 ± 0.33	15	5.0 ± 1.3	12	1.4 ± 0.26	15	1.9 ± 0.2	12
Fe	21 ± 2	15	28 ± 8	15	11 ± 3	15	14 ± 2.0	15
Co	0.12 ± 0.05	7*	0.16 ± 0.06	8*	0.062	1*	0.10 ± 0.05	4*
Ni	0.30 ± 0.45	15	0.51 ± 0.15	15	0.17 ± 0.04	15	0.51 ± 0.15	14*
Cu	1.4 ± 0.5	15	1.2 ± 0.39	12	0.44 ± 0.28	15	0.68 ± 0.29	14
Zn	9.9 ± 1.1	15	11 ± 2	15	4.2 ± 1.0	15	12 ± 4	15
Ga	0.14 ± 0.04	11	0.15 ± 0.058	6*	0.070 ± 0.010	6*	0.11 ± 0.02	5*
Ge	0.096 ± 0.013	5*	0.10 ± 0.01	3*	0.054 ± 0.002	2*	0.051 ± 0.01	2*
As	0.50 ± 0.10	12	0.36 ± 0.12	9*	0.27 ± 0.128	12*	0.39 ± 0.13	10*
Se	0.17 ± 0.03	11*	0.18 ± 0.06	13*	0.094 ± 0.085	12*	0.11 ± 0.02	9*
Br	1.2 ± 0.2	15	1.8 ± 0.4	15	0.43 ± 0.22	15	0.52 ± 0.10	15
Rb	0.24 ± 0.5	13*	0.29 ± 0.06	12*	0.088 ± 0.019	7*	0.28 ± 0.20	10*
Sr	0.82 ± 0.11	15	1.7 ± 0.2	15	0.24 ± 0.06	13*	0.38 ± 0.16	12*
Pb	6.3 ± 0.4	15	10 ± 3	15	3.5 ± 1.0	15	3.8 ± 0.64	15

[a] n is the number of samples taken into the mean value. If it is less than 15, it indicates that obvious cases of contamination have been excluded or that concentrations were below the detection limit (indicated by an *).

Table III. Arithmetic Mean Element Concentrations and Detection Limits for 12 Blanks Determined by PIXE (0.1 N HNO_3)[a]

	blank	n	detection limit
Si	5.1 ± 0.7	4	2.9 ± 0.9
P	4.4 ± 1.8	10	2.2 ± 0.7
S	35 ± 34	12	1.8 ± 0.6
Cl			1.5 ± 0.5
K	2.5 ± 1.5	9	0.69 ± 0.23
Ca	4.4 ± 2.3	12	0.35 ± 0.12
Ti	0.20 ± 0.7	9	0.13 ± 0.04
V	0.11 ± 0.01	2	0.091 ± 0.030
Cr			0.059 ± 0.019
Mn	0.33 ± 0.47	12	0.044 ± 0.014
Fe	2.9 ± 1.7	11	0.040 ± 0.017
Co	0.11 ± 0.3	2	0.080 ± 0.036
Ni	0.059 ± 0.032	9	0.030 ± 0.010
Cu	0.34 ± 0.23	12	0.035 ± 0.011
Zn	1.1 ± 0.4	12	0.043 ± 0.013
Ga	0.092 ± 0.051	3	0.069 ± 0.022
Ge			0.069 ± 0.022
As	0.077 ± 0.033	4	0.069 ± 0.021
Se			0.076 ± 0.024
Br	0.11 ± 0.04	6	
Rb	0.168	1	0.15 ± 0.05
Sr	0.256	1	0.18 ± 0.06
Pb	0.25 ± 0.17	2	0.21 ± 0.07

[a] Mean concentration ($\mu g\ L^{-1}$), standard deviation, and number of samples above the detection limit used for the mean calculation are given.

Table IV. Range of Ratios of Rainwater Concentrations to Blank Values Achieved by the PIXE Analysis[a]

Si	1–4	Ni	3–10
P	4–10	Cu	1.5–5
S	15–30	Zn	4–10
Cl	1–3*	Ga	1–1.5
K	10–200	Ge	1–1.5*
Ca	10–70	As	3–6
Ti	2–5	Se	1–2*
V	5–15	Br	3–10
Cr	1–3*	Rb	0.5–1.5
Mn	4–15	Sr	1–5
Fe	4–10	Pb	15–40
Co	1–1.5		

[a] If the blank values were lower than the detection limit, detection limits were used in the denominator (indicated by an *). Blank values and detection limits are given in Table III.

The PIXE technique detection limits and mean concentrations in 12 blanks (0.1 N HNO_3) are given in Table III. By dividing rainwater concentrations by the blank values, an estimate of the influence of the blank is achieved (Table IV). However, for Cl, Cr, Ge, and Se, blank concentrations were lower than the detection limit. Thus, detection limits were used in the denominator. Since concentrations of this group of elements are usually found in the range of their detection limits, little can be said about the influence of the blank. On the other hand, one can lower the detection limit by at least a factor of 2 by increasing sample volume or analysis time.

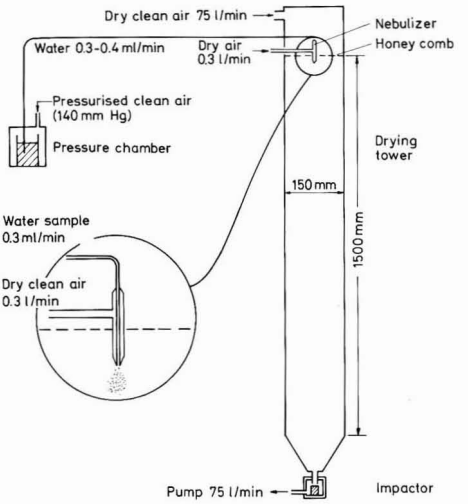

Figure 2. Schematic of preconcentrating sprayer device.

Elements most strongly influenced by the blank are Co, Ga, and Rb. In some instances, Si, Ti, Ni, Cu, and Sr are also influenced when concentrations are low. By comparing detection limits and blank concentrations, it appears that reducing the blank a substantial decrease in detection limits can be reached for several elements (e.g., a factor of 10 for Cu).

To determine the actual analytical uncertainty for the spray preconcentration together with the PIXE analysis, the elemental concentrations for each analysis was divided by the mean value for the three replicates. The standard deviation on the total data set then reflects the uncertainty of the total analytical procedure. The preconcentration and PIXE analysis had an uncertainty of 5–20% for P, S, K, Ca, Ti, V, Mn, Fe, Co, Ni, Zn, Ga, Ge, As, Rb, and Sr and between 20–30% for Si, Cr, Cu, Se, and Br.

Comparison of GFAAS and PIXE. Tables I and II are compiled into Table V for a general comparison of the results from the two analytical methods. The agreement for Mn and Fe are excellent. PIXE shows somewhat higher concentrations for Cu at station Aspvreten, for Zn at Liehittäjä, and for Pb at Arup. Otherwise the agreement is good and within the variation of the data. The results

Table V. Comparison of Measured Concentrations between GFAAS and PIXE Taken from Tables I and II[a]

	sampling site							
	Aspvreten	n	Arup	n	Bredkälen	n	Liehittäjä	n
Mn	3.8 ± 0.5	5	5.5 ± 1.6	5	1.3 ± 0.23	5	1.8 ± 0.1	5
Mn	3.4 ± 0.3	15	5.0 ± 1.3	12	1.4 ± 0.26	15	1.9 ± 0.2	12
Fe	19 ± 1	5	21 ± 2	5	8.4 ± 0.4	5	11 ± 1	5
Fe	21 ± 2	15	28 ± 8	15	11 ± 3.1	15	14 ± 2	15
Cu	0.65 ± 0.05	5	1.3 ± 0.5	3	0.20 ± 0.05	5	0.46 ± 0.06	5
Cu	1.4 ± 0.47	15	1.2 ± 0.4	12	0.44 ± 0.28	15	0.68 ± 0.29	14
Zn	11 ± 1	5	14 ± 1	5	3.6 ± 0.4	5	6.0 ± 0.5	4
Zn	9.9 ± 1.1	15	11 ± 2	15	4.2 ± 1.0	15	12 ± 4	15
Pb	5.5 ± 0.1	5	6.6 ± 0.2	5	3.0 ± 0.2	5	3.0 ± 0.42	5
Pb	6.3 ± 0.4	15	10 ± 3.1	5	3.5 ± 1.0	15	3.8 ± 0.64	15

[a] GFAAS results given on the first line of each element and PIXE results on the second line; n is the number of samples analyzed.

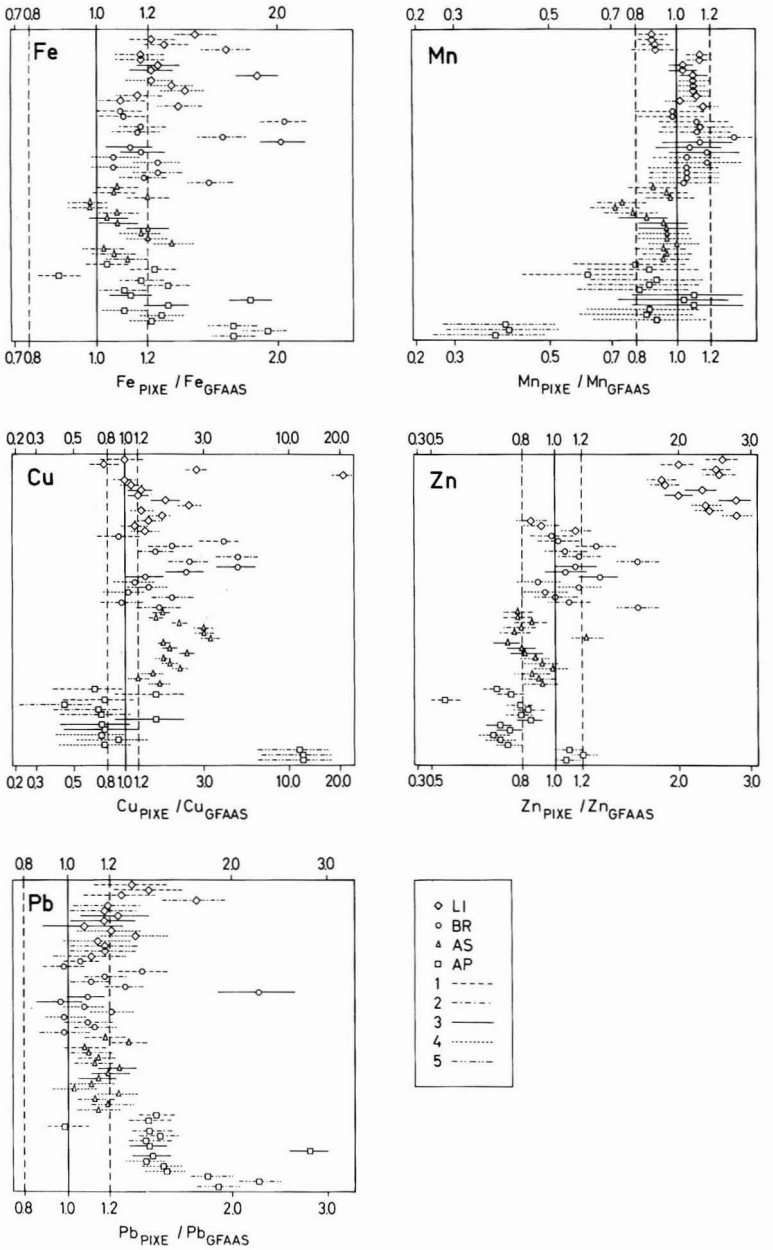

Figure 3. Sample by sample comparison of trace metal concentrations determined by GFAAS and PIXE. The different symbols indicate the station, while the various lines represent the sample from that station. The length of the line indicates the uncertainty in the PIXE analysis.

from PIXE generally have the most variation, especially for Cu, and this is probably due to influences from the blank.

A sample by sample comparison of the two analytical methods are shown in Figure 3. In these figures, the concentrations achieved by PIXE are divided by the associated GFAAS results. Concentrations of Fe and Mn are in excellent agreement, with just a few exceptions. The discrepancies may be due to contamination or the presence of small erosion particles in the sample. Much more water (10 mL) is used by the spray-drying technique than the GFAAS (≈20 μL), increasing the chance for particles to be resuspended and sampled. Other soil-related elements, such as, e.g., Si, also show a higher variability (Table II).

More serious cases of contamination can be seen for Cu. Excluding these obvious cases, a good agreement can be seen, even though there is a higher variability. The PIXE values are also probably affected by the blank. For Zn, the first samples from station Liehittäjä show a probable case of contamination, the rest are in good agreement. Pb also agrees well, but for the last sampling site slightly higher concentrations are found by PIXE.

Conclusions

The results showed that by using the spray column and PIXE analysis a number of elements in atmospheric precipitation, at relatively low concentrations, can be determined simultaneously (P, S, K, Ca, V, Mn, Fe, Ni, Zn, As, Br, and Pb). For other elements (Ti, Cr, Co, Cu, Ga, Ge, Se, Rb, and Sr) the potential of this technique is large, because considerable improvement in detection limit can be achieved by decreasing elemental content in the blank and increasing the water volume or analysis time.

GFAAS analysis showed high precision for the elements investigated (Cd, Cu, Fe, Mn, Pb, and Zn). A comparison of the results from the PIXE analysis and the detection limits for GFAAS indicates that to determine Ti, Cr, Co, Se, Ni, As, and V with GFAAS one will need to preconcentrate the samples.

Some of the differences between analytical methods may be due to the fact that acidification does not dissolve all of the metals. This would be particularly true for the refractory elements Fe, Mn, and Ti. For the anomalously enriched elements such as Cd, Pb, and Zn, 80–100% are solubilized (*30*). The point is however that PIXE measures total concentrations in solution, while GFAAS measures only the acid-soluble portion.

In general, a relatively good agreement is found between the two techniques. However, contamination during the analytical determinations with PIXE will need to be better controlled. Once contamination problems are solved, PIXE analysis with nonselective preconcentration will be a valuable analytical tool because it is a multielemental technique capable of determining elements that are not readily analyzed by GFAAS.

Registry No. H_2O, 7732-18-5; Si, 7440-21-3; P, 7723-14-0; S, 7704-34-9; Cl_2, 7782-50-5; K, 7440-09-7; Ca, 7440-70-2; Ti, 7440-32-6; V, 7440-62-2; Cr, 7440-47-3; Mn, 7439-96-5; Fe, 7439-89-6; Co, 7440-48-4; Ni, 7440-02-0; Cu, 7440-50-8; Zn, 7440-66-6; Ga, 7440-55-3; Ge, 7440-56-4; As, 7440-38-2; Se, 7782-49-2; Br_2, 7726-95-6; Rb, 7440-17-7; Sr, 7440-24-6; Pb, 7439-92-1.

Literature Cited

(1) Gough, L. P.; Schacklette, H. T.; Case, A. A. *U.S. Geol. Sur. Bull.* **1979**, *No. 1466*, 80 p.
(2) Hutton, H. In *Effects of Pollutants at the Ecosystems Level*; Scope Report 22; Aheehan, P. J., Miller, D. R., Butler, G. C., Bordeau, P., Eds.; Wiley: London, 1984; pp 365–375.
(3) Lindberg, S. E.; Harriss, R. C. *Water, Air, Soil Pollut.* **1981**, *16*, 13–31.
(4) Salomons, W.; Förstner, U. *Metals in the Hydrocycle*; Springer-Verlag: Berlin, 1984.
(5) Lantzy, R. J.; Mackenzie, F. T. *Geochim. Cosmochim. Acta* **1979**, *43*, 511–525.
(6) *International Conference Proceedings on Heavy Metals in the Environment*, Athens, Greece, Sept 1985; CEP Consultants: Edinburgh, UK, 1985.
(7) Chan, W. H.; Lusis, M. A. In *Toxic Metals in the Atmosphere*; Nriagu, J. O., Davidson, C. I., Eds.; Wiley-Interscience: New York, 1986; pp 113–144.
(8) Tyler, G. *Ambio* **1984**, *13*, 18–24.
(9) *Proceedings of the Workshop on Measurements of Trace Metals in Precipitation*, Atmospheric Environmental Service, Downsview, Ontario, Canada, Jan 29–30, 1986; Atmospheric Environmental Service: Downsview, Ontario, 1986.
(10) Slavin, W. *Anal. Chem.* **1986**, *58*, 589A–596A.
(11) Houk, R. S. *Anal. Chem.* **1986**, *58*, 97A–105A.
(12) Bass, D. A.; Holcombe, J. A. *Anal. Chem.* **1987**, *59*, 974–979.
(13) Adams, F.; Van Espen, P.; Maenhaut, W. *Atmos. Environ.* **1983**, *17*, 1521–1536.
(14) Dams, R.; Robbins, J. A.; Winchester, J. W. *Anal. Chem.* **1970**, *42*, 861–867.
(15) Hansson, H. C.; Martinsson, B.; Swietlicki, E.; Asking, L.; Heintzenberg, J.; Ogren, J. A. *Nucl. Instrum. Methods Phys. Res., Sect. B* **1987**, *B22*, 235–240.
(16) Heindryckx, R.; Dams, R. *J. Radioanal. Chem.* **1974**, *19*, 339–349.
(17) Johansson, T. B.; Van Grieken, R. E.; Nelson, J. W.; Winchester, J. W. *Anal. Chem.* **1975**, *47*, 855–860.
(18) Maenhaut, W.; Raemdonck, H.; Selen, A.; Van Grieken, R.; Winchester, J. W. *J. Geophys. Res. C: Oceans* **1983**, *88C*, 5353–5364.
(19) Winchester, J. W. *Nucl. Instrum. Methods Phys. Res., Sect. B* **1984**, *B3*, 454–461.
(20) Zoller, W. H.; Gordon, G. E. *Anal. Chem.* **1970**, *42*, 257–265.
(21) Hamilton, E. P.; Chatt, A. *J. Radioanal. Chem.* **1982**, *71*, 29–45.
(22) Sloot, H. A. *Neutron Activation of Trace Elements in Water Samples after Preconcentration on Activated Carbon*; Netherlands Energy Research Foundation: 1976; ECN-1, 215 p.
(23) Cawse, P. A.; Peirson, D. H. *An Analytical Study of Trace Elements in the Atmospheric Environment*; AERE Harwell Rep.; HMSO: London, 1972; AERE-R 7134.
(24) Johansson, E.-M.; Johansson, S. A. E. *Nucl. Instrum. Methods Phys. Res., Sect. B* **1984**, *B3*, 154–157.
(25) Hansson, H. C.; Johansson, E.-M.; Ekholm, A.-K. *Nucl. Instrum. Methods Phys. Res., Sect. B* **1984**, *B3*, 158–162.
(26) Kellogg, R.; Roache, N. F.; Dellinger, B. *Anal. Chem.* **1981**, *53*, 546–549.
(27) Ross, H. *Methodology for the Collection and Analysis of Trace Metals in Atmospheric Precipitation*; University of Stockholm, Department of Meteorology: Stockholm, Sweden, 1984; Report CM-67, 35 p.
(28) Ross, H. *Atmos. Eviron.* **1986**, *20*, 401–405.
(29) Ross, H. *Water, Air, Soil Pollut.*, in press.
(30) Lindberg, S. E.; Harriss, R. C. *J. Geophys. Res. C: Oceans* **1983**, *88C*, 5091–5100.

Received for review May 14, 1987. Accepted October 26, 1987. The collection and analysis of precipitation for trace metals are funded by the National Swedish Environmental Protection Board (SNV) Programme for Environmental Control (PMK). Partial funding for this intercalibration is from the Swedish Natural Science Research Council.

Environ. Sci. Technol. 1988, 22, 532–537

Trace Element Partitioning during the Retorting of Condor and Rundle Oil Shales

John H. Patterson,* Leslie S. Dale, and James F. Chapman

CSIRO, Division of Fuel Technology, Lucas Heights Research Laboratories, Menai, N.S.W. 2234, Australia

■ Composite oil shale samples from the Condor and Rundle deposits in Queensland were retorted under Fischer assay conditions at temperatures ranging from 300 to 545 °C. Trace elements mobilized to the shale oil and retort water were determined at each temperature. The results were comparable for both oil shales. Several elements including arsenic, selenium, chlorine, bromine, cobalt, nickel, copper, and zinc were progressively mobilized as the retort temperature was increased. Most elements partition mainly to the oil and to a lesser extent to the retort water in a similar manner to other oil shales. For Rundle oil shales, trace element abundances in oils, and the proportions of elements mobilized, generally increased with oil shale grade. This was attributed to the reduced effect of adsorption and/or coking of heavier oil fractions during retorting of higher grade samples. Nickel porphyrins, unidentified organometallic compounds, pyrite, and halite are considered to be the sources of mobile trace elements. The results are relatively favorable for oil shale processing and show that arsenic is the most significant element in relation to both shale oil refining and disposal of retort waters.

Introduction

Trace elements in oil shales are partially mobilized during retorting, can poison catalysts in oil refining, and may cause environmental pollution problems during processing and waste disposal. The mobilization of trace elements and their distribution during oil shale retorting are therefore important in processing studies, and a number of partitioning studies have been carried out on the retorting of Green River Formation (*1–3*) and Australian (*4, 5*) oil shales.

The Condor and Rundle oil shale deposits in Queensland are among the most prospective of the major Australian oil shale deposits. For both of these oil shales, trace element abundances are generally similar to or less than those for a typical shale, except for pyritic sulfur, arsenic, and manganese, which are sometimes above normal abundances (*6*). The trace element mineralogy of these shales has been previously reported (*6*), and the above elements may give rise to environmental problems especially in relation to solid waste disposal. Preliminary trace element partitioning studies (*4*) have revealed the elements that are mobilized during Fischer assay retorting. The work reported here examines the effects of retort temperature and oil shale grade on the mobilization of those trace elements.

Experimental Section

Samples for investigation were (i) a composite sample from the high-grade zone at the base of the Brown Oil Shale Sub-Unit, Condor deposit, borehole CDD 70, 382–414 m, and (ii) four ore type samples (*7*) from the Rundle deposit, Brick Kiln Member, borehole ERD 324.

Rundle samples were predried at 105 °C. All samples were crushed to −5.6 mm and blended before riffling into separate batches for retorting. Samples were retorted with Fischer assay procedures (ASTM D3904-80) at temperatures from 300 to 545 °C. Modifications to the standard procedure and details of sampling and sample storage prior to chemical analyses were as previously described (*5*).

Table I. Fischer Assay Yields at Different Retort Temperatures

sample	retort temp, °C	yields, g/100 g of shale: spent shale	oil	water	gas and losses
Condor	300	97.7	nil	2.3	nil
	360	96.9	0.55	2.35	0.2
	400	93.1	2.1	2.75	1.05
	445	89.0	6.4	3.0	1.6
	500[a]	87.0 ± 0.2	6.9 ± 0.05	3.6 ± 0.15	2.5 ± 0.08
	545	84.0	6.8	4.85	4.35
Rundle					
ore type 1	300	96.8	0.1	2.7	0.4
	350	95.1	0.65	3.25	1.0
	400	91.3	3.5	4.0	1.2
	450	79.1	12.9	4.4	3.6
	495[a]	76.4 ± 0.4	14.2 ± 0.3	4.6 ± 0.1	4.8 ± 0.15
	545	75.6	14.5	5.2	4.9
ore type 4	495	80.9	10.65	4.55	3.9
ore type 5	495	85.3	7.4	4.6	2.7
ore type 6	495	91.9	2.55	3.5	2.05

[a] Yields are the average of three runs.

Raw shales, spent shales, oils, and retort waters were chemically analyzed with instrumental neutron activation analysis (INAA) and inductively coupled plasma atomic emission spectrometry (ICPAES) as described elsewhere (*4*). Analyses for Na, Cl, V, Cr, Co, As, Se, and Br in all matrices were by INAA. Analyses for Ca, Ti, Fe, Ni, Cu, Zn, and Mo in all matrices were by ICPAES. Aluminum was analyzed by INAA for raw and spent shales and by ICPAES for oils.

Condor and Rundle (ore type 1) samples were Soxhlet extracted sequentially with chloroform and methanol, and the extracts analyzed for trace elements by the above techniques.

Results and Discussion

The Fischer assay yields of oil, retort water, and spent shale for the various samples and at the different retort temperatures are shown in Table I. Agreement between triplicate runs at about 500 °C was good. For both shales, oil evolution commenced at about 300 °C and was essentially complete at 500 °C. As expected, there were considerable differences in oil yield between the oil shales and especially between the different ore types from the Rundle deposit. Yields of retort water increased with retort temperature up to 545 °C. This was due in part to dehydroxylation of kaolinite, which is a major mineral component in the oil shales. Gas formation also increases progressively at temperatures from 300 to 500 °C. For Condor oil shale, gas formation was further increased at 545 °C due to formation of CO_2 from the partial decomposition of siderite.

Condor and Rundle oil shales are mineralogically different but contain similar levels of trace elements. This is well illustrated by the element abundances in the samples used for this work (Tables II and III). The mineralogical residences of most trace elements have been de-

 0013-936X/88/0922-0532$01.50/0

Table II. Element Abundances in Rundle Oil Shales[a]

element	ore type 4	ore type 5	ore type 6
Na	6500	7200	7900
Al, %	5.6	6.5	6.6
Cl	1280	1080	1120
Ca, %	3.0	2.4	2.7
Ti	3300	4600	4700
V	80	90	85
Cr	48	65	68
Fe, %	4.0	3.9	4.1
Co	19	19	15
Ni	57	45	36
Cu	13	32	31
Zn	65	75	80
As	9.5	9.5	5
Se	1	1	1
Br	7	6	5

[a] Concentrations expressed as $\mu g\ g^{-1}$ unless indicated.

termined and also show many similarities between the two oil shales (*6*, *8*). Chemical analyses of the raw and spent shales indicated that most trace elements remained substantially, if not completely, in the retorted shale (Tables III and IV). It was therefore not possible to establish reliably the mobilization of any of these elements on the basis of difference between raw and retorted shale assays.

Analyses of the product oils and retort waters allowed determination of the elements that were mobilized during retorting. The abundances of trace elements determined in the oils and retort waters are given in Table III for retorting at 500 °C. Mass balances over these triplicate retorting tests are satisfactory for most elements (Table IV). The aluminum concentrations in oils may well reflect fine dust carried over during retorting, and if this is correct, then dust levels were minimal at 30–100 $\mu g\ g^{-1}$ in the oils. This is consistent with results of earlier Fischer assay studies (*5*, *9*). At these levels only aluminum, titanium, calcium, and part of the iron contents can be accounted for as dust carryover to the oils. Since the oils were not dried prior to analysis, it is possible that chlorine levels may be at least partially derived from retort waters not completely separated from the oils. It can be seen that trace element abundances are very similar for Condor and Rundle shale oils with only chlorine, arsenic, and selenium concentrations being slightly higher in the Rundle oils (Table III).

In comparison with Green River shale oils (*10*, *11*), trace element concentrations are generally comparable or slightly lower for both Condor and Rundle oils. Molybdenum, arsenic, and selenium are the elements that are lower. Compared with conventional crude oils, vanadium and nickel levels are much lower and only arsenic concentrations are increased (*12*). Accordingly, the trace elements in Condor and Rundle shale oils do not appear to pose any particular problems with regard to oil refining. Total metal contents appear slightly lower than for Green River shale oils and much lower than for Julia Creek shale oils (*5*).

The abundance of several elements in Rundle shale oils, including arsenic, iron, nickel, cobalt, and chromium tended to increase with oil shale grade (Table V). However, the significance of such trends remains in some doubt because of uncertainities in shale sampling and/or precision of analyses at the low concentration levels. Probable reasons for such results will be discussed later.

Element abundances in retort waters are generally comparable for both oil shales and similar to those found in waters from Fischer assay testing of Green River Formation oil shales (*1*, *2*). Chlorine and arsenic concentrations are somwhat greater in the Rundle retort waters (Table III). The relatively high arsenic and selenium contents exceed Australian water quality criteria (*13*) for agricultural waters.

The total mass of a particular element in the oil or retort water has been used to indicate trends in trace element mobility with retort temperature. For Condor oil shale (Table VI) arsenic, nickel, and cobalt were increasingly mobilized to the oil as the retort temperature was increased. Copper and zinc showed similar trends up to 500 °C but were unexpectedly reduced at 545 °C. Arsenic, selenium, chlorine, bromine, and cobalt were increasingly mobilized to the retort waters at higher retort temperatures (Table VI). For Rundle oil shale (Table VII) arsenic, nickel, cobalt, selenium, chlorine, and bromine were increasingly mobilized to the oil at higher temperatures. These same elements, with the exception of nickel, also tended to be increasingly mobilized to the retort waters at higher retort temperatures (Table VII). However, elements in retort waters can be derived by aqueous extraction from the oils (*2*, *3*). Thus, in most cases the increased abundances in retort waters may simply be reflecting those in the oils.

The above trends, including the progressive mobilization of chlorine, arsenic, selenium, cobalt, nickel, and copper

Table III. Elemental Abundances in Raw Shales, Spent Shales, Oils, and Retort Waters

elemental	Condor raw shale	Condor spent shale	Condor oil	Condor retort water	Rundle, ore type 1 raw shale	Rundle, ore type 1 spent shale	Rundle, ore type 1 oil	Rundle, ore type 1 retort water
Na	3400 ± 140	3850 ± 40	–	17 ± 3	6000 ± 170	7700 ± 70	–[b]	11 ± 4
Al	6.5 ± 0.3[a]	7.7 ± 0.3[a]	2	–	5.5 ± 0.2[a]	6.8 ± 0.3[a]	1.0	–
Cl	<100	–[b]	15	80 ± 40	1300 ± 65	1500 ± 180	30 ± 5	715 ± 15
Ca	3400	3900	3	–	3.8 ± 0.2	4.9 ± 0.25	0.8 ± 0.2	–
Ti	3700	4200	0.2 ± 0.06	–	3000 ± 170	3900	<0.1	–
V	110 ± 10	130 ± 6	0.05	–	80 ± 3	105 ± 3	<0.3	–
Cr	55 ± 2	65 ± 4	–	–	45 ± 3	68 ± 2.6	0.7	–
Fe	4.5 ± 0.2[a]	5.3[a]	20 ± 20	2.5 ± 1.5	4.0 ± 0.2[a]	5.2[a]	15 ± 7	7 ± 1.2
Co	17 ± 0.6	25 ± 4	0.6 ± 0.2	0.3 ± 0.15	18 ± 3.3	21 ± 1.3	0.15 ± 0.05	0.10 ± 0.02
Ni	25	30	2.5 ± 0.4	–	37	35	0.9 ± 0.4	–
Cu	25	30	1.0 ± 1.2	–	21	25	0.8 ± 0.3	–
Zn	65	70	2.0 ± 1.5	–	55 ± 11	70 ± 16	0.15	0.2 ± 0.06
As	8.5 ± 0.4	9.5 ± 0.2	2.8 ± 0.4	1.0 ± 0.1	9 ± 0.8	10 ± 1.5	6.3 ± 3	5.5 ± 0.3
Se	<1	–	–	0.6 ± 0.1	<1	0.9	0.15 ± 0.1	0.15 ± 0.1
Br	2	–	0.1 ± 0.02	1.2 ± 0.4	10 ± 0.5	12 ± 1.5	0.12 ± 0.04	1.3 ± 0.2
Mo	1	–	<0.1	–	2	–	<0.1	–

[a] Concentrations as weight percent. All other concentrations expressed as $\mu g\ g^{-1}$. Values are for retorting at 495–500 °C and are the average of three samples ± 1σ when possible. [b] (–) indicates not detected.

Table IV. Elemental Mass Balances and Closures for Retorting at 495–500 °C

element	mass, μg: raw shale (1 g)	spent shale	oil	water	closure, %
Condor					
Na	3400	3350		0.6	98
Al	65000	67000	0.14		103
Ca	3450	3420	0.2		99
Ti	3700	3650	0.2		99
V	110	113	0.004		103
Cr	55	57			104
Fe	45000	46000	1.4	0.1	102
Co	17	22	0.6	0.3	135
Ni	25	26	0.2		105
Cu	25	26	0.1		104
Zn	65	61	0.1		94
As	8.4	8.3	0.2	0.04	102
Rundle					
Na	6000	5850	1.2	0.7	97
Al	55000	51700	0.1		94
Cl	1300	1140	5	33	91
Ca	38000	37200	0.1		98
Ti	3000	2960			99
V	80	80			100
Cr	45	50	0.1		111
Fe	40000	39500	2.5	0.3	99
Co	18	16	0.02	0.005	89
Ni	37	27	0.13		73
Cu	21	19	0.07		91
Zn	55	53	0.02	0.01	96
As	9	7.6	0.67	0.25	93
Se	<1	0.7	0.013	0.004	>72
Br	10	9	0.015	0.055	91

Table V. Elemental Abundances in Oils from Rundle Ore Types[a]

element	ore type at the indicated oil yield: 6 (2.6 wt %)	5 (7.4 wt %)	4 (10.7 wt %)	1 (14.2 wt %)
Cr	<0.1	<0.1	0.1	0.7
Fe	2	5	10	15 ± 7
Co	0.02	0.08	0.1	0.15 ± 0.05
Ni	<0.1	<0.1	0.25	0.9 ± 0.4
As	2	2.3	3.3	6.3 ± 3

[a] All concentrations expressed as $\mu g\ g^{-1}$.

with retort temperature, are similar to those previously reported for retorting of Julia Creek oil shale (*5*).

To compare the two oil shales and the different ore types for the Rundle deposit it is more appropriate to examine the partitioning of trace elements by calculating element mobility as a percentage of the quantity in the feed shale. Thus total mobility (%) is defined as the percentage of the element distributed to the product oil and water. Tables VIII and IX compare the total mobilities found in this work with those obtained by Fox et al. (*2*) for Green River oil shale. The mobilities for arsenic, selenium, chlorine, and bromine are high, and those for cobalt, nickel, copper, and zinc are also significant. The results are similar to those obtained for Green River oil shale, except that the mobilities for cobalt, nickel, and perhaps selenium are lower for Condor and Rundle oil shales. For Rundle oil shales, the mobilities for arsenic, selenium, cobalt, zinc, chromium, and iron tend to increase with oil shale grade (Tables I and IX).

The element mobilities to the oil and the water are shown separately for retorting at about 500 °C in Table X. Most elements, with the exception of chlorine and bromine, partition mainly to the oil as previously observed

Table VI. Total Elemental Masses in Condor Oils and Retort Waters[a]

element	retort temperature, °C: 300	360	400	445	500	545
for oils						
Cl	–[b]	5.5	–	–	97	34
Fe	–	–	34	26	140 ± 140	41
Co	–	0.7	0.2	4.5	4.2 ± 1.4	8.2
Ni	–	–	1.3	7	17.3 ± 2.8	13.6
Cu	–	–	0.5	3.2	6.9 ± 2.8	1.0
Zn	–	–	0.6	3.2	13.8 ± 10	1.4
As	–	0.8	3.8	15.4	19.4 ± 2.8	18.4
Br	–	3.3	1.7	3.8	0.5 ± 0.2	4.1
for waters						
Na	25	28	22	33	60 ± 11	39
Cl	46	16	55	165	280 ± 140	240
Fe	4.6	–	–	12	9 ± 5.4	–
Co	0.02	0.15	0.08	0.18	1.1 ± 0.5	7.3
As	0.23	0.47	1.93	1.2	3.6 ± 0.4	2.4
Se	–	–	0.55	1.5	2.2 ± 0.25	1.9
Br	0.11	0.12	1.0	1.8	4.3 ± 1.4	4.8

[a] All masses expressed as μg. Values at 500 °C are generally the average of three samples $\pm 1\sigma$. [b] – indicates insufficient sample or not detected.

for Green River oil shales (*2*, *3*) and Julia Creek oil shale (*5*). Selenium and arsenic partition more equally to both the oil and the water, again as was found for Green River and Julia Creek oil shales. Hence the general partitioning patterns are similar for all the oil shales even though the percentage mobilities vary from shale to shale.

As noted earlier, elemental abundance levels in Rundle oils tended to increase with oil shale grade. Results for arsenic in oils and waters show the most significant trends with oil shale grade, but similar trends are indicated for several other elements (Table V). The relevant results for arsenic are given in Table XI and show that abundances in oils and retort waters and mobilities (%) to oils and waters all increase significantly with oil yield. For Rundle oil shales there is often a direct relationship between pyrite contents and oil yield (*6*), and the ore type samples are no exception, as shown by pyritic sulfur values (Table XI).

There are several possible explanations for increased trace element abundances in the oils from higher grade Rundle oil shales. First, kerogen compositions could vary between ore types. Secondly, pyrite could be the source of particular elements, and lastly, secondary adsorption and/or coking reactions on mineral surfaces could reduce the trace element levels in oils from the lower grade shales. The first possibility may be the most likely and is supported by the identification (discussed later) of nickel porphyrin and the probable existence of unknown organometallic phases for all of the relevant metals. However, elemental compositions of kerogens from brown oil shales are similar throughout the deposit (*14*), and it would seem unlikely that a number of chemically different organometallic compounds in the shale could all vary in a similar manner with ore type. The samples come from adjacent intervals within the Brick Kiln Member and are comprised of very similar type I kerogens (*15*). The second possibility may be important in relation to arsenic (*2*), but again it seems unlikely that pyrite could be the source of all the metals. The third possibility would apply to all the metals and is supported by independent reports of adsorption and/or coking of primary oils during modified Fischer assay retorting (*16*) and of the high boiling point components of primary oils, in pilot plant retorting tests using hot ash recycle (*17*). These studies were on Stuart and Condor oil shales. Coking of both Stuart and Condor

Table VII. Total Elemental Masses in Rundle Oils and Retort Waters[a]

	ore type at the indicated temp									
	1 (495 °C)	4 (495 °C)	5 (495 °C)	6 (495 °C)	1 (300 °C)	1 (350 °C)	1 (400 °C)	1 (450 °C)	1 (495 °C)	1 (545 °C)
for oils										
Cl	425 ± 70	960	150	150	–[b]	40	140	260	425 ± 70	220
Cr	10	1	<0.7	<0.3	–	0.1	<0.4	<1.3	10	19
Fe	210 ± 100	105	37	5	–	–	<3.5	<13	210 ± 100	<15
Co	2.1 ± 0.7	1.1	0.6	0.05	–	0.1	0.1	0.8	2.1 ± 0.7	2.6
Ni	13 ± 5.7	2.7	<0.7	<0.3	–	–	1.3	2.5	13 ± 5.7	12.3
As	90 ± 40	35	17	5	–	8.5	19	48	90 ± 40	46
Se	2 ± 1.4	1.6	1.8	0.8	–	0.8	1.4	1.9	2 ± 1.4	2.9
Br	1.7 ± 0.6	3.7	1.8	0.8	–	0.5	1.0	1.9	1.7 ± 0.6	2.2
for waters										
Na	50 ± 18	36	37	25	46	20	28	26	50 ± 18	47
Cl	3300 ± 70	4400	3200	980	110	500	1280	1630	3300 ± 70	5560
Fe	32 ± 5.5	32	41	3.5	20	1.6	4	26	32 ± 5.5	29
Co	0.45 ± 0.1	0.3	0.5	0.07	0.14	0.03	0.12	0.9	0.45 ± 0.1	0.5
Zn	0.9 ± 0.3	–[b]	1.6	1.4	1.6	0.5	0.7	0.9	0.9 ± 0.3	0.8
As	25 ± 1.5	17	15	7	3.8	13.6	21	20	25 ± 1.5	35
Se	0.7 ± 0.5	0.5	0.2	0.07	0.1	0.8	0.4	0.65	0.7 ± 0.5	1.2
Br	6 ± 0.9	5.5	4.5	1.2	0.2	–	1.8	4	6 ± 0.9	12

[a] All masses expressed as μg. Values at 495 °C are the average of three samples ±1 σ. [b] – indicates insufficient sample or not detected.

Table VIII. Element Mobilities (%) at Different Retort Temperatures for Condor Oil Shale

	retort temperature, °C						
element	300	360	400	445	500	545	500[a]
Na	0.007	0.01	0.006	0.01	0.018 ± 0.005	0.011	0.19
Cl	>0.5	>0.22	>0.55	>2.0	>4.0	>2.9	–[b]
Fe	–	–	0.001	0.001	0.003 ± 0.003	–	0.084
Co	–	0.06	0.02	0.27	0.3 ± 0.08	0.9	3.8
Ni	–	0.06	0.05	0.28	0.7 ± 0.10	0.9	4.7
Cu	–	–	0.02	0.17	0.28 ± 0.32	0.05	0.27
Zn	–	–	0.01	0.25	0.21 ± 0.16	0.02	0.27
As	0.03	0.15	0.70	1.94	2.73 ± 0.3	2.50	3.8
Se	–	–	>0.6	>1.5	>2	>1.9	5.1
Br	0.06	1.8	1.3	2.8	2.4 ± 0.7	4.4	–

[a] Green River oil shale, after Fox et al. (2). [b] – indicates not detected.

oils has been reported on spent shale ash at temperatures as low as 500 °C (*18*). The Stuart and Rundle deposits are contiguous within The Narrows Graben (*16*), and thus, the above results are directly relevant to these studies.

The adsorption and/or coking of primary oils onto mineral surfaces can readily account for these results. It is known that trace metals in crude oils and shale oils are generally concentrated in the heavier oil fractions (*10*, *19*) and that these heavier fractions are preferentially adsorbed and/or coked on clay mineral surfaces (*20*, *21*). Delayed coking is a well-established method for removal of heavy metals from petroleum oils (*22*), and coking has been shown to reduce metal contents in shale oils (*19*). Accordingly, the preferential adsorption and/or coking of heavy oils during Fischer assay retorting would be expected to result in a reduction in trace element levels in the oils. The clay minerals, montmorillonite and kaolinite, are the major minerals present in Rundle oil shales (*6*, *15*), and it is known that their concentrations increase in lower grade samples. Thus the lower the grade, the greater is the ratio of clay minerals (or clay mineral surface area) to oil produced during retorting, the greater is the likelihood of adsorption and/or coking of the primary oil, and the lower should be the trace metal contents of the final oil product. The product oils should also become progressively depleted in heavier fractions as the oil shale grade decreases, and this was confirmed by results of simulated distillations of the whole oil products from this work. Depletion of the heavy gas oil fraction (bp > 450 °C) was particularly marked in the oil from the two lowest grade samples.

The partitioning of a particular trace element during retorting is controlled largely by operating conditions, the mineralogical residence of the element, and the occurrence of secondary reactions during retorting. The mineralogy and dominant mineralogical residences have been described elsewhere (*6*, *7*) as follows: (i) As, Ni, and Co are mainly resident in pyrite, but some Ni occurs as porphyrins. It is possible that some As and Co also occur as organometallic compounds, which are as yet unidentified. It is also considered that Se is associated with pyrite. (ii) Cl and Br occur in halite for Rundle oil shale. (iii) Zn and

Table IX. Element Mobilities (%) at Different Retort Temperatures for Rundle Oil Shales

	retort temperature, °C						ore types[a]			
element	300	350	400	450	495	545	1	4	5	6
Na	0.008	0.003	0.004	0.005	0.03 ± 0.003	0.01	0.03 ± 0.003	0.005	0.005	0.003
Cl	0.08	0.4	1.10	1.45	2.86 ± 0.1	4.42	2.86 ± 0.1	4.2	–[b]	2.4
Cr	0.07	0.08	0.11	0.12	0.33	0.57	0.33	0.07	0.08	0.06
Fe	–	–	–	–	0.006 ± 0.002	–	0.006 ± 0.002	0.003	0.001	–
Co	0.008	0.007	0.007	0.09	0.14 ± 0.05	0.17	0.14 ± 0.05	0.02	0.055	0.005
Ni	–	–	0.034	0.066	0.35 ± 0.15	0.34	0.35 ± 0.15	0.05	–	–
Zn	0.03	0.009	0.02	0.30	0.27	0.95	0.27	–	0.13	0.02
As	0.43	2.55	4.60	7.75	12.9 ± 4.6	9.4	12.9 ± 4.6	5.4	3.35	2.35
Se	>0.1	>1	>1.8	>2.6	>4.8	>3.0	>4.8	2.25	2.1	0.8
Br	0.02	0.12	0.25	0.56	0.70	1.31	0.7	1.32	1.02	0.43

[a] Retorted at 495 °C. [b] – indicates not detected.

Table X. Element Mobilities (%) to Oils and Retort Waters[a]

element	Condor		Rundle	
	oil	water	oil	water
Na	–[b]	0.018	0.02	0.01
Cl	>1	>4	0.33	2.53
Cr	–	0.06	0.22	0.11
Fe	0.003	0.0002	0.005	0.001
Co	0.24	0.06	0.12	0.02
Ni	0.7	–	0.35	–
Cu	0.28	0.003	0.54	–
Zn	0.21	0.002	0.25	0.02
As	2.3	0.43	10.0	2.9
Se	–	>2.1	>2	>2.8
Br	0.25	2.15	0.15	0.55

[a] For retorting at 495–500 °C. [b] – indicates not detected.

Table XI. Abundances and Mobilities (%) of Arsenic for Rundle Ore Types

ore type	yield, wt %		pyritic sulfur, %	abundance, $\mu g\ g^{-1}$		mobility, %	
	oil	water		oil	water	to oil	to water
1	14.2	4.6	1.1	6.3 ± 3	5.5 ± 0.3	10 ± 4.6	2.9 ± 0.1
4	10.7	4.55	0.7	3.3	3.7	3.7	1.7
5	7.4	4.6	0.5	2.3	3.3	1.75	1.6
6	2.6	3.5	0.3	2.0	2.0	1.0	1.35

Cu are mainly resident in sphalerite and chalcopyrite for Condor oil shale but not for Rundle oil shale.

To check for the presence of organometallic compounds in the shales, selected samples were Soxhlet extracted sequentially with chloroform and methanol. Significant amounts of several elements (which had been mobilized to the oils during retorting) were detected. These included cobalt, nickel, copper, zinc, chromium, and possibly iron. With one notable exception (nickel in Condor oil shale), more of the metals were extracted with methanol than with chloroform. Notable proportions of total nickel (0.6–4.5%), cobalt (about 1.5%), and zinc (0.5%) were extracted. This suggests the presence of a number of metal–organic complexes in the shales. The total amounts extracted from both shales were sufficient to account for the element mobilities found on retorting. Nickel porphyrins have been identified in the methanol extracts from both oil shales with UV–visible spectroscopy (Fookes, unpublished). Similar nickel porphyrins have previously been identified in Green River (*23*) and Julia Creek oil shales (*24*).

Hence for both Condor and Rundle oil shales, it is possible to account for the mobility of nickel, cobalt, copper, zinc, chromium, and possibly iron on the basis of volatility of metal–organic compounds. This would also logically account for their partitioning mainly to the oil rather than to the retort waters.

Of the other elements that are mobilized from the shale, chlorine and bromine most probably arise from the sodium salts, whereas arsenic and selenium may be derived from pyrite (*2, 5*) or metal–organic compounds (*25, 26*) as previously discussed (*5*). Arsenic and selenium were not detected in the organic extracts from Condor oil shale but were just detectable in the methanol extract from Rundle oil shale. About 3% of total arsenic was extracted with methanol compared with 12.9% mobilized during retorting. This suggests that organoarsenic compounds may be present in Rundle oil shales and that arsenic in oils and retort waters arises from both sources.

Summary and Conclusions

A number of trace elements, including chlorine, bromine, arsenic, selenium, iron, cobalt, nickel, chromium, copper, and zinc, are progressively mobilized from Condor and Rundle oil shales during retorting at temperatures from 300 to 545 °C. With the exceptions of chlorine, bromine, and to a lesser extent selenium, these elements partition mainly to the oil. Trace element partitioning patterns are similar to those for Green River Formation and Julia Creek oil shales.

For Rundle oil shales, elemental abundances in the oil generally increased with oil shale grade. This is attributed to the adsorption and/or coking of primary oils onto clay mineral surfaces. These effects preferentially remove trace metals from the oils and are enhanced in lower grade samples because of increased clay mineral content relative to oil produced during retorting.

The results suggest that nickel, cobalt, copper, zinc, chromium, and iron are derived from nickel porphyrins and other unidentified metal–organic compounds, that chlorine and bromine are derived from sodium salts, and that arsenic may be derived from both pyrite and organoarsenic compounds present in the raw shale.

Trace element abundances in oils and retort waters are relatively low compared with abundance levels for other oil shales. Arsenic would appear to be the most significant trace element in relation to shale oil refining and disposal of retort waters.

Acknowledgments

We acknowledge the following colleagues for their analytical work: J. J. Fardy, Y. J. Farrar, T. F. Gorman, D. A. Alewood, S. J. Buchanan, and G. D. McOrist. We also thank Southern Pacific Petroleum NL and Esso Australia Ltd for providing the oil shale samples, H. J. Loeh for conducting the organic solvent extractions, and P. Udaja for the simulated distillations.

Registry No. Na, 7440-23-5; Al, 7429-90-5; Cl_2, 7782-50-5; Ca, 7440-70-2; Ti, 7440-32-6; V, 7440-62-2; Cr, 7440-47-3; Fe, 7439-89-6; Co, 7440-48-4; Ni, 7440-02-0; Cu, 7440-50-8; Zn, 7440-66-6; As, 7440-38-2; Se, 7782-49-2; Br_2, 7726-95-6.

Literature Cited

(1) Shendrikar, A. D.; Faudel, G. B. *Environ. Sci. Technol.* **1978**, *12*, 332–334.
(2) Fox, J. P.; Mason, K. K.; Duvall, J. J. *Oil Shale Symp. Proc.* **1979**, *12th*, 58–71.
(3) Fruchter, J. S.; Wilkerson, C. L.; Evans, J. C.; Sanders, R. W. *Environ. Sci. Technol.* **1980**, *11*, 1374–1381.
(4) Dale, L. S.; Fardy, J. J. *Environ. Sci. Technol.* **1984**, *18*, 887–889.
(5) Patterson, J. H.; Dale, L. S.; Chapman, J. F. *Environ. Sci. Technol.* **1987**, *21*, 490–494.
(6) Patterson, J. H.; Dale, L. S.; Fardy, J. J.; Ramsden, A. R *Fuel* **1987**, *66*, 319–322.
(7) Coshell, L. *Geol. Soc. Aust. Abstr.* **1984**, *12*, 117–118.
(8) Patterson, J. H.; Ramsden, A. R.; Dale, L. S. *Chem. Geol.* **1988**, *67*, 327–340.
(9) Wildeman, T. R.; Meglen, R. R. *Adv. Chem. Ser.* **1978**, *No. 170*, 195–212.
(10) Wilkerson, C. L. *Fuel* **1982**, *61*, 63–70.
(11) Fox, J. P.; Hodgson, A. T.; Girvin, D. C. In *Energy and Environmental Chemistry, Fossil Fuels*; Keith, L. H., Ed.; Ann Arbor Science: Ann Arbor, MI, 1982; Vol. 1, pp 69–102.
(12) Ghassemi, M.; Panahloo, A.; Quinlivan, S. *Energy Sources* **1984**, *7*, 377–401.
(13) Hart, B. T. *Aust. Water Resour. Counc. Tech. Pap.* **1974**, *No. 7*, 1–349.
(14) Lindner, A. W. *ACS Symp. Ser.* **1983**, *No. 230*, 97–118.
(15) Hutton, A. C. *Proceedings of the First Australian Workshop on Oil Shale*, Lucas Heights, Australia; Australian Atomic Energy Commission: Sydney, 1983; pp 31–34.
(16) Gannon, A. J.; Henstridge, D. A.; Schoenheimer, A. N. *Proceedings of the First Australian Workshop on Oil Shale*,

Lucas Heights, Australia; Australian Atomic Energy Commission: Sydney, 1983; pp 101-104.
(17) Dung, N. V.; Wall, G. C.; Kastl, G. *Fuel* **1987**, *66*, 372-376.
(18) Levy, J. H.; Mallon, R. G.; Wall, G. C. *Fuel* **1987**, *66*, 358-364.
(19) Jackson, K. F.; Benedik, J. E.; Birkholz, F. A. *Oil Shale Symp. Proc.* **1981**, *14th*, 75-81.
(20) Schulman, B. L. *AIChE Symp. Ser.* **1976**, *72*, 39-43.
(21) Espitalie, J.; Madec, M.; Tissot, B. *AAPG Bull.* **1980**, *64*, 59-66.
(22) *Kirk-Othmer Encyclopedia of Chemical Technology*, 3rd ed.; Wiley: New York, 1982; Vol. 17, pp 210-215.
(23) Milton, C.; Dwornik, E. J.; Estep-Barnes, P. A.; Finkelman, R. B.; Pabst, A.; Palmer, S. *Am. Mineral.* **1978**, *63*, 930-937.
(24) Fookes, C. J. R. *J. Chem. Soc., Chem. Commun.* **1983**, 1472-1473.
(25) Fish, R. H.; Tannous, R. S.; Walker, W.; Weiss, C. S.; Brinckman, F. E. *J. Chem. Soc., Chem. Commun.* **1983**, 490-492.
(26) Fish, R. H. *ACS Symp. Ser.* **1983**, *No. 230*, 423-432.

Received for review November 24, 1986. Revised manuscript received August 12, 1987. Accepted December 8, 1987.

Proteins in Natural Waters and Their Relation to the Formation of Chlorinated Organics during Water Disinfection†

Frank E. Scully, Jr.,* G. Dean Howell, Robert Kravitz, and Jeffrey T. Jewell

Department of Chemical Sciences, Old Dominion University, Norfolk, Virginia 23508

Victor Hahn and Mark Speed

Utilities Department, 9500 Civic Center Drive, Thornton, Colorado 80229

■ Solutions of model proteins were chlorinated and found to produce yields of trihalomethanes and total organic chloride comparable to a humic acid. The concentrations of proteins (total dissolved amino nitrogen) and algal counts in a lake water were measured from April to November of 1985. Concentrations ranged from 0.07 to 0.3 mg/L as N while copper sulfate was added to the lake for algae control. Increases in protein concentration correlated with algal blooms. When copper sulfate treatment was suspended, a massive algal bloom was observed and the protein concentration increased to 0.96 mg/L as N. From this protein concentration a 5-day trihalomethane formation potential of 115 μg/L was estimated. Pretreatment with powdered activated carbon, alum coagulation, sedimentation, filtration, and disinfection processes were effective in removing about 70% of the proteins. Organic precursors in a natural water were fractionated by ultrafiltration and protein concentrations and trihalomethane formation potential (THMFP) measured in each fraction. Proteins appeared to account for 8-11% of the THMFP of each fraction. It was concluded that chlorination of proteins produced during algal blooms may make a significant contribution to the formation of trihalomethanes in chlorinated natural waters.

Introduction

Since the identification of carcinogenic trihalomethanes (THMs) in chlorinated drinking waters (*1*, *2*), utility companies and government regulatory agencies have invested considerable research and effort to determine the factors that affect the formation of these compounds and how to remove them.

Natural waters contain a complex mixture of organic compounds (*3*, *4*) that can react with aqueous chlorine to form THMs. The reaction of humic and fulvic acids, which compose the largest fraction of organic substances in natural waters, is believed to be the major source of these compounds. However, attempts to correlate the trihalomethane formation potential (THMFP) of natural waters with a simple chemical parameter such as total organic carbon have revealed only crude relationships and demonstrated the fact that the characteristics of the organic components of various waters differ widely (*5*).

In a number of instances seasonal variations in the THM concentrations in finished waters have been linked to the increased organic loading of a raw water produced by algal blooms (*6-9*). Studies have shown that chlorination of algae (*6*), algal biomass (*7*), and extracellular products produced by algae (*7-10*) all produce THMs. Although algae vary considerably in their metabolic activity and in the organic products of their metabolism, proteins generally represent the largest single fraction of organic components of many algae (*11-13*) and are especially important extracellular products of blue-green algae (*14*). For instance, approximately 60-70% of the dry weight of the algae *Monodus subterraneus* and *Spirulina maxima* is proteinaceous. Volesky et al. (*15*) report that higher protein content is found in the Chlorophyceae and Rhodophyceae families of algae than among others and that these may contain 20-50% protein in addition to smaller concentrations of carbohydrates and lipids.

The presence of algae can dramatically affect the organic nitrogen content of natural waters. Ram and Morris (*16*) have recorded 21.7 mg/L organic nitrogen in a freshwater lake during the bloom of a blue-green algae. Gardner and Lee (*17*) have found high concentrations of amino acids during a period of rapid algal decomposition. Tuschall and Brezonik (*18*) have found that 71% of the dissolved organic nitrogen in the filtrate of a culture of *Anabaena* sp. was proteinaceous. The full implications of these observations for the treatment of natural water affected by algal growth have not yet been fully realized, but Williams (*19*) has described problems of taste, odor, disinfection requirements, and cost of treatment associated with the presence of proteins in drinking water supplies.

The research described here was begun while investigating the impact of high organic nitrogen levels on two drinking water supplies. Until 1985 one of the principal raw water sources for the City of Thornton, CO, was a series of shallow gravel lakes that are adjacent to the South Platte River 1 mi downstream from the discharge point of the Denver Metro Wastewater Treatment Plant. Be-

†The material described herein was presented in part at the Fifth Conference on Water Chlorination, Williamsburg, VA, June 3-8, 1984, and that portion was published in the conference proceedings.

0013-936X/88/0922-0537$01.50/0

sides periodic groundwater intrusion from the river, the lakes are affected regularly by algal blooms. To suppress algal growth, 100–150 lb of copper sulfate was added daily to the central lake, N.E. Tani Lake (3.83×10^6 ft^3), from late May through mid September. Throughout the year, the lakes are found to be high in ammonia and dissolved organic nitrogen. The second water studied came from the main water supply for a community in southeastern Pennsylvania. In the late winter after the frozen ground begins to thaw, this reservoir is affected by heavy runoff from dairy farms. Since the ammonia level rises rapidly and the water develops an amine odor, it was suspected of containing the high concentrations of proteinaceous amino nitrogen.

The purpose of this study was to evaluate the significance of the formation of chlorinated organic byproducts from the reaction of aqueous chlorine with proteins found in natural waters. To make this evaluation, we have measured the yields of organohalogen compounds from the chlorination of model proteins and related these to the concentrations of proteins found in natural waters.

Total dissolved amino nitrogen (TDAN) is a measure of the primary amino organic nitrogen compounds present after acid hydrolysis. On the basis of the work of others (*17*, *18*), proteins were presumed to make the largest contribution to this measurement, and consequently the terms TDAN and proteins are used interchangeably.

Experimental Section

General. All chemicals were of reagent grade or better. Chlorine-demand-free water was prepared by chlorinating Milli-Q water to 2 mg/L, allowing this to stand overnight, boiling it for 1 h, irradiating it overnight with high intensity UV light until no residual chlorine was detected, and bubbling the water with nitrogen gas for 1 h. The water was sealed under a nitrogen atmosphere and stored in the refrigerator. All buffers and solutions used in THM and total organic chloride (TOCl) determinations were prepared in chlorine-demand-free (CDF) water. Solutions were chlorinated with standard hypochlorite (1000 ± 10 mg/L) prepared as described in EPA method 510.1 (*20*). Bromodichloromethane and chlorodibromomethane were obtained from Columbia Organic Chemicals. Bromoform (96%) and humic acid, sodium salt (lot no. 1204PE), were obtained from Aldrich Chemical Co. Bovine serum albumin (BSA), pepsin, rennin, and cytochrome *c* (type III) were obtained from Sigma Chemical Co.

Gas chromatography was performed on a Varian Aerograph 3700 gas chromatograph equipped with a ^{63}Ni electron capture detector (ECD). The carrier gas used throughout the experiments was high-purity nitrogen used at a flow rate of 20 mL/min. Glass columns (4 mm i.d. × 6 ft) were packed with 10% w/w squalane (Varian) on Chromosorb W 100/120 mesh (Analabs, Inc.). A column temperature of 67 °C, a detector temperature of 250 °C, and an injector temperature of 160 °C were used for all trihalomethane analyses. Chromatograms were recorded and peak areas measured on a Shimadzu Chromatopac C-R1B recording data processor. UV/vis spectrophotometric determinations were performed on a Cary Model 219 spectrophotometer in the auto slit mode. A Corning digital Model 110 pH meter with a Corning semimicro calomel combination electrode (calibrated before each measurement with standard buffers) was used for all pH measurements. Total organic carbon analyses were performed on a Dohrmann DC-54 TOC analyzer. Total organic chloride analyses were performed on a Dohrmann DX-20 total organic halide analyzer according to EPA method 450.1 (*21*). Free amino acid concentrations were determined by precolumn derivatization with orthophthalaldehyde (OPA) and high-performance liquid chromatography by a method similar to that of Jones et al. (*22*).

Preparation of Protein Stock Solutions. By using an analytical balance, the approximate amount of protein was weighed out to make up 250 mL of a 500 mg/L solution in CDF water. This solution was stored in an amber glass bottle in the refrigerator. A 50-mL portion of the protein stock solution was dialyzed overnight against deionized water using dialysis tubing with a nominal molecular weight cutoff of 8000 (1.25 in. inflated diameter; Thomas Scientific). An aliquot of CDF water was also dialyzed as a blank. The dialysis water was changed 3 times during the afternoon and evening. These dialyzed stock solutions were quantitated spectrophotometrically (*23*, *24*).

Chlorination of Protein Solutions. An aliquot of the dialyzed stock protein solution (generally containing 5.0 mg of protein) was pipetted into a 1-L volumetric flask and diluted to approximately 900 mL with 0.025 M phosphate buffer (pH 7.0, prepared from CDF water). The solution was mixed thoroughly, the desired amount of hypochlorite (1000 ± 10 mg/L Cl_2) was added with swirling, and the sample was diluted to the mark with buffer. After the solution was mixed thoroughly, it was decanted into 125-mL sample bottles capped with Teflon-lined caps and incubated without headspace at 20 °C.

Trihalomethane Analysis. In order to calibrate the ECD response, standard solutions of the trihalomethanes were prepared according to published procedures (*25*). Correlation coefficients for calibration curves were always greater than 0.95. Trihalomethanes were isolated and analyzed by the liquid/liquid extraction method prescribed by EPA protocol (*25*).

Handling of Natural Water Samples. Samples of raw water were obtained in 4-L amber glass bottles and sealed without headspace with Teflon-lined caps. Chlorinated samples were dechlorinated with sodium metabisulfite after sampling. Otherwise, no reagents were added to the samples before they were shipped overnight to Norfolk, VA. They were refrigerated at 4 °C and analyzed within 1 week of receipt.

Total Dissolved Amino Nitrogen (TDAN) Analysis. Samples were filtered through a Gelman type A/E glass-fiber filter. Total dissolved free and hydrolyzable amino nitrogen levels (protein concentrations) were measured with the following variation of the method of Gardner and Stephens (*26*). Eight vacuum hydrolysis tubes were used to which standard additions of glycine were made. Samples were hydrolyzed with a 50% solution of distilled propionic acid and ultrapure concentrated HCl (*26*) for 30 min at 145 °C. After lyophilization, derivatization with fluorescamine, and fluorescence analysis, a plot of relative fluorescence vs amount of added glycine, was generated as described previously (*26*). A least-squares analysis of the data was performed and the intercept calculated. The concentrations of glycine that would produce an equivalent amount of fluorescence was then determined from the plot. The variance in this number was a function of the mean squared residual σ^2:

$$\sigma^2 = [\sum(y - y')^2/(n - 2)]^{1/2}$$

$y - y'$ being the difference in actual measurements and the calculated regression line. The variance k is defined as

$$k = 2[\sigma^2/\beta^2[(1/n) + (\alpha + \beta\hat{x})^2/\mathrm{ss}_x\beta^2]]$$

where β = slope, α = intercept, n = number of data, $\hat{x}$ = average of glycine concentrations, and $\mathrm{ss}_x = \sum x^2 -$

$(\sum x)^2/n$. Since glycine contains 18.6% nitrogen, concentrations of TDAN (as glycine) were converted to TDAN (as N) with multiplication by 0.186.

Ultrafiltration of Raw Water Samples. A water sample from N.E. Tani Lake was fractionated with Amicon ultrafiltration membranes. The water was first filtered through a Gelman glass-fiber filter to remove particulates. A 250-mL volume of the sample was forced through an XM 50 [50 000 nominal molecular weight (M_r) cutoff] membrane with nitrogen (40 psi) until approximately 20 mL of water remained above the membrane. The concentrate was washed twice with 50 mL of CDF water and reconcentrated by filtration. A total volume of 300 mL was passed through the filter. The concentrate retained by the membrane was recovered by thoroughly washing the ultrafiltration cell twice with 100 mL of CDF water. Finally, a 50-mL volume of CDF water was added, stirred, removed, and combined to give a total volume of the retained material equal to the original water sample (250 mL).

The filtrate of the first membrane (a total volume of 300 mL) was next passed through a YM 5 membrane (M_r 5000 cutoff) following the same procedure. The retained material was removed and resuspended in CDF water to a volume of 250 mL. This filtrate was next passed through a YCO 5 membrane (M_r 500 cutoff), and again the material retained was resuspended in 250 mL of CDF water. To obtain a fraction of material with lower molecular weight than 500, a separate portion of the original glass-fiber filtered water was passed through the YCO 5 membrane until a 250-mL volume was recovered.

Chlorination of Nominal Molecular Weight Fractions. To 200 mL of each molecular weight fraction was added 2.00 mL of 2.5 M K_2HPO_4. With rapid stirring, 5.7 mL of hypochlorite (1055 mg/L as Cl_2) was added slowly to each solution and the pH adjusted to 8.25 ± 0.05 with 1 M NaOH in high-purity water. The solutions were decanted into glass bottles, sealed with Teflon-lined caps without headspace, and incubated in the dark in a constant-temperature bath at 20.0 ± 0.1 °C. After 5 days the pH of each solution was checked and found to be within 0.1 unit of its original value. Each solution was analyzed for free and total residual chlorine and found to contain at least 14 mg/L free chlorine. The solutions were then analyzed for THMs as described above.

Algal Counts. Counts were made within 3 h of collection of a water sample. Enumerations were performed with a Sedgwick–Rafter counting cell and a calibrated Whipple grid according to method 1002 F of *Standard Methods for the Examination of Water and Wastewater* (*28*). The strip counting method was used after concentration of 200 mL of water to 14 mL, producing a concentration factor of 0.07.

Results

Model Studies. Four commercially available proteins were chosen as models of proteins present in nature. They were chosen for their different molecular weights, which span the range found by Tuschall and Brezonik (*18*). Bovine serum albumin (BSA) is a readily available compound frequently used in model studies because its purity, secondary and tertiary chemical structures, activity, and function have been well characterized by biochemists. Pepsin and rennin are digestive enzymes found in the stomachs of many mammals. Cytochrome *c*, which contains an iron-porphyrin group, is a pigmented protein used by aerobic cells to transfer electrons to oxygen. Although the structure of cytochrome *c* isolated from different cells varies slightly, a cytochrome of the *c* type has been isolated from blue-green algae (*29*).

Table I. Yields of Chloroform and Total Organic Chloride (TOCl) Formed 5 Days after Chlorination of 5 mg/L Solutions of Proteins and Humic Acid at pH 7.0 and 20 °C

chlorination substrate	M_r	TOC, mg/L	THMs[a] µg/L	THMs[a] % yield	TOCl/TOC, µg/mg
bovine serum albumin (BSA)	66 000	2.25	97	0.44	246
pepsin	30 000	2.30	117	0.51	193
rennin[b]	30 000	2.70	117	0.49	
rennin	30 000	2.70	47	0.20	99
cytochrome *c*	12 500	2.25	93	0.42	308
humic acid	unknown	1.75	135	0.78	305

[a] Data taken from ref 36. [b] This solution of rennin was not dialyzed.

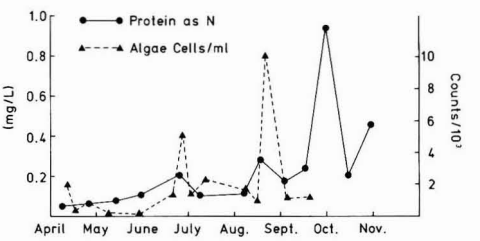

Figure 1. Variation of protein concentrations (TDAN) and total algal cell count in N.E. Tani Lake, Thornton, CO, in 1985.

Terminal 5-day THM and TOCl concentrations were measured in solutions of each protein with a carbon content of 2–3 mg/L in 0.025 M potassium phosphate at pH 7.0, chlorinated to 20 mg/L Cl_2, and incubated in the dark at 20 °C. The results are recorded in Table I. Control experiments showed that in all but one case (rennin) dialysis did not reduce the amount of chloroform produced. Commercial humic acid was used for comparison.

Solutions of BSA have a higher chlorine demand at pH 7.0 in 0.025 M phosphate buffer (20 ± 0.5 °C) than similar solutions of humic acid. Four days after chlorinating 1 mg/L (as C) solutions of each to 11.9 mg/L (Cl_2), the humic acid solution showed a chlorine demand of 5.9 mg/L per mg of TOC, while the BSA solution showed a demand of 8.2 mg/L per mg of TOC.

BSA shows a marked increase in the yield of chloroform as the pH is raised, especially above pH 9.0. Solutions of BSA (5 mg/L) in 0.025 M aqueous potassium phosphate (pH 7.0 and 8.0) or 0.025 M aqueous sodium borate (pH 9.0 and 10.0) were also chlorinated to 20 mg/L Cl_2 and incubated in the dark for 5 days at 20 °C (±0.5 °C). The relative yields of chloroform were 1.0 (pH 7.0), 1.2 (pH 8.0), 1.25 (pH 9.0), and 1.9 (pH 10.0).

Amino Nitrogen in Natural Waters. Copper sulfate, approximately 0.5 mg/L, was added daily to N.E. Tani Lake in Thornton, CO, from late May through mid September. The concentrations of total dissolved amino nitrogen (TDAN) were measured from April to November 1985. These concentrations as well as algal counts are plotted in Figure 1. TDAN concentrations in N.E. Tani Lake samples on September 11, 1984, measured 422 ± 78 µg/L. Amino acid concentrations measured (µg/L amino acid) were as follows: aspartic acid, 10.2; glutamic acid, 14.6; serine, 16.6; alanine, 19.0; valine, 12.6. This represented a total of 9 µg/L free amino acid nitrogen. Concentrations of other amino acids were much less.

Two studies were conducted to determine how water treatment processes affect the concentrations of proteins and the production of THMs in natural waters. On Feb-

Table II. Protein Concentrations[a] and 5-Day Total Trihalomethane Concentrations Produced from Chlorination of Raw Water [pH 8.2, 20 (±0.5) °C] from N.E. Tani Lake at Well 28,[a] Thornton, CO, Sampled on February 28, 1984

chlorine dose, mg/L	residual chlorine, mg/L	5-day TTHM, μg/L	TDAN,[b] μg/L
0	0		71 ± 11
2	0	26	78 ± 9
5	0	169	60 ± 8
7	0	217	77 ± 13
10	.6	274	54 + 9
12	1.8	286	35 ± 4

[a] Initial concentration of NH_3–N was 0.45 mg/L. [b] Protein concentration is defined as total dissolved amino nitrogen (TDAN) following acid hydrolysis measured by fluorescence after derivatization with fluorescamine (*25*). Data is recalculated from ref 36.

ruary 28, 1984, a study was conducted to determine the effect of different chlorine dosages along a breakpoint curve on the destruction of proteins and the concomitant formation of trihalomethanes over 5 days (Table II). The sample was collected from N.E. Tani Lake, which was found to contain approximately 71 (±11) μg/L TDAN, and had a 1-h chlorine demand of about 4 mg/L. It was chlorinated to various levels along the chlorine-demand curve of the water. The 5-day terminal THM concentrations as well as the TDAN concentrations at each dosage level are listed in Table II.

In a second study, water from a reservoir in southeastern Pennsylvania was found to contain 179 ± 30 μg/L TDAN. Water was obtained from several points in the local treatment plant to determine the effect of the different phases of water treatment on the removal of proteins. The utility adds powdered activated carbon to its raw water, followed within 5 min by a rapid mix with chlorine and alum and sometimes lime. The water is flocculated for 20 min, settled for 4–5 h, and filtered through a dual medium of sand and anthracite coal. Ammonia is added after filtration, followed by lime and chlorine before the water is held in the clear well. The filter effluent was found to contain 69 ± 11 μg/L TDAN, and the finished water was found to contain 48 ± 11 μg/L TDAN.

Nominal Molecular Weight Fractionation of Raw Water Organics: Proteins and Trihalomethane Production. Ultrafiltration was used to separate by nominal molecular weight the organics present in water from N.E. Tani Lake, sampled on September 11, 1984. The original sample contained 420 ± 78 μg/L TDAN. The protein concentrations and 5-day terminal THM concentrations for each fraction are plotted in Figure 2. The recovery of the raw water organics from the ultrafiltration membranes appeared to be quantitative from a comparison of the THMFP of the unfractionated water (298 mg/L) and the sum of the THMFP of each fraction (329 mg/L).

Discussion

Yields of THM and TOCl from Proteins. The yields of chloroform produced by proteins of widely varying structure and molecular weight are remarkably similar to each other. This is not surprising since, unlike humic or fulvic acids, proteins have well-defined subunits, the 20 essential amino acids, which are found in all proteins. The yields are about half that of humic acid (Table I, column 5).

Morris et al. (*30*) have measured the yields of chloroform from excess chlorination at pH 7 of various amino acids. In general, yields from most amino acids after a 24-h

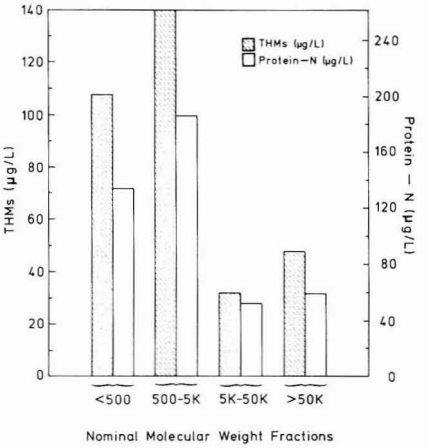

Figure 2. Protein concentrations in water from N.E. Tani Lake, Thornton, CO, which had been fractionated by nominal molecular weight using ultrafiltration. The fractions (in 0.025 M phosphate buffer at pH 8.25 ± 0.05) were chlorinated to 30 mg/L Cl_2 and incubated 5 day at 20 °C and the THM concentrations measured.

contact time are low. Tryptophan and hydroxyproline give the highest yields with alanine, phenylalanine, and proline giving much lower yields. However, BSA contains no hydroxyproline and only 0.35 mol % of tryptophan (*24*). According to Morris et al. (*30*), the yield of chloroform from tryptophan is 7.8% at pH 7.0 after a 24-h contact time. Consequently, the yield of chloroform from the excess chlorination of tryptophan residues in BSA is

$$\frac{2 \text{ mol of tryptophan}}{1 \text{ mol of BSA}} \frac{0.078 \text{ mol of chloroform}}{1 \text{ mol of tryptophan}} = \frac{0.16 \text{ mol of } CHCl_3}{1 \text{ mol of BSA}}$$

Alanine, because of its greater abundance in the protein, appears to be the largest producer of chloroform of the amino acids studied by Morris, even though the yield of chloroform from this amino acid is only 1%. If the same calculation is performed for each of the four amino acids examined by Morris using its abundance in BSA and the yields of chloroform from each determined by Morris et al. (*30*), then the total yield of chloroform expected from the chlorination of BSA is 1.09 mol of $CHCl_3$/mol of BSA. If a solution of 10 mg/L BSA (1.5×10^{-7} M, 4.4 mg/L as carbon) in 0.025 M aqueous potassium phosphate at pH 7.0 is chlorinated to 20 mg/L chlorine and incubated for 24 h at 20 °C, a chloroform concentration of $1.09 \times (1.5 \times 10^{-7}$ M) would be predicted. In fact, such a solution produces 80 μg/L or 6.7×10^{-7} M chloroform or 4.2 as much as the predicted value. To determine if the higher than predicted yield was due to an enhancement of the reaction catalyzed by neighboring groups in the large macromolecule, the protein was hydrolyzed before it was chlorinated. The yield of chloroform from the hydrolyzed protein was 84% of that from the unhydrolyzed protein. However, this difference is insignificant, since some amino acids, especially tryptophan, are decomposed by acid hydrolysis. Consequently, the discrepancy between the predicted and the observed yields of chloroform from the protein is probably due to very low yields of chloroform from amino acids not studied by Morris.

The fact that chlorination of the hydrolyzed protein produces almost as much chloroform in 5 days as the intact protein suggests that the chloroform is being produced

from side chains of the amino acid with little influence from the amide linkages.

Because BSA exerts a greater chlorine demand per milligram of TOC than humic acid, it was expected that the proteins would form significant concentrations of TOCl. There appears to be more variability in the TOCl yields from the different proteins than in the THM yields. Except for cytochrome *c*, the TOCl/TOC ratios for the proteins are lower than for humic acid. Bruchet et al. (*31*) reported a similar finding for a similar chlorine dosage and a 24-h contact time. If the chlorine demand of proteins is greater than humic acid but the TOCl levels are lower, then a greater part of the demand must be going to reduction of the chlorine to chloride. The reactions of aqueous chlorine with amino acids have been studied by many workers and have been reviewed by Burleson et al. (*32*) and Helz et al. (*33*). Recent work (*30*, *34*, *35*) has demonstrated new reactions of amino acids not previously noted. All of these studies have shown that a considerable amount of chloride is produced in oxidizing primary amino groups to carbonyls and carboxylic acid units to CO_2. Those TOCl-forming reactions that involve decarboxylation would also require scission of amide linkages, which may be more dependent on the tertiary structure of the protein than chloroform formation.

Seasonal Variations of Total Dissolved Amino Nitrogen Concentrations and Algal Counts in N.E. Tani Lake, Thornton, CO. Less than 3% of the TDAN in N.E. Tani Lake on September 11, 1984, was due to free amino acids. Proteins appeared to be the major portion of TDAN. These results are consistent with those of Tuschall and Brezonik (*18*), who found that free amino acid concentrations in two lake waters and an algae culture were between 3 and 8% of the TDAN levels.

When routine measuring of TDAN concentrations was begun in April 1985, levels were comparatively low. They increased gradually throughout the summer months (Figure 1). Several small algal blooms were recorded on June 26 and on August 20 (Figure 1), and the TDAN concentration was found to have increased in the nearest sampling. Addition of copper sulfate was suspended in mid September, and a massive algal bloom was recorded shortly thereafter. In the sampling at the end of September, the concentration of TDAN had jumped to 0.96 mg/L or greater than 4 times the concentration in the previous sampling. These data support the correlation between algal blooms and protein concentrations in natural waters.

Implication of Models for Natural Waters. Typical proteins (e.g., BSA in Table I) have carbon/nitrogen weight ratios of 3:1. To estimate the concentration of proteinaceous carbon, the TDAN value was multiplied by 3. Therefore, the water in Figure 1, which contained 0.96 mg/L TDAN, contained approximately 2.9 mg/L protein C. If the proteins in the natural water respond to chlorination like the BSA model, then with sufficient chlorine 0.4 mol % of the carbon will be converted to chloroform. This means that, regardless of any humic or fulvic acids in the water, the proteins alone have the potential for producing 115 μg/L $CHCl_3$, which exceeds the U.S. Environmental Protection Agency's (EPA) maximum contaminant level (MCL) for chloroform.

Water Treatment and the Removal of Proteins. The presence of ammonia in a natural water inhibits the destruction of proteins as well as the production of THMs. As shown in Table II, THM formation was minimized when a natural water containing ammonia was chlorinated to levels below the ammonia breakpoint (4 mg/L as Cl_2). THM concentrations begin to increase dramatically at dosage levels of 5 mg/L and above. However, the protein levels remain relatively constant in samples that contain no free chlorine after 5 days. When free chlorine is detected in a sample, the protein concentrations begin to decrease. This suggests that the peptide backbone, which would account for the major portion of amino nitrogen measured after hydrolysis, remains intact while more reactive side chains (as well as humic acid) react with active chlorine. This is consistent with the slow reaction rate of amide linkages with hypochlorite. Coagulation, sedimentation, filtration, and disinfection remove successively increasing amounts of proteins but do not remove them completely. Throughout the treatment process about 50% of the proteins was removed.

Nominal Molecular Weight Distribution of Proteins and THM Precursors. Veenstra and Schnoor (*36*) showed that greater than 85% of both the total organic carbon (TOC) and the total THM yields from chlorination of Iowa River water was produced by organic precursors with nominal molecular weights less than 3000. Figure 2 shows that 75% of the THM precursors and 74% of the TDAN in water from N.E. Tani Lake have a nominal molecular weight less than 5000. By using the calculation discussed above to estimate the amount of chloroform produced in 5 days by chlorination of each fraction, it appears that proteins contribute between 8 and 11% of the total chloroform produced in each of these fractions. The remainder presumably is derived from humic and fulvic precursors.

Conclusions

Proteins react with aqueous chlorine to produce chloroform and total organic chlorine compounds with yields slightly lower than, but comparable to, a model humic acid. Chlorination of ultrafiltrate fractions of one natural water suggested that proteins contribute about 10% of the THMFP of this water. However, seasonal variations in the concentrations of proteins in natural waters appear to be related to algal blooms. Consequently, their contribution to the THMFP of a natural water may be more significant during summer months of high algal growth. Since proteinaceous THM precursors differ from the classical polyhydroxylated phenolic precursors, it may be important for treatment plant operators to develop different treatment techniques to control the concentration of different types of precursor molecules. This may be especially important if the EPA lowers the MCL of total THMs in finished drinking waters, as recommended recently by the National Academy of Sciences (*38*).

Registry No. Pepsin, 9001-75-6; rennin, 9001-98-3.

Literature Cited

(1) Kraybill, H. F. *Ann. N.Y. Acad. Sci.* **1976**, *298*, 80–82.
(2) Loper, J. C. *Mutat. Res.* **1980**, *76*, 241–268.
(3) *Aquatic and Terrestrial Humic Materials*; Christman, R. F., Gjessing, E. T., Eds.; Ann Arbor Science: Ann Arbor, MI, 1983.
(4) Thurman, E. M. *Organic Geochemistry of Natural Waters*; Martinus Neijhoff/Dr. W. Junk: Dordrecht, The Netherlands, 1985.
(5) Symons, J. A.; Stevens, A. A.; Clark, R. M.; Geldreich, E. E.; Love, O. T., Jr.; DeMarco, J. *Treatment Techniques for Controlling Trihalomethanes in Drinking Water*; Municipal Environmental Research Laboratory, U.S. EPA: Cincinnati, OH, Sept 1981; EPA-600/2-81-156.
(6) Oliver, B. G.; Shindler, D. B. *Environ. Sci. Technol.* **1980**, *14*, 1502–1505.
(7) Hoehn, R. C.; Barnes, D. B.; Thompson, B. C.; Randall, C. W.; Grizzard, T. J.; Shaffer, P. T. B. *J.—Am. Water Works Assoc.* **1980**, *72*, 344–350.

(8) Hoehn, R. C.; Dixon, K. L.; Malone, J. K.; Novak, J. T.; Randall, C. W. *J.—Am. Water Works Assoc.* **1984**, *76*, 134–141.
(9) Wachter, J. K.; Andelman, J. B. *Environ. Sci. Technol.* **1984**, *18*, 811–817.
(10) Briley, K. F.; Williams, R. F.; Longley, K. E.; Sorber, C. A. In *Water Chlorination: Environmental Impact and Health Effects*; Jolley, R. L., et al., Eds.; Ann Arbor Science: Ann Arbor, MI, 1980; Vol. 3, pp 117–129.
(11) Fogg, G. E. In *Physiology and Biochemistry of Algae*; Lewin, R. A., Ed.; Academic: New York, 1962; pp 161–170.
(12) Fowden, L. In *Physiology and Biochemistry of Algae*; Lewin, R. A., Ed.; Academic: New York, 1962; pp 189–209.
(13) Fogg, G. E. *Algal Cultures and Phytoplankton Ecology*; University of Wisconsin Press: Madison, WI, 1975.
(14) Hellebust, J. A. In *Algal Physiology and Biochemistry*; Stewart, W. P. D., Ed.; University of California Press: Berkeley, CA, 1974; pp 838–863.
(15) Volesky, B.; Zajic, J. E.; Knettig, E. In *Properties and Products of Algae*; Zajic, J. E., Ed.; Plenum: New York, 1970; pp 49–82.
(16) Ram, N. M.; Morris, J. C. *Environ. Int.* **1980**, *4*, 397–405.
(17) Gardner, W. S.; Lee, G. F. *Limnol. Oceanogr.* **1975**, *20(3)*, 379–388.
(18) Tuschall, J. R., Jr.; Brezonik, P. L. *Limnol. Oceanogr.* **1980**, *25(3)*, 495–504.
(19) Williams, D. B. *J.—Am. Water Works Assoc.* **1951**, *43*, 837–846.
(20) Bellar, T. A.; Brass, H. J.; Stevens, A. A. *The Determination of the Maximum Total Trihalomethane Potential. Method 510.1*; U.S. Environmental Protection Agency: Cincinnati, OH, April 1982; EPA-600/4-81-044.
(21) Billets, S.; Lichtenberg, J. *Total Organic Halide, Method 450.1*; U.S. Environmental Protection Agency: Cincinnati, OH, April 1982; EPA-600/4-81-056.
(22) Jones, B. N.; Pääbo, S.; Stein, S. *J. Liq. Chromatogr.* **1981**, *4(4)*, 565–586.
(23) Massey, V. *Biochim. Biophys. Acta* **1959**, *34*, 255–256.
(24) *Handbook of Biochemistry and Molecular Biology: Proteins*, 3rd ed.; Farman, G., Ed.; CRC: Cleveland, OH, 1976; Vol. II, pp 383–545.
(25) *Fed. Regist.* **1979**, *44(231)*, 68683–68690.
(26) Gardner, W. S.; Stephens, J. A. *Mar. Chem.* **1978**, *6*, 335–342.
(27) Westall, F.; Hesser, H. *Anal. Biochem.* **1974**, *61*, 610–613.
(28) *Standard Methods for the Examination of Water and Wastewater*, 15th ed.; Franson, M. A., Ed.; American Public Health Association, American Water Works Association, and Water Pollution Control Federation: Washington, DC, 1980; pp 944–946.
(29) Fogg, G. E.; Stewart, W. D. P.; Fay, P.; Walsby, A. E. *The Blue-Green Algae*; Academic: London, 1973; pp 49–51.
(30) Morris, J. C.; Ram, N. M.; Baum, B.; Wajon, E. *Formation and Significance of N-Chloro Compounds in Water Supplies*; U.S. Government Printing Office: Washington, DC, 1980; EPA-600/2-80-031.
(31) Bruchet, A.; Tsutsumi, Y.; Duguet, J. P.; Mallevialle, J. In *Water Chlorination: Chemistry, Environmental Impact, and Health Effects*; Jolley, R. L., et al., Eds.; Lewis: Chelsea, MI, 1985; Vol. 5, pp 1165–1184.
(32) Burleson, J. L.; Peyton, G. R.; Glaze, W. H. *Environ. Sci. Technol.* **1980**, *14*, 1354–1359.
(33) Helz, G. R.; Dotson, D. A.; Sigleo, A. C. In *Water Chlorination: Environmental Impact and Health Effects*: Jolley, R. L., et al., Eds.; Ann Arbor Science: Ann Arbor, MI, 1983; Vol. 4, pp 181–190.
(34) Trehy, M. L.; Yost, R. A.; Miles, C. J. *Environ. Sci. Technol.* **1986**, *20*, 1117–1122.
(35) de Leer, E. W. B.; Baggerman, T.; van Schaik, P.; Zuydeweg, C. W. S.; de Galan, L. *Environ. Sci. Technol.* **1986**, *20*, 1218–1223.
(36) Veenstra, J. N.; Schnoor, J. L. In *Water Chlorination: Environmental Impact and Health Effects*; Jolley, R. L., et al., Eds.; Ann Arbor Science: Ann Arbor, MI, 1980; Vol. 3, pp 109–116.
(37) Scully, F. E., Jr.; Kravitz, R.; Howell, G. D.; Speed, M. A.; Arber, R. P. In *Water Chlorination: Chemistry, Environmental Impact, and Health Effects*; Jolley, R. L., et al., Eds.; Lewis: Chelsea, MI, 1985; Vol. 5, pp 807–820.
(38) National Academy of Sciences *Drinking Water and Health*; National Academy Press: Washington, DC, 1987; Vol. 7, Chapter 3.

Received for review February 9, 1987. Accepted November 24, 1987. This work was funded in part by the Department of Utilities of the City of Thornton, CO, and in part by the U.S. Environmental Protection Agency under Assistance Agreement CR-809333 to the City of Thornton, CO, by the Agency's Water Engineering Research Laboratory (Ben Lykins, Project Officer). This paper has been reviewed in accordance with U.S. EPA policy and approved for publication. Mention of trade names or commercial products does not constitute endorsement or recommendation for use.

Environ. Sci. Technol. 1988, 22, 543–548

Occurrence and Bioaccumulation of Organochlorine Compounds in Fishes from Siskiwit Lake, Isle Royale, Lake Superior

Deborah L. Swackhamer[†] and Ronald A. Hites*

School of Public and Environmental Affairs and Department of Chemistry, Indiana University, Bloomington, Indiana 47405

■ A wide range of chlorinated organic compounds was measured in different size classes of lake trout (*Salvelinus namaycush namaycush*) and whitefish (*Coregonus culpeaformis neohantoniensus*) from Siskiwit Lake, a remote lake on Isle Royale in Lake Superior. Our results confirm the long-range transport of several chlorinated pesticides and polychlorinated biphenyls (PCBs) and, in addition, indicate that technical chlordane constituents, octachlorostyrene, pentachloroanisole, and decachlorodiphenyl ether also are transported to remote locations. Chemical concentrations as a function of fish age (size) were not similar between species and were not consistent among compounds. Differences in bioaccumulation with age between species for a given compound indicated that physical–chemical properties alone do not determine bioaccumulation in a species; fish characteristics are also important. The relationship of the bioconcentration factor (BCF) and the octanol–water partition coefficient (K_{ow}) was examined. The correlation was weak ($r^2 = 0.73$) for pesticides and poor ($r^2 = 0.46$) for PCB congeners when compared to published relationships based on laboratory data.

Introduction

The contamination of aquatic environments by persistent organic compounds has affected biota at every point of the food web. Because of the concentration of these compounds at top levels, fishes are an excellent indicator organism for detecting trace organic compounds whose presence in water would be difficult to measure directly. The difference in contaminant concentration between water and fishes provides an indication of the bioavailability of these compounds. Although numerous data bases exist on organic compound concentrations in Great Lakes fishes (*1–9*), few data are available for more remote regions.

In this paper, the concentrations of a wide range of chlorinated organic compounds in lake trout (*Salvelinus namaycush namaycush*) and whitefish (*Coregonus culpeaformis neohantoniensus*) obtained from Siskiwit Lake, located near the south shore of Isle Royale National Park in Lake Superior, are reported. This remote lake is more than 50 km from the nearest city (Thunder Bay, Ontario). The island was designated as a national park in 1940 and has had little anthropogenic activity. Access to the lake is by backpack trail only. The lake is a recharge lake with no inflow from Lake Superior. Our intent was threefold: (1) to evaluate the extent of contamination by these compounds in a remote lake system as indicated by concentrations of contaminants in fish, (2) to assess the relative bioavailabilities of these compounds by looking at species differences and age differences within species, and (3) to determine the relationship of bioconcentration factor (BCF) and octanol–water partition coefficient (K_{ow}) and to compare these data to bioaccumulation models. Because these previously reported relationships have been based on laboratory rather than field studies, the models were tested for their applicability to natural systems.

Table I. Characteristics of Fish Composites from Siskiwit Lake

species	size class	N	mass range, kg (mean)	size range, cm (mean)	sex M	sex F
lake trout	XLG	4	2.5–3.1 (2.7)	62–67 (64)	2	2
	LG	6	2.1–2.3 (2.2)	58–62 (60)	2	4
	MED	5	1.7–2.0 (1.8)	53–58 (56)	2	3
	SM	3	1.1–1.6 (1.4)	48–56 (52)	3	0
whitefish	LG	6	1.4–2.1 (1.6)	52–53 (53)	1	5[a]
	MED	5	1.2–1.3 (1.2)	47–53 (51)	4	1[a]
	SM	4	1.0–1.2 (1.1)	46–48 (47)	2	2[b]

[a] One female not spawning at time of collection. [b] Two females not spawning at time of collection.

Methods

Fishes were collected by net. They included lake trout and whitefish. Specimens were frozen upon collection. Fish were grouped into composites of similar size and weight; their characteristics are described in Table I. Sex was determined by dissection.

Whole fish were ground with a commercial meat grinder, and composites were reground together to homogenize them. Samples (approximately 12 g, wet tissue) were mixed with anhydrous Na_2SO_4 (approximately 85 g) and Soxhlet extracted with hexane–acetone (1:1) for 24 h. The internal standard, 2,2′,3,4,4′,5,6,6′-octachlorobiphenyl, was added to the extraction solvent prior to extraction. Extracts were reduced in volume, solvent-exchanged to hexane, and subsampled for lipid analysis. The lipids were removed from the extracts by gel permeation chromatography (GPC) (*10*). Extracts were passed over a 2.5 × 38 cm column containing SX-2 Bio-Beads (Bio-Rad, Inc.) and eluted with cyclohexane–dichloromethane (3:2). The eluate was monitored by a fixed-wavelength UV flow detector (254 nm) in order to isolate the fraction containing the compounds of interest. Extracts were reduced in volume, solvent-exchanged to dichloromethane, and cleaned on a microcolumn (0.5 × 8 cm) of silica gel (1% deactivated, w/w). Extracts were eluted with 3 column volumes of dichloromethane followed by methanol. The dichloromethane fraction was solvent-exchanged to hexane, reduced to approximately 1 mL, and stored at −20 °C until analysis. Lipid content was determined gravimetrically by drying a 50.0-μL aliquot of sample extract at room temperature to constant weight (48–60 h).

Samples were analyzed by gas chromatographic mass spectrometry (GC–MS) in the electron capture, negative ion mode with methane as the enhancement gas. The gas chromatograph was a Hewlett-Packard 5840 equipped with splitless injection, a DB-5 capillary column (0.2 mm × 30 m, J&W Scientific), and helium carrier gas. The oven was programmed from 40 to 280 °C at 4 deg/min and held at 280 °C for 15 min after an initial 2-min hold. The splitless vent time was 0.9 min, and the column flow rate was 1.0

[†] Present address: Environmental and Occupational Health, School of Public Health, Box 197 Mayo, 420 Delaware St. SE, University of Minnesota, Minneapolis, MN 55455.

0013-936X/88/0922-0543$01.50/0

Table II. Contaminant Concentrations in Siskiwit Lake Fish Expressed as ng/g of Lipid

compound	lake trout concn					whitefish concn			
	SM	MED	LG	XLG	mean	SM	MED	LG	mean
BHC	140	110	180	110	130	150	180	280	200
pentachlorobenzene	3.3	2.2	3.0	4.7	3.3	3.9	6.4	8.8	6.4
hexachlorobenzene	48	40	62	110	65	64	88	100	85
heptachlor epoxide	74	30	45	85	58	210	190	120	170
dieldrin	470	180	310	1200	550	690	760	420	620
pentachloroanisole	3.1	3.1	3.8	4.4	3.6	4.4	6.3	8.8	6.5
DDE	3600	2800	4300	37000	12000	4700	7600	5100	5800
chlordane	320	230	380	770	420	320	330	140	260
octachlorostyrene	13	13	17	32	19	12	24	13	16
toxaphene	4400	15000	14000	8500	11000	6400	10000	4500	7000
nonachlor	290	360	600	1100	570	490	370	500	450
mirex	19	17	nd[a]	nd	9.1	11	nd	nd	3.7
decachlorodiphenyl ether	4.2	18	15	nd	9.3	8.4	53	31	31
Dacthal	43	28	42	38	38	37	30	70	46
oxychlordane	43	34	45	170	73	160	200	140	160
endosulfan	nd	1.5	nd	nd	0.4	nd	nd	nd	nd
PCBs									
2,2′	57	nd	nd	24	20	110	nd	nd	36
2,4′	460	420	400	320	400	490	570	360	480
4,4′	180	410	440	380	350	460	620	230	440
2,2′,5	23	80	84	71	64	54	80	48	60
2′,3,4	97	300	290	200	220	210	210	83	160
2,2′,3,3′	20	65	60	35	45	160	390	120	230
2,2′,4,5′	40	130	120	70	90	78	100	33	71
2,2′,5,5′	60	160	130	90	110	120	180	110	130
2,2′,3′,4,5	54	96	130	67	86	160	210	83	150
2,2′,4,5,5′	170	270	220	190	210	150	230	190	190
2,3′,4,4′,5	170	250	210	520	290	280	420	130	280
2,2′,3,4,4′,5	85	160	150	88	120	190	260	56	170
2,2′,3,4,4′,5′	530	790	560	1500	830	1000	1600	490	1000
2,2′,3,4′,5′,6	73	120	110	93	100	73	130	36	80
2,2′,3,4,4′,5,5′	230	290	250	1100	470	350	540	220	370
2,2′,3,4′,5,5′,6	180	320	180	330	250	150	250	96	160
2,2′,3,3′,4,4′,5,5′	49	76	56	260	110	95	140	70	100
2,2′,3,3′,4′,5,5′,6	85	130	110	260	150	120	180	86	130
2,2′,3,3′,4,4′,5,5′,6	nd	66	nd	160	56	nd	98	nd	33

[a] nd = not detected.

mL/min. The transfer lines, modified as described by Jensen et al. (*11*), and the injection port were kept at 285 °C. The MS was a Hewlett-Packard Model 5985B. The ion source temperature was 100 °C, and the methane pressure was 0.35 Torr as measured by a capacitance manometer (*12*).

Polychlorinated biphenyl (PCB) congeners were quantified with an HP 5890 GC equipped with an electron capture detector, splitless injection, HP 7376 autosampler, and HP 3392 integrator interfaced to an IBM XT computer. The column used was the same as above. GC conditions were as follows: injection port, 225 °C; detector, 325 °C; hydrogen carrier gas, 1.3 mL/min; 95/5% argon-in-methane makeup gas, 20 mL/min; splitless vent time, 0.9 min; initial temperature, 100 °C for 1 min; ramp to 160 °C at 30 deg/min; ramp to 260 °C at 2 deg/min; ramp to 280 °C at 10 deg/min.

Fish samples were examined for the following compounds: trichloroanisole, pentachloroanisole, pentachlorobenzene, hexachlorobenzene, α-, β-, γ-, and δ-hexachlorocyclohexane (BHC), chlordene, heptachlor, aldrin, Dacthal, octachlorostyrene (OCS), heptachlor epoxide, oxychlordane, α- and γ-chlordane, endosulfan I, *trans*-nonachlor, dieldrin, *p,p′*-DDE, *o,p′*-DDD, *p,p′*-DDT, mirex, photomirex, penta- and decachlorinated diphenyl ethers, total toxaphene, and 22 PCB congeners. The PCB congeners chosen for study were selected to span a wide range of chlorination, molecular weight, solubility, and vapor pressure, and because they were prominent in the samples and contribute significantly to the mass of commercial Aroclors. The detection limit for all compounds was approximately 1 ng/g, expressed on a fish lipid basis. Compounds were identified by comparing their mass spectra and GC retention times to those of known standards. All compounds except toxaphene and PCBs were quantitated by comparing the areas of representative mass chromatograms from the unknown and the internal standard (m/z 430) and from the relative response factor for the standard compound. New response factors were determined for each day's analyses.

Toxaphene was quantitated by a selected ion monitoring (SIM) program developed in this laboratory (*13*). PCB congeners were quantitated against standard response factors by the internal standard method. Response factors were determined from individual PCB congeners (Ultra Scientific) on the same day as analyses.

Procedural blanks were included with every five sample extractions. Blank levels were negligible. Three of the eight samples were extracted in duplicate, and three of the resulting 11 extracts were analyzed in duplicate. The coefficients of variation were 36 and 28% for duplicate extractions and duplicate GC–MS analyses, respectively. Because quantitation was done relative to an internal standard added at extraction, all reported concentrations are corrected for procedural losses. Duplicate lipid analyses varied by 6%.

Results and Discussion

The concentrations of compounds found in Siskiwit Lake fish are shown in Table II expressed as nanograms of compound per gram of fish lipid. Because these compounds are lipophilic, their concentrations are normalized

Table III. Concentrations of Selected Organochlorine Compounds in Lake Superior and Siskiwit Lake Lake Trout and Whitefish[a]

species	location	date	ref	PCB	DDE	dieldrin	HCB	BHC	hept epox
lake trout	Lake Superior	1975	15	14	4	0.4	0.08	0.1	0.05
	Lake Superior	1977–1979	5	5	2	0.3	0.05	0.1	nm[b]
	Siskiwit Lake	1975	15	34	68	0.3	0.1	0.3	0.2
	Siskiwit Lake	1983	*e*	*d*	12	0.5	0.06	0.1	0.06
whitefish	Lake Superior	1975	15	4	2	0.3	0.06	0.1	0.04
	Lake Superior	1977–1979	5	3	0.9	0.4	0.1	0.2	nm
	Siskiwit Lake	1975	15	3	2	0.2	nd[c]	0.2	0.2
	Siskiwit Lake	1983	*e*	*d*	6	0.6	0.09	0.2	0.2

[a] All concentrations are expressed in $\mu g/g$ of fish lipid. [b] Not measured. [c] Not detected. [d] Total PCB was not measured in this study, but based on congener analysis, PCB levels are estimated to be less than in 1975. [e] This study.

to lipid content to facilitate comparisons among samples having differing amounts of fat. Of the compounds targeted for study, trichloroanisole, β- and δ-BHC, chlordene, heptachlor, aldrin, DDD, photomirex, and pentachlorodiphenyl ethers were not found in the fish. DDT was detected in large and medium lake trout composites but not in amounts that could be reliably quantitated. Additional isomers of chlordane and nonachlor were also detected. For these compounds, an average response factor of the available isomer standards was used for their quantitation.

Toxaphene, a mixture of chlorinated camphenes, generally was the most abundant contaminant. The most abundant single pesticide in all the samples was DDE, followed by dieldrin and *trans*-nonachlor. PCB congeners were also present in high concentrations relative to other compounds. The least abundant compounds were pentachlorobenzene, pentachloroanisole, γ-BHC, and decachlorodiphenyl ether. Mirex was detected in only three fish composites, and endosulfan was in a single composite.

The high concentrations of DDE may partly be due to localized DDT application. Isle Royale National Park officials recall that some DDT was used on the island in the 1960s. However, no other pesticides were used.

Atmospheric Transport. Because Siskiwit Lake is remote and far from point sources, the presence of contaminants in Siskiwit Lake indicates their source is the atmosphere. Long-range atmospheric transport of PCBs, chlorobenzenes, DDT, BHC, dieldrin, heptachlor epoxide, and toxaphene have been documented (*14–18*). The occurrence of Dacthal, mirex, chlordane, nonachlor, oxychlordane, octachlorostyrene (OCS), pentachloroanisole, and decachlorodiphenyl ether (DPE) in a remote site has not been reported previously, and this indicates that these compounds are transported and deposited in sites far removed from their initial application or formation. Once they are transferred to the lake by wet and dry removal processes, they enter the food chain and are accumulated in fish.

It is not surprising that these pesticides are widely distributed in the environment because many of them were used extensively and are resistant to degradation. However, it is surprising to find OCS in Siskiwit Lake. This chemical was not manufactured directly for a specific use, but it was a byproduct in the manufacture of chlorine gas (*19*). High concentrations of OCS are found in the Lake Ontario ecosystem because of a point source on the Niagara River; there is little evidence of its presence in the upper Great Lakes (*6*). The presence of OCS in Siskiwit Lake fishes confirms that it is also subject to atmospheric transport to remote sites. Pentachloroanisole and DDE are biodegradation products of pentachlorophenol and DDT, respectively. These compounds were either transported directly or were formed after transport prior to uptake by fish. Decachlorodiphenyl ether (DPE), a byproduct in the formation of pentachlorophenol, apparently also is transported to remote sites.

Concentrations of chlorinated organic compounds in Siskiwit Lake fishes are generally similar to those in Lake Superior fishes (see Table III) and less than those in fishes from the other Great Lakes on a species basis (*1–5, 7*). The similarity in concentrations to Lake Superior fishes is expected because the atmosphere is thought to be the primary source of contaminants to Lake Superior (*20*).

Swain (*18*) conducted a study in 1976 that compared contaminant concentrations in lake trout and whitefish from several locations in Lake Superior to those in Siskiwit Lake. He found that when concentrations were normalized to lipid content, the Siskiwit lake trout had significantly higher concentrations of PCBs, HCB, BHC, heptachlor epoxide, and DDE than lake trout from Lake Superior. Siskiwit whitefish had higher concentrations of BHC and heptachlor epoxide. Further investigation revealed that concentrations of PCBs in Siskiwit Lake water were considerably greater than those in open Lake Superior waters. Thus, increased exposure led to higher contaminant concentrations in fishes. Although both lakes may receive similar inputs, differences in depth and particle removal mechanisms possibly account for the different aqueous concentrations. Recent findings by this laboratory support these observations (*21*).

Comparison of the contaminant concentrations in Siskiwit lake trout from 1975 and 1983 indicates that contaminant concentrations in fish generally have decreased over time. A quantitative comparison could not be made for PCBs because earlier studies measured total PCBs and this study measured selected congeners. However, a qualitative assessment of the data indicates that PCB concentrations have decreased with time. The observation of decreasing contaminant concentrations is supported by a comparison of the Lake Superior lake trout data from 1975 and 1977–1979. This decrease is consistent with a decrease in the input functions for these compounds; for example, PCBs are now banned for use by the EPA. This decreasing trend is not seen in the whitefish, where DDE and dieldrin are higher in the later measurements. This indicates that the source of contaminants to the whitefish has not decreased over time and is different from the source for lake trout. This observation may be explained by differences in fish food sources. The lake trout are deep-water pelagic piscivores, while the whitefish are benthic omnivores. Because of low sedimentation rates, mixing, and resuspension, concentrations of PCBs in sediments (and in benthic biota) would respond more slowly to decreased atmospheric inputs than would the water column and its biota.

Species and Age Differences. Concentrations averaged across all size groups were not consistently higher in

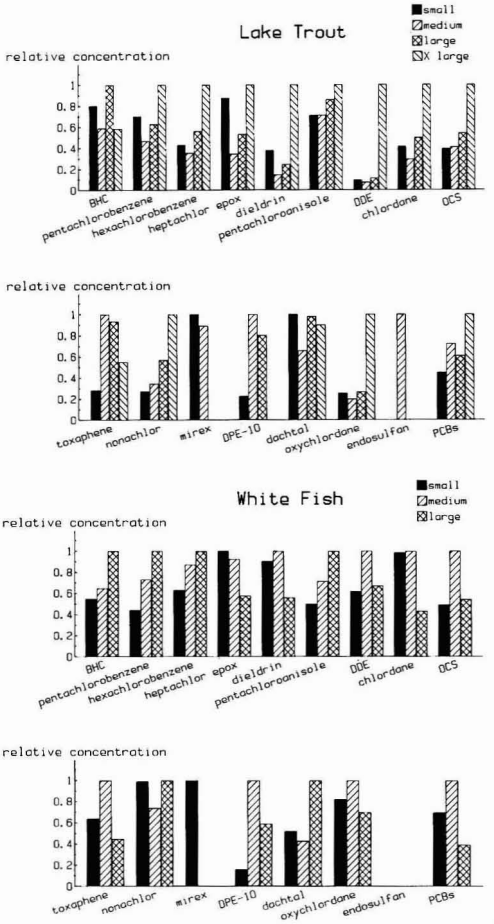

Figure 1. The distribution of concentrations relative to fish size for 17 compounds in Siskiwit lake trout and whitefish. Concentrations of each compound are normalized to the highest concentration in the species size classes. PCBs are the sum of selected congeners and are not total PCB.

one species compared to the other. This is probably because they are both near the top of their respective, but separate, food webs. To compare relative differences among size classes for each of the compounds in a given species, concentrations were expressed as a fraction of the highest concentration. The results are displayed in Figure 1 for both species.

Among lake trout, the extra-large (XLG) size group generally had the highest concentration of contaminants. If one assumes that size is directly correlated to age, then longer exposure times would lead to increased concentrations of compounds in these fish. The large class usually had higher concentrations than the medium class. For most compounds, the small size class also had higher concentrations than the medium size class. It is possible that this is an artifact due to the sexual composition of the composites. The small lake trout contained no females (see Table I), and thus, they would have no way to lower body burdens of lipophilic contaminants by spawning (*22*). Excluding the small class from the comparison, the general trend is medium < large < extra-large for many of the compounds, which suggests that bioaccumulation of compounds is related to length of exposure or to dietary intake. The food sources for the extra-large lake trout may have a greater contaminant burden than those for smaller lake trout, thus contributing to the higher contaminant concentration in the larger fish. The profiles of BHC, mirex, DPE, and Dacthal suggest that length of exposure does not affect bioaccumulation of these compounds.

The concentration distribution with age in whitefish differed among compounds to a greater extent than the same distributions did in lake trout. No one size class consistently had the highest concentrations. Although the medium size class usually had higher concentrations than the small size class, this trend did not extend to include the large size class. Because the latter consisted of 80% females, it is possible that spawning may have decreased their body burdens. Thus, fish sex may be an important variable to consider when compositing fish.

Note that the size profile for a given compound was not the same between species for about half of the compounds studied. This indicates that contaminant properties alone, such as K_{ow} or solubility, do not determine uptake but that species factors may play an equally important role. Possible factors may include lipid compositional differences (relative amounts of saturated and unsaturated fatty acids), metabolic differences, contaminant source differences, or dietary intake. However, because the number of fish in each size class is small, the conclusions offered here are not definitive.

Bioconcentration. Bioaccumulation of compounds in fish is the process by which chemicals are enriched in the organisms relative to the water in which they reside. It is well accepted for fishes and many other animals that hydrophobic compounds preferentially accumulate in lipids relative to other compartments. Accumulation of contaminants in fish lipids can occur by two routes: (a) diffusion from the water across the gills into the body and (b) transfer from the gut into the body after consumption of contaminated food. The relative importance of these routes is affected by species, locale, food web, and contaminant physical–chemical properties.

The bioconcentration factor, BCF, has been used to quantitatively describe bioaccumulation. It is defined as the dimensionless ratio of wet-weight contaminant concentration in fish, C_F, to the water concentration, C_W:

$$\mathrm{BCF} = C_F/C_W$$

It also describes the equilibrium reached between uptake and depuration of a contaminant by fish and is the ratio of the respective rate constants for those processes.

The association of contaminants with fish lipids has led several researchers to model bioaccumulation on the basis of lipid–water equilibrium partitioning and to develop correlations between BCF and K_{ow}, the octanol–water partition coefficient (*23–29*). These models assume that octanol is suitable for modeling fish lipids and that the contaminant is recalcitrant. Mackay (*28*) argues that the slope of a plot of log BCF vs log K_{ow} should be unity if octanol is a good surrogate for fish lipids, and his model supports this. Significant correlations have been observed for a wide range of hydrophobic organic compounds having K_{ow} and BCF values spanning 4–5 orders of magnitude. These models serve as a reasonable approximation for modeling BCF, but they can have errors of up to 1 log unit. The BCF data for these older studies were all derived from laboratory tank studies where fish were exposed to water having a known contaminant concentration. Thus, consumptive uptake was not included.

How well do these models explain the real world? BCF values were calculated for 27 compounds in our data set where contaminant concentrations in water were obtained.

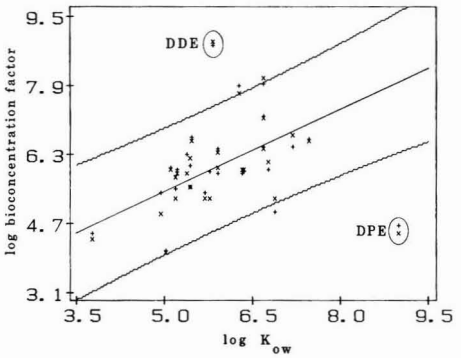

Figure 2. Least-squares linear regression of log BCF vs log K_{ow} for Siskiwit lake trout (×) and whitefish (+). The BCFs are lipid-normalized. The 90% confidence limits about the population mean are shown. DDE and decachlorodiphenyl ether (DPE) were omitted from the regression.

Whitefish and lake trout values were normalized to lipid content, and the resulting log BCF values were plotted against log K_{ow} (see Figure 2). Lipid normalization facilitates comparison of the two species and affects the intercept but not the slope of the relationship. While a trend is observed between log BCF and log K_{ow}, there is considerable scatter in the data. Omitting DDE and DPE from the regressed data set (because of highly enhanced and depressed BCF values, respectively), a regression coefficient (r^2) of 0.46 was obtained. While this is a statistically significant correlation ($r^2 = 0.18$ at $p = 0.01$), it is much less than the regression coefficients obtained in the aforementioned laboratory studies, all of which were >0.9. Thus, laboratory-derived models may be poor approximations of bioaccumulation of these compounds in fish in the environment.

Oliver and Niimi (*30*) developed a log BCF–log K_{ow} relationship for chlorinated benzenes in laboratory experiments with rainbow trout and then tested their model against fish from Lake Ontario. They found that, with the exception of hexachlorobenzene (HCB), their model accurately predicted the field contaminant concentrations in fish. They concluded that lake exposure rather than consumptive processes controlled the chlorinated benzene concentrations in rainbow trout (except for HCB). However, Thomann and Connolly (*31*), in their model of the Lake Michigan lake trout food chain, found that concentrations of PCBs in lake trout could not be predicted by a simple log BCF–log K_{ow} relationship and that >99% of the PCBs in lake trout were derived from food chain uptake rather than lake water exposure. This was also found for PCBs in Lake Michigan lake trout by Weininger (*32*). Farrington and co-workers reported that the BCF values of selected PCB congeners in mussels, lobster, and flounder were poorly predicted by log K_{ow} (*33*, *34*). Thus, evidence exists that this relationship cannot be strictly applied to PCB bioaccumulation in the field. Possible explanations for this PCB anomaly include selective metabolism of different congeners, differential uptake, or depuration rate variations due to chlorine configuration differences affecting membrane transport.

If PCBs are excluded from our data set, the regression becomes log BCF = 1.05 log K_{ow} + 0.39 with $r^2 = 0.73$. This correlation more closely resembles that of Mackay (*28*). However, substantial deviations still exist. The regression underestimates the BCF for DDE by more than 2 orders of magnitude. The observed enhanced bioconcentration may be due to preferential membrane transport because of its more planar configuration compared to the other compounds in the data set. The planarity of a molecule has been implicated in controlling bioavailability of dioxin congeners in fish (*35*).

The BCF for DPE is several orders of magnitude lower than predicted by the regression. It has been postulated that accumulation of certain high molecular weight compounds is prohibited when the width of the compound is >9.5 Å (*36*). This may explain why octachlorodioxin and octachloronaphthalene are not readily accumulated, whereas decachlorobiphenyl is accumulated. The low accumulation of DPE is consistent with this model.

Clearly, the log BCF–log K_{ow} model is only useful as a rough approximation of bioaccumulation in the field, and it fails completely for some classes of compounds such as PCBs. The assumption that octanol can be used to approximate lipids may be incorrect. The thermodynamics for equilibrium partitioning between water–fish lipid and water–octanol may not be similar (*37*, *38*). Inclusion of metabolism, lipid composition, and molecular size and configuration is needed to reliably model bioaccumulation of contaminants in fish in the environment.

Acknowledgments

We thank I. Basu for technical assistance and D. Weidner for preparation of the manuscript. The cooperation of the National Park Service is gratefully acknowledged. A special thanks to B. McVeety for his trips to Siskiwit Lake and helpful discussions.

Registry No. BHC, 58-89-9; DDE, 72-55-9; 2,4′-DCB, 34883-43-7; 4,4′-DCB, 2050-68-2; 2,2′,5-TCB, 37680-65-2; 2′,3,4-TCB, 38444-86-9; 2,2′,3,3′-TCB, 38444-93-8; 2,2′,4,5′-TCB, 41464-40-8; 2,2′,5,5′-TCB, 35693-99-3; 2,2′,3′,4,5-PCB, 41464-51-1; 2,2′,4,5,5′-PCB, 37680-73-2; 2,3′,4,4′,5-PCB, 31508-00-6; 2,2′,3,4,4′,5-HCB, 35694-06-5; 2,2′,3,4,4′,5′-HCB, 35065-28-2; 2,2′,3,4′,5′,6-HCB, 38380-04-0; 2,2′,3,4,4′,5,5′-HCB, 35065-29-3; 2,2′,3,4′,5,5′,6-HCB, 52663-68-0; 2,2′,3,3′,4,4′,5,5′-OCB, 35694-08-7; 2,2′,3,3′,4′,5,5′,6-OCB, 52663-75-9; 2,2′,3,3′,4,4′,5,5′,6-NCB, 40186-72-9; C_6HCl_5, 608-93-5; C_6Cl_6, 118-74-1; heptachlor epoxide, 1024-57-3; dieldrin, 60-57-1; pentachloroanisole, 1825-21-4; chlordane, 12789-03-6; octachlorostyrene, 29082-74-4; toxaphene, 8001-35-2; nonachlor, 3734-49-4; mirex, 2385-85-5; decachlorodiphenyl ether, 31710-30-2; dacthal, 1861-32-1; oxychlordane, 27304-13-8; endosulfan, 115-29-7.

Literature Cited

(1) Veith, G. D.; Kuehl, D. W.; Puglisi, F. A.; Glass, G. E.; Eaton, J. G. *Arch. Environ. Contam. Toxicol.* **1977**, *5*, 487–499.
(2) Frank, R.; Holdrinet, M.; Braun, H. E.; Dodge, D. P.; Sprangler, G. E. *Pestic. Monit. J.* **1978**, *12*, 60–68.
(3) Schmitt, C. J.; Ludke, J. L.; Walsh, D. F. *Pestic. Monit. J.* **1981**, *14*, 136–208.
(4) Hesselberg, R. J.; Seelye, J. G. "U.S. Fish and Wildlife Service Report USFWS-GLFL/AR-82-1"; U.S. Fish and Wildlife Service: Ann Arbor, MI, 1982.
(5) Schmitt, C. J.; Ribick, M. A.; Ludke, J. L.; May, T. W. "U.S. Fish and Wildlife Service Resource Publication 152"; U.S. Fish and Wildlife Service: Washington, DC, 1983.
(6) Jaffe, R.; Stemmler, E. A.; Eitzer, B. D.; Hites, R. A. *J. Great Lakes Res.* **1985**, *11*, 156–162.
(7) DeVault, D. *Arch. Environ. Contam. Toxicol.* **1985**, *14*, 587.
(8) DeVault, D.; Wilford, W.; Hesselberg, R.; Northrup, D.; Rundberg, B.; Lawan, A. K.; Batistea, C. *Arch. Environ. Contam. Toxicol.* **1986**, *15*, 349.
(9) DeVault, D.; Weisaar, J.; Clark, J.; Loharts, G. *J. Great Lakes Res.*, in press.
(10) Stalling, D. L.; Tindle, R. C.; Johnson, J. L. *J. Assoc. Off. Anal. Chem.* **1972**, *55*, 32–38.
(11) Jensen, T. E.; Kaminsky, R.; McVeety, B. D.; Wozniak, T. J.; Hites, R. A. *Anal. Chem.* **1982**, *54*, 2385–2388.
(12) Stemmler, E. A.; Hites, R. A. *Anal. Chem.* **1985**, *57*, 684–692.

(13) Swackhamer, D. L.; Charles, M. J.; Hites, R. A. *Anal. Chem.* **1987**, *59*, 913.
(14) Harvey, G. R.; Steinhauer, W. G. *Atmos. Environ.* **1974**, *8*, 777-782.
(15) Bidleman, T. F.; Olney, E. E. *Nature (London)* **1975**, *257*, 475-477.
(16) Atlas, E.; Giam, C. S. *Science (Washington, D.C.)* **1981**, *211*, 163-165.
(17) Ballschmiter, K.; Zell, M. *Int. J. Environ. Anal. Chem.* **1980**, *8*, 15-35.
(18) Swain, W. R. *J. Great Lakes Res.* **1978**, *4*, 398-407.
(19) Kaminsky, R.; Hites, R. A. *Environ. Sci. Technol.* **1984**, *18*, 275-279.
(20) Eisenreich, S. J.; Hollod, G. J.; Johnson, T. C. *Environ. Sci. Technol.* **1979**, *13*, 569-573.
(21) Swackhamer, D. L.; McVeety, B. D.; Hites, R. A. *Environ. Sci. Technol.*, in press.
(22) Niimi, A. J. *Can. J. Fish. Aquat. Sci.* **1983**, *40*, 306-312.
(23) Neely, W. B.; Branson, D. R.; Blau, G. E. *Environ. Sci. Technol.* **1984**, *8*, 1113-1115.
(24) Chiou, C. T.; Freed, V. H.; Schmedding, D. W.; Kohnert, R. L. *Environ. Sci. Technol.* **1977**, *11*, 475-478.
(25) Veith, G. D.; DeFoe, D. L.; Bergstedt, B. V. *J. Fish. Res. Board Can.* **1979**, *36*, 1040-1048.
(26) Kenaga, E. E. *Environ. Sci. Technol.* **1980**, *14*, 553-556.
(27) Konemann, H.; Leeuwen, K. V. *Chemosphere* **1980**, *9*, 3-19.
(28) Mackay, D. *Environ. Sci. Technol.* **1982**, *16*, 274-278.
(29) Chiou, C. T. *Environ. Sci. Technol.* **1985**, *19*, 57-62.
(30) Oliver, B. G.; Niimi, A. J. *Environ. Sci. Technol.* **1983**, *17*, 287-291.
(31) Thomann, R. V.; Connolly, J. P. *Environ. Sci. Technol.* **1984**, *18*, 65-71.
(32) Weininger, D. Ph.D. Dissertation, University of Wisconsin, Madison, WI, 1978.
(33) Farrington, J. W.; Westall, J. In *The Role of the Oceans as a Waste Disposal Option*; Kullenberg, G., Ed.; Reidel: Dordrecht, The Netherlands, 1986; pp 361-425.
(34) Farrington, J. W.; Davis, A. C.; Brownawell, B. J.; Tripp, B. W.; Clifford, C. H.; Livramento, J. B. In *Organic Marine Geochemistry*; Sohn, M. L., Ed.; ACS Symposium Series 305; American Chemical Society: Washington, DC, 1986; pp 174-197.
(35) Kuehl, D. W.; Cook, P. M.; Batterman, A. R.; Lothenbach, D. B. *Chemosphere* **1985**, *14*, 427-437.
(36) Opperhuizen, A.; van der Velde, E. W.; Gobas, F. A. P. C.; Liem, D. A. K.; van der Steen, J. M. D. *Chemosphere* **1985**, *14*, 1871-1896.
(37) Opperhuizen, A. Ph.D. Dissertation, University of Amsterdam, Netherlands, 1986.
(38) Matsuo, M. *Chemosphere* **1980**, *9*, 671-675.

Received for review February 10, 1987. Revised manuscript received November 3, 1987. Accepted December 16, 1987. This work was supported by the U.S. Environmental Protection Agency through Grant R808865.

Comparative Toxicology for Risk Assessment of Marine Fishes and Crustaceans†

Glenn W. Suter II* and Aaron E. Rosen

Environmental Sciences Division, Oak Ridge National Laboratory, Oak Ridge, Tennessee 37831

■ The goal of this study was to collect data on the effects of chemicals on marine fishes and crustaceans and to evaluate the predictive power of the data for assessing risks to marine resources. The data sets consisted of acute median lethal concentrations (LC_{50}s) and chronic maximum acceptable toxicant concentrations (MATCs). They were analyzed with regression models and simple comparisons. The conclusions include the following: (1) the variability found in the marine data was comparable to that found in freshwater data; (2) the standard marine test fish *Cyprinodon variegatus* appears to be representative of marine fishes; (3) the responses of marine crustaceans are so highly diverse that the concept of a representative crustacean is questionable; (4) mysid and penaeid shrimp appear to be particularly sensitive to toxic chemicals. These conclusions are subject to the constraints of the existing limited data base and should be confirmed by a systematic study of the relative sensitivity of marine organisms to chemicals with diverse modes of action.

Introduction

Fishes and crustaceans inhabiting coastal marine waters are subject to the effects of a variety of pollutants plus habitat loss, harvesting, entrainment in water intakes, and natural stresses. Changes in the abundance of these organisms are apparent but difficult to explain. The goal of this study was to collect data on the effects of chemicals on marine fishes and crustaceans and evaluate the predictive power of the data using environmental risk assessment methods developed for the U.S. Environmental Protection Agency (EPA) (*1*). The results would be a tool for determining where pollutants may be affecting coastal stocks of fishes and crustaceans.

The specific objectives were as follows: (1) to evaluate the utility of existing marine toxicity data for developing the types of taxonomic and acute–chronic extrapolation formulas that have been used for risk analysis of toxic effects on freshwater organisms (*2*, *3*), (2) to examine the representativeness of the standard marine test species, (3) to compare the relative sensitivities of toxicants of different marine species, (4) to evaluate the feasibility of extrapolating from freshwater to marine species.

Methods

Data Sets. We used four data sets in this study. The first is a marine chronic toxicity data set consisting of data from studies reporting acceptable life cycle, partial life cycle, or early life stage maximum acceptable toxicant concentrations (MATCs) for marine or estuarine fishes or crustaceans. The MATC is the geometric mean of the lowest concentration producing a statistically significant effect and the highest concentrationproducing no such effect on survival, growth, or fecundity in any life stage in a life cycle, partial life cycle, or early life stage test. It is used as a threshold for toxic effects in exposures of indefinite duration but does not correspond to any particular level or type of effect on any particular life stage. The MATCs and associated 96-h median lethal concentrations (LC_{50}s) for 114 species–chemical pairs are listed in Table I. The second is an equivalent set of chronic data for freshwater fishes, containing the results of 177 chronic tets (*1*). The third is a set of chronic data (MATCs and

† Publication No. 2792, Environmental Sciences Division, Oak Ridge National Laboratory.

 0013-936X/88/0922-0548$01.50/0

Table I. Marine Chronic Data Set

chemical	species[a]	LC_{50}, μg/L	MATC, μg/L	MATC type[b]	ref
AC 222, 705	CV	1.1	0.04	ELS	4
acenaphthene	CV	3100	710	ELS	5
acephate	MB	73000	900	LC	6
silver nitrate	MB	249	19	LC	7
	MB	141	15	LC	8
	MB		59	LC	8
	MB	300	53	LC	8
aldicarb	MB	16	1.2	LC	6
ammonium jarosite	CV	500000	180000	ELS	9
Aroclor 1016	CV		7.1	ELS	10
Aroclor 1254	CV		0.098	ELS	11
arsenic	MB	1740	893	LC	7
atrazine	MB	1000	123	LC	12
	CV	16000	2542	ELS	12
bis(tributyltin) oxide	CV	0.96	3.7	LC	13
bromoform	CV	71000	6400	ELS	5
carbofuran	CV	386	19	LC	14
carbophenothion	PP	2.9	0.28	LC	6
	MB	3.0	0.76	LC	6
	CV	2.8	1.9	ELS	6
cadmium	MB	15.5	5.5	LC	15, 16
	MB	110	7.1	LC	17
chlordane	CV	12.5	0.6	LC	18
	CV	24.5	11	ELS	19
oxidants	MP	0.054	0.072	ELS	20
chlorpyrifos	MM	1.7	0.37	ELS	21
	LT	1.3	1.2	ELS	21
	MY	4.2	0.54	ELS	21
	MP	1.3	46	ELS	21
	CV		2.3	ELS	22
	OB	560	<3.7	ELS	23
chlorine	MP	54	46	ELS	24
cyanide	MB	113	(0	LC	7
	CV	300	36	ELS	7
chromium	MB	2030	132	LC	24
copper	MB	181	54	LC	7
DEF (*S,S,S*-tributyl phosphotrithioate)	MB	4.55	<0.34	LC	25
diazinon	MB	4.82	1.94	LC	25
diazinon	CV	1.470	<0.47	LC	26
dieldrin	EA	23	1.4	LC	27
dieldrin	MB	4.5	0.73	LC	28
dimilin	MB	2.06	<0.075	LC	29
endosulfan	MB	1.37	0.48	LC	28
	MB	1.30	0.48	LC	8
	MB	1.05	0.21	LC	8
	MB	5.00	0.41	LC	8
	MB	4.60	0.25	LC	8
	CV	0.95	0.40	ELS	28
	CV		0.68	ELS	30
	CV		0.41	ELS	30
	CV		0.41	ELS	30
	CV		0.37	ELS	30
	CV		1.77	ELS	30
	CV		0.29	ELS	30
	CV		0.86	ELS	30
	CV		0.83	ELS	30
	CV		0.27	ELS	30
	CV		0.45	ELS	30
endrin	PP	0.35	0.04	LC	31
	MB	0.185	0.01	LC	32
	CV	0.34	0.19	LC	33
	CV	0.38	0.31	ELS	34
EPN [*O*-ethyl *O*-(*p*-nitrophenyl) phenylthiophosphonate]	MB	3.01	1.35	LC	25
	CV		5.7	LC	35
ethoprop	MB	7.5	0.47	LC	6
	CV	180	16	ELS	6
fenvalerate	CV	5	1.1	ELS	4
fluoranthene	MB	40	16	LC	28
guthion	CV		0.35	LC	35
heptachlor	CV	3.68	1.58	ELS	36
	CV	10.5	1.4	LC	37
mercury	MB	3.5	1.1	LC	38, 39
isophorone	CV	140000	110000	ELS	5
kepone	EA	40	7.1	LC	40
	MB	10.1	0.043	LC	15
	CV	69.5	0.094	LC	41
	CV	69.5	0.08	LC	42
leptophos	MB	3.31	1.06	LC	25
malathion	CV	51	6	LC	14
methoxychlor	CV	49	17	LC	14
methyl parathion	MB	0.77	0.13	LC	25
nickel	MB	508	93	LC	38
lead	MB	3130	25	LC	7
pentachlorobenzene	CV		26	ELS	30
	CV		29	ELS	30
	CV		66	ELS	30
	CV		87	ELS	30
	CV		145	ELS	30
	CV		73	ELS	30
	CV		155	ELS	30
	CV		88	ELS	30
	CV		74	ELS	30
pentachloroethane	MB	5060	580	LC	28
pentachlorophenol	CV	420	64	LC	18
permethrin	CV	7.8	1.06	ELS	4
phorate	MB	0.33	0.11	LC	25
	CV	1.3	0.31	ELS	6
selenium	MB	15000	212	LC	43
	CV	7400	675	ELS	43
tetrachloroethylene	MB	10200	450	LC	28
thiobencarb	MB	330	28	LC	8
thallium	CV	20900	6000	ELS	28
toluene	CV	13000	5000	ELS	5
toxaphene	MB	2.69	0.10	LC	25
	CV	1.1	1.7	ELS	36
trifluralin	CV	190	2.5	LC	18
zinc	MB	499	166	LC	7
1-chloronaphthalene	CV	690	555	ELS	5
1,2,4-trichlorobenzene	CV	214000	222	ELS	28
1,2,4,5-tetrachlorobenzene	CV	330	129	ELS	5
1,3-dichloropropane	MB	10300	3040	LC	28
2,4-dichloro-6-methylphenol	CV	3700	360	ELS	5
2,4-dinitrophenol	CV	29400	7900	ELS	28
4-nitrophenol	CV	32000	12650	ELS	5

[a] CV = *Cyprinodon variegatus*; EA = *Eurytemora affinis*; LT = *Leuresthes tenuis*; MB = *Mysidopsis bahia*; MM = *Media menidia*; MP = *Menidia peninsulae*; MY = *Menidia beryllina*; OB = *Opsanus beta*; PP = *Palaemonetes pugio*. [b] ELS = early life stage; LC = life cycle or partial life cycle.

associated 48-h LC_{50}s) for *Daphnia*, the standard freshwater crustacean test species. The *Daphnia* data were taken from the EPA's national water quality criteria support documents (*24*, *28*). The fourth data set consists of the 2580 96-h LC_{50} values for saltwater fishes and crustaceans in the EPA aquatic toxicity data base AQUIRE.

Regression Analysis. To extrapolate data between taxa and between test end points (numeric expressions of the results of toxicity tests, e.g., LC_{50}s and MATCs), we used an errors-in-variables regression model (*3*). The choice of extrapolation model for this method was based on the following characteristics of toxicity data: (1) the observed values of both the independent variable (X) and dependent variable (Y) are subject to error of measurement and to inherent variability; (2) X is not a controlled variable (like settings on a thermostat); (3) values assumed by X and Y are open-ended and nonnormally distributed (*44*).

These characteristics suggest that an ordinary least-squares regression model would be inappropriate and an errors-in-variables model should be used (*44*). Because values of λ, the ratio of the error variances of Y to X, can be determined from duplicate test results, a functional

errors-in-variables model is identifiable and provides maximum likelihood estimators of the regression parameters. For further discussion of errors-in-variables regression models, see papers by Ricker (*44*) and Mandel (*45*).

The estimators of the slope (β) and intercept (α) are

$$b = \{\sum y^2 - \lambda\sum x^2 + [(\sum y^2 - \lambda\sum x^2)^2 + 4\lambda(\sum xy)^2]^{1/2}\}/2\sum xy$$

and

$$a = \bar{y} - b\bar{x}$$

where $x = X_i - \bar{X}$ and $y = Y_i - \bar{Y}$ for $i = 1 \ldots n$.

The variance of a single predicted Y value for a given X value ($X = X_0$) is the sum of the error variance of Y and the variance of a fitted value as given by Mandel (*46*). It is estimated as

$$\mathrm{var}(Y|X_0) = s_e^2\{1 + 1/n + [1 + (b^2/\lambda)][(X_0 - \bar{X})^2/\sum u^2]\}$$

where $s_e^2 = (b^2\sum x^2 - 2b\sum xy + \sum y^2)/n - 2$ and $\sum u^2 = \sum x^2 + (2b)/\lambda\sum xy + (b/\lambda)^2\sum y^2$.

This variance is the appropriate value to use in calculating confidence intervals and risk estimates because the interest in this case is the certainty concerning an individual future observation of Y, such as a toxic threshold for an untested species–chemical combination. This variance is larger than the variance on the mean of a $Y|X_0$, which in turn is larger than the variance of the regression coefficient. Confidence intervals calculated from this variance are larger than those that are conventionally reported and are referred to as prediction intervals (*46*).

For ease in using this method, we reduce the variance formula to

$$\mathrm{var}(Y|X_0) = F_1 + F_2(X_0 - \bar{X})^2$$

and, where the inverse regression is useful, the variance of a predicted X value is

$$\mathrm{var}(X|Y_0) = G_1 + G_2(Y_0 - \bar{Y})^2$$

We provide values for F_1, F_2, G_1, and G_2 in Tables II, IV, VI, and VII. These variances are used to calculate 95% prediction intervals and can be used in calculating risks of toxic effects (*3*).

This model requires that λ, the ratio of the point variances of Y to X, be estimated. When extrapolating between common bench marks for organisms aggregated at the same taxonomic level, λ was set to 1. Otherwise λ was set to the ratios of the n-weighted means of the variances of bench marks from replicate tests. When extrapolating from LC_{50}s to MATCs for fishes, λ was set to the ratio of the mean of variances of all sets of replicate fish MATCs to the mean of variances of all sets of replicate fish LC_{50}s.

Relative Sensitivity. The possibility that certain species might be particularly sensitive or insensitive to toxic chemicals was examined by ranking and by using the ratio LC_{50}(sp.x)/LC_{50}(sp.r), where sp.r is any species in the AQUIRE data set for which there are at least eight 96-h LC_{50} values and sp.x is any species that has a 96-h LC_{50} for any chemical in common with sp.r. MATC values from the acute–chronic data set were assessed analogously. The geometric mean, standard error, and range of the quotients of these ratios were determined for each sp.r.

General. All the data used in the regressions are log transformed, and the reported results are for the transformed values. Log transformations were used to induce homogeneity of variance. Test results expressed as greater than or less than values were not used except for ranking. Where replicate data existed for a single combination of test type, species, and chemical, one replicate was chosen at random for each analysis (using the mean of replicates would have artificially reduced the variance).

Results

Taxonomic Extrapolations. Taxonomic extrapolations of marine acute LC_{50}s from the AQUIRE data set are presented in Table II. The extrapolations are performed between taxa having the next higher taxonomic level in common rather than simply matching all possible species combinations. This approach permits extrapolation to species that have rarely or never been tested by assuming that they are represented by those members of a taxon to which they belong that have been tested. It is based on the concept that taxonomic similarity implies toxicological similarity (*2*, *3*, *47*, *48*). Only those regressions for which there were at least five data pairs and significant correlations were included.

We use the 95% prediction intervals (PIs) on Y at mean X as indicators of the quality of the extrapolations because we are interested in the ability of the model to predict future observations. Comparison of correlation coefficients (r values) is done only to compare the ability of different models to explain the variance in a particular set of existing data. The average PIs for each taxonomic level of marine fishes and crustaceans are presented in Table III and compared to earlier results for freshwater taxa (*3*). The extrapolation uncertainty, represented by the average PIs, increases by almost a factor of 2 as we move up the taxonomic hierarchy from congeneric species to orders within Osteichthyes and Crustacea. The mean PIs are quite similar to those for freshwater fishes and arthropods at the same taxonomic levels even though the freshwater data, which came from the Columbia National Fisheries Research Laboratory (*48*), would be expected to have less extraneous variance than the AQUIRE data, which came from numerous laboratories. This result suggests that the uncertainty in these extrapolations is primarily due to variance in the response of the organisms rather than to the test methods and conditions.

Representativeness of Standard Test Species. Recently, the atheriniform fish *Cyprinodon variegatus* (sheepshead minnow) and the mysid shrimp *Mysidopsis bahia* have become the most commonly used marine test species. Eighty-eight percent of the marine MATCs were for one of these species (Table I), and they are becoming predominant in acute toxicity studies. Table IV contains the results of regressions to predict the response of higher taxa of fish and crustaceans from test results for these two species. As expected, *C. variegatus* LC_{50}s are reasonably representative of LC_{50}s for other members of the order Atheriniformes (i.e., the slope and intercept are near 1 and 0, and the PI is ±1 order of magnitude, which is comparable to the family-level extrapolations in Table III). There is somewhat greater uncertainty in predicting LC_{50}s for all Osteichthyes from *C. variegatus* (PI = 1.49), and considerably greater uncertainty associated with the prediction of LC_{50}s for Crustacea (PI = 2.15; Figure 1a) and MATCs for Crustacea (PI = 1.80; Figure 1b). On the basis of the regression parameters, *C. variegatus* appears to be less sensitive than Perciformes and Crustacea, more sensitive than Gasterosteiformes, and fairly typical of Osteichthyes in general.

There are not enough MATCs for marine fishes, other than *C. variegatus*, to examine the representativeness of *C. variegatus* chronic responses for all Osteichthyes. However, analogy to the extrapolationi of *C. variegatus* LC_{50}s (Table IV) and to the extrapolation of *Pimephales promelas* MATCs to all freshwater Osteichthyes [PI = 1.12

Table II. Taxonomic Extrapolations of log LC_{50} Values from the AQUIRE Data Set

taxonomic level	taxon X	taxon Y	n^a	PI[b]	slope	intercept	F_1	F_2	G_1	G_2	$\bar{X}$	$\bar{Y}$
				Osteichthyes								
species	*Fundulus heteroclitus*	*Fundulus majalis*	12	0.75	1.12	−0.32	0.15	0.01	0.12	0.01	1.67	1.56
genus	*Cyprinodon*	*Fundulus*	9	0.82	0.96	0.21	0.17	0.12	0.19	0.01	0.33	1.49
family	Atherinidae	Cyprinodontidae	32	0.83	0.90	0.50	0.18	0.003	0.22	0.004	1.42	1.77
	Mugilidae	Labridae	12	1.74	0.82	0.70	0.79	0.04	1.17	0.09	1.33	1.79
	Cyprinodontidae	Poeciliidae	12	0.53	0.75	0.19	0.07	0.02	0.13	0.05	0.15	0.31
order	Anguiliformes	Tetraodontiformes	12	1.08	1.89	1.09	0.30	0.02	0.38	0.02	1.40	2.34
	Anguiliformes	Perciformes	34	1.40	0.96	0.21	0.51	0.01	0.55	0.01	1.11	1.28
	Anguiliformes	Gasterosteiformes	8	1.22	1.04	0.52	0.39	0.10	0.36	0.08	0.85	1.40
	Anguiliformes	Atheriniformes	46	0.94	1.05	0.06	0.23	0.003	0.21	0.002	1.31	1.43
	Atheriniformes	Cypriniformes	7	2.69	0.82	1.93	1.89	0.03	2.77	0.08	2.26	3.79
	Atheriniformes	Tetraodontiformes	46	1.06	0.88	1.00	0.29	0.004	0.38	0.01	1.43	2.26
	Atheriniformes	Perciformes	148	1.41	0.92	0.10	0.51	0.001	0.61	0.002	1.27	1.27
	Atheriniformes	Gasterosteiformes	36	0.97	0.94	0.49	0.24	0.01	0.28	0.01	0.92	1.35
	Gasterosteiformes	Tetraodontiformes	8	1.27	1.12	0.31	0.42	0.10	0.33	0.06	1.40	1.887
	Gasterosteiformes	Perciformes	33	1.55	1.15	−0.67	0.62	0.04	0.47	0.02	1.47	1.03
	Perciformes	Tetraodontiformes	34	1.40	0.91	0.93	0.52	0.01	0.62	0.02	1.28	2.10
	Cypriniformes	Perciformes	6	0.84	0.46	−0.35	0.18	0.01	0.86	0.18	3.13	1.10
	Perciformes	Salmoniformes	7	0.15	0.19	−0.76	0.01	0.00	0.01	0.00	2.80	2.80
				Crustacea								
family	Cacridae	Crangonidae	5	0.94	1.33	−2.25	0.23	0.24	0.13	0.08	4.29	3.46
	Crangonidae	Palaemonidae	21	1.09	0.98	0.48	0.31	0.01	0.32	0.01	1.29	1.74
	Crangonidae	Pandalidae	10[c]	0.61	0.81	0.6.	0.10	0.03	0.15	0.06	4.26	4.13
	Crangonidae	Portunidae	9[c]	0.58	1.18	−0.33	0.09	0.03	0.06	0.01	4.00	4.41
	Palaemonidae	Penaeidae	11	1.18	1.14	−1.19	0.37	0.02	0.18	0.004	1.32	0.68
	Palaemonidae	Portunidae	5	1.79	0.71	1.33	0.84	0.03	1.67	0.14	3.68	3.94
	Pandalidae	Portunidae	7[c]	0.48	0.97	0.59	0.06	0.03	0.06	0.04	4.04	4.51
order	Amphipoda	Decapoda	50	2.22	1.23	−0.69	1.29	0.02	0.82	0.01	1.93	1.68
	Calanoidea	Decapoda	14	2.83	3.05	−3.12	2.08	1.27	0.22	0.01	1.82	2.42
	Decapoda	Harpacticoidea	23	3.16	1.18	1.06	2.59	0.09	1.84	0.05	3.38	3.88
	Decapoda	Mysidae	10	0.75	0.35	0.16	0.15	0.01	1.18	0.49	1.38	0.65

[a] n = number of points, each consisting of LC_{50}s for species from the X and Y taxa tested for the same chemical and duration. [b] Prediction interval ($\alpha = 0.05$) at the mean ($\bar{X}$) is $\bar{Y} \pm$ PI. [c] Derived from 48-h tests; all others are from 96-h tests.

Table III. Summary of Freshwater and Marine Taxonomic Extrapolations for LC_{50}s

taxonomic level	n^a	n-weighted mean of 95% prediction intervals
species		
marine fish	1	0.75
freshwater fish	8	0.76
freshwater arthropods	2	1.10
genera		
marine fish	1	0.82
freshwater fish	8	0.74
freshwater arthropods	2	0.78
families		
marine fish	3	0.96
freshwater fish	4	0.97
marine crustaceans	7	0.94
freshwater arthropods	3	1.37
orders		
marine fish	13	1.27
freshwater fish	10	1.35
marine crustaceans	4	2.38
freshwater arthropods	10	2.06

[a] n = the number of pairs of taxa at that taxonomic level.

with n = 51; (*3*)] suggests that the PI for MATCs for marine Osteichthyes would fall within ±1–1.5 orders of magnitude of *C. variegatus* MATCs.

Extrapolations from *M. bahia* to higher taxa are more uncertain (i.e, the PIs are larger) than those from *C. variegatus*. While the differences in PIs for the same Y taxon are not large, it is surprising that *M. bahia* does no better than a fish in predicing the acute or chronic response of crustaceans as a group (Figure 2). The crustaceans are highly diverse, and perhaps no single member can serve any better as a representative of the class than can a fish.

Relative Sensitivity. The geometric means of ratios of LC_{50}s show two shrimp, *Penaeus duorarum* and *M. bahia*, to be, on average, the most sensitive species of marine fishes or crustaceans in the AQUIRE data set (Table V). While they were, on average, 13 and 42 times as sensitive as other species, neither mean ratio was more than 1 SE greater than 1 (i.e., equal average toxicity). The high standard errors were due to the 18 cases where a species was more than 3 orders of magnitude less sensitive than either *M. bahia* or *P. duorarum*, all of which involved fishes and all but one of which involved a pesticide. Other species were more sensitive in only 15% of cases for *P. duorarum* and 17% of cases for *M. bahia*. In the one case where a species was 2 orders of magnitude more sensitive than *M. bahia*, that species was *P. duorarum*. In the two cases where a species was 2 orders of magnitude more sensitive than *P. duorarum*, the species were *M. bahia* and *Marinogammarus obtusatus*. Thus, these species are

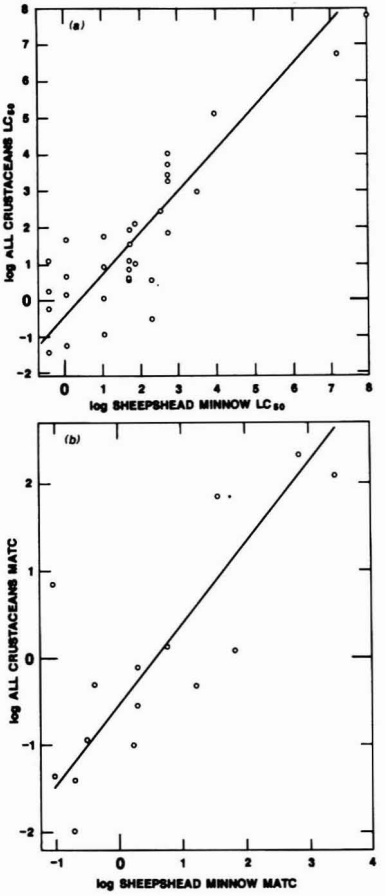

Figure 1. (a) Regression of LC_{50} for all crustaceans against those for *Cyprinodon variegatus* (sheepshead minnow). Units are log (μg/L); n = 34; PI = 2.15. (b) Regression of MATC values for all crustaceans against those for *C. variegatus*. Units are log (μg/L); n = 15; PI = 1.80.

generally, but not invariably, more sensitive than other species with which we are able to compare them. Two species, the cyprinid minnow *Alburnus alburnus* and the tetraodontid puffer *Sphoeroides maculatus*, have geometric mean ratios that are more than 2 SE less than 1, suggesting that they are relatively insensitive to chemicals. The other 17 species considered have ratios near 1.

It is considerably more difficult to draw conclusions about the relative sensitivity of marine species in chronic

Table IV. Extrapolations from the Standard Test Species *Cyprinodon variegatus* and *Mysidopsis bahia*

species X	taxon Y	bench mark	n^a	PI[b]	slope	intercept	F_1	F_2	$\bar{X}$	$\bar{Y}$
C. variegatus	Osteichthyes	LC_{50}	51	1.49	0.97	0.03	0.58	0.01	1.25	1.24
	Atheriniformes	LC_{50}	17	1.00	1.02	0.04	0.26	0.01	1.22	1.28
	Perciformes	LC_{50}	20	1.56	0.85	−0.12	0.63	0.02	1.36	0.99
	Gasterosteiformes	LC_{50}	5	1.10	1.08	0.43	0.31	0.07	0.81	1.30
	Crustacea	LC_{50}	34	2.15	1.14	−0.41	1.21	0.11	1.78	1.62
	Crustacea	MATC	15	1.80	0.93	−0.54	0.84	0.03	0.53	−0.05
M. bahia	Crustacea	LC_{50}	14	2.46	2.89	−0.55	1.57	0.53	0.71	1.50
	Osteichthyes	LC_{50}	29	1.85	1.08	0.35	0.88	0.01	2.42	2.96
	Crustacea	MATC	5	2.22	0.80	0.43	1.28	0.27	−0.57	−1.28
	Osteichthyes[c]	MATC	12	1.40	1.02	0.75	0.51	0.28	0.03	0.78

[a] n = number of points, each consisting of a toxicological bench mark value for a standard test species and an equivalent value for a species belonging to the Y taxon for the same chemical. [b] Prediction interval (α = 0.05) at the mean ($\bar{X}$) is $\bar{Y}$ ± PI. [c] All are *C. variegatus*.

Table V. Ratios of LC_{50}s of All Marine Fish and Crustaceans to Potential Reference Species

reference species	n^a	geometric mean ratio	SE
Alburnus alburnus	53	0.07	0.10
Anguilla rostrata	149	1.06	0.71
Cancer magister	36	0.99	14.76
Crangon crangon	13	0.97	12.08
Crangon septemspinosa	162	6.37	247.32
Cyprinodon variegatus	85	0.86	1.07
Fundulus heteroclitus	167	0.39	0.38
Fundulus majalis	149	0.76	0.91
Gasterosteus aculeatus	139	0.42	17.40
Menidia beryllina	11	0.68	4.00
Menidia menidia	174	2.15	90.81
Morone saxatilis	23	1.09	0.79
Mugil cephalus	161	0.47	1.15
Mysidopsis bahia	30	41.97	3321.4
Nitocra spinipes	97	0.09	0.88
Pagurus longicar	154	1.01	74.25
Palaemonetes pugio	92	0.68	45.36
Palaemonetes vulgaris	162	1.83	164.75
Penaeus duorarum	81	13.51	516.35
Sphoeroides maculatus	149	0.10	0.06
Thalassoma bifas	149	1.35	2.83

[a] n = number of ratios.

tests. However, the results tend to confirm the relative sensitivity of *M. bahia*. *M. bahia* is more sensitive than other crustaceans in three out of four cases. It was more sensitive than *C. variegatus* in 10 out of 13 cases and less sensitive once (cyanide), and the comparison was inconclusive twice. *C. variegatus* was never more sensitive than other fishes; however, all but one of the matches with four other fish species were for a single chemical, chlorpyrifos. The geometric mean ratio of the MATCs for all other marine species to the MATCs for *M. bahia* is 7, but this value is less than 1 SE greater than 1.

Acute–Chronic Extrapolations. MATCs for fishes and crustaceans were regressed against LC_{50} values for the same species determined in the same study (Figure 3). The data are given in Table I, and the results are presented in Table VI. The PI for all marine fishes and all chemicals (1.27) is smaller than the analogous regression for freshwater fishes [PI = 1.53; (*3*)], and the PIs for all marine crustaceans and all chemicals (0.90, which is based on 90% *M. bahia* data) is smaller than the analogous regression for *Daphnia* [PI = 1.35; (*3*)].

Freshwater–Marine Extrapolations. Because of the relatively small number of marine MATCs available, it would be useful to extrapolate from freshwater to saltwater MATCs. The results of such extrapolations for the standard marine and freshwater fishes and crustaceans are presented in Table VII and in Figure 4. Since *Pimephales promelas* and *C. variegatus* are in different orders of Osteichthyes and *Daphnia* and *M. bahia* are in different orders of Crustacea, these extrapolations are between distantly related organisms as well as between major ha-

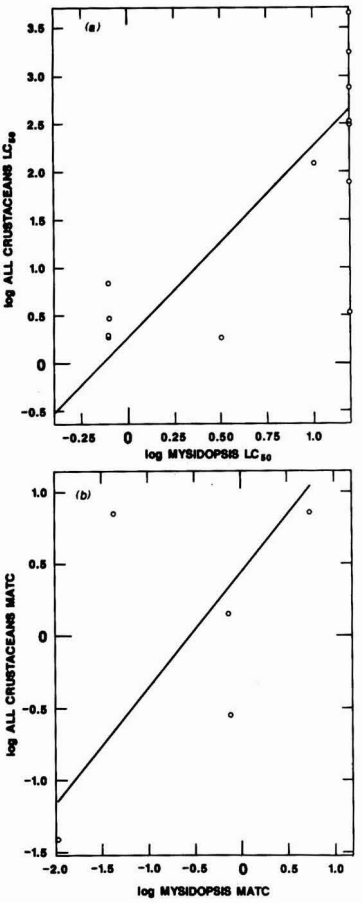

Figure 2. (a) Regression of LC_{50} values for all crustaceans against those for *Mysidopsis bahia*. Units are log (μg/L); n = 14; PI = 2.46. (b) Regression of MATCs for all crustaceans against those for *M. bahia*. Units are log (μg/L); n = 5; PI = 2.22.

Table VI. Extrapolation from 96-h LC_{50}s to MATCs for Marine Fishes and Crustaceans

taxon	n^a	PI[b]	λ	slope	intercept	F_1	F_2	$\bar{X}$	$\bar{Y}$
Osteichthyes	41	1.27	1.4	0.98	−0.60	0.42	0.004	1.80	1.16
Crustacea	43	0.90	1.4	1.00	−0.88	0.21	0.003	1.58	0.70

[a] n = number of points, each consisting of an LC_{50} and an MATC for the same species and chemical in the same laboratory. [b] Prediction interval (α = 0.05) at the mean ($\bar{X}$) is $\bar{Y} \pm$ PI.

Table VII. Freshwater to Marine Extrapolations

species X	taxon Y	bench mark	n^a	PI[b]	slope	intercept	F_1	F_2	$\bar{X}$	$\bar{Y}$
P. promelas	*C. variegatus*	MATC	16	1.58	0.99	−0.02	0.65	0.01	1.10	1.07
D. magna	*M. bahia*	MATC	15	1.70	1.01	−0.06	0.76	0.04	1.38	1.33
	marine crustaceans	MATC	17	1.90	0.95	0.00	0.94	0.04	1.31	1.24

[a] n = the number of points, each consisting of an MATC for species X and an MATC for species Y for the same chemical. [b] Prediction interval (α = 0.05) at the mean ($\bar{X}$) is $\bar{Y} \pm$ PI.

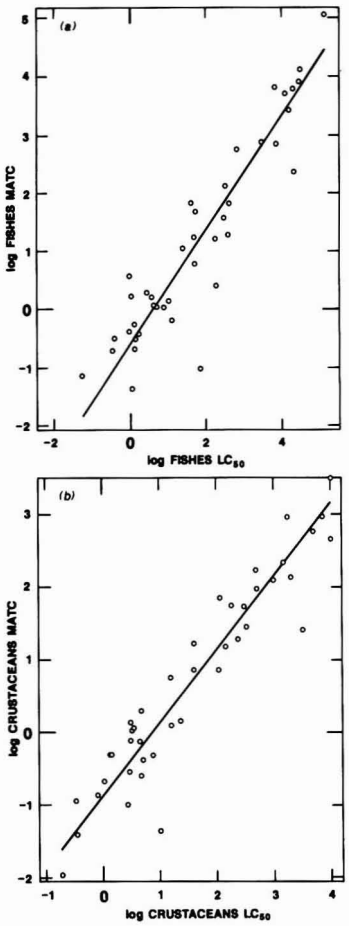

Figure 3. (a) Regression of MATC values against LC_{50} values for fish. Units are log (μg/L); n = 41; PI = 1.27. (b) Regression of MATC values against LC_{50} values for crustaceans. Units are log (μg/L); n = 43; PI = 0.90.

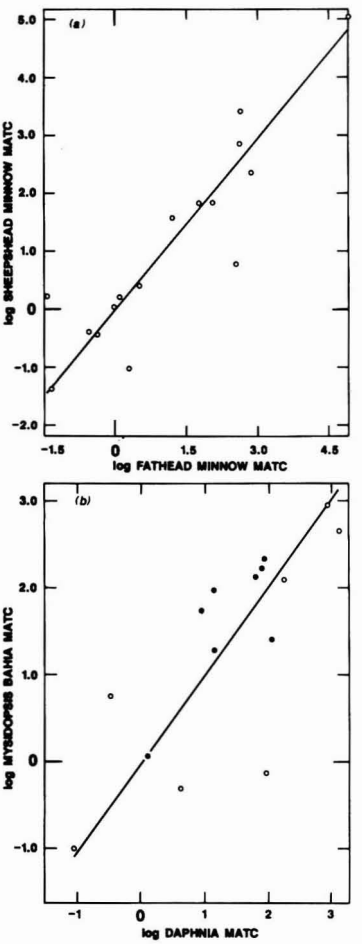

Figure 4. (a) Regression of MATCs for *Cyprinodon variegatus* (sheepshead minnow) against those for *Pimephales promelas* (fathead minnow). Units are log (μg/L); n = 16; PI = 1.58. (b) Regression of MATCs for *Mysidopsis bahia* against those for *Daphnia*. Points marked with a closed circle are metals; those marked an open circle are nonmetals. Units are log (μg/L); n = 15; PI = 1.70.

bitat types. The PI for the *P. promelas* to *C. variegatus* extrapolation (1.58) is a little worse than the PIs for extrapolating LC_{50}s between orders of saltwater fish and between orders of freshwater fish (Table III). The PI for the *Daphnia* to *M. bahia* extrapolation (1.70) falls below the mean PI for extrapolating LC_{50}s between orders of marine crustaceans and that for extrapolating between orders of freshwater arthropods (Table III). The slopes and intercepts for these two regressions are very close to 1 and 0, indicating that the members of both species pairs have very similar average sensitivities.

These results are somewhat surprising, since salinity affects the toxicity of some chemicals, particularly metals (*49*). However, there is no evidence that metals are particularly difficult to extrapolate between freshwater and saltwater. While there are no MATCs for common metals for the two fishes, more than half of the MATC pairs for crustaceans are for metals, and they cluster around the slope 1, intercept 0 line (Figure 4b). The results are consistent with the finding of Klapow and Lewis (*50*) that LC_{50}s for freshwater and saltwater species have indistinguishable distributions for nine metals and four other chemicals. They are also consistent with the finding of LeBlanc (*47*) that the LC_{50}s for *C. variegatus* and *M. bahia* are significantly correlated with those for *P. promelas* and *D. magna*, respectively, and with the finding of Zaroogian et al. (*51*) that structure–activity models for *P. promelas* and *Poecilia reticulata* (guppy) can be used to predict LC_{50} values for *C. variegatus* and *M. bahia*.

Discussion

While the parameters of the regression lines presented above can be used to indicate relative sensitivity, they should not be used simply to generate point predictors. Since there is no such organism as the mean fish or mean shrimp, the variance about the line cannot be treated as measurement error about a true value. Rather, the variance about the line should be used to determine the probability that the LC_{50} or MATC for an untested species from the specified taxon will be less than a particular ambient concentration, given a test result for a standard test species.

For example, if a chemical has an LC_{50} of 17.8 μg/L (log 17.8 = 1.25) for *C. variegatus*, then from Table IV we can see that, given a two-tailed 95% PI of 1.24 ± 1.49 at X =

1.25, 97.5% of marine Osteichthyes would be expected to have an LC_{50} greater than 0.56 $\mu g/L$ (log 0.56 = −0.25 = 1.24–1.49). In other words, the risk that the median lethal concentration for any particular fish species would be less than 0.56 is 0.025. Calculations of probabilities for other predicted test results or for particular ambient concentrations are performed analogously; for detailed instructions, see Suter et al. (*3*).

The analyses of relative sensitivity confirm prior results for freshwater species, indicating that no species is consistently the most sensitive (*48*, *52*, *53*). Since there is no most sensitive species, some correction must be made when the results of a single species test is used to determine a safe or acceptable concentration for a taxon or biota. These corrections can be used on the risks of not protecting the species of interest or of affecting more than x% of members of a taxon calculated from the variances on these regressions.

Alternatively, the results of the analyses of relative sensitivity can be used as a guide for planning monitoring studies or interpreting their results. While no species can be counted on to respond first to pollution, monitoring efforts would be best concentrated on the species with the greatest average sensitivity. Of the taxa considered, penaeid shrimp and mysid shrimp appear to have the highest average sensitivity, and crustaceans appear to be more sensitive than fish.

These analyses depend on the assumption that the data sets used are representative. Specifically, we assume that the array of species tested are randomly chosen from the higher taxa in which they occur. This is clearly not the case: test species are chosen for their ability to be maintained in the laboratory for at least the duration of the test; for their availability to the investigators; and in some cases, for their relevance to a particular pollution problem, but not by some random process. However, they have not, in general, been chosen for their sensitivity because relative sensitivities are only now becoming apparent. Therefore, we do not believe, for example, that the nine atherinid fish in the AQUIRE data set are a biased sample of Atherinidae with respect to sensitivity to pollutants. What is problematical is the ability of the tested species to represent marine fishes and crustaceans in general. Many important marine taxa such as *Clupeiformes*, *Gadiformes*, and *Pleuronectiformes* are clearly underrepresented, and some taxa such as *Scombridae* will never lend themselves to testing. Therefore, it is possible, and even likely, that highly sensitive marine species exist that do not appear in this analysis.

The other aspect of representativeness of the data sets is the assumption that the tested chemicals are representative of those that will be important in the field. This assumption is difficult to verify, and we know that the mode of action of a chemical can affect the extrapolations (*3*). This assumption can be minimized by parititioning the data sets by chemical class, but in most cases the data sets are not large enough to tolerate partitioning. That being the case, we must assume that the investigators had a reasonable grasp of the relative importance of pollutants when they chose their test chemicals or that the chemicals chosen for testing are at least a reasonable assortment.

Conclusions

Data extrapolations are required to assess the risk of almost any chemical to any marine fish or crustacean because of the large number of species and chemical to be assessed. These extrapolations must often be made at very high taxonomic levels, and even when they can be made between closely related species, nontrivial uncertainties are involved. In general, toxic effects can be predicted with ±1–2 order of magnitude precision. These uncertainties are comparable to those associated with extrapolations of freshwater data (*3*). The practical significance of these uncertainties depends on the individual assessment. Given the extremely wide range of concentrations at which chemicals occur in the environment, most environmental concentrations can be expected to fall outside the prediction intervals for most predicted-effects concentrations. When environmental concentrations do fall within the uncertainty bounds of a predicted-effects concentration, the uncertainty can be considered to constitute a risk, that is, a probability of an undesired effect (*2*). The uncertainty and associated risk can be decreased by additional testing.

Another conclusion that may be drawn from this study is that more systematic testing needs to be done to determine the relative sensitivity of marine organisms to chemical pollutants. Better knowledge of relative sensitivity will allow better estimation of risk and greater confidence in the appropriateness of criteria. The existing data, particularly that for chronic toxicity, cannot said to be representative of the marine biota. Particular emphasis must be placed on invertebrates because of their great diversity relative to fish. A testing program that examines the responses of a taxonomic array of species to a set of chemicals with diverse modes of action could greatly improve the confidence with which data from standard test species can be used in risk assessments.

Acknowledgments

We thank L. R. Goodman, D. J. Hansen, S. M. Lussier, and P. R. Parrish for supplying toxicity data. We also thank L. W. Barnthouse, C. T. Hunsaker, A. Mearns, and D. M. Soballe for their helpful comments and J. S. O'Connor for his support and guidance.

Literature Cited

(1) Barnthouse, L. W.; Suter, G. W., II *User's Manual for Ecological Risk Assessment*; Oak Ridge National Laboratory: Oak Ridge, TN, 1986; ORNL-6251.

(2) Suter, G. W., II; Vaughan, D. S.; Gardner, R. H. *Environ. Toxicol. Chem.* **1983**, *2*, 369–378.

(3) Suter, G. W., II; Rosen, A. E.; Linder, E. In *User's Manual for Ecological Risk Analysis*; Barnthouse, L. W., Suter, G. W., II, Eds.; Oak Ridge National Laboratory: Oak Ridge, TN, 1986; ORNL-6251, pp 49–81.

(4) Hansen, D. J.; Goodman, L. R.; Moore, J. C.; Higdon, P. K. *Environ. Toxicol. Chem.* **1983**, *2*, 251–258.

(5) Ward, G. S.; Parrish, P. R.; Rigby, R. A. *J. Toxicol. Environ. Health* **1981**, *8*, 225–240.

(6) Environmental Protection Agency *Acephate, Aldicarb, Carbophenothion, DEF, EPN, Ethoprop, Methyl Parathion, and Phorate: Their Acute and Chronic Toxicity, Bioconcentration Potential, and Persistence as Related to Marine Environments*; U.S. EPA, Environmental Research Laboratory: Gulf Breeze, FL, 1981; EPA-600/4-81-041.

(7) Lussier, S. M.; Gentile, J. H.; Walker, J. *Aquat. Toxicol.* **1985**, *7*, 25–35.

(8) McKenny, C. L., Jr. *Interlaboratory Comparison of Chronic Toxicity Testing Using the Estuarine Mysid* (Mysidopsis bahia); final report; U.S. Environmental Protection Agency: Gulf Breeze, FL, no date.

(9) Ward, G. S.; Cramm, G. C.; Parrish, P. R.; Petrocelli, S. R. *Mar. Pollut. Bull.* **1982**, *13*, 191–195.

(10) Hansen, D. J.; Schimmel, S. C.; Forester, J. *Trans. Am. Fish. Soc.* **1975**, *104*, 584–588.

(11) Schimmel, S. C.; Hansen, D. J.; Forester, J. *Trans. Am. Fish. Soc.* **1974**, *103*, 582–586.

(12) Ward, G. S.; Ballentine, L. *Estuaries* **1985**, *8*, 22–27.

(13) Ward, G. S.; Cramm, G. C.; Parrish, P. R.; Trachman, H.; Slesinger, A. In *Aquatic Toxicology and Hazard Assess-*

ment: Fourth Conference; Branson, D. R., Dickson, K. L., Eds.; American Society for Testing and Materials: Philadelphia, PA, 1981; ASTM STP 737, pp 183–200.
(14) Parrish, P. R.; Dyar, E. E.; Lindberg, M. A.; Shanika, C. N.; Enos, J. M. *Chronic Toxicity of Methoxychlor, Malathion, and Carbofuran to Sheepshead Minnows (Cyprinodon variegatus)*; U.S. Environmental Protection Agency: Gulf Breeze, FL, 1977; EPA-600/3-77-059.
(15) Nimmo, D. R.; Bahner, L. H.; Rigby, R. A.; Sheppard, J. M.; Wilson, A. J., Jr. In *Aquatic Toxicology and Hazard Evaluation*; Mayer, F. L., Hamelink, J. L., Eds.; American Society for Testing and Materials: Philadelphia, PA, 1977; ASTM STP 634, pp 109–116.
(16) Nimmo, D. R.; Rigby, R. A.; Bahner, L. H.; Sheppard, J. M. *Bull. Environ. Contam. Toxicol.* **1978**, *7*, 80–85.
(17) Gentile, S. M.; Gentile, J. H.; Walker, J.; Heltshe, J. F. *Hydrobiologia* **1982**, *93*, 195–204.
(18) Parrish, P. R.; Dyar, E. E.; Enos, J. M.; Wilson, W. G. *Chronic Toxicity of Chlordan, Trifluralin, and Pentachlorophenol to Sheepshead Minnow (Cyprinodon variegatus)*; U.S. Environmental Protection Agency: Gulf Breeze, FL, 1978; EPA-600/3-78-010.
(19) Parrish, P. R.; Schimmel, S. C.; Hansen, D. J.; Patrick, P. M.; Forester, J. *J. Toxicol. Environ. Health* **1976**, *1*, 485–494.
(20) Goodman, L. R.; Middaugh, D. P.; Hansen, D. J.; Higdon, P. K.; Cripe, G. M. *Environ. Toxicol. Chem.* **1983**, *2*, 337–342.
(21) Goodman, L. R.; Hansen, D. J.; Middaugh, D. P.; Cripe, G. M.; Moore, J. C. In *Aquatic Toxicology and Hazard Assessment, Seventh Symposium*; Cardwell, R. D., Purdy, R., Bahner, R. C., Eds.; American Society for Testing and Materials: Philadelphia, PA, 1985; pp 145–154.
(22) Cripe, G. M.; Hansen, D. J.; Macauley, S. F.; Forester, J. In *Aquatic Toxicology and Hazard Assessment, Ninth Symposium*; Poston, T. M., Purdy, R., Eds.; American Society for Testing and Materials: Philadelphia, PA, 1986; pp 450–460.
(23) Hansen, D. J.; Goodman, L. R.; Cripe, G. M.; Macauley, S. F. *Ecotoxicol. Environ. Saf.* **1986**, *11*, 15–22.
(24) Environmental Protection Agency *Fed. Regist.* **1985**, *50*, 30784–30796.
(25) Nimmo, D. R.; Hamaker, T. L.; Mathews, E.; Moore, J. C. In *Biological Monitoring of Marine Pollutants*; Vernberg, J., Calabrese, A., Thurberg, F., Vernberg, W. B., Eds.; American Press: New York, 1981; pp 3–19.
(26) Goodman, L. R.; Hansen, D. J.; Coopage, D. L.; Moore, J. C.; Mathews, W. *Trans. Am. Fish. Soc.* **1979**, *108*, 479–488.
(27) Daniels, R. E.; Allan, J. D. *Can. J. Fish. Aquat. Sci.* **1981**, *38*, 485–494.
(28) Environmental Protection Agency *Fed. Regist.* **1980**, *45*, 79318–79379.
(29) Nimmo, D. R.; Hamaker, T. L.; Moore, J. C.; Wood, R. A. In *Aquatic Toxicology*; Eaton, J. G., Parrish, P. R., Hendricks, A. C., Eds.; American Society for Testing and Materials: Philadelphia, PA, 1980; ASTM STP 707, pp 366–376.
(30) Hansen, D. J.; Cripe, G. M. *Interlaboratory Comparison of the Early Life-Stage Test Using the Sheepshead Minnow (Cyprinodon variegatus)*; U.S. Environmental Protection Agency: Gulf Breeze, FL, 1984; EPA-600/X-84-081.
(31) Tyler-Schroeder, D. B. In *Aquatic Toxicology*; Marking L. L., Kimerle, R. A., Eds.; American Society for Testing and Materials: Philadelphia, PA, 1979; ASTM STP 667, pp 159–170.
(32) McKenny, C. L., Jr. *Interrelationships Between Energy Metabolism, Growth Dynamics and Reproduction During the Life-Cycle of Mysidopsis bahia as Influenced by Sublethal Endrin Exposure*; U.S. Environmental Protection Agency: Gulf Breeze, FL, 1982; EPA 600/D-82-080.
(33) Hansen, D. J.; Schimmel, S. C.; Forester, J. *J. Toxicol. Environ. Health* **1977**, *3*, 721–733.
(34) Schimmel, S. C.; Parrish, P. R.; Hansen, D. J.; Patrick, J. M., Jr.; Forester, J. In *Proceedings, 28th Conference, Southeastern Association of Game and Fish Commissioners*; Southeastern Association of Game and Fish Commissioners: Baton Rouge, LA, 1974; pp 187–194.
(35) Cripe, G. M.; Goodman, L. R.; Hansen, D. J. *Aquat. Toxicol.* **1984**, *5*, 255–266.
(36) Goodman, L. R.; Hansen, D. J.; Crouch, J. A.; Forester, J. In *Proceedings, 30th Annual Conference, Southeastern Association of Game and Fish Commissioners*; Southeastern Association of Game and Fish Commissioners: Baton Rouge, LA, 1976; pp 192–202.
(37) *Aquatic Toxicity and Hazard Evaluation*; Hansen, D. J.; Parrish, P. R.; Mayer, F. L.; Hamelink, J. L., Eds.; American Society for Testing and Materials: Philadelphia, PA, 1977; ASTM STP 634, pp 117–126.
(38) Gentile, J. H.; Gentile, S. M.; Hairston, N. G., Jr.; Sullivan, B. K. *Hydrobiologia* **1982**, *93*, 179–187.
(39) Gentile, J. H.; Gentile, S. M.; Hoffman, G.; Heltshe, J. F.; Hairston, N., Jr. *Environ. Toxicol. Chem.* **1983**, *2*, 61–68.
(40) Allan, J. D.; Daniels, R. E. "Sublethal Effects of Pollutants: Life Table Evaluation of Chronic Exposure of *Eurytemora affinis* (Copepoda) to Kepone"; Technical Report No. 61; Water Resources Research Center, University of Maryland: College Park, MD, 1980.
(41) Goodman, L. R.; Hansen, D. J.; Manning, C. S.; Faas, L. F. *Arch. Environ. Contam. Toxicol.* **1982**, *11*, 335–342.
(42) Hansen, D. J.; Goodman, L. R.; Wilson, A. J., Jr. *Chesapeake Sci.* **1977**, *18*, 227–232.
(43) Ward, G. S.; Hollister, T. A.; Parrish, P. R. *Northeast Gulf Sci.* **1981**, *2*, 73–78.
(44) Ricker, W. E. *J. Fish. Res. Board Can.* **1973**, *30*, 409–434.
(45) Mandel, J. *J. Qual. Technol.* **1984**, *16*, 1–14.
(46) Wonnacott, R. J.; Wonnacott, T. H. *Introductory Statistics*, 4th ed.; Wiley: New York, 1985.
(47) LeBlanc, G. A. *Environ. Toxicol. Chem.* **1984**, *3*, 47–60.
(48) Mayer, F. L.; Ellersieck, M. R. *Manual of Acute Toxicity: Interpretation and Data Base for 410 Chemicals and 66 Species of Freshwater Animals*; U.S. Fish and Wildlife Service: Washington, DC, 1986; Resource Pub. 160.
(49) Engel, E. W.; Fowler, B. A. *EHP, Environ. Health Persp.* **1979**, *28*, 81–88.
(50) Klapow, L. A.; Lewis, R. H. *J.—Water Pollut. Control Fed.* **1979**, *51*, 2054–2070.
(51) Zaroogian, G.; Heltshe, J. F.; Johnson, M. *Aquat. Toxicol.* **1985**, *6*, 251–270.
(52) Kenaga, E. E. *Environ. Sci. Technol.* **1978**, *12*, 1322–1329.
(53) Patrick, R.; Cairns, J.; Scheier, A. *Prog. Fish-Cult.* **1968**, *30*, 137–140.

Received for review September 15, 1986. Revised manuscript received September 14, 1987. Accepted December 8, 1987. Research sponsored by the National Oceanographic and Atmospheric Administration (NOAA) through Interagency Agreement 40-1535-84 with the U.S. Department of Energy, under Contract DE-AC05-840R21400 with Martin Marietta Energy Systems, Inc. This paper has been reviewed by NOAA and approved for publication. Such approval does not signify that the contents of this paper necessarily represent the official position of the U.S. Government or of NOAA, nor does the mention of trade names or commercial products constitute endorsement or recommendation for their use.

Environ. Sci. Technol. 1988, 22, 557–561

Catalytic Oxidation of Polychlorinated Biphenyls in a Monolithic Reactor System

Prasad Subbanna, Howard Greene,* and Faredoon Desai

Department of Chemical Engineering, University of Akron, Akron, Ohio 44325

■ Air containing 200–1000 ppm of Aroclor 1254 vapors [a mixture of polychlorinated biphenyls (PCBs)] was passed through a 22.86 cm long heated section of 0.64 cm i.d. monolithic α-alumina support, which had been previously treated with one or more catalytic agents. At 600 °C, with a residence time of about 9.4 s, results showed that the overall PCB destruction efficiency ranged from a high of 97.3% for supported CuO to a low of 69.3% for Cr_2O_3. Supported catalysts of Co_3O_4, $CuCr_2O_4$, and Pt–Pd were intermediate in activity. Relative activity for this group of p-type catalysts in deep oxidation was in accordance with Sabatier's principle, decreasing with increasing heats of O_2 chemisorption. Selectivity toward oxidation of the more toxic high-chlorine-containing PCBs was found to be greater for catalysts made from transition metal oxides than for noble metal systems or homogeneous (thermal) decomposition.

Introduction

Because thermal destruction of polychlorinated biphenyls (PCBs) requires temperatures of at least 1200 °C and residence times of over 1 s, standard municipal incinerators merely vaporize and release PCBs into the atmosphere (*1*) or result in the formation of even more toxic polychlorinated dibenzofurans (PCDFs) and polychlorinated dibenzo-*p*-dioxins (PCDDs) (*2–4*). Hence, there is a compelling need for development of economically viable lower temperature processes capable of effectively treating incinerator flue gas or other effluents that may be contaminated with PCB vapors.

Previous work by Lombardi et al. (*5*) has shown some success in destroying PCB vapors by two-stage contact with Cr_2O_3–Al_2O_3 particles in fluidized-bed reactors at temperatures between 595 and 695 °C. However, the relatively complex system suffers from a high-pressure drop and requires pumps, cyclones, and multiple stages for good conversion. In addition, no fundamental kinetic data (which could be applied to the design of simpler reactor geometries) are reported.

Chemical treatment methods (patented by Franklin Institute, SunOhio, and Goodyear), which use a reagent containing sodium or calcium to strip chlorine from the PCBs, are portable but involve dangerously exothermic reactions (*6*) and apply primarily to liquids. Other methods of PCB disposal (activated-carbon adsorption, microwave plasma, chlorinolysis, dehydrochlorination, wet-air oxidation, and biological destruction) suffer from various defects; none has been shown to be workable for large-scale destruction (*7, 8*).

Scope. The objective of this study was primarily to determine PCB destruction efficiencies and product selectivities for each catalyst studied at temperatures between 500 and 600 °C, utilizing low-pressure drop monolith supports treated with noble metals or transition metal oxides. Mathematical modeling of these results and the role of diffusion in PCB reactivity was also of importance but has been reported on elsewhere (*9*).

Experimental Section

Apparatus. A schematic of the reactor system is shown in Figure 1. At the beginning of a run, approximately 1 g of Aroclor 1254 (a mixture of chlorinated biphenyl isomers with an average of five chlorine atoms per molecule, 54% chlorine by weight, and a molecular weight of 325) was placed in the sample vaporizer (a shallow cup attached to a long quartz tube) and vaporized at controlled temperatures in the lower tube furnace. A stream of dry, preheated primary air from a Linde high-purity compressed air cylinder carried the PCB vapors generated in the lower heated sections upwards into the separately heated/controlled catalytic reaction chamber. Products comprising condensable organics and water were collected in a train of dry ice/acetone traps attached to the reactor; unconverted PCBs were trapped in a Florisil Sep-Pak cartridge and analyzed quantitatively with electron capture gas chromatography (*10*). Vapors emerging from the exit of the last trap were vented to the hood. Vapor samples for analysis were taken periodically, above and below the catalyst tube from sampling ports A and B, by syringes with 15.24 cm long needles in order to just reach the center of the gas stream.

The lower furnace, manufactured by Lindberg, was controlled by an ERC Co. West Model 10 on/off controller, while the heating rate was manipulated by means of a Superior Electric Co. powerstat. The catalytic reaction chamber was heated by a HEVI-DUTY Electric Co. Model 70 tube furnace and controlled by a West Gardsman II proportional controller. The tube furnaces were capable of maximum temperatures of 1010 °C, but the limit on the upper furnace controller was 600 °C. All system temperatures, including reactor wall and centerline, during a run were measured with chromel-alumel thermocouples connected to an Analog Devices Type K scanning digital thermometer. Thermolyne Co. heating tapes connected to Superior Electrical Co. powerstats and insulated with fiberglass prevented condensation of vapors on exposed surfaces of the quartz tube.

Catalyst Preparation. The catalyst support tubes used in all experiments were ceramic α-alumina monoliths, either 22.86 or 15.24 cm long by 1.59 cm o.d. and 0.64 cm i.d. The blank for studying the homogeneous reaction was made of thin-walled Pyrex of similar dimensions. These monoliths were provided by the Norton Co. with the following specifications: surface area, 0.48 m^2/g; apparent porosity, 31.94% (by weight); water absorption, 14.61% (by weight); apparent specific gravity, 3.21; particle density, 2.19 g/cm^3; mercury pore volume, 0.23 cm^3/g; median pore diameter, 1.45 μm.

The outer surface of the monoliths was glazed to prevent the diffusion (and consequent loss) of reactants and/or products from the gas stream to the surrounding furnace. It should be noted that these hollow ceramic tubes have a number of other advantages when used as catalyst supports, including excellent thermal shock resistance, high strength, light weight, chemical inertness, and reasonably high melting temperatures (*11*).

The method of incipient wetness was used to impregnate the various catalytic agents on the support substrates by dissolving a known weight of metal ions, usually in the form of the nitrate salt, in water and/or dilute HCl. The solution was used to physically saturate the support, care being taken to ensure uniformity in distribution. Water

0013-936X/88/0922-0557$01.50/0

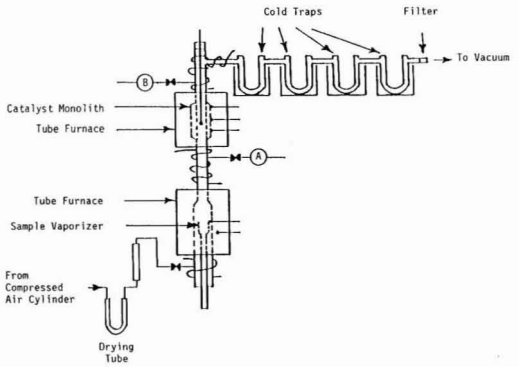

Figure 1. Experimental apparatus.

and other volatiles were first driven off by heating the treated monoliths to 110 °C in a drying oven for 24 h. The monoliths were subsequently installed in the upper tube furnace and then calcined at 600 °C with airflow for a period of 24 h. Refractory baffles were placed at various intervals along the outer length of the monolith when installed in the upper furnace to minimize the effects of free convection. The resultant catalyst tubes were subsequently used directly in the oxidation studies. In all, five different monolith catalyst systems were used, four *p*-type transition metal oxides (4% Cr_2O_3, 10% $CuCr_2O_4$, 6% Co_3O_4, and 10% CuO), and one noble metal type (0.05% Pt plus 0.05% Pd).

In the case of the $CuCr_2O_4$ catalyst, an unglazed tube was used, and a solution containing the nitrates of copper and chromium (with excess copper) was impregnated on the support. The monolith was oven-dried and the temperature subsequently increased to 200 °C to facilitate decomposition of the metal nitrates. It was then fired at 600 °C for 6 h, when CuO and $CuCr_2O_4$ were formed. The monolith was then leached in 3 M HCl, thoroughly washed, and subsequently fired to 800 °C to leave $CuCr_2O_4$ as the only remaining active species.

Procedures. The basic run procedure was to meter air at a flow rate of 500 mL/min (STP) through the catalyst monolith section. Product traps consisting of cooled preweighed Pyrex U-tubes (250 mL of acetone in 600-mL Pyrex beaker with dry ice to fill) were attached to the top of the reactor; the U-tubes were connected by Tygon tubing, and a cellulose filter was installed after the last U-tube to pick up the remainder. The entire system was allowed to attain thermal equilibrium prior to commencing a run.

To initiate a run, the sample holder, containing a preweighed amount of liquid Aroclor 1254, was inserted into the lower furnace causing controlled vaporization of the sample. The lower furnace was maintained at 300 °C for 12 min, elevated to 400 °C at the rate of 10 deg/min, and held at this temperature for 5 min. The temperature programming procedure allowed for reasonably constant rates of PCB vaporization over the entire run period, as the more volatile (low-chlorine isomers) were gradually replaced by less volatile (high-chlorine isomers) in the vapor stream. Temperature data were obtained from all thermocouples with the digital scanner. Vapor samples before and after passage though the monolith reactor were taken at designated times with syringes inserted through sampling ports A and B.

At the end of the run (27 min), the sample holder was removed from the lower furnace, cooled, and reweighed. The U-tubes containing products were disconnected, removed, dried, and reweighed; power to the system was disconnected, and the airflow was stopped.

The vapor samples removed periodically from ports A and B were analyzed for H_2, O_2, N_2, CO, CH_4, and CO_2 (water-free basis), with a Varian 90P-3 gas chromatograph (GC) equipped with a thermal conductivity detector maintained at 225 °C. The column was 2.44 m long by 0.32 cm i.d. stainless steel and packed with 100/120-mesh Carbosieve-S. The samples were injected with the column temperature initially at 27 °C; this was raised to 190 °C at the rate of 20 deg/min once the O_2 peak had been observed on the associated Leeds and Northrup Speedomax W strip-chart recorder. A Columbia CSI-Model 38 digital integrator was used to obtain the peak areas.

Analysis of reactor products during this study was limited to PCB isomers, CO_2, O_2, N_2, and CO. It is unlikely that detectable quantities of dioxins or dibenzofurans were formed at reactor temperatures of 500–600 °C on the basis of the literature (*12*), which reports that chlorinated phenols, not chlorinated biphenyls, are the necessary precursors for significant PCDD formation. However, analysis for these compounds or other chlorinated hydrocarbons was not performed during this study.

To determine the residual PCBs in the condensate from the U-tubes, 20 mL of pesticide-grade hexane was injected into each tube. Solutions from all U-tubes were thoroughly mixed in a beaker where PCBs deposited on the filter were also dissolved. One milliliter of the mixed solution was injected into a Florisil Sep-Pak cartridge (Waters Associates) that had been preeluted with 10 mL of hexane. The eluate was collected in a 100-mL volumetric flask, and PCBs deposited in the cartridge were flushed into the flask by repeated injections of hexane; interfering organics and unnecessary compounds remained behind (*13*, *14*). The liquid in the flask was brought up to the mark by addition of hexane. Five-microliter samples of this liquid were injected into a Bendix-2200 GC equipped with tritium foil electron capture detector maintained at 200 °C. The glass column (1.83 m × 0.64 cm i.d., packed with 3% SE-30 on 100/120-mesh Gas-Chrom Q) was operated in the isothermal mode at 192 °C. Peak areas were determined in a Columbia CSI-Model 38 digital integrator. Each of the 11 prominent isomer peaks was previously calibrated by means of injecting a series of standard PCB solutions into the electron capture gas chromatography (EC) and determining the resultant concentration-dependent response factors based on the method developed by Goodyear (*15*). The product of each isomer concentration and the liquid sample volume (in appropriate units) gave the total weight of each PCB isomer in the condensate.

Summation over all isomers present yielded the total weight of all PCBs collected. An iterative procedure (*10*) was utilized when running reactor effluent samples that allowed convergence to the correct isomer concentrations. A typical chromatogram of Aroclor 1254 is shown in Figure 2. (The key for Figure 2 is shown in Table I.)

On the basis of peak areas from these chromatograms and the method outlined above, the weights of each PCB isomer before and after passage through the catalytic reactor were calculated. By using these results, destruction efficiencies for each PCB isomer as well as overall destruction efficiencies (total PCB destroyed/total PCB charged) were obtained. The average rate of PCB destruction (PCB destroyed/unit catalyst, unit time) was also found.

Results and Discussion

Catalyst Activity. Experimental values of overall PCB destruction rates and overall PCB destruction efficiences

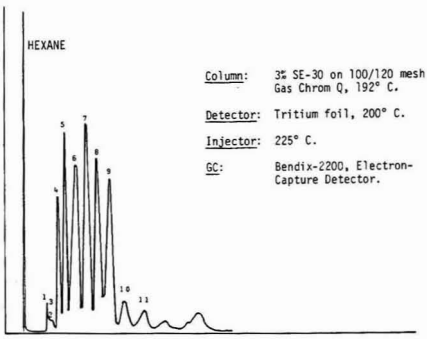

Figure 2. Typical chromatogram of Aroclor 1254.

Table I. Key to Figure 2

peak no.	RRT[a]	no. of Cl's on isomer	mean wt %
1	47	4	6.8
2	54	4	3.2
3	58	4	1.5
4	70	4 (25%)	14.5
		5 (75%)	
5	84	5	19.0
6	104	5	14.9
7	125	5 (70%)	16.4
		6 (30%)	
8	146	6 (30%)	11.4
		6 (70%)	
9	174	6	9.2
10	203	6	2.0
11	232	7	1.1
total			100.0

[a] Retention time in seconds relative to p,p'-DDE = 100. Measured from first appearance of solvent (hexane).

of the blank Pyrex tube (assumed to represent homogeneous reaction only) as well as the five monolithic catalyst systems are summarized in Table II. Comparative results, listed in order of increasing catalyst activity, are shown at both 500 and 600 °C and in all cases are an average of two or three separate experimental determinations.

Only one relatively low level of noble metal (0.05% Pt plus 0.05% Pd) catalyst was formulated and tested. Hence, it is possible that higher noble metal loaded monoliths would have outperformed all transition metal oxide (TMO) catalysts activitywise. Nevertheless, comparative economics would probably mitigate against such a commercial catalyst because of the high cost.

The four p-type TMOs were formulated with sufficient catalytic agent to potentially attain at least monolayer coverage for the metal cations throughout the entire pore structure of the support. These levels are generally in line with TMO loadings for commercially available catalysts.

Passage of PCB vapors through the Pyrex blank, a measure of homogeneous reaction rate, yielded almost no

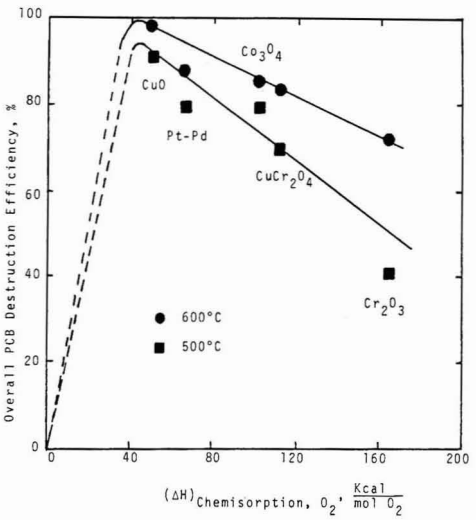

Figure 3. Catalyst activity versus heat of chemisorption for O_2.

activity at 500 °C (0.2%) increasing to 7.2% PCB destruction efficiency at 600 °C. All of the catalytic monoliths showed heterogeneous activity for PCB disposal, which was 1 or more order of magnitude above that obtained in the homogeneous Pyrex system. Differences in rate for homogeneous versus heterogeneous system are especially noticeable (3 orders of magnitude) at 500 °C but diminish to 1 order of magnitude difference at 600 °C. Temperature insensitivity (low activation energy) for heterogeneous reactions at high temperatures is not unusual. Limits on the rate of reactant diffusion to the catalyst surface sites within the pores, especially at higher temperatures, are probably responsible for this phenomenon, a result which has subsequently been supported by separate modeling studies (*9*).

Activities of the p-type TMOs and the noble metal catalyst are plotted versus initial heats of oxygen chemisorption in Figure 3. In catalytic deep oxidation processes, activity often decreases with an increase in the strength of the oxygen–catalyst surface bond energy (measured here by the initial heat of oxygen chemisorption) basically because these bonds must be broken during the oxidation process (often called the principle of Sabatier). Figure 3 shows good correlation with this relationship for all four TMOs tested. Had diffusion limits not blunted activities of the best catalysts, the trend might have been even more pronounced. Results for the noble metal Pt–Pd catalyst (not a TMO) are also shown in Figure 3 for purposes of comparison.

It is not surprising that destruction efficiencies do not extend above 99%. First, the monolith is (importantly) a low-pressure drop device useful in treating high vapor

Table II. Catalyst Activity

	500 °C		600 °C	
catalyst	overall PCB dest rate, g of PCB cm^{-3} of cat. s^{-1}	overall PCB dest eff, %	overall PCB dest rate, g of PCB cm^{-3} of cat. s^{-1}	overall PCB dest eff, %
Pyrex	6.26×10^{-8}	0.2	2.63×10^{-6}	7.2
4% Cr_2O_3	1.46×10^{-5}	39.2	2.46×10^{-5}	69.3
10% $CuCr_2O_4$	2.48×10^{-5}	68.3	3.13×10^{-5}	83.0
0.05% Pt, 0.05% Pd	2.86×10^{-5}	78.4	3.20×10^{-5}	87.4
6% Co_3O_4	2.93×10^{-5}	80.1	3.14×10^{-5}	85.9
10% CuO	3.37×10^{-5}	92.4	3.56×10^{-5}	97.3

Table III. Catalyst Selectivity for Deep Oxidation of PCB

catalyst	deep oxidation efficiency, % (PCB carbon → CO and CO_2) 500 °C	600 °C
Pyrex	1.0 (1.00)[a]	4.9 (1.00)[a]
4% Cr_2O_3	40.5 (0.864)	50.3 (0.817)
10% $CuCr_2O_4$	51.4 (0.871)	85.1 (0.810)
0.05% Pt, 0.05% Pd	38.3 (0.798)	75.6 (0.792)
6% Co_3O_4	45.5 (1.00)	81.0 (0.975)
10% CuO	55.5 (1.00)	75.4 (1.00)

[a] Represents fraction present as CO_2, with balance as CO.

flow rate streams. However, without the inherent mixing found in packed or fluidized beds, film diffusion may limit reactivity. Second, low surface area supports (<1 m^2/g) were purposely chosen for this study so that surface reaction rates (not just diffusion rates) play a role in catalyst activity. Future studies using higher surface areas, thin-walled supports, and closely spaced multicell monoliths will effectively maximize the destruction efficiency.

Catalyst Selectivity. Many reaction products are possible for the oxidation of mixed polychlorinated biphenyls depending largely on the relative amounts of combined hydrogen and chlorine. When combined hydrogen is in excess, considerable water and HCl should be anticipated; when combined chlorine is in excess, products such as CCl_4, Cl_2, and $COCl_2$ might be expected.

In this study, only individual PCB isomer destruction rates along with CO and CO_2 formation rates were quantitatively measured. Hence, conclusions as to catalyst selectivity are necessarily limited by these available data.

One criterion for the effectiveness and potential environmental usefulness of any catalyst system is its preferential selectivity toward deep oxidation of the PCB isomers (i.e., total formation of CO and CO_2 from PCB carbon). Deep oxidation selectivities for each of the five catalysts and blank reactor at both 500 and 600 °C are shown in Table III.

Table III shows that even at 600 °C deep oxidation efficiencies for the best catalysts appear to level out, never exceeding the 75–85% range. This is in contrast to overall PCB destruction efficiences, which were found to exceed 90% at both 500 and 600 °C. One possible explanation for this is that the initial PCB oxidation step is most likely heterogeneous (occurs on the surface of the catalyst), whereas one or more of the subsequent steps in the oxidation process, which eventually leads to CO and CO_2, may well be homogeneous and hence relatively independent of the nature of the catalyst surface.

The fraction of deep oxidation product present as CO_2 for each catalyst system is also shown (brackets) in Table III and projects a minimum value of 0.792 with a high of 1.00. High fractional CO_2 formation is obviously preferred; however, in making comparisons it should be realized that high CO_2 fractions for systems showing minimal deep oxidation efficiencies are not of significant merit.

A third measure of catalyst selectivity is its effectiveness in destroying PCB isomers with high-chlorine levels (6 or more Cls per PCB molecule) versus low-chlorine levels (4 or less Cls per PCB molecule). An important physiological ramification is that high-chlorine-containing isomers are much more carcinogenic than low-chlorine-containing isomers.

This selectivity comparison was accomplished in this study for each catalyst by determining GC/EC areas for each of the 11 peaks observed in the commercial mixture of PCB isomers (Aroclor 1254), before and after passage of the mixed vapors (plus excess air) through the catalytic reactor of 600 °C. Areas were then converted to weight fractions for each isomer by the method previously outlined under Procedures. The results are shown in Table IV. Changes in isomer weight fraction (averaged for three determinations in each case) were lumped into three categories: peaks 1–4 (low-chlorine-content isomers with 4 Cls), peaks 5–7 (medium-chlorine-content isomers with 5 Cls), peaks 8–11 (high-chlorine-content isomers with 6–7 Cls).

Several interesting results emerge from these comparisons. First, the Pyrex blank reactor, representing the homogeneous reaction, yielded not only poor overall PCB destruction (4.9%) but also showed an increase (+22.4%) in the fraction of more toxic high-chlorine isomers after passage through the reactor. With thermal stability generally increasing with chlorine content, this relative result was not surprising, although the actual pyrosynthesis of the high-chlorine isomers was not anticipated.

Second, comparisons from Table IV show that TMO catalyst activity and selectivity can be significantly more favorable than the homogeneous case and even more favorable than the noble metal counterpart. For example, the CuO catalyst shows not only high overall PCB destruction activity (97%) but also excellent selectivity (>99%) in removing high-chlorine-containing isomers. Of course, other concerns must be satisfied before settling on a given catalyst system for commercial application.

Long term deactivation and stability of the catalytic agent must be determined. In the case of the CuO catalyst, one would expect slow conversion to $CuCl_2$ on the basis of contact with HCl formed during the dechlorination reactions. Since the melting point of $CuCl_2$ is only slightly above 600 °C, slow volatilization of the catalytic agent is probable. Thermal stabilization is possible, however, through use of promoters such as KCl, and it is probable that the resultant Deacon-process-type catalyst would be quite acceptable.

Conversely, Pt–Pd catalysts are known to slowly deactivate under conditions where HCl and Cl_2 are prevalent, another good reason to focus on TMOs when searching for a commercial catalyst system.

In summary, the high degree of flexibility for catalytic versus thermal means of destruction is clearly demonstrated. Product distribution, which may be more im-

Table IV. PCB Destruction Levels versus Isomer Chlorine Content (600 °C)

catalyst	av change in isomer weight for peaks 1–4 (low Cl), wt %	av change in isomer weight for peaks 5–7 (med Cl), wt %	av change in isomer weight for peaks 8–11 (high Cl), wt %
Pyrex	−31.7	−11.7	+22.4
4% Cr_2O_3	−67.6	−73.6	−69.0
10% $CuCr_2O_4$	−94.9	−87.5	−98.6
0.05% Pt, 0.05% Pd	−92.8	−87.8	−85.4
6% Co_3O_4	−92.4	−83.5	−92.6
10% CuO	−99.1	−96.9	−99.7

portant than activity, can be tailored to fit needs and conditions by changing catalytic agents and/or mixtures thereof.

The low surface area, thick-walled monlithic reactor used in this study was not designed for direct commercial application. Thin-walled multicellular cores with higher surface area could pack at least 100 times more active catalytic sites into each cubic centimeter of catalyst system. Nevertheless, estimation of scaleup potential with the present 10% CuO catalyst on low surface area Al_2O_3 monolith shows that a 1000-L vapor-phase reactor operating at 500–600 °C would convert 50–70 kg of PCB/h. However, with higher surface area commerical multicell cores, reactivity could be at least 1 order of magnitude higher.

Registry No. Aroclor 1254, 11097-69-1; $C_6H_5C_6H_5$, 92-52-4; Cr_2O_3, 1308-38-9; Pt, 7440-06-4; Pd, 7440-05-3; Co_3O_4, 1308-06-1; CuO, 1317-38-0; $CuCr_2O_4$, 12018-10-9.

Literature Cited

(1) Farrell, J. B.; Salotto, B. V. *Effect of Incineration on Metals, Pesticides and PCBs in Sewage Sludge*; National Symposium on the Ultimate Disposal of Wastewaters, and Their Residuals: Raleigh, NC, 1973.
(2) Buser, H. R.; Bosshardt, H. P.; Rappe, C. *Chemosphere* **1978**, *1*, 109.
(3) Buser, H. R.; Bosshardt, H. P.; Rappe, C. *Chemosphere* **1978**, *2*, 165.
(4) Olie, K.; Vermuelen, P. L.; Hutzinger, O. *Chemosphere* **1977**, *8*, 455.
(5) Lombardi, E. F.; Johnson, A. J.; Meyer, F. G.; Hunter, D. I. *Incineration of PCBs Using a Fluidized Bed Incinerator*; Rockwell International: Golden, CO, 1981.
(6) *Chem. Eng.* **1981**, *88(16)*, 37–41.
(7) Akerman, L. C.; Scinta, L. L.; Bakshi, P. S.; Delumyea, R. G.; Johnson, R. J.; Richard, G.; Takata, A. M.; Sworzyn, E. M. *Destruction and Disposal of PCBs by Thermal and Non-Thermal Methods*; Noyes Data: Park Ridge, NJ, 1983.
(8) Akerman, D. G. "Guidelines for the Disposal of PCBs and PCB Items by Thermal Destruction"; U.S. EPA Report 600/281-022; U.S. Government Printing Office, Washington, DC, 1981.
(9) Desai, F. N.; Greene, H. L.; Subbanna, P. *Ind. Eng. Chem. Res.* **1987**, *26*, 1965.
(10) Subbanna, P. M.S. Thesis, University of Akron, 1985.
(11) Prasad, R.; Kennedy, L. A.; Ruckenstein, E. *Combust. Sci. Technol.* **1980**, *22*, 271–80.
(12) "State-of-the-Art Review: PCDDs and PCDFs in Utility PCB Fluid"; final report EPRI CS-3308, Project 1263-11; Electric Power Research Institute: Palo Alto, CA, Nov 1983.
(13) Lerman, S. I.; Gordon, H.; Hendricks, J. P. *Am. Lab. (Fairfield, Conn.)* **1982**, *14(2)*, 176–81.
(14) *Sep-Pak Cartridges, A New Dimension in Sample Cleanup*; Waters Associates: Milford, MA, 1981.
(15) *A Safe, Efficient Chemical Disposal Method for PCBs*; Goodyear Tire and Rubber: Akron, OH, 1980.

Received for review December 29, 1986. Revised manuscript received November 9, 1987. Accepted December 15, 1987.

A Numerical Solution for Mass Transport in Membrane-Based Diffusion Scrubbers

Richard L. Corsi,* Daniel P. Y. Chang, and Bruce E. Larock

Department of Civil Engineering, University of California, Davis, California 95616

■ The Galerkin finite element method was used to develop a numerical model for the design of porous-wall diffusion scrubbers, devices which may be used as alternatives to diffusion denuders, and to selectively separate dissolved components from a liquid stream. It was found that the analytical Gormley–Kennedy solution for a tube with an ideally absorbing interior wall is appropriate for scrubbers characterized by a gas–liquid interface at the wall. However, the major conclusion of this work is that the Gormley–Kennedy solution is often inappropriate for application to diffusion scrubbers based upon a liquid–liquid interface at the wall. For such scrubbers, the unknown concentration boundary condition at the interior wall can be accounted for with the numerical solution, thus providing a design tool that has not been previously available. A set of penetration curves was generated for design purposes, and example applications are provided.

Introduction

The diffusion denuder is a device which can be used to remove a gaseous component selectively from a gas mixture or aerosol. Denuders are typically constructed from a cylindrical tube or concentric tubes with the inner wall(s) coated with a substance to sorb a specific component. They have been used to remove water selectively from a nebulized aerosol sample while permitting the passage of sulfate particles (*1*), to remove sulfur dioxide from airstreams containing sulfur particles (*2–4*), and to remove ammonia in order to prevent neutralization of sulfuric acid aerosol collected on downstream filters (*5*). Additional applications for denuders have been suggested (*6–8*), but specific design and operational limitations have also been cited (*3, 9*). Limitations include a finite adsorptive capacity (*3*), the choice of sorbents, the sorbent concentration and form, the wall material, the denuder geometry, and the sample flow rate (*9*).

Dasgupta (*10*) investigated alternative device configurations for the collection of atmospheric gases. His work led to the construction of a diffusion scrubber, a device which is similar in principle to the diffusion denuder but which employs a thin membrane tube as the collection element. In subsequent work a porous-membrane tube was found to be the material of choice (*11*). A schematic representation of the hollow cylindrical diffusion scrubber is shown in Figure 1. It consists of a porous-wall hollow fiber. Molecules of interest diffuse through the wall and are removed by a scrubber liquid flowing counter to the transport medium. Applications of diffusion scrubbers include not only diffusion denuders for gas separation but also the separation of dissolved species from a liquid stream (*12–15*). Diffusion scrubbers have also been used as concentrators for continuous chemical analysis (*16*). In addition, Dasgupta (*17*) described the use of an annular helical diffusion scrubber in ion chromatography as an efficient conductance suppressor column having both low dispersion and low dead volume.

Models to describe species transport in diffusion devices can be used to determine design parameters such as denuder length and the sample flow rate required to achieve

0013-936X/88/0922-0561$01.50/0

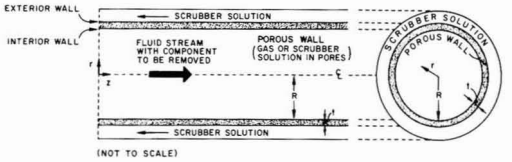

Figure 1. A simplified diagram of the porous-wall diffusion scrubber illustrating the internal fluid stream, porous wall, and scrubber solution.

a desired species collection or removal efficiency. Analytical solutions exist to predict the penetration Pt, defined as

$$\mathrm{Pt} = \bar{C}_e/\bar{C}_o \tag{1}$$

where $\bar{C}_o$ and $\bar{C}_e$ are the average concentrations at the tube inlet and outlet, respectively, of a chemical species in fully developed, laminar flow in a cylindrical tube, given either an ideally absorbing wall or known concentration profiles at the wall (*18–21*). These solutions are applicable to laminar flow in diffusion denuders or other devices satisfying the boundary conditions such as diffusion through silicone tubing or possibly ion-exchange membranes. The authors are unaware of any extant solutions which predict concentration profiles and penetration in a diffusion scrubber for which a nonuniform concentration boundary condition applies, but cannot be initially prescribed, at the inside surface of the porous wall (see Figure 1). This study was undertaken in order to investigate the effects of such a condition and to develop a numerical finite element model for use as a design tool in cases not described by existing analytical solutions such as the Gormley–Kennedy (*19*) solution. The latter is expressed as

$$\mathrm{Pt} = 0.819e^{-14.6272b} + 0.976e^{-89.22b} + 0.01896e^{-212b} + \ldots \tag{2}$$

where

$$b = Dz/(4\bar{u}R^2) \tag{3}$$

and D is the diffusion coefficient of the species of interest, z is the axial distance from the tube inlet, $\bar{u}$ is the average axial velocity, and R is the tube's inner radius. Equation 2 has been used successfully to model denuder systems with interior walls that act as perfect sinks (*19–21*).

In order to verify model results for a porous wall, in this study a simplified case corresponding to an impermeable adsorbing inner wall which behaves as a perfect sink for the species of interest was solved by a finite element approach. The penetration of a component was then compared with values obtained from the Gormley–Kennedy solution, an analytical solution which has been widely used and tested in the field of aerosol science. A permeable wall boundary condition and the inclusion of a hydrodynamic entrance region were subsequently added to examine their effects on species transport. It should be emphasized that the numerical solution only treats the condition of laminar flow, which is the dominant flow regime for most diffusion scrubber applications.

Model Methodology

Governing Equations. The steady-state convective–diffusion equation governs diffusion through a homogeneous medium flowing in a cylindrical tube. It may be written as

$$u\frac{\partial C}{\partial z} + v\frac{\partial C}{\partial r} = D\left(\frac{1}{r}\frac{\partial}{\partial r}\left(r\frac{\partial C}{\partial r}\right) + \frac{\partial^2 C}{\partial z^2}\right) \tag{4}$$

where u is the velocity in the axial (z) direction, v is the velocity in the radial (r) direction, and C is the concentration of the component of interest. Axial symmetry has been assumed, along with the assumption that there are no sources or chemical transformations occurring within the tube.

Equation 4 can be simplified by assuming that the radial velocity component and the axial diffusion term are negligible. It is assumed that there is no bulk flow of fluid through the wall. Following the arguments of Tan (*22*), the assumption of a negligible radial velocity is valid for typical flow rates, scrubber geometries, and species diffusion coefficients for which diffusion scrubbers are applied. Ingham (*20*) and Tan and Hsu (*21*) noted the conditions for which axial diffusion is insignificant. These conditions are also easily met for typical diffusion scrubber geometries and flows (*10*). Use of these assumptions allows eq 4 to be simplified to

$$u\frac{\partial C}{\partial z} \simeq \frac{D}{r}\frac{\partial}{\partial r}\left(r\frac{\partial C}{\partial r}\right) \tag{5}$$

Introduction of the dimensionless variables

$$C' = C/C_0 \qquad u' = u/2\bar{u} \qquad r' = r/R \qquad z' = z/L$$

leads to the nondimensional equation

$$u'\frac{\partial C'}{\partial z'} \simeq \frac{\tilde{D}}{r'}\frac{\partial}{\partial r'}\left(r'\frac{\partial C'}{\partial r'}\right) \tag{6}$$

where L is the effective scrubber length. The characteristic nondimensional Fourier parameter $\tilde{D}$ is

$$\tilde{D} = DL/(2\bar{u}R^2) \tag{7}$$

For reasons which will become apparent in a later example application, $\tilde{D}$ is chosen for design purposes. The choice of $\tilde{D}$, $\bar{u}$, and R, together with a known value for D, defines a characteristic scrubber length, L. The design, or actual, scrubber length, x, is obtained as the product of L and the dimensionless axial distance z'. The selection of an appropriate value for z' is demonstrated later in this paper.

For fully developed laminar flow, the appropriate dimensionless velocity distribution is

$$u' = 1.0 - r'^2 \tag{8}$$

If a significant entrance length exists, eq 8 is not an accurate representation of the velocity profile for the entire flow domain. Instead, a solution for the developing velocity field is required as input data for the numerical model. For this study, an equation based upon the linearization of momentum was used to describe the entrance region velocity field (*23*).

Boundary Conditions. The dimensionless concentration at the inlet, $z' = 0$, was prescribed with a uniform value of 1.0. At the outlet, $z' = 1$, both a zero concentration boundary condition and a second boundary condition were investigated. The alternative boundary condition was based upon a parabolic fit of the penetration which was obtained by the Gormley–Kennedy solution. Results obtained with the two boundary conditions were not significantly different. The latter condition was arbitrarily chosen for this study. Either condition imposes limitations on the minimum value which may be chosen for $\tilde{D}$, since small values of $\tilde{D}$ correspond to conditions associated with high penetration that would violate the assumed boundary condition at the outlet.

For permeable walls at steady state, the flux at the interior surface of the wall must necessarily be equal to the flux through the wall. It was assumed that the transport through the wall is such that a linear concentration gradient exists in the wall and that only radial diffusion is significant in the wall. This leads to

$$C'_{i,1} = [1.0/(1.0 + W\Delta r'/t')]C'_1 \tag{9}$$

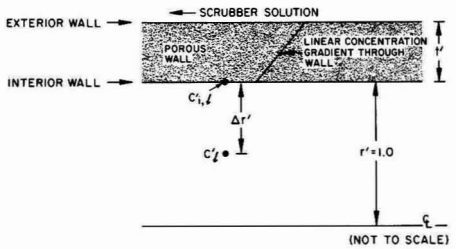

Figure 2. An illustration of the region near the porous wall. Important wall assumptions and dimensionless parameters are noted.

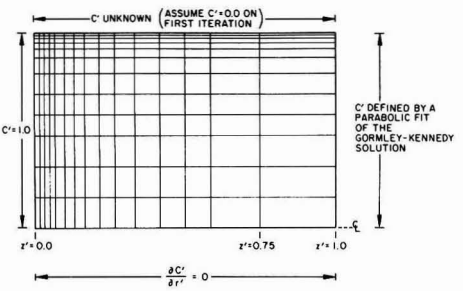

Figure 3. A typical finite element grid. Boundary conditions are noted.

where $C'_{i,l}$ is the dimensionless concentration in the liquid phase at the inner surface of the wall, C'_l is the dimensionless concentration at a dimensionless radial distance $\Delta r'$ from the inner surface of the wall, and t' is the dimensionless wall thickness defined to be the ratio of the actual wall thickness t to the scrubber radius R (see Figure 2). The term W is a nondimensional wall parameter. For the case of a liquid flow medium and a gas space in the porous wall (liquid–gas interface), W is

$$W = D_g K/(D_l R_u T) \tag{10}$$

where D_g and D_l are diffusion coefficients of the species of interest in the gas and liquid phases, respectively, K is the Henry's law coefficient governing its partition between the two phases, R_u is the universal gas constant, and T is the absolute temperature. For a liquid–liquid interface of two immiscible liquids, the wall parameter is

$$W = D_{l2}K'/D_{l1} \tag{11}$$

where D_{l2} is the diffusion coefficient of the species of interest in the outer acceptor liquid (which occupies the pore space in the wall or the wall itself), D_{l1} is the diffusion coefficient in the donor liquid bearing the species of interest flowing through the tube, and K' is the equilibrium partition coefficient of the species of interest between the two immiscible liquid phases. Specifically, K' is the ratio of the species concentration in the acceptor liquid to that in the donor liquid at equilibrium.

Numerical Solution. To determine concentration and penetration values, a Galerkin finite element numerical model (*24*, *25*) was developed. Bilinear interpolation functions were used along with four-node, isoparametric, quadrilateral elements to describe the geometry of, and concentration within, elements subdividing the diffusion scrubber volume. Figure 3 depicts a typical grid system with nodes at which concentrations were computed. The boundary conditions for this study are also denoted. Axial symmetry was assumed, and computed values of C' were numerically integrated across the scrubber cross-section to solve for the penetration at specified values of z'.

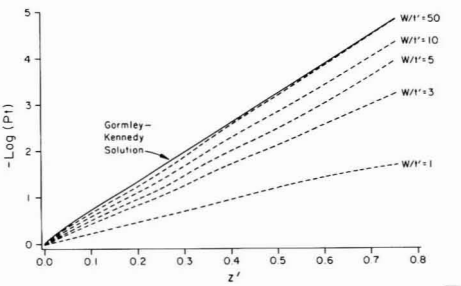

Figure 4. Penetration as a function of the dimensionless axial distance (z') and properties of the porous wall (W/t'). The Gormley–Kennedy solution is shown by the solid line. $\tilde{D} = 2.0$.

Results

The model was solved with the aid of a grid system similar to the one shown in Figure 3. A sensitivity analysis of concentration profiles near the scrubber wall suggested that $\tilde{D}$ should exceed a value of 1.0 to be consistent with the outlet boundary condition. A value of $\tilde{D}$ equal to 2.0 was used for this study. The algorithm of the numerical model was verified for the simplified case of an ideally adsorbing wall by comparison of model results with values obtained from the Gormley–Kennedy solution. For typical scrubber geometries and sample flow rates, the effect of a hydrodynamic entrance region was determined to be insignificant.

The permeability of the scrubber wall was found to be a significant factor only for values of W/t' less than 50.0. Given typical values of t' less than 0.25 for porous-membrane tubes and typical values of W calculated according to eq 10, the value of W/t' is nearly always greater than 50.0 for systems composed of a liquid transport medium and a gas phase in the scrubber wall. Thus, the Gormley–Kennedy solution for laminar flow in a cylindrical tube, strictly applicable to an ideally adsorbing wall, can also be used as an accurate model for predicting penetration in porous-wall gas–liquid scrubbers. The Gormley–Kennedy solution does not, however, yield accurate results for systems with values of W/t' significantly less than 50.0. Such systems might be based upon the interface of two immiscible liquids at the scrubber wall.

Figure 4 consists of a plot of $-\log$ Pt versus z' for various values of W/t' and $\tilde{D} = 2.0$. Curves are shown only to $z' = 0.75$, which was the nondimensional distance corresponding to the last set of grid nodes at which concentrations were numerically solved. The next set of nodes corresponded to the outlet nodes where concentrations were specified as mentioned previously. The solid line indicates the Gormley–Kennedy solution. Figure 4 can be used for diffusion scrubber design in those cases where the Gormley–Kennedy solution would be inappropriate. The following examples are provided to illustrate the use of Figure 4.

Example Application 1. A diffusion scrubber is to be used to remove a specific compound from a liquid stream which requires pretreatment before chemical analysis. With 1-octanol as the scrubber solution and water as the transport medium, the values of D_{l2} and D_{l1} are 3.0×10^{-6} cm^2/s and 3.0×10^{-5} cm^2/s, respectively. The octanol–water partition coefficient is 30.0. A scrubber tube with an inner diameter equal to 0.625 mm and a wall thickness of 0.125 mm is available. It is desired to find the minimum scrubber length x required to remove 99% or more of the compound. The sample flow rate is expected to be less than 0.25 mL/min:

Step 1: Solve for $D_{l2}/D_{l1} = 3.0 \times 10^{-6}/3.0 \times 10^{-5} = 0.1$.
Step 2: Solve for $t' = 0.125/0.3125 = 0.4$.
Step 3: Solve for $W/t' = 0.10(30.0)/0.4 = 7.5$.
Step 4: Solve for $-\log Pt = -\log (1.0–0.99) = 2.0$.
Step 5: Solve for z' at $-\log Pt = 2.0$ for $W/t' = 7.5$. From Figure 4, $z' = 0.365$.
Step 6: Compute the maximum average sample velocity for a flow rate of 0.25 mL/min and a radius of 0.3125 mm. The average velocity is calculated by dividing the sample flow rate by the cross-sectional area of the scrubber tube. $\bar{u} = 1.36$ cm/s.
Step 7: Let $L = x/z'$ and use eq 7 along with the known or calculated values of $\tilde{D}$, D, z, $\bar{u}$, and R to solve for x; $x = 65$ cm.

Use of the Gormley–Kennedy equation leads to a value of x equal to 53 cm. For $W/t' = 7.5$, this corresponds to a penetration of 3%. Thus, use of the Gormley–Kennedy equation for this application may lead to an undersized (in length) scrubber and too low of a removal efficiency for the intended end use of the sample.

Often, a specific length of scrubber tube is available, and the removal efficiency that can be achieved with that length is desired to be known. The following example shows how the removal efficiency can be calculated with the use of Figure 4.

Example Application 2. A 30-cm segment of a scrubber tube is available to remove a compound from a liquid stream. With 1-octanol as the scrubber solution and water as the transport medium, the values of D_{l2} and D_{l1} are 2.0×10^{-6} cm^2/s and 2.5×10^{-5} cm^2/s, respectively. The octanol–water partition coefficient is 25.0. The scrubber tube has an inner radius equal to 0.5 mm and a wall thickness of 0.1 mm. It is desired to find the compound removal efficiency given a sample flow rate of 0.2 mL/min:

Step 1: Solve for $D_{l2}/D_{l1} = 2.0 \times 10^{-6}/2.5 \times 10^{-5} = 0.08$.
Step 2: Solve for $t' = 0.1/0.5 = 0.2$.
Step 3: Solve for $W/t' = 0.08(25.0)/0.2 = 10.0$.
Step 4: Solve for the average velocity of the sample; $\bar{u} = 0.42$ cm/s.
Step 5: Solve for $L = x/z'$ given $\tilde{D}$, D, $\bar{u}$, and R. Use $\tilde{D} = 2.0$ for consistency with Figure 4. From eq 7, $L = 168$ cm.
Step 6: Solve for $z' = x/L = 30/168 = 0.18$.
Step 7: Solve for the penetration (Pt) using Figure 4 with $z' = 0.18$ and $W/t' = 10.0$; Pt = 0.1.

Thus, a 90% removal efficiency is expected with the 30-cm length of scrubber tube. Given the specific tubing, the removal efficiency could be improved by lowering the sample flow rate. This will lead to a decrease in L and a subsequent increase in z'. Figure 4 could again be used to solve for the appropriate flow rate to achieve the desired removal efficiency.

Summary

A numerical solution of diffusion of a single component from a fluid flowing in laminar conditions through a permeable-wall cylindrical tube has been completed. The results demonstrate that a dimensionless ratio, W/t', can be used as a criterion for satisfactory application of the Gormley–Kennedy solution to the mass-transfer problem. In cases where W/t' is less than 50, the numerical solution would provide more accurate results. The application of diffusion scrubbers extends to several disciplines, and the penetration curves presented in this paper should be of assistance in the design of such devices. The analysis presented here is based on the assumption of smooth walls without local mixing due to surface irregularities and pores. Future work should be directed toward verifying such an assumption for typical porous-wall diffusion scrubbers.

Acknowledgments

We thank Dr. Purnendu Dasgupta for his valuable comments regarding his study of diffusion scrubber design and application and Virginia Roy and Barbara Sullivan for assistance with the preparation of the manuscript.

Glossary

b	diffusion parameter used in the Gormley–Kennedy equation; $b = Dz/(4\bar{u}R^2)$
r	radial coordinate (cm)
r'	dimensionless radial coordinate; $r' = r/R$
t	scrubber wall thickness (cm)
t'	dimensionless wall thickness; $t' = t/R$
u	axial velocity component (cm/s)
u'	dimensionless axial velocity; $u' = u/2\bar{u}$
$\bar{u}$	average axial velocity (cm/s)
v	radial velocity component (cm/s)
z	axial coordinate (cm)
z'	dimensionless axial coordinate: $z' = z/L$
C	concentration (g/cm^3)
C_0	concentration at the scrubber inlet (g/cm^3)
C'	dimensionless concentration; $C' = C/C_0$
C'_1	dimensionless concentration at a dimensionless distance $\Delta r'$ from the interior wall of the scrubber
$C'_{i,l}$	dimensionless concentration at the interior surface of the scrubber wall
$\bar{C}_e$	average concentration across the scrubber outlet (g/cm^3)
$\bar{C}_o$	average concentration across the scrubber inlet (g/cm^3)
D	diffusion coefficient of the species of interest (cm^2/s)
$\tilde{D}$	nondimensional Fourier parameter; $\tilde{D} = 2b$
D_g	diffusion coefficient in air (cm^2/s)
D_l	diffusion coefficient in liquid (cm^2/s)
D_{l1}	diffusion coefficient in the liquid flowing through the scrubber (cm^2/s)
D_{l2}	species diffusion coefficient in the scrubber liquid which permeates the porous wall (cm^2/s)
K	Henry's law constant of the diffusing species (atm·m^3/mol)
K'	liquid–liquid partition coefficient
L	length of the diffusion scrubber (cm)
Pt	penetration through the scrubber; $Pt = \bar{C}_e/\bar{C}_o$
R	scrubber inner radius (cm)
R_u	universal gas constant (atm·m^3/mol·K)
T	absolute temperature of the gas phase (K)
W	nondimensional wall parameter

Literature Cited

(1) Crider, W. L.; Barkley, N. P.; Knott, M. J.; Slater, R. W. *Anal. Chim. Acta* **1969**, *47*, 237.
(2) Durham, J. L.; Wilson, W. E. *Atmos. Environ.* **1978**, *12*, 883.
(3) Kaplan, D. J.; Himmelblau, D. M.; Chikao, K. *Environ. Sci. Technol.* **1981**, *15*, 558.
(4) Lewin, E. E.; Klockow, D. *Proceedings of the 2nd European Symposium on the Physico-Chemical Behavior of Atmospheric Pollutants*; Commission of the European Communities: Luxembourg, 1981; p 54.
(5) Appel, B. R.; Hoffer, E. M.; Tokiwa, Y.; Kothney, E. *Atmos. Environ.* **1982**, *16*, 589.
(6) Shaw, R. W.; Stevens, R. K.; Bowermaster, J. *Atmos. Environ.* **1982**, *16*, 845.
(7) Smith, B. M.; Wagman, J.; Fish, B. R. *Environ. Sci. Technol.* **1969**, *3*, 558.
(8) Stevens, R. K.; Dzubay, T. G. *Atmos. Environ.* **1978**, *12*, 55.
(9) Ferm, M. *Atmos. Environ.* **1979**, *13*, 1385.
(10) Dasgupta, P. K. *Atmos. Environ.* **1984**, *18*, 1593.
(11) Dasgupta, P. K.; McDowell, W. L.; Rhee, J. S. *Analyst (London)* **1986**, *111*, 87.
(12) Aoki, T.; Munemori, M. *Anal. Chem.* **1983**, *55*, 209.

(13) Aoki, T.; Uemura, S.; Munemori, M. *Anal. Chem.* **1983**, *55*, 1620.
(14) Hallowell, A.; Pacey, G. E.; Gordon, G. *Anal. Chem.* **1985**, *57*, 2851.
(15) Kiani, A.; Bhave, R. R.; Sirkar, K. K. *J. Membr. Sci.* **1984**, *20*, 125.
(16) Carlson, R. M. *Anal. Chem.* **1978**, *50*, 1528.
(17) Dasgupta, P. K. *Anal. Chem.* **1984**, *56*, 96.
(18) Davies, C. N. *J. Aerosol Sci.* **1973**, *4*, 317.
(19) Gormley, P.; Kennedy, M. *Proc. R. Ir. Acad., Sect. A* **1949**, *52A*, 163.
(20) Ingham, D. B. *J. Aerosol Sci.* **1975**, *6*, 125.
(21) Tan, C. W.; Hsu, C.-J. *J. Aerosol Sci.* **1971**, *2*, 117.
(22) Tan, C. W. *Heat Mass Transfer* **1969**, *12*, 471.
(23) Sparrow, E. M.; Lin, S. H.; Lundgren, T. S. *Phys. Fluids* **1964**, *7*, 338.
(24) Finlayson, B. A. In *Finite Elements in Fluids*; Gallagher, R. H., et al., Eds.; Wiley: London, 1975; Vol. 1, p 1.
(25) Becker, E. B.; Carey, G. F.; Oden, J. T. *Finite Elements: An Introduction*; Prentice-Hall: Englewood Cliffs, NJ, 1981; Vol. 1, p 10.

Received for review September 8, 1986. Accepted November 3, 1987.

Development and Evaluation of a Procedure for Determining Volatile Organics in Water

Larry C. Michael and Edo D. Pellizzari*

Research Triangle Institute, Research Triangle Park, North Carolina 27709

Roger W. Wiseman

National Institute of Environmental Health Sciences, Research Triangle Park, North Carolina 27709

■ A comprehensive procedure for isolation of volatile organic compounds from various waters was developed through the use of representative volatile organic compounds as part of the EPA Master Analytical Scheme. Preliminary recoveries were determined for a broad range of analytes in distilled water, municipal wastewater effluent, and industrial (energy-related) wastewater effluent. The apparatus for isolation of the compounds from water was interfaced directly to a gas chromatograph/mass spectrometer/computer, and recoveries were determined for compounds comprising different functional groups in drinking water and municipal/industrial wastewater.

Introduction

Analysis of organic compounds in water has traditionally been approached by selecting analytical methods on the basis of the target compounds. Examples of such an approach are the 600 series methods presented in the *Federal Register* (*1*). Alternatively, broad spectrum analytical methods provide a comprehensive assessment of all sample components. This philosophy was embraced by the U.S. EPA "Master Analytical Scheme" program (*2*). Analytical methods developed under this program were designed to encompass all gas chromatographable compounds with the fewest analytical methods.

The overall approach to development of a comprehensive analytical scheme for purgeables in water was to employ gas chromatography/mass spectrometry/computer (GC/MS/COMP) in conjunction with an isolation technique which would include the volatile (bp < 150 °C), water-insoluble compounds and also many compounds considered to be semivolatile and semi water soluble. An additional objective was to detect and quantitate these compounds at 0.1 μg/L in drinking water, 1 μg/L in surface waters, and 10 μg/L in effluent waters. On the basis of a comprehensive review of the current literature (*3*), only two techniques possessed adequate sensitivity to warrant experimental investigation of their range of applicability: (1) purge and trap (*4*) and (2) closed-loop gas stripping (Grob) analysis (CLSA) (*5–7*). Preliminary evaluation of both of these methods revealed that the conventional purge and trap method had a significantly shorter analysis time per sample and was inherently freer from interferences than closed-loop gas stripping analysis. In particular, the carbon disulfide used for desorption of the carbon trap in CLSA chromatographically obscured early-eluting analytes. Consequently, extensive method optimization was performed only on the purge and trap method. This was accomplished with ^{14}C-labeled compounds and is too extensive for inclusion here (*2*). This paper addresses method refinement, interface of the purge and trap apparatus to the GC/MS/COMP, and the method evaluation. Nonradiolabeled purgeable compounds, encompassing a broad range of compound types, were employed for method evaluation.

Experimental Section

Method Refinement Studies. Recovery determinations with representative compounds followed the analytical protocol outlined below:

(1) Organic-free water was prepared by purging deionized water for 2 h at 90 °C with 100 mL/min helium followed by continued purging while cooling to 30 °C.

(2) Aliquots (200 mL) were transferred to purge flasks containing 60 g of anhydrous Na_2SO_4 and were shaken to dissolve the salt.

(3) The 30% Na_2SO_4 solution was spiked with 5 μL of the appropriate standard mixture in methanol, mixed gently, and equilibrated at 30 °C for 10 mins.

(4) After the Tenax GC cartridge was attached, 500 mL of helium was passed through the solution at 25 mL/min.

(5) Exposed cartridges were analyzed by thermal desorption gas chromatography with flame ionization detection (GC/FID) on either a 180 × 0.2 cm Tenax GC (80/100 mesh) packed column or a 65 m × 0.5 mm SE-30 WCOT column.

(6) Recoveries were calculated by comparison to standard cartridges using electronic peak height measurements.

(7) In experiments involving municipal and energy effluent samples, 20 mL of effluent was combined with 180 mL of distilled water prior to introduction into the purge flask.

Evaluation of an Integrated GC/MS/COMP Purge and Trap System. A purge and trap system (Figure 1) consisting of a purge and trap module (A), an injection

0013-936X/88/0922-0565$01.50/0

Table I. Component Identification: Purge and Trap System

item	description
1	rope heaters—Hotwatt Inc., 250 W, 120 V, 60 in.
2	insulation—glass wool sleeve $^1/_2$ in. × $^1/_6$ in. thick
3	glass fiber tape—Scotch 27 (3M Co.)
4	sorbent trap—1.5 g of Tenax GC (Enka Research Institute, The Netherlands); 35/60 mesh
4A	$^3/_8$ in.–$^1/_{16}$ in. stainless steel, fritted (10 μm) reduction union
4B	$^3/_8$-in. stainless steel nut
4C	10 in. × $^3/_8$ in. o.d. × $^1/_{56}$ in. i.d. stainless steel tubing
5	heated/insulated nickel transfer line from six-port valve to GC injection system, $^1/_{16}$ in. o.d. × 0.040 in. i.d. × 30 in.
6	heated/insulated nickel transfer line from six-port valve to sorbent trap, $^1/_{16}$ in. o.d. × 0.040 in. i.d. × 14 in.
7	support and heater for six-port valve, Valco HA-1 (Valco Instruments Co., Inc.)
8	six-port valve, Valco C-6-T, $^1/_{16}$ in. zero dead volume fittings
9	support bracket for sample valve
10	sample valve, Tekmar 14036 (Tekmar Co.)
11	sample introduction needle, Tekmar 14217
12	Teflon (E. I. du Pont de Nemours and Co.) tubing ($^1/_{16}$ in. o.d. × 0.040 in. i.d. × 20 in.) with needle (18 gauge × 55 in.)
13	Teflon tubing ($^1/_{16}$ in. o.d. × 0.040 in. i.d. × 8 in.) with Cheminert (LDC/Milton Roy) connector for connecting to item 20
14	sampler union, Tekmar 14049
15	same as item 14
16	sample container, 243 mL, glass, 24-mm septum cap
17	three-finger clamp, Fisher 05-742 (Fisher Scientific Co.)
18	clamp holder, Fisher 05-754
19	aluminum rod, $^1/_2$ in., Fisher 14-666
20	heated/insulated nickel transfer line from purge flask connecting line to six-port valve, $^1/_{16}$ in. o.d. × 0.040 in. i.d. × 14 in.
21	heated/insulated nickel transfer line from six-port valve to sorbent trap, $^1/_{16}$ in. o.d. × 0.040 in. i.d. × 20 in.
22	heated/insulated nickel transfer line from sorbent trap to six-port valve, $^1/_{16}$ in. o.d. × 0.040 in. i.d. × 5 in.
23	clamp
24	soap bubble flowmeter
25	purge flask approximate dimensions—18 in. × 1.5 in. purge gas inlet—$^1/_{16}$ in. o.d. frit porosity—medium material—borosilicate glass (A) Microflex valve, Kontes K-749100-21 (Kontes Scientific Glassware/Instruments) (B) Chromaflex column valve, Kontes K-423600 (C) Chromaflex column valve, Kontes K-423600
26	spring, 1.5 in.
27	dry purge valve, four-port, Valco C-4-T, $^1/_{16}$ in. zero dead volume fittings
28	aluminum panel, 16 in. × 26 in. × $^1/_8$ in.
29	Flexframe foot plate, Fisher 14-666-25
30	purge gas line, Teflon tubing ($^1/_{16}$ in. o.d. × 0.040 in. i.d. × 20 in.) with Cheminert fitting
31	Teflon tubing ($^1/_{16}$ in. o.d. × 0.040 in. i.d.) with stainless steel needle (18 gauge × 1 in.)
32	purge gas flow metering valve, Nupro SS-2SG (Nupro Co.), $^1/_8$ in. fittings
33	temperature controller/readout no. 1

port/cryofocusing trap (B), and other ancillary devices was evaluated for analysis of volatile organic compounds. Parts listings are given in Tables I and II.

Organic-free water was transferred into a 250-mL bottle equipped with a magnetic stirrer and a silicone–Teflon septum closure until the bottle was filled to capacity (no head space). Compounds of interest were introduced through the septum in 2 μL of a methanol solution containing 200–300 ng/μL of each compound and deuteriated internal standards ([$^2H_5$]bromoethane; [$^2H_3$]anisole; [$^2H_5$]chlorobenzene) and then stirred for 2 min.

Gaseous solutions of the external standard perfluorotoluene (PFT) were prepared in a 1-L gas bulb which had been flushed with helium and heated with a heating mantle to 35 °C. With continual magnetic stirring, PFT was injected into the bulb through a septum to produce 200 ng of PFT/1 mL of gas; the system was equilibrated for 30 min.

Sixty grams of anhydrous powdered sodium sulfate (Baker) was added to the dry 200-mL purge vessel. The vessel was equipped with a foam trap on the purge gas exit and Teflon valves on the purge gas inlet and exit lines. Following the introduction of salt, the vessel was purged (with the exit line disconnected from the Tenax trap) at 25 mL/min for 20 min to simultaneously purge the salt and displace the void volume of the flask. The Teflon valves on the flask were then closed, and the flask was shaken to redistribute the salt for easier dissolution. After the valve on the exit line leading to the Tenax trap was opened (to allow head-space displacement), 200 mL of sample was introduced into the vessel by a pressurized delivery system (Figure 2) using helium. When delivery was complete, the valves on the flask were closed, and the flask was shaken to dissolve the salt. The foam trap and Teflon valves prevent water from entering the system lines during the shaking procedure. After the salt was dissolved,

Table II. Component Identification: Injection System

1	injection block, containing six-port valve
2	liquid nitrogen cooled, nickel capillary trap
3	gas chromatograph carrier gas inlet to injector
4	septum purge outlet (closed during operations)
5	injection splitter exit (closed)
6	vent
7	heated/insulated transfer line inlet from purge and trap system, $^1/_6$ in. o.d. × 0.040 in. i.d. × 30 in. (other end of item 5, Table I)
8	purge flask heater, $^3/_4$ in. diameter × 8 in., Watlow 01808081 (Watlow Winona, Inc.)
9	electrical connection to injector body
10	electrical connection to cryogenic trap heater
11	gas chromatograph bulkhead
12	gas chromatograph injection port
13	fused-silica capillary column
14	temperature controller/readout no. 2

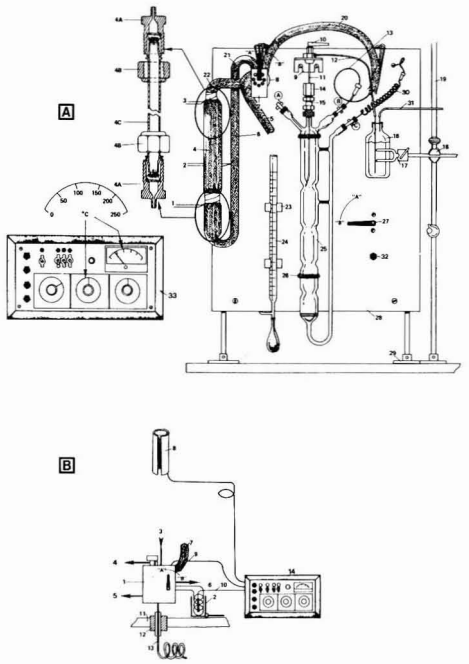

Figure 1. (A) Purge and trap system; (B) injection system.

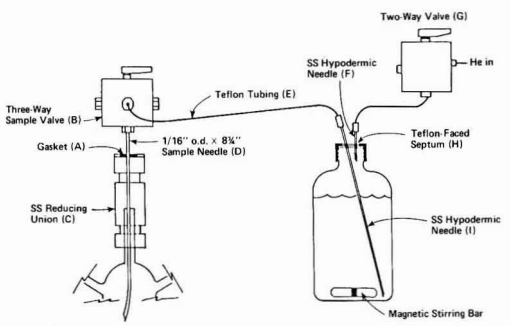

Figure 2. Pressurized sample delivery system.

the valves were reopened, and the sample was purged for 20 min at 25 mL/min. At the conclusion of the normal purge cycle, the purge gas was diverted (part 27, Figure 1) around the purge flask for an additional 5 min to remove residual water vapor from the Tenax trap. During this "dry" purge (18 min into the cycle), 1 mL of gaseous PFT in helium was injected with a 5-mL gas-tight syringe into the cold cryogenic trap. Trapped compounds were desorbed from the Tenax trap at 200 °C onto the cryogenic trap for 8 minutes at 15 mL/min. The cryofocused eluent was then flash evaporated onto the capillary column by ballistic heating of the cryotrap to 200 °C. All experiments were conducted in triplicate.

Results and Discussion

Method Refinement Studies. Recovery studies with representative compounds were performed in triplicate at 1 ppb in tap water and 100 ppb in municipal and energy effluents. These studies encompassed ten different functional group classifications including aldehydes, ketones, esters, ethers, aromatic hydrocarbons, aliphatic hydrocarbons, halogenated aromatic hydrocarbons, halogenated aliphatic hydrocarbons, miscellaneous nitrogen compounds, and miscellaneous sulfur compounds. The two effluent waters were diluted 1:10 prior to purging to minimize foaming. Recovery data (Table III) indicate compound classes which are amenable to purge and trap as described here. Recoveries for aldehydes, ketones, esters, and miscellaneous nitrogen compounds were extremely low (<50%) and demonstrate that purge and trap cannot be applied successfully to these compounds at 1 ppb. Three exceptions to this conclusion were ethyl butyrate, butyl propionate, and ethyl hexanoate, all of which exhibited recoveries of 90% or better, presumably because of an optimum relationship between volatility and water solubility not possessed by other esters. Recovery experiments were not performed for aldehydes, ketones, and miscellaneous nitrogen compounds in the effluent media.

A poorly defined but general decrease in recovery was observed with decreasing volatility for all three water types. The data predict that compounds in chemical classes amenable to purge and trap, including ethers, aromatic hydrocarbons, aliphatic hydrocarbons, halogenated aromatic hydrocarbons, halogenated aliphatic hydrocarbons, and certain sulfur compounds, can be determined up to a boiling point of approximately 220 °C. This range of volatilities affords appreciable overlap with compound isolation procedures employing solvent extraction.

On the basis of the research described above, an interim protocol for volatile organics was prepared. The interim protocol was tested with field samples fortified with internal standards and model compounds. Two studies were conducted to test the interim protocol. An intralaboratory study was first conducted by Research Triangle Institute (RTI) on distilled and drinking water (one each) and on energy (three each), industrial (three each), and municipal (two each) effluents. The interim protocol was applied in triplicate to spiked and unspiked (control) water samples. Subsequently, an interlaboratory study was performed on water samples spiked with model compounds and then analyzed by EPA/Athens, GA, and RTI. The samples represented distilled, drinking, and surface waters and municipal, energy, and industrial effluents. Spiked and unspiked samples were analyzed by both laboratories.

Several problems in the interim protocol became apparent during the interlaboratory study. Further research addressed improvements to the purge and trap protocol: (1) simplification of the sample transfer, (2) improvement in the procedures for adding internal and external standards, and (3) design and validation of a purge and trap apparatus interfaced directly to a gas chromatograph/mass spectrometer/computer. This last modification was to significantly reduce background interferences associated with the Tenax GC trap.

Evaluation of an Integrated GC/MS/COMP Purge and Trap System. Candidate closed-system designs for purge and trap included (1) a modification of the Tekmar LSC-3 system (Tekmar Co., Cincinnati, OH), (2) the UNACON 810A (Envirochem, Inc., Kemblesville, PA), and (3) an RTI-designed system. All three designs were evaluated under nearly identical criteria. Ultimately, the RTI-designed purge and trap system was selected for inclusion in the final analytical protocol on the basis of its superior overall performance relative to the other two systems.

The injection component of the RTI system provided for introduction of gas or liquid samples, or the introduction of desorbed analytes from the trap of a purge and trap system, onto glass or fused-silica capillary columns. As part of this system, cryofocusing was utilized to faci-

Table III. Recovery Studies with Representative Volatile Compounds

class	compound	bp (°C)	mean percent recovery (% RSD) distilled water	municipal effluent (10%)	energy effluent (10%)
esters	ethoxyethyl acetate	156	ND[a]	ND	ND
	ethyl hexanoate	168	108 (12)	95 (3)	100 (3)
	furfuryl acetate	177	ND	ND	ND
	diethyl oxalate	186	ND	ND	ND
	phenyl acetate	196	ND	ND	ND
	dimethyl adipate	≫200	20 (26)	ND	ND
	benzyl acetate	216	94 (10)	4 (25)	5 (20)
ethers	diethyl ether	35	100 (14)	100 (49)	*b*
	propylene oxide	35	12 (12)	*b*	*b*
	2-methylfuran	63	ND	28 (90)	87 (21)
	tetrahydrofuran	66	24 (39)	24 (22)	11 (10)
	diisopropyl ether	69	*b*	109 (11)	100 (4)
	diallyl ether	94	*b*	100 (8)	89 (11)
	1,4-dioxane	101	*b*	6 (40)	3 (12)
	epichlorohydrin	118	26 (9)	3 (33)	4 (16)
	dibutyl ether	142	*b*	*b*	*b*
	anisole	156	76 (7)	83 (7)	65 (10)
	dihexyl ether	223	66 (23)	40 (12)	45 (11)
	diphenyl ether	259	97 (14)	70 (6)	85 (4)
	dibenzyl ether	298	78 (116)	5 (50)	10 (60)
aliphatic hydrocarbons	pentane	36	185 (58)	*b*	109 (14)
	cyclopentane	49	115 (10)	*b*	124 (26)
	hexane	68	97 (7)	*b*	124 (26)
	cyclohexene	83	81 (11)	124 (4)	115 (14)
	heptane	98	110 (10)	121 (27)	130 (10)
aldehydes	propionaldehyde	49	*b*	*b*	*b*
	n-butyraldehyde	75	13 (14)	*b*	*b*
	crotonaldehyde	104	*b*	*b*	*b*
	heptaldehyde	153	34 (16)	*b*	*b*
	furfural	162	ND	*b*	*b*
	benzaldehyde	179	ND	*b*	*b*
	salicycladehyde	196	ND	*b*	*b*
	p-tolualdehyde	200	ND	*b*	*b*
	anisaldehyde	248	ND	*b*	*b*
ketones	acetone	57	*b*	*b*	*b*
	methyl ethyl ketone	80	*b*	*b*	*b*
	cyclopentanone	131	ND	*b*	*b*
	acetylacetone	141	ND	*b*	*b*
	2-heptanone	151	53 (10)	*b*	*b*
	cyclohexanone	57	*b*	*b*	*b*
	2-octanone	173	ND	*b*	*b*
	fenchone	194	ND	*b*	*b*
	acetophenone	202	*b*	*b*	*b*
	phenylacetone	217	ND	*b*	*b*
	trans-4-phenyl-3-butene		ND	*b*	*b*
esters	methyl formate	32	36 (31)	95 (24)	110 (23)
	methyl acetate	57	25 (24)	*b*	*b*
	ethyl acetate	77	23 (9)	29 (12)	30 (31)
	tert-butyl acetate	98	34 (3)	98 (13)	74 (26)
	propyl acetate	102	*b*	64 (20)	58 (23)
	allyl acetae	104	34 (7)	22 (14)	26 (31)
	ethyl butyrate	120	90 (4)	82 (4)	85 (9)
	butyl propionate	146	126 (2)	94 (3)	94 (4)
aliphatic hydrocarbons	1-octane	~122	104 (7)	110 (21)	143 (20)
	octane	125	104 (7)	98 (23)	102 (22)
	nonane	151	57 (11)	70 (5)	70 (20)
	dipentene	~170	87 (11)	92 (5)	79 (12)
	decane	174	38 (21)	66 (7)	66 (17)
	dodecane	~216	48 (30)	64 (4)	65 (9)
	tetradecane	254	27 (40)	22 (22)	36 (10)
	hexadecane	287	ND	5 (25)	10 (26)
halogenated aliphatic hydrocarbons	methylene chloride	40	99 (3)	105 (14)	*b*
	allyl chloride	45	113 (11)	*b*	*b*
	trans-1,2-dichloroethylene	48	116 (13)	103 (10)	106 (5)
	chloroform	61	79 (14)	105 (18)	95 (7)
	bromochloromethane	68	79 (14)	*b*	110 (18)
	1,2-dichloroethane	83.5	80 (9)	82 (6)	*b*
	trichloroethylene	87	87 (2)	84 (12)	97 (7)
	1,2-dichloropropane	96	84 (13)	111 (11)	97 (5)
	1,1,2-trichloroethane	113	86 (7)	87 (3)	85 (2)
	1-bromo-3-methylbutane	122	100 (12)	101 (4)	113 (12)
	1,2-dibromoethane	131	90 (6)	80 (6)	96 (7)
	1-chlorohexane	132	100 (7)	*b*	103 (10)
	1,2-dibromopropane	141	96 (6)	99 (3)	98 (5)

Table III (Continued)

class	compound	bp (°C)	mean percent recovery (% RSD) distilled water	municipal effluent (10%)	energy effluent (10%)
	3-bromo-1-chloropropane	142.5	*b*	101 (2)	102 (4)
	1,4-dichlorobutane	161.3	86 (2)	91 (2)	91 (6)
	1,4-dibromobutane	197	92 (11)	86 (4)	*b*
	1-bromodecane	238	27 (15)	45 (12)	38 (30)
aromatics	benzene	80	76 (9)	104 (5)	111 (87)
	toluene	111	74 (15)	103 (4)	107 (5)
	ethylbenzene	163	66 (15)	94 (4)	101 (4)
	xylene	139	66 (15)	100 (1)	100 (5)
	cumene	152	59 (20)	99 (1)	96 (10)
	tert-butylbenzene	134	*b*	*b*	97 (11)
	1,2,4-trimethylbenzene	170	84 (10)	99 (2)	97 (11)
	diethylbenzene	~182	60 (16)	86 (1)	81 (15)
	triethylbenzene	217	42 (24)	68 (3)	66 (22)
	naphthalene	218	83 (8)	85 (2)	*b*
	diphenylmethane	266	63 (9)	66 (5)	64 (22)
halogenated aromatics	fluorobenzene	85	91 (10)	107 (5)	101 (9)
	α,α,α-trifluorotoluene	103	83 (12)	103 (8)	101 (9)
	chlorobenzene	132	93 (8)	101 (4)	95 (3)
	bromobenzene	156	92 (4)	95 (2)	91 (7)
	p-bromotoluene	184	92 (2)	91 (4)	86 (14)
	iodotoluene	189	92 (4)	91 (3)	87 (9)
	1,2,4-trichlorobenzene	214	103 (7)	84 (8)	93 (1)
	α,α,α-trichlorotoluene	221	*b*	*b*	*b*
	1,2,4,5-tetrachlorobenzene	244	79 (7)	56 (12)	*b*
sulfur (misc)	carbon disulfide	47	93 (29)	93 (15)	*b*
	thiophene	84	64 (13)	*b*	*b*
	tert-butyl disulfide	~200	ND	*b*	*b*
	benzyl sulfide	296	*b*	*b*	*b*
nitrogen (misc)	propionitrile	97	25 (34)	*b*	*b*
	nitroethane	114	6 (7)	*b*	*b*
	1-nitropropane	132	9 (4)	*b*	*b*
	benzonitrile	191	ND	*b*	*b*
	nitrobenzene	210	30 (7)	*b*	*b*

[a] Compound not detected. [b] Recovery not determined.

Table IV. Recovery of Volatile Organic (VO) Compounds from Drinking Water and Industrial/Municipal Wastewater

compound	mean percent recovery (% RSD)[a] drinking water	wastewater	compound	mean percent recovery (% RSD)[a] drinking water	wastewater
n-pentane	*c*	25 (16)	chloroform	74 (6)	82 (15)
n-hexane	90 (19)	120 (8)	tetrachloroethylene	82 (8)	73 (7)
n-heptane	120 (3)	*c*	1,2-dibromoethane	68 (8)	86 (6)
n-octane	103 (11)	104 (30)	1,4-dibromobutane	94 (7)	*c*
n-nonane	80 (40)	78 (4)	allyl chloride	*c*	48 (2)
n-decane	70 (14)	51 (10)	1-chlorohexane	128 (9)	
n-dodecane	64[b]	71 (5)	bromochloromethane	48 (7)	144 (7)
n-tridecane	52 (34)	36[b]	2-bromobutane	117 (3)	*c*
n-tetradecane	58 (38)	40 (12)	2-bromo-1-chloropropane	99 (4)	*c*
dipentene	96 (16)	83 (22)	1-bromohexane	129 (5)	*c*
cyclopentane	*c*	131 (3)	1,2-dibromopropane	90 (4)	*c*
cyclohexane	79 (10)	91 (2)	trichloroethylene	118 (8)	*c*
propylene oxide	67 (22)	*c*	1,2-dichloroethane	102 (10)	*c*
diethyl ether	*c*	115 (4)	*trans*-1,2-dichloroethylene	82 (7)	93 (10)
dihexyl ether	68 (23)	72 (8)	chlorobenzene	98 (10)	84 (16)
diallyl ether	87 (10)	109 (3)	1,2-dichlorobenzene	116 (9)	*c*
diphenyl ether	*c*	47[b]	1,2,4-trichlorobenzene	88 (3)	86 (4)
2-methylfuran	65 (5)	95 (2)	*p*-iodotoluene	96 (8)	117 (3)
benzene	78 (7)	74 (13)	bromobenzene	123 (10)	*c*
p-xylene	108 (12)	89 (13)	α,α,α-trifluorotoluene	*c*	58 (2)
tert-butylbenzene	113 (3)	*c*	2-bromochlorobenzene	73 (4)	112 (10)
1,2,4-trimethylbenzene	97 (2)	91 (18)	4-bromochlorobenzene	90 (5)	106 (2)
1,3,5-trimethylbenzene	65 (5)	90 (3)	1,4-dichlorobenzene	83 (4)	*c*
ethylbenzene	96 (5)	*c*	*p*-bromotoluene	104 (3)	*c*
p-deithylbenzene	61 (6)	101 (6)	1,3-dichlorobenzene	90 (5)	116 (2)
o-diethylbenzene	98	*c*	anisole	62 (2)	74 (5)
toluene	125 (5)	*c*	thiophene	120 (6)	149 (1)
(3-methylisopropyl)benzene	100 (5)	*c*	carbon disulfide	*c*	100 (3)
naphthalene	*c*	74 (3)	diphenylmethane	59 (9)	*c*

[a] Triplicate determinations; percent recoveries were calculated relative to the nearest eluting deuteriated internal standard ($[^2H_5]$bromoethane, $[^2H_3]$anisole, and $[^2H_5]$chlorobenzene). [b] Single determination. [c] Not determined.

litate sharp, discrete sample injection. Specific features of this sample introduction mechanism are described at length elsewhere (*2*).

Experiments conducted with the RTI purge and trap design equipped with injection port/cryofocusing showed this system to be compatible with capillary GC/MS for the isolation of volatile organic compounds from water. Table IV illustrates the recoveries and precision of the volatile organic model compounds from drinking water and industrial/municipal wastewater calculated relative to the nearest eluting internal standard.

Acknowledgments

We acknowledge technical support from J. Bursey, J. Harry, R. Porch, J. Turlington, and M. Parker and editorial assistance from C. Sparacino and R. Zweidinger. Sincere appreciation is also offered to A. W. Garrison of the U.S. Environmental Protection Agency for his guidance during this effort.

Registry No. Ethoxyethyl acetate, 111-15-9; ethyl hexanoate, 123-66-0; furfuryl acetate, 623-17-6; diethyl oxalate, 95-92-1; phenyl acetate, 122-79-2; dimethyl adipate, 627-93-0; benzyl acetate, 140-11-4; diethyl ether, 60-29-7; propylene oxide, 75-56-9; 2-methylfuran, 534-22-5; tetrahydrofuran, 109-99-9; diisopropyl ether, 108-20-3; diallyl ether, 557-40-4; 1,4-dioxane, 123-91-1; epichlorohydrin, 106-89-8; dibutyl ether, 142-96-1; anisole, 100-66-3; dihexyl ether, 112-58-3; diphenyl ether, 101-84-8; dibenzyl ether, 103-50-4; pentane, 109-66-0; cyclopentane, 287-92-3; hexane, 110-54-3; cyclohexene, 110-83-8; heptane, 142-82-5; propionaldehyde, 123-38-6; *n*-butyraldehyde, 123-72-8; crotonaldehyde, 4170-30-3; heptaldehyde, 111-71-7; furfural, 98-01-1; benzaldehyde, 100-52-7; salicylaldehyde, 90-02-8; *p*-tolualdehyde, 104-87-0; anisaldehyde, 123-11-5; acetone, 67-64-1; methyl ethyl ketone, 78-93-3; cyclopentanone, 120-92-3; acetylacetone, 123-54-6; 2-heptanone, 110-43-0; cyclohexanone, 108-94-1; 2-octanone, 111-13-7; fenchone, 1195-79-5; acetophenone, 98-86-2; phenylacetone, 103-79-7; *trans*-4-phenyl-3-butene, 1005-64-7; methyl formate, 107-31-3; methyl acetate, 79-20-9; ethyl acetate, 141-78-6; *tert*-butyl acetate, 540-88-5; propyl acetate, 109-60-4; allyl acetate, 591-87-7; ethyl butyrate, 105-54-4; butyl propionate, 590-01-2; 1-octane, 111-65-9; nonane, 111-84-2; dipentene, 138-86-3; decane, 124-18-5; dodecane, 112-40-3; tetradecane, 629-59-4; hexadecane, 544-76-3; methylene chloride, 75-09-2; allyl chloride, 107-05-1; *trans*-1,2-dichloroethylene, 156-60-5; chloroform, 67-66-3; bromochloromethane, 74-97-5; 1,2-dichloroethane, 107-06-2; trichloroethylene, 79-01-6; 1,2-dichloropropane, 78-87-5; 1,1,2-trichloroethane, 79-00-5; 1-bromo-3-methylbutane, 107-82-4; 1,2-dibromoethane, 106-93-4; 1-chlorohexane, 544-10-5; 1,2-dibromopropane, 78-75-1; 3-bromo-1-chloropropane, 109-70-6; 1,4-dichlorobutane, 110-56-5; 1,4-dibromobutane, 110-52-1; 1-bromodecane, 112-29-8; benzene, 71-43-2; toluene, 108-88-3; ethylbenzene, 100-41-4; xylene, 1330-20-7; cumene, 98-82-8; *tert*-butylbenzene, 98-06-6; 1,2,4-trimethylbenzene, 95-63-6; diethylbenzene, 25340-17-4; triethylbenzene, 25340-18-5; naphthalene, 91-20-3; diphenylmethane, 101-81-5; fluorobenzene, 462-06-6; α,α,α-trifluorotoluene, 98-08-8; chlorobenzene, 108-90-7; bromobenzene, 108-86-1; *p*-bromotoluene, 106-38-7; iodotoluene, 61878-58-8; 1,2,4-trichlorobenzene, 120-82-1; α,α,α-trichlorotoluene, 98-07-7; 1,2,4,5-tetrachlorobenzene, 95-94-3; carbon disulfide, 75-15-0; thiophene, 110-02-1; *tert*-butyl disulfide, 110-06-5; benzyl sulfide, 538-74-9; propionitrile, 107-12-0; nitroethane, 79-24-3; 1-nitropropane, 108-03-2; benzonitrile, 100-47-0; nitrobenzene, 98-95-3; water, 7732-18-5.

Literature Cited

(1) "Guidelines Establishing Test Procedures for the Analysis of Pollutants Under the Clean Water Act"; *Fed. Regist.* **1984**, Oct 26.
(2) Pellizzari, E. D.; Sheldon, L S.; Bursey, J. T.; Michael, L. C.; Zweidinger, R. A.; "Master Analytical Scheme for Organic Compounds in Water"; final report on U.S. EPA Contract 68-03-2704; U.S. EPA: Washington, DC, 1985.
(3) Pellizzari, E. D.; Sheldon, L. S.; Bursey, J. T.; Michael, L. C.; Zweidinger, R. A. "Master Scheme for the Analysis of Organic Compounds in Water, State-of-the-Art Review of Analytical Operations"; U.S. EPA Contract 68-03-2704; U.S. EPA: Washington, DC, 1985.
(4) Bellar, T. A.; Lichtenberg, J. J. *The Determination of Volatile Organic Compounds at the Microgram per Liter in Water by Gas Chromatography*; U.S. EPA: Washington, DC, 1974; EPA-670/4-74-009.
(5) Grob, K. *J. Chromatogr.* **1973**, *84*, 255–73.
(6) Grob, K.; Grob, G. *J. Chromatogr.* **1974**, *90*, 303–13.
(7) Grob, K.; Grob, K., Jr.; Grob, G. *J. Chromatogr.* **1975**, *106*, 299–315.

Received for review July 18, 1986. Revised manuscript received November 24, 1987. Accepted December 18, 1987. Although the research described in this article has been funded wholly or in part by the U.S. EPA through Contract 68-03-2704 to the Research Triangle Institute, it has not been subjected to the agency's required peer and administrative review and therefore does not necessarily reflect the views of the agency, and no official endorsement should be inferred.

Environ. Sci. Technol. 1988, 22, 571–578

Influence of Vapor-Phase Sorption and Diffusion on the Fate of Trichloroethylene in an Unsaturated Aquifer System

Michele S. Peterson,† Leonard W. Lion,* and Christine A. Shoemaker

Department of Environmental Engineering, Cornell University, Ithaca, New York 14853

■ This research evaluates the influence of vapor-phase sorption and diffusion on the fate and transport of a common volatile pollutant, trichloroethylene (TCE). Vapor-phase sorption of TCE by a porous aluminum oxide surface coated with humic acids (to simulate an aquifer material) was observed to be highly dependent on moisture content. Linear partition coefficients for binding of TCE vapor under a range of unsaturated conditions were 1–4 orders of magnitude greater than the value measured for the saturated sorbent. In addition, laboratory measurement of the TCE diffusion coefficient through the simulated aquifer material indicated that an existing empirical formula used to estimate this parameter can be in error by as much as 400%. The significance of differences in sorptive partition coefficients and diffusion coefficients was examined with an existing one-dimensional vertical transport model for the unsaturated zone. Model calculations indicate that the common practice of assuming saturated partition coefficients apply to unsaturated conditions should be avoided to obtain accurate predictions of volatile contaminant transport.

Introduction

Most studies dealing with the transport and sorption of groundwater contaminants have focused on chemical, biological, and physical activity in the saturated zone. However, a major category of groundwater pollutants are volatile organic compounds that can readily move between the aqueous phase and vapor phase in aquifers that have saturated and unsaturated zones. An understanding of the extent and significance of vapor-phase transport and reaction may be important for accurately forecasting the movement of volatile contaminants and in evaluating the usefulness of alternative remedial methods for removing pollutants.

Compared to our understanding of pollutant behavior in saturated systems, our present knowledge of vapor-phase reactions in soils is relatively deficient. For example, the aqueous-phase sorptive partitioning coefficient of a wide array of nonionic organic compounds may generally be estimated (within a factor of 3–10) from a knowledge of two parameters: (1) a measure of the pollutant hydrophobicity such as the octanol–water partitioning coefficient or aqueous solubility and (2) a measure of soil hydrophobicity such as the weight fraction of organic carbon (*1*, *2*). By comparison, our understanding of organic vapor adsorption allows no such empirical prediction. Vapor-phase sorption reactions are anticipated to depend on specific soil properties that may not play a significant role in control of sorption in saturated systems. For example, the results of Chiou and Shoup (*3*) suggest that competition between organic vapors and water vapor for adsorption sites on soil minerals may be extremely important.

Transport processes for organic solutes in saturated systems include advection, dispersion, and diffusion. In the absence of vapor pressure gradients, gaseous diffusion is expected to be the major mechanism for vapor transport. Since vapor-phase diffusion coefficients greatly exceed those in the aqueous phase, movement of organic vapors in the gaseous headspace of unsaturated aquifers may be a significant aspect of volatile pollutant transport.

It is the purpose of this paper to report the results of a sequence of laboratory experiments and model simulations performed to determine the potential impact of vapor-phase adsorption and gaseous diffusion on the movement of trichloroethylene (TCE) in unsaturated aquifer systems. Linear sorptive partitioning coefficients for TCE were measured both from aqueous solution and from the vapor phase onto a synthetic soil. Vapor-phase sorption was evaluated for several moisture contents. The gaseous diffusion coefficient for TCE in the synthetic soil was also measured. This information was incorporated into an existing one-dimensional behavior assessment model for volatile organic materials to illustrate the impact of vapor-phase sorption and diffusion on the fate of TCE.

TCE was selected as the subject for the study because it is one of the most common groundwater pollutants in the nation. In 1980, 18 states surveyed reported a total of 2894 wells containing volatile organics, of which TCE was the most often detected compound (*4*).

Determination of Partition Coefficients. Methods used to determine sorptive partition coefficients include bottle-point equilibrium and/or soil column retardation studies. We have employed a recently developed headspace technique (*5*) to measure the aqueous partition coefficient for TCE. The procedure was also modified to obtain TCE vapor-phase partition coefficients.

In analysis of solute sorption in aqueous systems, difficulties can arise if results are based on direct sampling of the aqueous phase, particularly if the compound of interest is bound to colloidal solids or dissolved macromolecules that are not removed in separation processes such as filtration or centrifugation. Experimental artifacts of this nature are one of the explanations offered to describe the "solids effect", in which linear sorptive partition coefficients are observed to decrease with increasing solids concentration (*6–8*). Since headspace analysis obviates the need for separation of solids from the aqueous phase, solids effects that result from incomplete separation should be avoided. In the results described below, we have compared the TCE sorptive partitioning coefficient obtained with the headspace batch equilibration procedure (over a range of solids concentrations) with the results of a soil column study.

Headspace Theory: Aqueous-Phase Partition Coefficient. The headspace procedure makes use of Henry's law, which interrelates the concentration of a compound in aqueous and gaseous phases at equilibrium:

$$\gamma C_L = C_G/K_H \quad (1)$$

where C_L is the liquid concentration, C_G is the gaseous concentration, K_H is Henry's constant (dimensionless), and γ is the aqueous activity coefficient correcting for nonideal behavior. To evaluate the sorption process, a system with known liquid volume, gas volume, and mass of sorbent is compared to a control, which contains no sorbent. If the

†Present address: Black and Veatch, Tacoma, WA 98409-6896.

0013-936X/88/0922-0571$01.50/0

total mass of the volatile compound in each system is the same, then the mass balance equations for each system may be equated. If, in addition, a linear adsorption isotherm is used to describe the relationship between the sorbed and liquid concentrations, then

$$C_s = X/M = K_d C_L \quad (2)$$

where C_s = sorbed concentration (mass sorbed/mass solid), X = mass sorbed, M = mass of solid sorbent, and K_d = the solid–liquid partition coefficient (cm^3/gm). Following the procedure of Garbarini and Lion (*5*), a combination of the mass balance equations for the control and the system containing sorbent, and substitution of eq 1 and 2 gives

$$(C_{G_1}/C_{G_2})\frac{V_{G_1}K_H\gamma + V_{L_1}}{V_{G_2}K_H\gamma + V_{L_2}} = K_d[M/(V_{L_2} + K_H\gamma V_{G_2})] + 1 \quad (3)$$

with V_{L_1} and V_{G_1} being the volume of liquid and gas in a standard control bottle without sorbent (mL), V_{L_2} and V_{G_2} being the liquid and gas volumes in bottles containing sorbent, C_{G_1} being the headspace vapor concentration in the control, and C_{G_2} being the vapor concentration in the bottle with sorbent.

Headspace Theory: Vapor-Phase Partition Coefficient. The linear partition coefficient K_d' (where $C_s = K_d'C_G$) for the vapor–solid adsorption isotherm may also be obtained by mass balance principles. A system with known gas volume and mass of sorbent may again be compared to a control, which contains no sorbent. If the same mass of contaminant vapor is introduced into each system, the mass balance equations must be equal:

$$C_{G_1}V_{G_1} = C_{G_2}V_{G_2} + X \quad (4)$$

where X is the mass of vapor that is adsorbed (g). The quantity X may be determined if the vapor adsorption isotherm is known. The adsorption model of Brunauer et al. (*9*) is commonly used to characterize the adsorption of gases by solids. At low vapor pressures of the adsorbate gas, the Brunauer–Emmett–Teller (BET) model equation reduces to a linear isotherm:

$$X/M = K_d'C_{G_2} \quad (5)$$

where K_d' is the soil–vapor partition coefficient (cm^3/g). Combining eq 4 and 5 results in

$$(C_{G_1}/C_{G_2})(V_{G_1}/V_{G_2}) = K_d'(M/V_{G_2}) + 1 \quad (6)$$

The parameters K_d and K_d' may be determined by calculating the slope of a plot of the left-hand side of eq 3 and 6 vs $M/(V_{L_2} + K_H\gamma V_{G_2})$ or M/V_{G_2}, respectively.

Experimental Methods and Materials

A simulated soil was used in all experiments to ensure the uniformity of sorbent properties and the ability to reproduce samples. Alumina oxide (Fisher Scientific adsorption alumina, 80–200 mesh) was coated with humic acid (Aldrich Chemical Co.) to provide a surface to serve as a sorbent for TCE. The coating procedure described by Garbarini and Lion (*5*) was followed.

The organic carbon content of the coated material was measured as 0.48% by the Walkley–Black method for soil analysis (*10*). This value is characteristic of the low carbon content of aquifer materials, whereas surface soils often have a higher carbon fraction. A specific gravity of 3.04 in the simulated soil was measured by using the method of Lambe (*11*). The BET surface area of the coated particles was determined to be 206 m^2/g by N_2 adsorption with a Quantachrome Quantasorb surface area analyzer.

Measurement of Soil–Liquid Partition Coefficient. Adsorption experiments were carried out in 50-mL glass hypovials of known volume containing various masses of coated alumina. To determine the aqueous-phase partition coefficient, 20 mL of 0.1 M NaCl was added to each bottle. This electrolyte was found to adequately swamp out any ionic influences attributed to the sorbent (*5*). In addition, Garbarini and Lion (*5*) have shown that the sorptive partition coefficient of TCE is unaffected by the presence of the 0.1 M NaCl electrolyte relative to that obtained in distilled water. TCE-saturated water (100 μL) was added, and the bottles were immediately sealed with Teflon-lined rubber septa and an aluminum crimp cap (Supelco, Inc.). Four to six replicates were prepared for each mass of sorbent evaluated. The bottles were then rotated for 6 h in a chamber maintained at 25 °C (±0.1 °C) by a circulating water bath. A 1-mL sample of the gaseous headspace was analyzed with a Varian 1440 gas chromatograph with a column of 20% SP 2100 and 0.1% Carbowax on 100/120 Supelcoport (Supelco, Inc.) operated isothermally at 135 °C.

The measurements of Henry's Law constant for TCE and the activity coefficient for 0.1 M NaCl were not repeated for this study. The values obtained by Garbarini and Lion (*5*), $K_H = 0.397$ and $\gamma = 1.055$, were used and are consistent with other reported values (*12–14*).

Measurement of Soil–Vapor Partition Coefficients. The above experimental procedure required slight modifications to adapt it for vapor sorption analysis. Bottles contained oven-dry or moist (see below) adsorbent in the absence of an aqueous phase. a 1.0-mL sample of TCE vapor taken from the headspace over pure liquid TCE at 25 °C was delivered to each sample bottle with a gas-tight syringe. The adsorbent and vapor were equilibrated for 12 h.

Two different moisture content values were obtained by exposing the synthetic soil sample to water vapor. The soil was placed in a chamber with water maintained at a constant temperature and allowed to equilibrate over a 3-day period. A moisture content of 8.2% (grams of H_2O/g dry weight) was obtained at 15 °C, and at 40 °C the water content achieved was 11.6%. The moist soil was weighed into desiccated 50-mL sample bottles, injected with 1 mL of TCE vapor, and immediately sealed with Teflon/rubber septa and an aluminum crimp cap. The headspace analysis procedure followed was then the same as that described above.

Validation of Headspace Technique with Soil Column Measurements. The validity of the headspace result for the soil–liquid partitioning was confirmed by performing a column study using the simulated soil. The experimental procedure developed by Zhong et al. (*15*) was employed for the column experiments. A Sage Model 220 syringe pump operated two Hamilton 1-mL gas-tight syringes for a continuous, pulse-free delivery. A 60-cm borosilicate glass column (Spectrum) with a 2.5-cm diameter was encased in a water jacket for precise temperature control at 25 °C. The porosity of the packed column was calculated gravimetrically to be 0.56 cm^3/cm^3. A steady-state flow of 0.1 M NaCl at a rate of 6.27 ± 0.02 (±0.4%) mL/h was established, resulting in an estimated pore-water velocity of 2.3 cm/h.

The TCE concentration of the column effluent was monitored with the use of a radiolabeled ^{14}C tracer. A 3-mL pulse input of water containing ^{14}C-labeled TCE was injected into the column with a gas-tight syringe. The

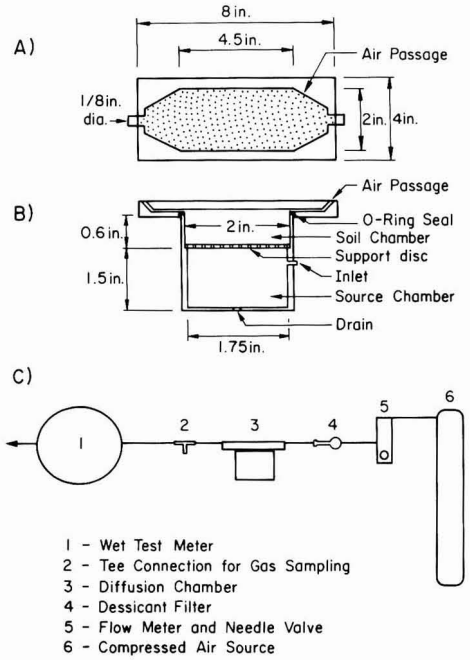

Figure 1. Diffusion test cell [(after Farmer et al. (*16*)]: (A) top view, (B) side view, and (C) schematic of test assembly.

column effluent was collected in scintillation cocktail (Fisher Scinti-Verse E) and analyzed on a Tracor analytic scintillation counter, Model 6882. A mass balance calculation indicated that 79% of the TCE applied was accounted for in the column effluent. The volatile nature of TCE is likely to be the major factor responsible for any loss.

Diffusion of Pollutant Vapors. In an unsaturated system, the steady-state diffusive flux is determined by the diffusion coefficient characteristic of the compound in transport, D_G, and the concentration gradient across the soil layer. This relationship is expressed by Fick's first law:

$$J = -D_G(C_m - C_{vp})/L \quad (7)$$

with J being the vapor flux through the soil (g/cm^2 day), C_{vp} being the concentration of the volatilizing material at one face of a soil layer, C_m being the measured concentration at the other face (g/mL), and L being the depth of the soil layer (cm).

A diffusion cell was constructed on the basis of the design of Farmer et al. (*16*) to measure diffusion of gaseous TCE through the simulated soil and is shown in Figure 1. An airstream was passed across the synthetic soil and carried TCE vapor out of the cell. The airflow rate through the cell was measured with a wet-test meter. Diffusion experiments were carried out in a constant-temperature room at 21.5 °C. A 1-mL sample of the flowing gas stream was periodically withdrawn by a gas-tight precision sampling syringe and analyzed on a Hewlett-Packard 5890A gas chromatograph with an HP3392A integrator; a standard methanol solution of known TCE concentration was used for calibration.

At a constant temperature, the TCE vapor concentration in the sample chamber below the soil can be calculated from TCE vapor pressure with the ideal gas law. The vapor pressure P of liquid TCE is a temperature-dependent relationship expressed by (*17*)

$$\log P(t) = A - B/(t + C) \quad (8)$$

where $A = 6.5183$, $B = 1018.6$, $C = 192.7$, t = temperature, and P is in millimeters of Hg (*17*). At the experimental temperature of 21.5 °C, P is 57.9 mmHg, or 0.076 atm.

The vapor flux J through the apparatus at a gasflow rate Q (cm^3/day) and soil-surface area A (cm^2) may be determined from the concentration of diffused pollutant C_m:

$$J = QC_m/A \quad (9)$$

Combining eq 7 and 9 gives the following equation for the diffusion coefficient:

$$D_G = QC_mL/(C_{vp} - C_m)A \quad (10)$$

Experimental Results and Discussion

Soil–Liquid Partition Coefficient. The results of the saturated sorption experiments fit to eq 3 are shown in Figure 2A. The mass of sorbent in the saturated system ranged from 0 to 20.000 g (giving a maximum of a 1:1 ratio of grams of sorbent mass to milliliter of solution). The solid–liquid partition coefficient of TCE onto humic-coated alumina adsorption was found to be 0.29 mL/g (or cm^3/g) by calculating the slope of the line ($r^2 = 0.94$). Normalizing this value for organic carbon content yields a K_{oc} of 61.1 cm^3/g ($K_{oc} = K_d$/fraction organic content).

Since the headspace procedure does not require a physical separation of solids, the solids effect that results from such separations should be avoided. As a check of this hypothesis, a TCE column experiment was performed to validate the partition coefficient obtained with the bottle equilibration procedure.

In saturated column experiments, the velocity of a sorbed contaminant (which obeys a linear sorption isotherm) may be related to that of an inert tracer through the retardation factor R where

$$R = 1 + (\rho_b/\phi)K_d \quad (11)$$

with ρ_b = bulk density of soil (g/cm^3) and ϕ = porosity.

The nonlinear least-squares inversion method of Parker and van Genuchten (*18*) was used to determine the soil retardation factor for TCE from the column breakthrough curve. The model was run for a deterministic linear equilibrium adsorption isotherm and an input of a pulse of known concentration. The degradation rate for TCE was assumed to be negligible. The resulting retardation factor (R) was calculated as 1.79 with an r^2 of 0.83. With a bulk density of 1.17 g/cm^3, the resulting partition coefficient is 0.38 cm^3/g. Given the experimental difficulties inherent in measuring small partition coefficients, this value agrees reasonably well with the value of 0.29 measured with the headspace technique. Since solids effects should result in a lower value of K_d for the column experiment (in which sorbent concentration is highest), differences in the two values may not be attributed to this phenomenon.

Soil–Vapor Partition Coefficients. The solid–vapor partition coefficient K_d' for TCE onto the oven-dried (105 °C) simulated soil (calculated from the slope of the adsorption isotherm plotted in Figure 2B) is 11 870 cm^3/g, which is over 10^5 times greater than the aqueous-phase linear partition coefficient. Hence, the percentage of material that would be expected to be sorbed onto the dry soil in much greater than would have been predicted by the partition coefficient measured under saturated conditions (as is often the practice). As the sorptive capacity of the dry soil was much higher than a soil that is saturated, less sorbent was needed in the experiments to yield

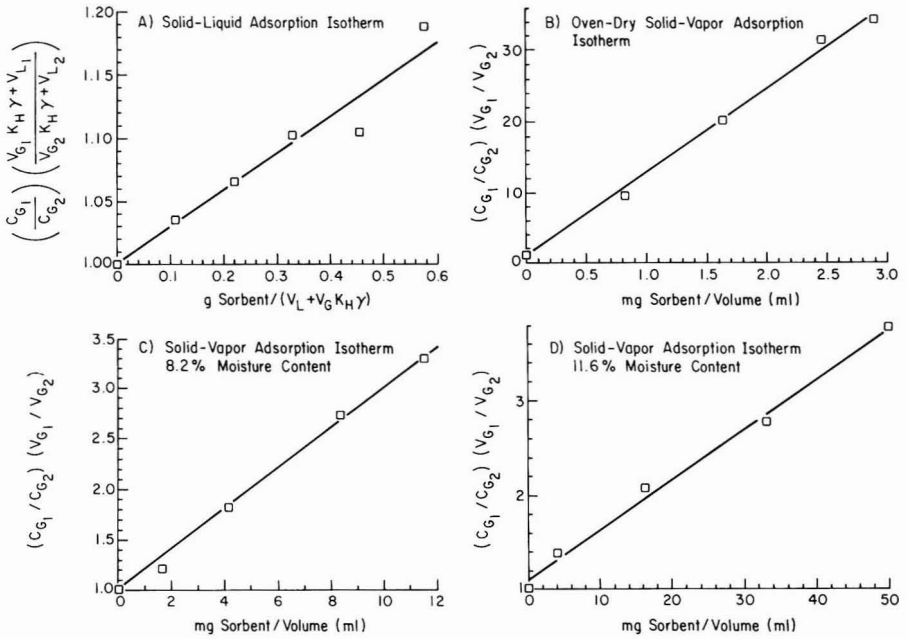

Figure 2. Reaction of TCE with humic-coated alumina: (A) sorption of dissolved TCE (saturated solid), (B) sorption of TCE vapor by oven-dry solid, and (C and D) sorption of TCE vapor by moist solid.

measurable changes in gas concentrations. The mass of sorbent used for sorption of TCE vapor ranged from 0.0500 to 0.1750 g.

Vapor sorption partition coefficients were not normalized with respect to soil organic content. Chiou and Shoup (*3*) have experimentally demonstrated that at subsaturation soil minerals may control organic vapor partitioning. However, in saturated aqueous systems, water displaces nonionic organic sorbates from hydrophilic soil mineral surfaces, and soil organic matter is most likely to account for binding of hydrophobic pollutants.

The soil region overlying the water table could conceivably contain moisture contents ranging from a few percent to near saturation. A typical field moisture content for the intermediate zone of a partially saturated soil layer is approximately 10%. The adsorption isotherms for the synthetic soil with moisture contents of 8.2% and 11.6% are presented in Figure 2, parts C and D. The TCE partition coefficient at 8.2% water content was 207 cm^3/g, and at 11.6% the value decreased to 53.9 cm^3/g. Both of these values are still 2 or more orders of magnitude greater than that determined for the saturated synthetic soil (K_d = 0.29). Therefore, in spite of the fact that hydrophilic mineral surfaces strongly bind water vapor, it may be very important to consider organic vapor-phase partitioning equilibria in unsaturated aquifer systems.

The experimental results given here are specific to the synthetic aquifer material (i.e., humic acid coated alumina) that was employed in this study. This surface's principle characteristics are a high specific area and low carbon content. It can be anticipated that the magnitude of TCE vapor partition coefficients and their dependence on moisture content will be different on different sorbents. The physical–chemical nature of soils can, of course, vary widely. Aquifer sands, for example, have much lower specific surface areas than the synthetic soil and would therefore be expected to have lower vapor partition coefficients. The choice of a commercial humic acid as the experimental organic coating also will influence the results. Malcom and MacCarthy (*19*) have reported pronounced differences between ^{13}C NMR spectra of commercial humic acids and natural organic materials. It is also clear that natural organic materials can vary widely in their pollutant-binding properties depending upon their hydrophobicity (*20*) and degree of aromaticity (*21*).

The purpose of this research was to illustrate the possible importance of vapor-phase sorption reactions. The experimental results for humic-coated alumina indicate that the assumption that vapor sorption partition coefficients may be equated with saturated partition coefficients can lead to large errors unless experimental data are available demonstrating that this assumption is reasonable for the soil of interest. The functional dependencies of specific soil characteristics on vapor-phase sorptive partitioning will be the subject of later research.

Estimation of the Wet versus Dry Sorption-Site Distribution in an Unsaturated Soil. As a first approximation, the sorptive partitioning coefficients for the oven-dried and water-saturated synthetic soil may be considered as end members of a continuum of possible sorption partition coefficients that will be observed at intermediate moisture contents. By using this approach it is possible to estimate the fraction of dry surface sites that would be needed to account for the measured partition coefficients of the partially wet synthetic soil. If the sorbent mass M is considered to be composed of some fraction F_w of water-saturated sites of mass M_{ws} and a fraction F_d of dry sites of mass M_{ds}, then $F_w + F_d = 1.0$ and

$$F_w = M_{ws}/M \tag{12}$$

$$F_d = M_{ds}/M \tag{13}$$

If each site type is also assumed to obey a linear isotherm, then

$$M_{sl} = C_L K_d M_{ws} \tag{14}$$

$$M_{sg} = C_G K_{d'dry} M_{ds} \quad (15)$$

where M_{sl} and M_{sg} are contaminant masses sorbed onto the wet and dry sites, respectively, and $K_{d'dry}$ is the vapor partition coefficient for the dry surface. The mass sorbed onto the partially wet solid X is considered to be the sum of the contribution of each site type. Therefore, from eq 5

$$X = M_{sl} + M_{sg} = K_{d'obsd} C_G M \quad (16)$$

where $K_{d'obsd}$ is the vapor partition coefficient at an intermediate moisture content.

Combination of eq 12–16 and Henry's law ($C_G = K_H C_L$) gives

$$K_{d'obsd} = F_w K_H K_d + F_d K_{d'dry} \quad (17)$$

Given the values of $K_{d'obsd}$ in Figure 2 and given $K_d = 0.29$ cm^3/g (our measured value for the saturated synthetic soil) as well as $K_{d'dry} = 11\,870$ cm^3/g (the value for the oven-dry soil), the values of F_w calculated from eq 17 are 0, 0.983, and 0.995 at 0, 8.2, and 11.6% moisture contents, respectively. Hence, F_w is a highly nonlinear function of the moisture content. Apparently only a very small fraction of dry sites would be required to mathematically account for the higher partitioning coefficient of the moist, unsaturated solid relative to saturated conditions.

An alternative explanation for the magnitude of K_d' vs K_d is that totally dry sites do not exist on the unsaturated moist solid but that (for reasons which are not known) the moist surface has a sorptive binding strength that is greater than that of the saturated sorbent. In this regard it is noteworthy that taking the surface area occupied by a water molecule as 11.4 Å^2 (*22*) and the measured BET surface area of 206 m^2/g gives an average coverage of 1.6 and 2.4 monolayers of water on the Al_2O_3 surface at the moisture contents of 8.2 and 11.6%. Multiple layers of water were therefore likely to have been present. Regardless of the interpretation of the results, the relationship between soil moisture and linear TCE sorption coefficients is highly nonlinear. Identifying the specific sorption mechanisms responsible for this relationship will require further study.

Gaseous Diffusion Coefficient. The TCE vapor diffusion coefficient of a soil system was monitored over a 6-day period. The carrier (air) flow rate was 1.70 ± 0.21 ft^3/h. The system stabilized (i.e., reached steady state) after 69 h, and the average diffusion coefficient (D_G computed from eq 10) after this point in time was 1195 ± 108 (±9.0%) cm^2/day at a soil porosity of 0.722.

It is instructive to compare the measured value of D_G to the value that would be predicted by empirical formulas such as the model proposed by Millington and Quirk (*23*), which is often used to estimate the vapor-phse diffusion coefficient for a soil system. This formula predicts the soil–vapor diffusion coefficient D_G (cm^2/day) on the basis of the known diffusion coefficient of the compound in air $D_{G_{air}}$. The specific geometric effects of the soil are accounted for by applying a retardation factor based on the soil's volumetric air content a and porosity ϕ:

$$D_G = a^{10/3}/\phi^2 D_{G_{air}} \quad (18)$$

A $D_{G_{air}}$ value of 6875 cm^2/day at 21.5 °C was estimated for TCE with the Hirschfelder correlation (*24*). Given this value, the value of D_G predicted by eq 18 was 4450 cm^2/day, 3.7 times greater than the experimentally measured coefficient. The experiment was repeated for a second porosity of 0.56, and again the predicted and measured values differed significantly. The measured diffusion coefficient was 700 cm^2/day (±5.1), and the predicted value was 3160 cm^2/day, which is over 4 times greater than the measured value.

It is apparent that the uncertainty associated with empirical relationships can, in some cases, be high. As two empirical formulas (Millington–Quirk and Hirschfelder) must be applied to estimate the soil gaseous diffusion coefficient for TCE, the uncertainty associated with the predicted coefficient D_G is the result of the combination of errors for the two equations. Reid and Sherwood (*24*) evaluated several methods of estimating diffusion coefficients and reported an average error of 6% in the Hirschfelder correlation. However, deviations as high as 39% were observed. Millington and Quirk (*23*) compared, predicted, and measured soil diffusion coefficients using the data of several researchers and found an average deviation of approximately 15%, with variations of 100% resulting in some cases. The results of Farmer et al. (*16*) show a closer agreement between the measured and predicted values for the diffusivity of hexachlorobenzene (approximate error of 15%).

Impact of Vapor-Phase Sorption on Contaminant Transport: Model Analysis

The significance of the uncertainty in vapor diffusivity on volatile pollutant behavior as well as the importance of considering the soil–vapor partitioning equilibria may be evaluated through the use of models. To illustrate effects, the model developed by Jury et al. (*25–28*) for contaminant transport in the unsaturated zone was employed. This model incorporates the effects of volatilization, leaching, and degradation to describe the major loss pathways of soil-applied organic chemicals as a function of specific environmental variables and soil conditions.

The model is an analytical solution to the one-dimensional advection–diffusion equation describing the vertical transport and volatilization loss of soil-applied compounds. Model equations are summarized in the Appendix. A homogeneous porous medium, a linear equilibrium adsorption isotherm, and a linear equilibrium liquid–vapor partitioning are assumed. Initial conditions include a uniform concentration of a compound incorporated to a specified depth L (cm). Volatilization at the soil surface is assumed to be controlled by gaseous diffusion through a stagnant air boundary layer of thickness d (cm). The model is intended for use as a screening tool to assess behavior under prototype conditions rather than to make precise predictions under specific circumstances.

As is the common practice for models of contaminant transport in the unsaturated zone, Jury et al. (*25*) assume that sorption is described by the partitioning coefficient determined by experiments on the basis of saturated conditions. However, as the preceding results indicate, the sorption partitioning coefficient can vary considerably with the phase in which the reaction occurs.

Figure 3 indicates the impact of changes in the value of the partition coefficient on model predictions of the transport of TCE through the unsaturated zone. Each line on the graph represents the results of the Jury et al. (*25*) model for a different value of the partition coefficient. For the "saturated" case, a K_d of 0.76 cm^3/g was used on the basis of our measured $K_{oc} = 61.1$ and a model soil with weight-fraction organic content $f_{oc} = 1.25\%$. The vapor partition coefficients at 11.6% moisture, 8.2% moisture, and 0.0% moisture were $K_d' = 53.9$, 207, and 11 870, respectively, and are based on our measured values for the vapor-phase partitioning coefficient. These were converted to an aqueous-phase basis [by noting $K_d = C_s/C_L = C_s/(C_G/K_H\gamma) = K_d'K_H\gamma$] prior to use in the model. Other

Table I. Model Input Parameters

symbol	term	units	value	source
$D_{G_{air}}$	TCE air diffusion coefficient	cm^2/day	7030	Hirschfelder formula at 25 °C, Reid and Sherwood (*24*)
$D_{L_{water}}$	TCE water diffusion coefficient	cm^2/day	0.8304	Wilke and Chang (*29*) at 25 °C
ϕ	porosity	cm^3/cm^3	0.5	
ρ_b	bulk density	g/cm^3	1.35	
f_{oc}	fraction organic content	%	1.25	
θ	water content		0.25	
a	air content		0.25	
L	incorporation depth	cm	10	
d	boundary layer thickness	cm	0.475	
K_H	Henry's Law constant		0.397	Garbarini and Lion (*5*)
C_0	uniform initial concentration	$\mu g/(cm^3 \cdot ppm)$	100	
T	elapsed time	days	10	
J_w	groundwater velocity	cm/day	1	
μ	degradation rate	day^{-1}	0	

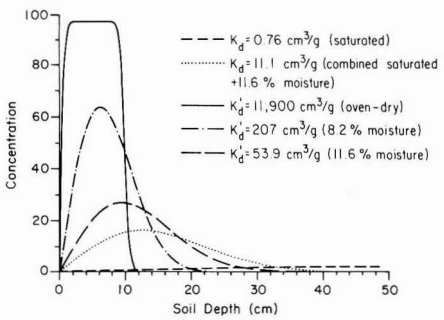

Figure 3. Calculated TCE concentration profiles assuming uniform sorption of TCE equivalent to that observed in saturated systems and unsaturated systems of varying moisture content.

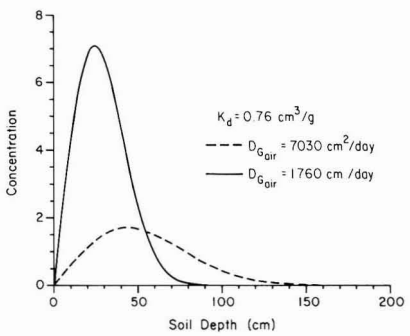

Figure 4. Calculated TCE concentration profiles with differing soil diffusion coefficients.

model input parameters are summarized in Table I.

As expected, the model predictions of transport down through the unsaturated zone vary markedly with the values used for the partition coefficient. Using the saturated partition coefficient to describe sorption in the unsaturated zone results in model predictions of much faster transport than is predicted when any of the unsaturated partition coefficients are used.

The results in Figure 3 illustrate only the impact of changing sorptive characteristics of the soil; they do not incorporate the impact of changes in vertical velocity associated with changes in soil moisture. Soil moisture and vertical velocity are positively correlated. Clearly decreases in vertical velocity will retard the downward transport of a contaminant. The results of Figure 3 illustrate that the decreases in soil moisture and associated increases in sorption will also retard the downward transport. The combined effect of reduction in soil moisture and in vertical transport is expected to be greater than either process acting by itself.

In saturated soils, it is reasonable to assume that portions of the solid phase behave as though they are surrounded by liquid water, and therefore their reactions with a nonionic organic pollutant may be described by a saturated sorptive partition coefficient. Other portions of the soil may behave as though they are in contact with both water and organic vapors, and a vapor-phase partition coefficient for the moist (but unsaturated) sorbent would be appropriate. Therefore, if a single partition coefficient for an organic pollutant is to be used in a model, a value that is intermediate between the saturated and moist–unsaturated partition coefficients may be a reasonable choice. As a first approximation for the selection of a value for a single partition coefficient in a soil with heterogeneous moisture conditions, we may wish to weigh the saturated and moist but unsaturated partition coefficients by the volumetric moisture content of the soil θ giving

$$K_{d\,combined} = (\theta/\phi)K_d + (a/\phi)K_d'K_H\gamma \qquad (19)$$

where a and ϕ are as previously defined (see eq 18).

Figure 3 also shows the results of a simulation trial using a partition coefficient K_d of 11.1 cm^3/g, which results from $\theta = 0.25$, $a = 0.25$, and $\phi = 0.5$, a saturated $K_d = 0.76$ cm^3/g (based on our $K_{oc} = 61.1$ and $f_{oc} = 0.0125$), and our unsaturated (11.6% moisture) $K_d' = 53.9$ cm^3/g values. It may be seen that the calculated profile for this case still lies nearer to the results for the case based on the K_d' for 11.6% moisture.

A more appropriate procedure for handling the unsaturated case where both gas- and liquid-phase partitioning occur would be to compartmentalize the unsaturated soil phase into portions that behave as though they are saturated (from the perspective of sorption reactions) and portions in which vapor-phase partitioning occur. The modified model could then employ both a soil–liquid and soil–vapor partition coefficient. Such a model has been developed (*30*) and will be the subject of a subsequent paper.

Sensitivity of Results to Gaseous Diffusion Rates. The model of Jury et al. (*25*) was also used to evaluate the significance of gaseous diffusion in determining the concentration profile. The results obtained for a case in which the gaseous diffusion coefficient was predicted with empirical models is compared to a trial in which this value was reduced by a factor of 4. This was roughly the magnitude of difference between the measured value for TCE in this study and the predicted diffusion coefficient estimated from empirical relationships. Figure 4 illustrates

the expected slower net transport of TCE when the diffusion coefficient is reduced.

Conclusions

This study demonstrates that an experimental headspace procedure can be used to measure linear solid–vapor partition coefficients. A significant range of values for the vapor sorptive partition coefficient for TCE was observed depending upon the moisture content of the sorbent.

Vapor-phase partition coefficients for a simulated soil were substantially greater than the saturated aqueous partition coefficient. The results of our study indicate that the current practice of using saturated partition coefficients in models of the unsaturated zone may underestimate the amount of sorption and hence overestimate the amount and rate of material moving into the groundwater. We note that the curves obtained are model dependent and that calculations performed with a different model may result in smaller or larger differences between predictions based on saturated vs unsaturated partition coefficients. The magnitude of differences in partition coefficients will also depend on the physical–chemical characteristics of the sorbent. However, if the saturated and unsaturated partition coefficients vary by several orders of magnitude (as they do for the synthetic sorbent employed in this research), the differences in predictions are expected to be similar to those described here.

The vapor-phase diffusion coefficient measured for TCE did not agree with the value predicted empirically. The model results indicate that the differences in calculation using measured vs empirically estimated values are significant. These results are important since field measurements of vapor diffusion coefficients are experimentally difficult and field conditions are likely to be heterogeneous. The model results indicate that any pollutant transport analysis based on empirically estimated values of the gaseous diffusion coefficient should be subjected to extensive sensitivity analysis to examine how the results of the analysis would change over a range of values.

Acknowledgments

Ann Lemley provided assistance with soil column test procedures and William Jury graciously provided us a copy of the computer code for the one-dimensional behavior assessment model. The assistance of Daniel Yoon and Terresa Culver with the model computations is gratefully acknowledged.

Appendix

The one-dimensional equations governing mass flux of solute and solute mass balance are respectively

$$J_s = -D_E\frac{dC_T}{dZ} + V_E C_T \qquad \text{(A1)}$$

$$\frac{dC_T}{dt} = D_E\frac{d^2C_T}{dZ^2} - V_E\frac{dC_T}{dZ} - \mu C_T \qquad \text{(A2)}$$

where J_s = solute mass flux in the soil (g/cm^2 day), C_T = total mass of solute per soil volume (g/cm^3), i.e., $C_T = C_L\theta + C_G a + C_s\rho_b$, Z = distance from surface (cm), t = time (day), μ = net degradation rate (day^{-1}), D_E = effective diffusion coefficient (cm^2/day), V_E = effective velocity (cm/day), and θ = volumetric water content ($\theta + a = \phi$).

The effective diffusivity D_E and velocity V_E take into account the retardation of transport due to sorption and volatilization and are functions of K_d, D_G, and K_H as derived by Jury et al. (*23*):

$$D_E = (K_H D_G + D_L)/(\rho_b K_d + \theta + aK_H)$$

and

$$V_E = J_w/(\rho_b K_d + \theta + aK_H)$$

where D_L is the aqueous diffusion coefficient of the solute in soil and J_w is the groundwater advective velocity.

The boundary conditions employed for solution were as follows: $C(Z,O) = C_o$ if $O < Z < L$, $C(Z,O) = O$ if $Z > L$, $C(\infty,t) = O$, and $J_s(O,t) = -hC_G(O,t)$. Here h is a transport coefficient across the boundary layer of thickness d (cm) and $C_G(O,t)$ is the gaseous concentration at the soil surface below the boundary layer. Equations A1 and A2 were solved for the above boundary and initial conditions (*23*); other input parameters used in the calculations performed here were based on the soil properties assumed in the original calculations of Jury et al. (*23*) and are summarized in Table I.

The analytic solution is as follows [note that the original paper by Jury et al. (*23*) contained a typographical error in this equation]:

$$C_T(Z,t) = (1/2)C_o \times \exp(-\mu t)\left\{\left[\operatorname{erfc}\frac{Z - L - V_E t}{\sqrt{4D_E t}} - \operatorname{erfc}\frac{Z - V_E t}{\sqrt{4D_E t}}\right] + [(1 + V_E/H)\exp(V_E Z/D_E)] \times \left(\operatorname{erfc}\frac{Z + L + V_E t}{\sqrt{4D_E t}} - \operatorname{erfc}\frac{Z + V_E t}{\sqrt{4D_E t}}\right) + [(2 + V_E/H)\exp\{[H(H + V_E)t + (H + V_E)Z]/D_E\}] \times \left(\operatorname{erfc}\frac{Z + [(2H + V_E)t]}{\sqrt{4D_E t}} - [\exp(HL/D_E)] \times \operatorname{erfc}\frac{Z + L + (2H + V_E)t}{\sqrt{4D_E t}}\right)\right\} \qquad \text{(A3)}$$

where $H = D_{G_{air}}(\rho_b C_s/C_G + \theta C_L/C_G + a)^{-1}/d$.

Registry No. $Cl_2C{=}CHCl$, 79-01-6; Al_2O_3, 1344-28-1.

Literature Cited

(1) Karickhoff, S. W.; Brown, D. S.; Scott, T. A. *Water Res.* **1979**, *13*, 241–248.
(2) Rao, P. S. C.; Davidson, J. M. In *Environmental Impact of Nonpoint Source Pollution*; Overcash, M. R., Davidson, J. M., Eds.; Ann Arbor Science: Ann Arbor, MI, 1980; pp 23–67.
(3) Chiou, C. T.; Shoup, T. D. *Environ. Sci. Technol.* **1985**, *19*(*12*), 1196–1200.
(4) Council and Environmental Quality *Contamination of Groundwater by Toxic Organic Chemicals*; Council on Environmental Quality: Washington, DC, Jan 1981.
(5) Garbarini, D. R.; Lion, L. W. *Environ. Sci. Technol.* **1985**, *19*(*11*), 1122–1128.
(6) O'Connor, D. J.; Connally, J. P. *Water Res.* **1980**, *14*(*10*), 1517–1523.
(7) Voice, T. C.; Rice, C. P.; Weber, W. J., Jr. *Environ. Sci. Technol.* **1983**, *17*(*9*), 513–517.
(8) Gschwend, P. M.; Wu, S. *Environ. Sci. Technol.* **1985**, *19*(*1*), 90–96.
(9) Brunauer, S.; Emmett, P. H.; Teller, E. *J. Am. Chem. Soc.* **1938**, *60*, 309–319.
(10) Allison, L. E. In *Methods of Soil Analysis: Part 2, Chemical And Microbiological Properties*; Black, C. A., Ed.; American Society of Agronomy: Madison WI, 1965; pp 1367–1378.
(11) Lambe, T. W. *Soil Testing for Engineers*; Wiley: New York, 1951.
(12) Lincoff, A. H.; Gossett, J. M. In *Gas Transfer at Water Surfaces*; Brutsaert, W., Jirka, G. H., Eds.; Reidel: Dordrecht, Holland, 1984; pp 17–25.

(13) Leighton, D. T.; Calo, J. M. *J. Chem. Eng. Data* **1981**, *26*, 382–385.
(14) Lincoff, A. H. MS. Thesis, Cornell University, 1983.
(15) Zhong, W.; Lemley, A. T.; Wagenet, R. J. In *Evaluation of Pesticides in Ground Water*; Garner, W. Y., Honeycutt, R. C., Nigg, H. N., Eds.; ACS Symposium Series 315; American Chemical Society: Washington, DC, 1986; pp 61–77.
(16) Farmer, W. J.; Yang, M. S.; Letey, J.; Spencer, W. F. *Soil Sci. Soc. Am. J.* **1980**, *44*, 676–680.
(17) *Lange's Handbook of Chemistry*, 13th ed.; Dean, J. A., Ed.; McGraw-Hill: New York, 1985; p 10-52.
(18) Parker, J. C.; van Genuchten, M. Th Virginia Agricultural Experiment Station, Bulletin 84–3, 1984.
(19) Malcolm, R. L.; MacCarthy, P. *Environ. Sci. Technol.* **1986**, *20*, 904–911.
(20) Garbarini, D. R.; Lion, L. W. *Environ. Sci. Technol.* **1986**, *12*, 1263–1268.
(21) Gauthier, T. D.; Seitz, W. R.; Grant, C. L. *Environ. Sci. Technol.* **1987**, *21*, 243–248.
(22) Himenz, P. C. *Principles of Colloid and Surface Chemistry*; Dekker: New York, 1981.
(23) Millington, R. J.; Quirk, J. M. *Trans. Faraday Soc.* **1961**, *57*, 1200–1207.
(24) Reid, R. C.; Sherwood, T. K. *Properties of Gases and Liquids*, 3rd ed.; McGraw-Hill: New York, 1977.
(25) Jury, W. A.; Spencer, W. F.; Farmer, W. J. *J. Environ. Qual.* **1983**, *12*(*4*), 558–564.
(26) Jury, W. A.; Spencer, W. F.; Farmer, W. J. *J. Environ. Qual.* **1984**, *13*(*4*), 567–572.
(27) Jury, W. A.; Spencer, W. F.; Farmer, W. J. *J. Environ. Qual.* **1984**, *13*(*4*), 572–579.
(28) Jury, W. A.; Spencer, W. F.; Farmer, W. J. *J. Environ. Qual.* **1984**, *13*(*4*), 580–586.
(29) Wilke, C. R.; Chang, P. *AIChE J.* **1955**, *1*, 264–270.
(30) Gustafson (Peterson), M. M.S. Thesis, Cornell University, 1986.

Received for review March 16, 1987. Accepted November 19, 1987. This research was supported by the Jessie Noyes-Smith Foundation and the USGS through the Water Resources Institute for New York State.

Atmospheric Reactions of a Series of Dimethyl Phosphoroamidates and Dimethyl Phosphorothioamidates

Mark A. Goodman,† Sara M. Aschmann, Roger Atkinson,* and Arthur M. Winer

Statewide Air Pollution Research Center, University of California, Riverside, California 92521

■ The kinetics of the atmospherically important gas-phase reactions of a series of dimethyl phosphoroamidates and dimethyl phosphorothioamidates with OH and NO_3 radicals and O_3 were investigated at 296 ± 2 K and ~740 Torr total pressure of air. The rate constants obtained for the OH radical, NO_3 radical, and O_3 reactions (in units of cm^3 $molecule^{-1}$ s^{-1}) were respectively as follows: $(CH_3O)_2P(O)N(CH_3)_2$, $(3.19 \pm 0.24) \times 10^{-11}$, $<3.9 \times 10^{-14}$, and $<2 \times 10^{-19}$; $(CH_3O)_2P(S)N(CH_3)_2$, $(4.68 \pm 0.14) \times 10^{-11}$, $(3.1 \pm 1.0) \times 10^{-14}$, and $<2 \times 10^{-19}$; $(CH_3O)_2P(S)NHCH_3$, $(2.32 \pm 0.13) \times 10^{-10}$, $(3.0 \pm 0.4) \times 10^{-13}$, and $<2 \times 10^{-19}$; $(CH_3O)_2P(S)NH_2$, $(2.44 \pm 0.09) \times 10^{-10}$, $(3.9 \pm 0.8) \times 10^{-13}$, and $<4 \times 10^{-19}$. These data show that for the dimethyl phosphorothioamidates both the OH and NO_3 radical reactions are important atmospheric loss processes, with calculated lifetimes ranging from ~1 h to ~1 day. The mechanistic implications of these data are discussed.

Introduction

It is now known that chemicals emitted into the troposphere, including volatilization from soil and aqueous systems (*1*), are removed from the troposphere by photolysis, by chemical reaction (mainly with OH and NO_3 radicals and O_3), and by wet and dry depositions (*2*, *3*). In order to assess the atmospheric lifetimes and dominant loss process(es) for organic chemicals emitted into the troposphere, and hence human exposures to such compounds and their atmospheric reaction products, it is necessary to know, or to reliably predict, the reaction rates for the potentially important atmospheric processes.

While a large data base is now available for the kinetics and mechanisms of the gas-phase reactions of organic compounds with OH radicals (*4*), O_3 (*5*), and NO_3 radicals (*2*), the only organophosphorous compounds for which data exist are trimethyl phosphate (*6*) and a series of trimethyl phosphorothioates (*7*), despite the fact that organophosphorous compounds are widely used in agricultural operations as insecticides and herbicides (*8*).

A class of organophosphorous compounds related to the phosphorothioates are the phosphoroamidates and the phosphorothioamidates:

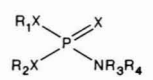

where X = O or S, respectively, R_1 and R_2 are alkyl groups, and R_3 and R_4 are H or alkyl. The insecticidal properties of many of these compounds have been investigated (*9*, *10*).

Acephate

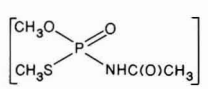

and methamidophos

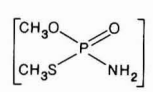

are two examples of this class of organophosphorous compounds presently used as insecticides (*8*), with several more having been in use previously (*8*).

In order to investigate the atmospherically important reaction pathways of this class of structurally interesting chemicals, and to further extend structure–reactivity relationships (*4*, *7*, *11*) to these compounds, we have investigated the gas-phase atmospheric chemistry of the dimethyl phosphoroamidates and dimethyl phosphorothioamidates (DMPs) $(CH_3O)_2P(O)N(CH_3)_2$, $(CH_3O)_2P(S)N(CH_3)_2$, $(CH_3O)_2P(S)NHCH_3$, and $(CH_3O)_2P(S)NH_2$. The DMP $(CH_3O)_2P(O)NHCH_3$ could not be studied, presumably due to its low volatility and/or to adsorption onto the reaction chamber walls, and hence we did not attempt to

†Present address: ICI Americas, Richmond, CA.

 0013-936X/88/0922-0578$01.50/0

study the less volatile DMP $(CH_3O)_2P(O)NH_2$.

Experimental Section

The experimental techniques and procedures used have been described previously (*6*, *7*, *12–16*) and are hence not discussed in detail here. All experiments were carried out in a 6400-L all-Teflon environmental chamber equipped with black lamp irradiation.

The OH radical reaction kinetics were determined with a relative rate technique, as described previously (*7*, *12*, *13*, *16*). With this method, the relative decay rates of the DMPs and a reference organic, which does not photolyze and whose OH radical reaction rate constant is reliably known, were monitored in the presence of OH radicals. Hydroxyl radicals were generated from the photolysis of methyl nitrite (CH_3ONO) in air at wavelengths >300 nm:

$$CH_3ONO + h\nu \rightarrow CH_3O + NO$$

$$CH_3O + O_2 \rightarrow HCHO + HO_2$$

$$HO_2 + NO \rightarrow OH + NO_2$$

Nitric oxide was added to the reaction mixtures to avoid the formation of O_3 and NO_3 radicals. Additionally, irradiations were carried out in the absence of CH_3ONO to assess the contribution, if any, of photolysis as a removal process for the DMPs in these experiments (*16*). The irradiations were carried out at either 20% or 50% of the maximum light intensity (corresponding to CH_3ONO lifetimes of ~10–25 min), and the irradiation times were varied from 0.5 to 9 min.

Propene and 2,3-dimethyl-2-butene were used as the reference organics and isoprene (2-methyl-1,3-butadiene) was also included with the 2,3-dimethyl-2-butene to check that reaction with O_3 was a negligible removal process for the 2,3-dimethyl-2-butene during these irradiations (*17*). [Thus, while isoprene and 2,3-dimethyl-2-butene react with the OH radical with similar rate constants (*4*), 2,3-dimethyl-2-butene is more reactive by a factor of ~100 toward O_3 than is isoprene (*5*).] The approximate initial reactant concentrations in the reaction mixtures were (in units of molecule cm^{-3}): CH_3ONO (when present), 2.4×10^{14}; NO, 2.4×10^{14}; reference organic and DMP, 2.4×10^{13}.

The experimental technique used to determine the NO_3 radical reaction rate constants was also a relative rate method (*14*, *15*) in which the relative decay rates of the DMPs and a reference organic (*trans*-2-butene) were monitored in the presence of NO_3 radicals. NO_3 radicals were generated by the thermal decomposition of N_2O_5:

$$N_2O_5 \rightleftarrows NO_3 + NO_2$$

NO_2 was added to the reactant mixtures to reduce the concentrations of NO_3 radicals and to extend the reaction times well beyond the mixing times. The approximate initial reactant concentrations in the reaction mixtures were (in units of molecule cm^{-3}) as follows: NO_2, $(1.2–2.4) \times 10^{14}$; DMP and *trans*-2-butene, 2.4×10^{13}, with four or five additions of N_2O_5 $[(0.5–8) \times 10^{13}$ molecule cm^{-3} in the chamber per addition] being made to the chamber during the reactions.

Provided that both the DMP and the reference organic were consumed only by reaction with OH or NO_3 radicals, then (*7*, *13–15*)

$$\ln\left(\frac{[DMP]_{t_0}}{[DMP]_t}\right) - D_t = \frac{k_1}{k_2}\left[\ln\left(\frac{[\text{reference organic}]_{t_0}}{[\text{reference organic}]_t}\right) - D_t\right] \quad (I)$$

where $[DMP]_{t_0}$ and $[\text{reference organic}]_{t_0}$ are the concentrations of the DMP and the reference organic, respectively, at time t_0, $[DMP]_t$ and $[\text{reference organic}]_t$ are the corresponding concentrations at time t, D_t is any dilution at time t caused by addition of reactants to the chamber (D_t was 0.0028 per addition of N_2O_5 to the chamber and zero for the OH radical reactions), and k_1 and k_2 are the rate constants for reactions 1 and 2, respectively. Hence,

$$\left.\begin{matrix}OH\\NO_3\end{matrix}\right\} + DMP \rightarrow \text{products} \quad (1)$$

$$\left.\begin{matrix}OH\\NO_3\end{matrix}\right\} + \text{reference organic} \rightarrow \text{products} \quad (2)$$

plots of $\ln([DMP]_{t_0}/[DMP]_t) - D_t$ against $\ln([\text{reference organic}]_{t_0}/[\text{reference organic}]_t) - D_t$ should yield straight lines of slope k_1/k_2 and zero intercept.

Rate constants, or upper limits thereof, for the reactions of O_3 with the DMPs were obtained by monitoring the decay rates of the DMPs in the presence of known excess concentrations of O_3 $[(5–7) \times 10^{13}$ molecule $cm^{-3}]$ over reaction times of approximately 3 h. Cyclohexane or ethane [at concentrations of $(2.4–24) \times 10^{14}$ molecule cm^{-3}] was also added to the reactant mixtures in these experiments to act as an OH radical scavenger.

All experiments were carried out at 296 ± 2 K and 1 atm (740 Torr) total pressure, using pure dry air as the diluent gas. Ozone was monitored by a Monitor Labs chemiluminescence ozone analyzer, and the DMPs and the reference organics were monitored by gas chromatography with flame ionization detection (GC-FID). Isoprene, 2,3-dimethyl-2-butene, and *trans*-2-butene were analyzed with a 20 ft × 0.125 in. stainless steel column of 5% DC703/C20M on 100/120 mesh AW, DMCS Chromosorb G, operated at 333 K. Propene was analyzed with a 36 ft × 0.125 in. stainless steel column of 10% 2,4-dimethylsulfolane on C-22 firebrick (60/80 mesh), operated at 273 K. For the DMPs, gas samples of 100 cm^3 volume were collected from the chamber onto Tenax GC solid adsorbent packed in Pyrex tubes. These samples were then transferred by the carrier gas at ~525 K to the head of a 6 ft × 0.25 in. glass column packed with Super Pak 20M, held at 353 K. The column was then temperature programmed, either from 353 to 413 K at 8 K min^{-1} or from 353 to 433 K at 12 K min^{-1}.

Methyl nitrite was prepared as described by Taylor et al. (*18*) and stored under vacuum at 77 K. N_2O_5 was prepared by reacting NO_2 with O_3 and collecting the products at 196 K (*14*), with subsequent storage at 77 K under vacuum. Ozone was generated by a Welsbach T-408 ozonizer.

DMPs were synthesized by the reaction of dimethyl chlorophosphate $[(CH_3O)_2P(O)Cl]$ or dimethyl chlorophosphorothioate $[(CH_3O)_2P(S)Cl]$ with NH_3, CH_3NH_2, or $(CH_3)_2NH$, using the general method described by Magee (*19*):

$$(CH_3O)_2P(X)Cl + R_1R_2NH \rightarrow (CH_3O)_2P(X)NR_1R_2 + HCl$$

$(CH_3O)_2P(S)Cl$ was obtained from the Aldrich Chemical Co. and used as received. Dimethyl chlorophosphate was prepared by reacting trimethyl phosphite with chlorine gas. Trimethyl phosphite (50 g, Aldrich Chemical Co.) was added to a 250-mL three-neck round bottom flask maintained at ice temperature and equipped with a gas bubbler and a reflux condenser fitted with a $CaCl_2$ drying tube. Excess chlorine was passed through the trimethyl phosphite until the mixture turned yellow. Excess Cl_2 was then

Table I. Rate Constant Ratios k_1/k_2 for the Gas-Phase Reactions of NO_3 and OH Radicals with a Series of DMPs at 296 ± 2 K

	k_1/k_2[a]		
	NO_3	OH	
DMP	relative to k_2(*trans*-2-butene) = 1.00	relative to k_2(propene) = 1.00	relative to k_2(2,3-dimethyl-2-butene) = 1.00
$(CH_3O)_2P(O)N(CH_3)_2$	<0.092	1.20 ± 0.09	
$(CH_3O)_2P(S)N(CH_3)_2$	0.083 ± 0.024	1.76 ± 0.05	
$(CH_3O)_2P(S)NHCH_3$	0.799 ± 0.032	8.75 ± 0.54	2.09 ± 0.11
$(CH_3O)_2P(S)NH_2$	1.04 ± 0.17		2.20 ± 0.08

[a] Indicated errors are two least-squares standard deviations.

Table II. Rate Constants k for the Gas-Phase Reactions of NO_3 and OH Radicals and O_3 with a Series of DMPs at 296 ± 2 K

	k, cm^3 molecule^{-1} s^{-1}		
DMP	NO_3[a]	OH[b]	O_3
$(CH_3O)_2P(O)N(CH_3)_2$	$<3.9 \times 10^{-14}$	$(3.19 \pm 0.24) \times 10^{-11}$	$<2 \times 10^{-19}$
$(CH_3O)_2P(S)N(CH_3)_2$	$(3.1 \pm 1.0) \times 10^{-14}$	$(4.68 \pm 0.14) \times 10^{-11}$	$<2 \times 10^{-19}$
$(CH_3O)_2P(S)NHCH_3$	$(3.0 \pm 0.4) \times 10^{-13}$	$(2.32 \pm 0.13) \times 10^{-10}$[c]	$<2 \times 10^{-19}$
$(CH_3O)_2P(S)NH_2$	$(3.9 \pm 0.8) \times 10^{-13}$	$(2.44 \pm 0.09) \times 10^{-10}$	$<4 \times 10^{-19}$

[a] Indicated errors are two least-squares standard deviations. Placed on an absolute basis by use of a rate constant of k_2(*trans*-2-butene) = $(3.78 \pm 0.41) \times 10^{-13}$ cm^3 molecule^{-1} s^{-1} (*20*). [b] Indicated errors are two least-squares standard deviations. Placed on an absolute basis by use of rate constants of k_2(propene) = 2.66×10^{-11} cm^3 molecule^{-1} s^{-1} and k_2(2,3-dimethyl-2-butene) = 1.11×10^{-10} cm^3 molecule^{-1} s^{-1} (*4*). [c] From irradiations with 2,3-dimethyl-2-butene as the reference organic. Value of $k = (2.33 \pm 0.15) \times 10^{-10}$ cm^3 molecule^{-1} s^{-1} obtained from the irradiation with propene as the reference organic.

removed by bubbling dry nitrogen through the mixture for 15–30 min. The product was distilled to give a clear liquid with a boiling point of 321–323 K at 3.5 mmHg.

DMPs were then synthesized as described by Magee (*19*), with slight modification. The starting $(CH_3O)_2P(O)Cl$ or $(CH_3O)_2P(S)Cl$ (0.1–0.2 mol) was dissolved in 150–200 mL of dry toluene and placed in a 250-mL Erlenmeyer flask equipped with a stirrer and cooled in an ice–water bath. The appropriate amine gas (ammonia, monomethylamine, or dimethylamine) was bubbled through the solution in excess. The solid amine chloride salt was allowed to settle and the solution filtered. Toluene was removed under reduced pressure. The remaining DMPs were further purified by distillation and their identities established by mass spectrometry and NMR spectroscopy.

Results

NO_3 Radical Reactions. The kinetics of the reactions of all four DMPs with the NO_3 radical were investigated with *trans*-2-butene as the reference organic. No reaction of $(CH_3O)_2P(O)N(CH_3)_2$ was observed within the measurement uncertainties of ~5–10%, leading to the upper limit of the rate constant ratio given in Table I. The other three DMPs were observed to react, and the data obtained are plotted in accordance with eq I in Figure 1. Variation of the initial NO_2 concentration by a factor of 2 (from 1.2×10^{14} to 2.4×10^{14} molecule cm^{-3}) had no effect on the measured rate constant ratios within the experimental uncertainties, showing that these reactions proceeded by reaction with the NO_3 radical and not with N_2O_5.

The rate constant ratios k_1/k_2 obtained from least-squares analyses of these data are given in Table I. These rate constant ratios k_1/k_2 can be placed on an absolute basis by use of a rate constant for the reaction of NO_3 radicals with *trans*-2-butene of $(3.78 \pm 0.41) \times 10^{-13}$ cm^3 molecule^{-1} s^{-1} (*20*), and the rate constants k_1 [including the upper limit to the rate constant for $(CH_3O)_2P(O)N(CH_3)_2$] are given in Table II.

Ozone Reactions. The gas-phase concentrations of the DMPs were monitored in the presence of ~(5–7) × 10^{13} molecule cm^{-3} of O_3, with the O_3 being in excess of the DMP concentrations. Cyclohexane or ethane was also present in order to scavenge any OH radicals formed and hence prevent secondary chain reactions (*7*). For $(CH_3O)_2P(S)N(CH_3)_2$ and $(CH_3O)_2P(O)N(CH_3)_2$, no loss of the DMP, within the measurement uncertainties of ~10%, was observed over reaction times of ~210 min, leading to the upper limits to the rate constants given in Table II. However, for both $(CH_3O)_2P(S)NHCH_3$ and $(CH_3O)_2P(S)NH_2$, a rapid decrease in the DMP concentration was observed immediately after addition of O_3 (~15% and ~40%, respectively, within 13 min of the time of O_3 addition), followed by a much slower decrease in the DMP concentration (<10% over a further ~200 min for both DMPs). This behavior is indicative of an initial radical chain reaction, possibly involving impurities, which was suppressed by the presence of the radical scavenger. From the slow decays of these two DMPs over the time periods 13–201 min [$(CH_3O)_2P(S)NHCH_3$] and 13–323 min [$(CH_3O)_2P(S)NH_2$] after the addition of O_3, the upper limits

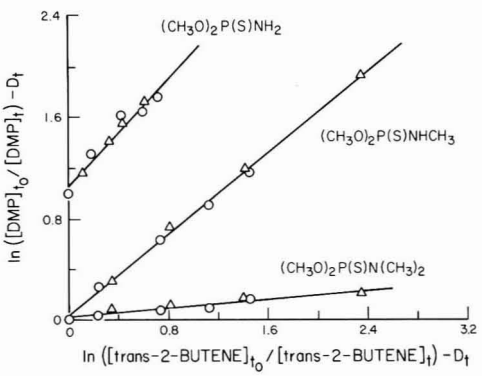

Figure 1. Plots of eq I for the reactions of the NO_3 radical with $(CH_3O)_2P(S)N(CH_3)_2$, $(CH_3O)_2P(S)NHCH_3$, and $(CH_3O)_2P(S)NH_2$, with *trans*-2-butene as the reference organic [the data for $(CH_3O)_2P(S)NH_2$ have been displaced vertically by 1.0 unit for clarity]. Initial concentrations of NO_2: (O) 1.2×10^{14} molecule cm^{-3}; (Δ) 2.4×10^{14} molecule cm^{-3}.

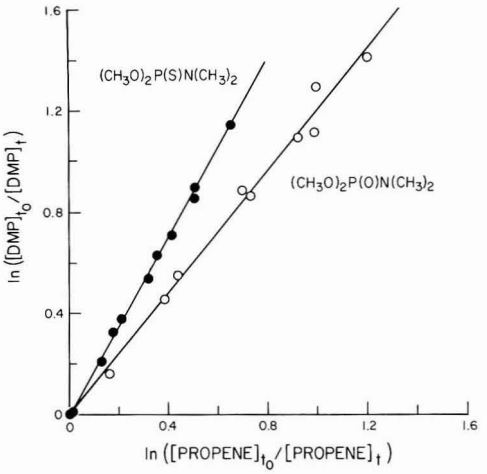

Figure 2. Plots of eq I for the reactions of the OH radical with $(CH_3O)_2P(O)N(CH_3)_2$ and $(CH_3O)_2P(S)N(CH_3)_2$, with propene as the reference organic.

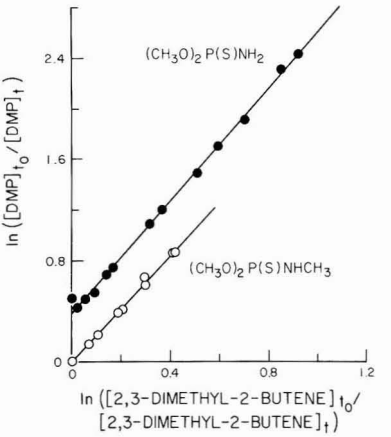

Figure 3. Plots of eq I for the reactions of the OH radical with $(CH_3O)_2P(S)NHCH_3$ and $(CH_3O)_2P(S)NH_2$, with 2,3-dimethyl-2-butene as the reference organic [the data for $(CH_3O)_2P(S)NH_2$ have been displaced vertically by 0.5 unit for clarity].

to the rate constants given in Table II were obtained.

OH Radical Reactions. CH_3ONO–NO–air and NO–air irradiations were carried out for $(CH_3O)_2P(O)N(CH_3)_2$, $(CH_3O)_2P(S)N(CH_3)_2$, and $(CH_3O)_2P(S)NHCH_3$ with propene as the reference organic and for $(CH_3O)_2P(S)NH_2$ with 2,3-dimethyl-2-butene as the reference organic. In addition, CH_3ONO–NO–$(CH_3O)_2P(S)NHCH_3$–2,3-dimethyl-2-butene–air irradiations were carried out. The average OH radical concentrations in the irradiated CH_3ONO–NO–DMP–reference organic–air mixtures, as calculated from the decay rates of the reference organics, were in the range (2–10) $\times 10^7$ molecule cm^{-3}. The calculated average OH radical concentrations in the NO–DMP–reference organic–air irradiations ranged from $<1.5 \times 10^6$ molecule cm^{-3} for those involving $(CH_3O)_2P(O)N(CH_3)_2$ and $(CH_3O)_2P(S)N(CH_3)_2$ to (4–5) $\times 10^6$ molecule cm^{-3} for the irradiations involving $(CH_3O)_2P(S)NHCH_3$ and $(CH_3O)_2P(S)NH_2$. During these NO–air irradiations, <5% disappearance of $(CH_3O)_2P(S)N(CH_3)_2$ and $(CH_3O)_2P(S)NHCH_3$ was observed over a 9-min irradiation period at 50% of the maximum light intensity, showing that photolysis of these two DMPs was negligible under these conditions.

The experimental data obtained from the CH_3ONO–NO–air and NO–air irradiations of all four of the DMPs are plotted in accordance with eq I in Figures 2 and 3. These plots show good linearity within the measurement uncertainties. In particular, the data for $(CH_3O)_2P(S)NH_2$ and $(CH_3O)_2P(O)N(CH_3)_2$ showed no evidence for any contribution of photolysis to the observed DMP disappearance rates. For the CH_3ONO–NO–air irradiations involving $(CH_3O)_2P(S)NHCH_3$ and $(CH_3O)_2P(S)NH_2$, the observed decay rate of isoprene was as high, or higher, than that of 2,3-dimethyl-2-butene, despite previous data which show that the OH radical reaction rate constant for 2,3-dimethyl-2-butene is ~8% higher than that for isoprene (*4*). These enhanced decays of isoprene were clearly not due to reaction with O_3, since 2,3-dimethyl-2-butene reacts faster than isoprene (*5*), and the known reaction of NO_2 with isoprene (*21*) was calculated to contribute <5% of the overall decay rates of isoprene. It thus appears that there was a further small loss process for isoprene (which is a reactive conjugated diene) in these systems, possibly with a reactive product or intermediate formed from these two DMPs. Accordingly, we used 2,3-dimethyl-2-butene as the reference organic for these irradiations, and the validity of this procedure was shown by the excellent agreement of the data obtained from the CH_3ONO–NO–$(CH_3O)_2P(S)NHCH_3$–propene–air and CH_3ONO–NO–$(CH_3O)_2P(S)NHCH_3$–2,3-dimethyl-2-butene–air irradiations (see Table II).

The rate constant ratios k_1/k_2 obtained from least-squares analysis of the experimental data are given in Table I and can be placed on an absolute basis by use of rate constants k_2 for propene and 2,3-dimethyl-2-butene of 2.66×10^{-11} cm^3 $molecule^{-1}$ s^{-1} and 1.11×10^{-10} cm^3 $molecule^{-1}$ s^{-1}, respectively (*4*). The resulting rate constants k_1 are given in Table II.

Discussion

The data given in Table II show that the dimethyl phosphorothioamidates react with both the NO_3 and the OH radical. For both of these radical reactions, the rate constants increase along the series $(CH_3O)_2P(S)N(CH_3)_2$ < $(CH_3O)_2P(S)NHCH_3$ ~ $(CH_3O)_2P(S)NH_2$, and for reaction with the OH radical $(CH_3O)_2P(O)N(CH_3)_2$ is somewhat less reactive than $(CH_3O)_2P(S)N(CH_3)_2$. In particular, $(CH_3O)_2P(S)NHCH_3$ and $(CH_3O)_2P(S)NH_2$ are highly reactive toward the OH radical, with room temperature rate constants of (2.3–2.4) $\times 10^{-10}$ cm^3 $molecule^{-1}$ s^{-1}.

Using these data, the atmospheric lifetimes of the DMPs studied can be calculated. We have used atmospheric concentrations of 2.4×10^8 molecule cm^{-3} of NO_3 radicals during a 12-h nighttime period (*22*, *23*), 1×10^6 molecule cm^{-3} of OH radicals during a 12- h daytime period (*24*), and 7×10^{11} molecule cm^{-3} of O_3 throughout a 24-h period (*25*, *26*) for these calculations. Lifetimes of the DMPs due to reaction with O_3 are calculated to be >40 day for $(CH_3O)_2P(S)NH_2$ and >80 day for the other three DMPs, and these reactions with O_3 are of negligible importance as an atmospheric removal process for these DMPs. The calculated lifetimes due to the nighttime NO_3 radical reaction range from >2.5 days for $(CH_3O)_2P(O)N(CH_3)_2$ to ~3 h for $(CH_3O)_2P(S)NH_2$, while those for daytime reaction with the OH radical range from ~9 h for $(CH_3O)_2P(O)N(CH_3)_2$ to ~1.1 h for $(CH_3O)_2P(S)NH_2$. Clearly, both the NO_3 radical and OH radical reactions must be considered in assessments of the atmospheric lifetimes and fates of the

dimethyl phosphorothioamidates.

The NO_3 and OH radical reaction rate constants can be compared to those for trimethyl phosphate (*6*) and the trimethyl phosphorothioates (*7*) to obtain information concerning the possible reaction pathways for the DMPs studied. No reactions of the trimethyl phosphorothioates with the NO_3 radical were observed, with upper limits to the NO_3 radical reaction rate constants of 3×10^{-14} cm^3 molecule^{-1} s^{-1} or lower being measured (*7*). Hence, the NO_3 radical reactions with the dimethyl phosphorothioamidates appear to proceed by initial NO_3 radical interaction with the $-NR_1R_2$ groups, with the $-NH_2$ and $-NHCH_3$ groups being significantly more reactive than the $-N(CH_3)_2$ group. This observation suggests that these NO_3 radical reactions with $(CH_3O)_2P(S)NHCH_3$ and $(CH_3O)_2P(S)NH_2$ proceed by H atom abstraction from the N–H bond(s):

$$NO_3 + (CH_3O)_2P(S)NHR \rightarrow HNO_3 + (CH_3O)_2P(S)\dot{N}R$$

The room temperature OH radical reaction rate constants for $(CH_3O)_3PO$, $(CH_3O)_2P(O)SCH_3$, and $(CH_3S)_2P(O)OCH_3$ are all $\sim 8 \times 10^{-12}$ cm^3 molecule^{-1} s^{-1} (*6*, *7*), while those for $(CH_3O)_3PS$ and $(CH_3O)_2P(S)SCH_3$ are $\sim 6 \times 10^{-11}$ cm^3 molecule^{-1} s^{-1} (*7*). The OH radical reactions with these trimethyl phosphorothioates are thus postulated to proceed by two pathways (*7*): H atom abstraction from the CH_3O- and CH_3S- groups with a rate constant at room temperature of $\sim(2.5\text{–}3.2) \times 10^{-12}$ cm^3 molecule^{-1} s^{-1} per CH_3O- or CH_3S- group, and OH radical addition to the P=S bond with a room temperature rate constant of $\sim 5.5 \times 10^{-11}$ cm^3 molecule^{-1} s^{-1} (*6*, *7*). For $(CH_3O)_2P(O)N(CH_3)_2$, $(CH_3O)_2P(S)NHCH_3$, and $(CH_3O)_2P(S)NH_2$, a significant amount of the OH radical reaction appears to proceed by OH radical interaction (presumably initial addition followed by decomposition of the intermediate complex) with the $-N(CH_3)_2$, $-NHCH_3$, and $-NH_2$ groups. Analogous to the NO_3 radical reactions, the observation that $(CH_3O)_2P(S)NHCH_3$ and $(CH_3O)_2P(S)NH_2$ are significantly more reactive than $(CH_3O)_2P(S)N(CH_3)_2$ suggests that the OH radical reactions with $(CH_3O)_2P(S)NHCH_3$ and $(CH_3O)_2P(S)NH_2$ occur to a major extent by H atom abstraction from the N–H bond(s).

However, the rate constant for the reaction of OH radicals with $(CH_3O)_2P(S)N(CH_3)_2$ of 4.7×10^{-11} cm^3 molecule^{-1} s^{-1} (Table II) is lower than that for the reaction of OH radicals with $(CH_3O)_3PS$ [7.0×10^{-11} cm^3 molecule^{-1} s^{-1} (*7*)], showing that synergistic effects between the structural units and/or steric effects must occur for these compounds. These observations make the extension of our present structure–activity relationship for the calculation of OH radical reaction rate constants (*4*, *7*, *11*) to these phosphoroamidates and phosphorothioamidates difficult.

In this relationship, the calculation of H atom abstraction rate constants from C–H bonds is based upon the estimation of $-CH_3$, $-CH_2-$, and >CH– group rate constants. These depend on the nature of the substituents around these groups:

$$k(CH_3\text{–}X) = k^\circ_{prim}F(X)$$

$$k(X\text{–}CH_2\text{–}Y) = k^\circ_{sec}F(X)F(Y)$$

$$k\left(X\text{—}CH\begin{matrix}\diagup Y\\ \diagdown Z\end{matrix}\right) = k^\circ_{tert}F(X)F(Y)F(Z)$$

where k°_{prim}, k°_{sec}, and k°_{tert} are the rate constants per $-CH_3$, $-CH_2-$, and >CH– for a standard substituent ($-CH_3$, with $F(-CH_3) = 1.00$), X, Y and Z are the substituent groups, and $F(X)$, $F(Y)$, and $F(Z)$ are the corresponding substituent factors. At room temperature, the values of k°_{prim}, k°_{sec}, and k°_{tert} are (in units of 10^{-12} cm^3 molecule^{-1} s^{-1}) 0.144, 0.838, and 1.83, respectively, and the factors $F(-CH_2-)$, $F(>CH-)$, and $F(>C<)$ are all 1.29 (*4*, *11*). The group rate constants for OH radical interaction with $-NH_2$, >NH, and >N– groups are (in units of 10^{-11} cm^3 molecule^{-1} s^{-1}) 2.0, 6.0, and 6.0, respectively, with factors $F(-NH_2) = F(>NH) = F(>N-) = 10$ (*11*). Our previous data for trimethyl phosphate and the trimethyl phosphorothioates (*6*, *7*) yield the factors $F(-OP-) = F(-SP-) = 20$ and the group rate constants $k_{-P=O} \simeq 0$ and $k_{-P=S} = 5.5 \times 10^{-11}$ cm^3 molecule^{-1} s^{-1} (*7*).

Use of these group rate constants and substituent factors, with no assumed effect of the P atom on the $-NR_2$ group rate constants, leads to predicted room temperature rate constants (in units of 10^{-11} cm^3 molecule^{-1} s^{-1}) for $(CH_3O)_2P(O)N(CH_3)_2$, $(CH_3O)_2P(S)N(CH_3)_2$, $(CH_3O)_2P(S)NHCH_3$, and $(CH_3O)_2P(S)NH_2$ of 6.9, 12.4, 12.1, and 8.1, respectively, compared to our measured values of (in the same units) 3.2, 4.7, 23.2, and 24.4, respectively. Clearly, discrepancies of up to a factor of 3 exist, and without making the structure–activity relationship too detailed and cumbersome for easy use, these may well represent the inherent uncertainties for more complex chemicals containing multiple substituent groups.

However, our calculated data show, for example, that the agriculturally used chemical Methamidophos will be reactive, with room temperature OH and NO_3 radical reaction rate constants of $\sim 1 \times 10^{-10}$ cm^3 molecule^{-1} s^{-1} and $\sim 3 \times 10^{-13}$ cm^3 molecule^{-1} s^{-1}, respectively. The calculated atmospheric lifetimes are then ~ 3 h for OH radical reaction and ~ 4 h for NO_3 radical reaction, for ambient OH and NO_3 radical concentrations of 1×10^6 molecule cm^{-3} and 2.4×10^8 molecule cm^{-3}, respectively.

Acknowledgments

We thank R. Fukuto and S. Keadtisuke of the Department of Entomology, University of California, Riverside, for valuable assistance in the syntheses.

Registry No. NO_3, 12033-49-7; HO•, 3352-57-6; O_3, 10028-15-6; $(CH_3O)_2P(O)N(CH_3)_2$, 597-07-9; $(CH_3O)_2P(S)N(CH_3)_2$, 28167-51-3; $(CH_3O)_2P(S)NHCH_3$, 31464-99-0; $(CH_3O)_2P(S)NH_2$, 17321-47-0.

Literature Cited

(1) Jury, W. A.; Winer, A. M.; Spencer, W. F.; Focht, D. D. *Rev. Environ. Contam. Toxicol.* **1987**, *99*, 119–164.
(2) Finlayson-Pitts, B. J.; Pitts, J. N., Jr. *Atmospheric Chemistry: Fundamentals and Experimental Techniques*; Wiley: New York, 1986.
(3) Atkinson, R. In *Air Pollution, The Automobile and Public Health*; Bates, R. R., Kennedy, D., Eds.; National Academy Press: Washington, DC, 1988; in press.
(4) Atkinson, R. *Chem. Rev.* **1986**, *86*, 69–201.
(5) Atkinson, R.; Carter, W. P. L. *Chem. Rev.* **1984**, *84*, 437–470.
(6) Tuazon, E. C.; Atkinson, R.; Aschmann, S. M.; Arey, J.; Winer, A. M.; Pitts, J. N., Jr. *Environ. Sci. Technol.* **1986**, *20*, 1043–1046.
(7) Goodman, M. A.; Aschmann, S. M.; Atkinson, R.; Winer, A. M. *Arch. Environ. Contam. Toxicol.*, in press.
(8) Worthing, C. R. *The Pesticide Manual*, 7th ed.; The British Crop Protection Council Publications: Croydon, UK, 1983.
(9) Quistad, G. B.; Fukuto, T. R.; Metcalf, R. L. *J. Agric. Food Chem.* **1970**, *18*, 189–194.
(10) Magee, P. S. In *Insecticide Mode of Action*; Academic: New York, 1982; pp 101–161.
(11) Atkinson, R. *Int. J. Chem. Kinet.* **1987**, *19*, 799–828.
(12) Atkinson, R.; Carter, W. P. L.; Winer, A. M.; Pitts, J. N., Jr. *J. Air Pollut. Control Assoc.* **1981**, *31*, 1090–1092.
(13) Atkinson, R.; Aschmann, S. M.; Winer, A. M.; Pitts, J. N., Jr. *Int. J. Chem. Kinet.* **1982**, *14*, 507–516.
(14) Atkinson, R.; Plum, C. N.; Carter, W. P. L.; Winer, A. M.; Pitts, J. N., Jr. *J. Phys. Chem.* **1984**, *88*, 1210–1215.

(15) Atkinson, R.; Pitts, J. N., Jr.; Aschmann, S. M. *J. Phys. Chem.* **1984**, *88*, 1584-1587.
(16) Carter, W. P. L.; Atkinson, R.; Winer, A. M.; Pitts, J. N., Jr. *Experimental Protocol for Determining Photolysis Reaction Rate Constants*; EPA-600/3-83-100; U.S. Government Printing Office: Washington, DC, Jan 1984.
(17) Atkinson, R.; Aschmann, S. M.; Carter, W. P. L. *Int. J. Chem. Kinet.* **1983**, *15*, 1161-1177.
(18) Taylor, W. D.; Allston, T. D.; Moscato, M. J.; Fazekas, G. B.; Kozlowski, R.; Takacs, G. A. *Int. J. Chem. Kinet.* **1980**, *12*, 231-240.
(19) Magee, P. S. U.S. Patent 3 309 266, March 14, 1967.
(20) Ravishankara, A. R.; Mauldin, R. L., III *J. Phys. Chem.* **1985**, *89*, 3144-3147.
(21) Atkinson, R.; Aschmann, S. M.; Winer, A. M.; Pitts, J. N., Jr. *Int. J. Chem. Kinet.* **1984**, *16*, 697-706.
(22) Platt, U. F.; Winer, A. M.; Biermann, H. W.; Atkinson, R.; Pitts, J. N., Jr. *Environ. Sci. Technol.* **1984**, *18*, 365-369.
(23) Atkinson, R.; Winer, A. M.; Pitts, J. N., Jr. *Atmos. Environ.* **1986**, *20*, 331-339.
(24) Crutzen, P. J. In *Atmospheric Chemistry*; Goldberg, E. D., Ed.; Springer-Verlag: Berlin, West Germany, 1982; pp 313-328.
(25) Singh, H. B.; Ludwig, F. L.; Johnson, W. B. *Atmos. Environ.* **1978**, *12*, 2185-2196.
(26) Oltmans, S. J. *J. Geophys. Res. C: Oceans Atmos.* **1981**, *86*, 1174-1180.

Received for review August 7, 1987. Accepted December 14, 1987. The financial support of the University of California, Riverside, Toxic Substances Research and Training Program is gratefully acknowledged.

Xenon-133 in California, Nevada, and Utah from the Chernobyl Accident

Robert W. Holloway* and Chung-King Liu

Environmental Monitoring Systems Laboratory, U.S. Environmental Protection Agency, P.O. Box 93478, Las Vegas, Nevada 89193-3478

■ The accident at the Chernobyl nuclear reactor in the USSR introduced numerous radioactive nuclides into the atmosphere including the noble gas xenon-133. EPA's Environmental Monitoring Systems Laboratory, Las Vegas, NV, detected xenon-133 from the Chernobyl accident in air samples from a monitoring network that consists of 15 stations located in Nevada, Utah, and California. The peak concentration of xenon-133 was found in weekly air samples collected during May 6-13, 1986. The network average concentration of xenon-133 was 41 pCi/m^3 during that time. A lower average was found in air samples collected in the following week. These concentrations are comparable to or less than that of natural radionuclides (such as radon) normally present in the atmosphere and are much lower than the peak xenon-133 concentration measured in New York State following the accident at the Three Mile Island reactor.

Introduction

The Chernobyl nuclear accident, which occurred in the Soviet Union on April 26, 1986, released various radioactive nuclides into the atmosphere. An early report (*1*) indicated that xenon-133 was one of several isotopes detected in Sweden by April 29, 1986. Xenon-133 is a convenient tracer to detect leakage from a reactor or recent nuclear explosion since it is a noble gas and its short 5.3 day half-life prevents the accumulation of a significant inventory in the atmosphere.

Since 1972, the Environmental Protection Agency's Environmental Monitoring Systems Laboratory at Las Vegas has maintained a network of noble gas monitoring stations in Nevada, Utah, and California as a part of the radiation monitoring program for the region near the Nevada Test Site. The network was established to measure the concentrations of radioactive noble gases released into the atmosphere either from underground nuclear detonations, from posttest operations, or from seepage from previous underground tests. The locations of the 15 stations in the network are shown in Figure 1. The network is approximately 200 miles wide (east to west) and 300 miles along a line from Las Vegas to Austin.

The concentration of radioactive xenon is routinely measured in air samples collected from the network, and therefore no special sampling program was required to monitor for xenon-133 emission from the Chernobyl accident.

Analytical Procedures

Air samples are collected by two methods. One method employs air-compressing units as described by Andrews (*2*). The other method is a cryogenic technique in which whole air samples are collected in the field at the temperature of liquid nitrogen and returned to the laboratory where they are allowed to warm to room temperature and are analyzed as compressed air. In both methods, approximately 1 m^3 of air is collected during continuous operations over a 1-week period.

All samples are analyzed in our laboratory by the procedure described by Johns et al. (*3*). The procedure involves the separation and purification of krypton and xenon by adsorption on chromatographic columns and the subsequent analysis of the radioactivity in the krypton and xenon fractions by liquid scintillation counting.

The accuracy of the method is checked periodically with samples of known radioactivity. The error involved in the analysis of known samples has been 10% or less. The errors reported with each xenon-133 determination are 2-σ errors derived from the statistics of counting the sample and background. Both the xenon-133 results and the error terms are decay corrected back to the midpoint of collection.

The minimum detectable concentration (MDC) of xenon-133 varies with each sample but is usually 10-25 pCi/m^3. The calculation of MDC of xenon-133 includes a correction for the decay of xenon-133 during the several days between the midpoint of collection and sample analysis. Thus, the MDC refers to the midpoint of collection and not to the date of analysis. The MDCs reported for these samples are roughly twice as high as would be obtained for grab samples analyzed immediately after collection.

In analyzing samples that are only slightly above the normal background of the counting equipment, statistical methods must be used to ensure that results above zero are caused by real activity rather than normal background fluctuations. For the results reported in Table I, all nu-

0013-936X/88/0922-0583$01.50/0

Table I. ^{133}Xe Concentrations by Station before and after the Chernobyl Accident

station	April 22–29, pCi/m^3	April 29–May 6, pCi/m^3	May 6–13, pCi/m^3	May 13–20, pCi/m^3	May 20–27, pCi/m^3
Shoshone, CA	ND[a]	ND	25 ± 8	28 ± 7	ND
Alamo, NV	30 ± 7	ND	40 ± 7	18 ± 7	ND
Austin, NV	ND	ND	55 ± 13	25 ± 12	ND
Beatty, NV	lost	ND	39 ± 13	51 ± 25	lost
Ely, NV	ND	ND	36 ± 9	29 ± 11	ND
Goldfield, NV	ND	ND	45 ± 10	32 ± 13	ND
Indian Springs, NV	ND	lost	43 ± 8	37 ± 11	ND
Las Vegas, NV	lost	ND	67 ± 15	25 ± 10	ND
Lathrop Wells, NV	ND	ND	37 ± 19	37 ± 11	ND
Overton, NV	ND	lost	31 ± 11	21 ± 9	ND
Pahrump, NV	lost	lost	lost	24 ± 6	12 ± 7
Rachel, NV	28 ± 7	21 ± 8	45 ± 8	17 ± 10	10 ± 8
Tonopah, NV	ND	ND	58 ± 18	35 ± 11	ND
Cedar City, UT	ND	lost	lost	33 ± 16	ND
St. George, UT	ND	ND	ND	lost	lost

[a] ND indicates that the ^{133}Xe concentration was below the minimum detectable concentration. The minimum detectable concentration usually ranges from 10 to 25 pCi/m^3 for ^{133}Xe.

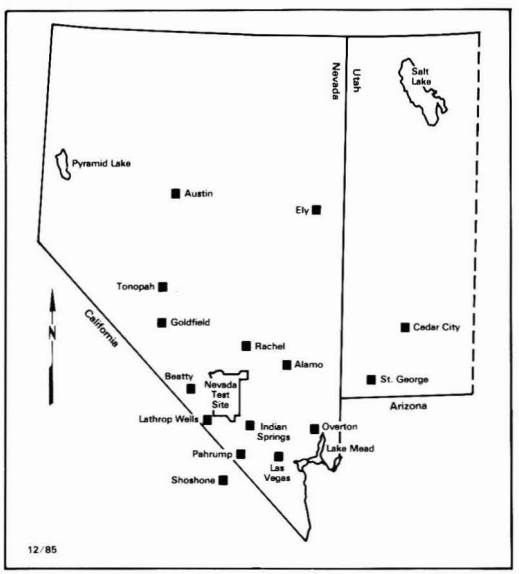

Figure 1. Noble gas sampling stations.

meric results were above the MDC, and the MDC was calculated for a 95% confidence level. Therefore, we can be reasonably sure that each numeric result represents real activity.

Discussion

As shown in Table I, xenon-133 was detected at two network stations (Alamo and Rachel, NV) for the sampling period of April 22–29, 1986. Although the explosion at the Chernobyl reactor is believed to have occurred on April 26, 1986, the reactor accident cannot be the source of the xenon-133 observed at Alamo and Rachel since more time is required for the radioactive cloud to reach Nevada. We have attributed the trace concentrations of xenon-133 observed at those two stations to the controlled purging of a tunnel used for an underground nuclear test at the Nevada Test Site during April (*4*). It is important to note that only noble gases escaped from the site during purging. Other fission products were removed by appropriate filtration so that the concentration was too low to be detected offsite. During the week of April 29 to May 6, 1986, xenon-133 was detected again at Rachel. This xenon also is likely to have come from the tunnel purging.

The first indication of xenon-133 from the Chernobyl accident was found in samples collected during the period from May 6 to May 13, 1986. Coincidently, fission products other than xenon appeared in samples from all air sampling stations operated by the Environmental Monitoring Systems Laboratory (Las Vegas), including those colocated with the noble gas samplers. An important finding was the presence of cesium-134 in the air samples because this radionuclide is indicative of a reactor release rather than a nuclear test explosion. We also found iodine-131 (47 pCi/L) in snow which fell 30 miles northwest of Las Vegas on May 7. The xenon-133 measured during this period was present at all stations except St. George, UT, where it was below the detection limit, and possibly Cedar City, UT, where the sample was lost in analysis. Excluding Cedar City, St. George is the easternmost station of the network. It seems likely that the air mass containing xenon-133 had not yet reached St. George or had bypassed it during that time.

Beiriger et al. (*5*) recently discussed the arrival of Chernobyl debris in the vicinity of Lawrence Livermore National Laboratory. Their samples were air filters with a 2–3-day collection period and analysis by γ spectroscopy. They detected initial low levels of Chernobyl debris on May 6, followed by a peak during the May 7–9 collection. They noted that the Chernobyl activity decreased rapidly but with oscillations over the next few weeks. Our network is 300–400 miles to the southeast of Livermore. The detection of Chernobyl xenon in our network indicates an arrival time soon after May 6, so the expected near coincidence of arrival times is present.

This is the only time in at least 5 years that we have detected xenon-133 simultaneously at virtually all of the sampling locations. Operations at the Nevada Test Site on rare occasions produce detectable xenon-133 at one or two stations such as those during the period of April 22 to May 6, 1986. The widely distributed nature of the xenon-133 during the May 6–20 period is not typical of a local source. In addition, the arrival time of the xenon-133 detected after May 6 is consistent with other reports of the arrival of Chernobyl fallout in the United States. It is interesting to compare the observed xenon-133 concentrations with what might be expected from an accident of this type. An early report quoted from Lawrence Livermore National Laboratory (*1*) suggested that at least 50% of the estimated inventory of 80 MCi of iodine-131 escaped

from the reactor. This represents a release of approximately 40 million Ci. The maximum activity ratio of xenon-133 to iodine-131 after the fission of uranium-235 by thermal neutrons can be obtained from basic decay equations and is given by

$$\text{activity ratio of } {}^{133}\text{Xe}/{}^{131}\text{I} = \left(\frac{\text{cumulative yield of } {}^{133}\text{Xe}}{\text{cumulative yield of } {}^{131}\text{I}}\right)\left(\frac{\text{half-life of } {}^{131}\text{I}}{\text{half-life of } {}^{133}\text{Xe}}\right)$$

The cumulative yields of xenon-133 and iodine-131 given by Meek and Rider (*6*) are 6.77% and 2.77%, respectively. The term "cumulative" in this case means the fission yield of the nuclide plus the yield of the radioactive precursors in that decay chain. These percentages indicate the relative number of atoms, not activity. An inverted half-life ratio is required because activity is inversely proportional to half-life. The half-life of iodine-131 is 8.07 days and that of xenon-133 is 5.27 days. The activity ratio calculated from the above equation is 3.74. This is a maximum value that will never be fully attained. The reason is that most of the xenon-133 is not created directly by fission but is produced from the decay of the iodine-133 precursor (half-life 20.8 h). During the time that the xenon-133 is being produced from the precursor, the shorter half-life of xenon-133 relative to iodine-131 will tend to reduce the activity ratio for a given generation of fission fragments. On the basis of these considerations, a xenon-133/iodine-131 activity ratio of 2–3 at the time of release seems reasonable. If we assume that the xenon-133/iodine-131 activity ratio in the Chernobyl reactor was 2–3 and that all the noble gas escaped, then this leads to an estimate of 160–240 million Ci of xenon-133 released at Chernobyl.

It is interesting to consider the concentration of xenon-133 that would result if that amount of xenon-133 were evenly distributed throughout the troposphere of the Northern Hemisphere. Poldervaart (*7*) gave an estimate of 4.3×10^{18} M^3 for the volume of the earth's troposphere. Considering half of that as the volume of the Northern Hemisphere gives a xenon-133 concentration of 74–111 pCi/m^3, assuming a uniform distribution of xenon-133 from the accident. The period from May 6 to May 13 represents the first passage of the debris across the United States, and it is clear that homogeneous mixing of the debris throughout the troposphere would not be expected, even at a later time. In addition, approximately 2–3 half-lives of xenon-133 elapsed between the first emissions and the midpoint of our collection. Considering decay and nonuniform dilution then the 41 pCi/m^3 average observed in our network appears to be reasonable.

The Chernobyl reactor was rated at 1000 MW. Chitwood (*8*) gave the expected xenon-133 inventory for a 1000-MW light water reactor at steady state after 3 years of operation with one-third of the core replaced each year. Chitwood's estimated inventory of xenon-133 was 165 million Ci. Assuming all was released, this 165 million Ci is in good agreement with the 160–240 million Ci range derived from the early report of the estimated iodine-131 release.

The average concentration of xenon-133 decreased to 29 pCi/m^3 during the second week but not to the extent that would be expected if all of the xenon had been released at one time and then decreased by decay and dilution. This seems consistent with news accounts of emissions lasting for 1 week or longer at Chernobyl.

During the week of May 20–27, 1986, xenon-133 was above detection limits at only two sampling locations. The network average of 12 pCi/m^3 (including those below MDC) during this period was still slightly above the network averages before the Chernobyl accident, possibly indicating some fading influence of the Chernobyl xenon.

It is interesting to compare these xenon-133 results with the concentrations of xenon-133 reported downwind of the Three Mile Island accident of 1979. Wahlen et al. (*9*) found xenon-133 in air samples taken in Albany, NY, some 375 km from the reactor. Their highest concentrations ranged from 3120 to 3900 pCi/m^3 in air samples collected on March 30, 1979. On the basis of a figure presented by Wahlen et al. (*9*), the estimated release rate of xenon-133 from the damaged reactor was 10–30 Ci/s during that time or from 0.8–2.5 million Ci/day. Although the emissions from the Chernobyl reactor were substantially greater than those of the Three Mile Island reactor, the concentration of Chernobyl xenon detected in our network is much less than the maximum concentrations found downwind of the Three Mile Island reactor, as would be expected. The measurements are not fully comparable, however, since our collection time was approximately 1 week while the maximum found by Wahlen et al. (*9*) was collected over 10 h. It is possible that 1-day sampling times in our network might have revealed peak concentrations somewhat higher than we report here. The xenon-133 measured by Wahlen et al. (*9*) had little time to decay enroute from Three Mile Island to Albany. They estimated a transit time of 18–24 h. The much longer transit times involved in the transport of Chernobyl fallout to Nevada corresponds to 2–3 half-lives of xenon-133 and allowed substantial decay. In addition, dilution would surely be more effective over the longer distance from Chernobyl.

Because the collection time was long compared to the movement of air masses across the network, there is no reason to expect great variation between stations. This seems to be confirmed by the results, especially when the error term is considered.

The derived air concentration standard (*10*) adjusted for continuous exposure and an 0.1 rem/year exposure guide for populations is 480 000 pCi/m^3 (annual average). Because the observed xenon-133 concentrations are much lower, the dose to the population of the area from this xenon-133 is negligible. For example, the xenon-133 concentration at Las Vegas during the period from May 6 to May 20 corresponds to a whole body γ-ray dose of 0.0004 mrem. This compares to 150 mrem/year received by the average person from all sources of exposure.

Conclusions

Xenon-133 was detected in air samples from California, Nevada, and Utah during May 6–27, 1986. The wide distribution of activity, the simultaneous detection of other fission products, and the time of arrival suggests that the source of the emissions was the Chernobyl accident.

The observed activity was much less than the peak xenon-133 activity detected in New York State after the Three Mile Island accident. The xenon-133 concentrations reported here are minuscule compared to the derived air concentration guides for continuous exposure. This xenon activity was present for only 2 weeks, and the dose to the population of the area from this xenon was negligible.

Acknowledgments

We thank Stuart Black, Charles Costa, and Erich Bretthauer for their helpful suggestions.

Registry No. Xenon-133, 14932-42-4.

Literature Cited

(1) Marshal, E. *Science (Washington, D.C.)* **1986**, *232*, 814–815.

(2) Andrew, V. E. *Noble Gas Sampling System*; National Technical Information Service: Springfield, VA, 1977; EMSL-LV-539-7.
(3) Johns, F. B.; Hahm, P. B.; Thome', D. J.; Bretthauer, E. W. *Radiochemical Analytical Procedures for Analysis of Environmental Samples*; National Technical Information Service, U.S. Department of Commerce: Springfield, VA, 1979; EMSL-LV-0539-17.
(4) Black, S. C.; Smith, A. E.; Costa, C. F. *Offsite Monitoring for the Mighty Oak Nuclear Test*; Environmental Monitoring Systems Laboratory, EPA: Las Vegas, NV, 1986; EPA 600/4-86-030.
(5) Beiriger, J. M.; Failor, R. A.; Marsh, K. V.; Shaw, G. E. *Proc. Annu. Conf. Bioassay, Anal. Environ. Radiochem.* **1987**, *No. 33.*
(6) Meek, M. E.; Rider, B. F. *Compilation of Fission Product Yields*; General Electric Co., Vallecitors Nuclear Center: Pleasanton, CA, 1972; NEDO-12154.
(7) *Crust of the Earth*; Poldervaart, A., Ed.; Geological Society of America: New York, 1955; pp 121–123.
(8) Chitwood, R. B. *Noble Gases*; Stanley, R. E., Moghissi, A. A., Eds.; National Technical Information Service, U.S. Department of Commerce: Springfield, VA, 1973; CONF-730915, pp 69–80.
(9) Wahlen, M.; Kunz, C. O.; Matuszek, J. M.; Mahoney, W. E.; Thompson, R. C. *Science (Washington, D.C.)* **1980**, *207*, 639–640.
(10) International Commission on Radiological Protection *Limits for Intakes of Radionuclides by Workers*; Pergamon: New York, 1979; Publication 30, Suppl. Part 2, pp 374.

Received for review March 20, 1987. Revised manuscript received November 19, 1987. Accepted December 18, 1987. Mention of trade names or commercial products does not constitute endorsement or recommendation for use.

Rate Constant for the Reaction of NO_2 with Sulfur(IV) over the pH Range 5.3–13

Carol L. Clifton, Nisan Altstein, and Robert E. Huie*

Chemical Kinetics Division, National Bureau of Standards, Gaithersburg, Maryland 20899

■ Rate constants have been determined for the reactions of NO_2 with SO_3^{2-} and HSO_3^- in aqueous solutions. The rate constant increases from about 1.2×10^7 M^{-1} s^{-1} near pH 5 to 2.9×10^7 M^{-1} s^{-1} at pH 13. The reaction appears to involve the formation of an intermediate complex that may undergo subsequent reaction with NO_2 to yield the ultimate products or may react with other substrates present. The formation of a long-lived intermediate would have implications on the chemistry of flue gas scrubbers and on luminol-based NO_2 detectors.

Introduction

Air pollution by both sulfur dioxide and nitrogen oxides has been recognized as major problems almost since the start of the industrial revolution. These pollutants have been in the spotlight more recently as precursors to the strong mineral acids HNO_3 and H_2SO_4 in precipitation. Yet, an effective, reliable, and inexpensive technique for removing these gases from emission sources, mainly coal-fired power plants, remains an elusive goal (*1*). Although a considerable amount of work has been done on the development of water-based flue gas scrubbers, there are major gaps in our understanding of the basic chemistry involved in their operation, particularly the free radical chemistry. Of particular importance are the reactions of the free radical NO_2, which may be formed in the gas phase through normal combustion reactions or deliberately formed in the flue gas to aid in the removal of NO_x. In a combined SO_x/NO_x scrubber, the NO_2 radical may react with dissolved S(IV) [$SO_2(aq)$, HSO_3^-, or SO_3^{2-}], effecting the removal efficiency of both.

An improved understanding of the underlying chemistry of the atmospheric conversion of SO_2 to SO_4^{2-} is also needed in order to allow the development of reliable atmospheric models. In atmospheric droplets, the reaction of NO_2 with HSO_3^- may serve as an additional pathway for acidification of the droplet. The reaction of NO_2 with SO_3^{2-} may also play an important role in the chemistry of the luminol-based chemiluminescence detector for NO_2. The addition of Na_2SO_3 has been found not only to reduce the interference from O_3 but also to increase greatly the sensitivity of that detector (*2*, *3*).

There has been some work on the effect of NO_2 on HSO_3^-/SO_3^{2-} oxidation (*4–8*) and the effect of SO_3^{2-} autoxidation on the absorption of NO_2 into an aqueous solution (*9*). Of particular interest is the observation that while NO_2 will oxidize SO_3^{2-}, it does not initiate SO_3^{2-} autoxidation (*8*) (which is a free radical chain reaction) (*10*). Also, it is interesting to note that NO serves as an inhibitor of SO_3^{2-} autoxidation (*6*) and that the efficiency of NO_2 absorption into SO_3^{2-} solutions decreased if autoxidation is permitted (*9*).

Recently, we investigated the reactions of NO_2, generated by pulse radiolysis in aqueous solutions, with several organic and inorganic reactants (*11*). The pulse radiolysis apparatus employed in that study could operate only in a single-shot mode. This makes it difficult to follow very small absorbance changes. Since the optical absorption due to NO_2 is very weak, its reactions were followed by monitoring a product radical from the other reactant. For the reaction with SO_3^{2-}, however, this was not possible, so the rate constant had to be measured relative to the reaction of NO_2 with phenol. The results were not completely satisfactory, and only an approximate number was reported and only at pH 12.1. In this work, we have employed a pulse radiolysis apparatus with signal averaging, which has allowed us to monitor the decay of NO_2 directly and to measure rate constants for the reaction of NO_2 with SO_3^{2-} and HSO_3^- over the pH range 5.3–13.

Experimental Section

The pulse radiolysis apparatus, capable of repeated pulses under computer control, will be described in detail elsewhere (*12*). It employs a Van de Graaff accelerator which, in these experiments, delivers 0.5-μs pulses of 2.8 MeV electrons to the reaction cell. The temporal history of a reactant or product is monitored by absorption spectroscopy. A decay curve from each individual pulse is recorded by a transient analyzer and transferred to the

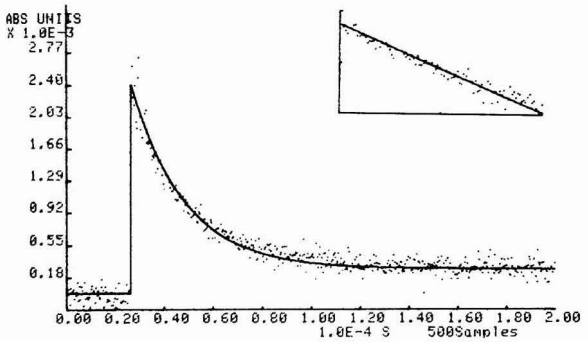

Figure 1. Decay of absorbance due to NO_2 at 400 nm. Solution containing 10 mM $NaNO_2$ and 1.5 mM Na_2SO_3 at pH 11.75. Average of 50 pulses. Insert: log Abs vs t.

computer. If the dose delivered by the Van de Graaff accelerator is within a preset range, the data are added to memory. This procedure is repeated enough times to produce a signal sufficient for analysis. The data are then analyzed by a linear least-squares program.

Reagent-grade chemicals were used as supplied; water was purified by an ion-exchange system. Separate solutions of $NaNO_2$ and of several concentrations of Na_2SO_3 were prepared. The solutions were saturated with N_2O and mixed just upstream of the 2 cm long irradiation cell, making use of a peristaltic pump. This procedure prevented possible complications due to the reaction of HNO_2 with HSO_3^-.

The irradiation of aqueous solutions at pH 3–13 produces the hydroxyl radical and the hydrated electron in similar concentrations, along with a small (<10%) yield of hydrogen atoms. In N_2O saturated solutions, the hydrated electron is converted to OH:

$$H_2O \rightarrow \rightarrow \rightarrow e_{aq}^-, H, OH \quad (1)$$

$$e_{aq}^- + N_2O + H_2O \rightarrow N_2 + OH + OH^- \quad (2)$$

The OH radical then reacts with NO_2^- to produce NO_2 ($k \sim 1 \times 10^{10}$ M^{-1} s^{-1}) (*13*):

$$OH + NO_2^- \rightarrow OH^- + NO_2 \quad (3)$$

Under our experimental conditions, about 5 μM NO_2 typically is produced. With no added solute, NO_2 equilibrates with its dimer N_2O_4 ($k = 4.5 \times 10^8$ M^{-1} s^{-1}; $K = 1.53 \times 10^{-5}$ M) (*14*), which then disproportionates to NO_2^- and NO_3^- (*15*).

Results and Discussion

The pulse irradiation of a N_2O saturated NO_2^- solution produced a very weak optical absorption due to NO_2 with maxima at 400 and 420 nm. We have not attempted to determine the absorptivity quantitatively, but our results appear compatible with the value of $\epsilon = 200$ M^{-1} cm^{-1} at 400 nm reported previously (*14*). To obtain an adequate signal for analysis, from 20 to 200 pulses were needed, depending upon conditions. Rate constants for the decay of the signal due to NO_2 were determined upon the addition of a great excess of S(IV). A sample experimental decay curve is given in Figure 1. In all cases, good first-order behavior was observed. Replicate runs were made at each S(IV) concentration, and typically, four concentrations between 5×10^{-4} and 2×10^{-3} M were employed to derive a second-order rate constant (Figure 2). Rate measurements were carried out over the pH range 5.3–13, with the results given in Table I and plotted

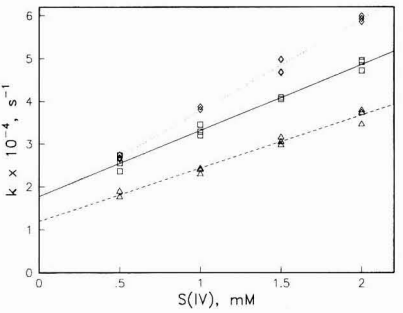

Figure 2. Concentration dependence of the first-order rate constant for the reaction of NO_2 with S(IV). Triangles, pH 5.3; squares, pH 6.7, 0.5 M phosphate buffer; diamonds, pH 11.75.

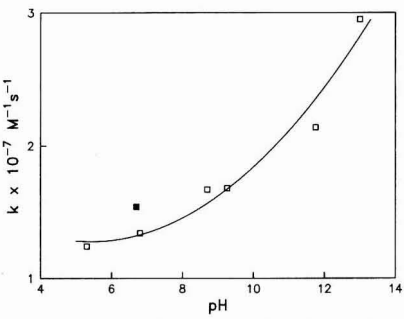

Figure 3. Dependence of the second-order rate constant for the reaction of NO_2 with S(IV) on pH. Solid square, 0.5 M phosphate buffer.

Table I. Rate Constants for the Reaction of NO_2 with SO_3^{2-}/HSO_3^-

pH	$k \times 10^{-7}$, M^{-1} s^{-1}	conditions
5.3	1.24	1 mM phosphate
6.7	1.54	0.5 M phosphate
6.8	1.34	$NaHSO_3 + Na_2SO_3$, no buffer
8.7	1.67	1 mM borate
9.3	1.68	1 mM borate
11.8	2.14	1 mM phosphate + KOH
13	2.95	0.1 M KOH

against pH in Figure 3. Rate measurements were not attempted at lower pH to avoid complications from the reaction of HNO_2 with HSO_3^-.

The pK for the deprotonation of bisulfite

$$HSO_3^- \rightleftarrows H^+ + SO_3^{2-} \quad (4)$$

is 7.19 (*16*). In general, free radicals react with SO_3^{2-} more rapidly than with HSO_3^- (*10*, *17*). This reflects the decrease in one-electron redox potential in going from HSO_3^- to SO_3^{2-} and leads to an inflection in the rate constant around the pK for HSO_3^-, with a lower rate constant below pH 7.19 and a higher value above that pH. Yet, in Figure 3 there is no indication of any inflection around that point. This suggests that the change in rate constant with pH does not result simply from the increased amount of SO_3^{2-} but involves general or specific base catalysis. Indeed, although the increase in rate constant with pH appears very sharp, the total increase in going from pH 5.3 to pH 13 is only about a factor of 2.5.

Although the change in rate constant with pH is not coincident with the transition from HSO_3^- to SO_3^{2-}, there is certainly an increase in rate constant with pH. To

investigate the possible importance of a general base catalyzed path, we determined the rate constant in the presence of 0.5 M phosphate buffer. The rate constant increased, but only slightly. This suggests that the increase in rate constant is associated primarily with the increase in OH^- concentration. Since the increase in rate constant with pH is so small, we have not attempted to derive an OH^--dependent rate expression.

In our earlier work on the reaction of NO_2 with SO_3^{2-}, we concluded that the reaction did not take place by a simple electron transfer. We arrived at this conclusion by comparing the rate constants for reactions of NO_2 with comparable reactions of ClO_2. In all other cases, where electron transfer was confirmed by observing the product radicals, the reaction of ClO_2 with a substrate was faster than the reaction of NO_2. The reaction of NO_2 with SO_3^{2-}, however, was faster than for ClO_2. The present results support that conclusion, since if the reaction were a simple electron transfer, the change in rate constant with pH should reflect the relative amounts of SO_3^{2-} and HSO_3^-.

There is also other information in the literature that, in conjunction with the present observations, sheds further light on the nature of this reaction. First is the observation, mentioned above, that whereas NO_2 can oxidize HSO_3^- or SO_3^{2-} directly, it does not appear to initiate their autoxidation. Second, the products and stoichiometry suggest that the overall reaction is mainly (*7*)

$$2NO_2 + HSO_3^- + H_2O \rightarrow 2NO_2^- + 3H^+ + SO_4^{2-} \quad (5)$$

with the yield of NO_2^- relative to HSO_3^- consumed 1.5 ± 0.4 and the yield of H^+ 2.5 ± 0.4. There appeared to be essentially no NO or NO_3^- produced. Third, the rate constant ($d[H^+]/dt$) determined by bubbling NO_2 through a HSO_3^- solution (>2 × 10^6 M^{-1} s^{-1} at pH 6.4 and 1.4 × 10^5 M^{-1} s^{-1} pH 5) (*18*) was much lower than the rate constant determined here. That work also showed that the reaction was not second order in NO_2, as the stoichiometry would suggest. Finally, it was observed that there was a small induction period in the generation of H^+ and that the generation of H^+ would continue for several minutes after NO_2 had been purged from the solution.

In our earlier work, we suggested that the reaction was a simple oxygen-atom transfer:

$$NO_2 + HSO_3^- \rightarrow NO + SO_4^{2-} + H^+ \quad (6)$$

The observations summarized above suggest that this is not likely to be the case. Rather, our observations and these other results suggest that the initial step involves the formation of an addition complex, which can undergo subsequent reaction with further NO_2:

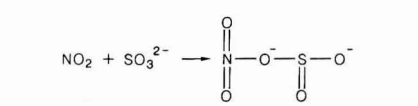

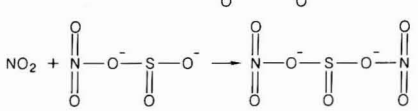

This second intermediate, which is potentially long lived, can then decompose, possibly in a base-catalyzed reaction, to NO_2^- and SO_4^{2-}:

In our experiments, the low initial NO_2 concentration (<10^{-5} M) will probably ensure that reaction 7 predominates. The occurrence of reaction 8 cannot be ruled out completely, however, but the very good first- and second-order plots (Figures 1 and 2) suggest that it is not important. Therefore, the rate constant we measure should correspond to the formation of the first complex. Indeed, there does seem to be a very small residual absorption at long time (Figure 1) that could be due to this complex. The production of acid upon bubbling NO_2 through a HSO_3^- solution, however, requires reactions 8–10 and would be expected to be much slower, as observed (*18*).

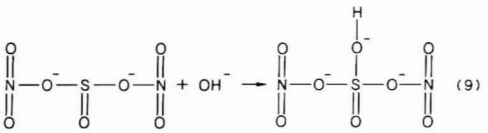

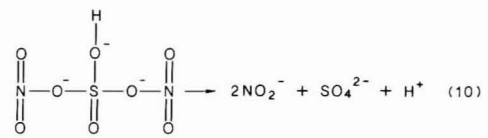

Relatively slow secondary steps also would be expected to lead to an induction period for the production of acid and the continued production of acid after the NO_2 was removed.

There is certainly considerable precedence for an addition reaction in the interactions of sulfite and bisulfite with nitrogen oxides and their anions. Nitrous acid reacts with bisulfate, first to form nitrososulfonic acid (*19*), which can then react further with bisulfate to form hydroxylaminedisulfonate (*20*):

$$HNO_2 + HSO_3^- \rightarrow ONSO_3^- + H_2O \quad (11)$$

$$ONSO_3^- + HSO_3^- \rightarrow HON(SO_3)_2^{2-} + H_2O \quad (12)$$

This product may hydrolyze or react with additional HSO_3^- to form aminetrisulfonate:

$$HON(SO_3)_2^{2-} + HSO_3^- \rightarrow N(SO_3)_3^{3-} + H_2O \quad (13)$$

In these reactions, three sulfites substitute onto the nitrogen, with the elimination of water. The reaction of nitric oxide with sulfite (*21*, *22*), however, appears to be more similar to what we are proposing here for nitrogen dioxide:

$$NO + SO_3^{2-} \rightarrow ONSO_3^{2-} \quad (14)$$

$$NO + ONSO_3^{2-} \rightarrow {}^-ON(NO)SO_3^- \quad (15)$$

$${}^-ON(NO)SO_3^- \rightarrow N_2O + SO_4^{2-} \quad (16)$$

In an atmospheric droplet, the fate of the initial intermediate formed from the reaction of NO_2 with SO_3^{2-} might not be simply to react with another NO_2, since that radical will be at such a low concentration in the droplet. The compound might serve as a one-electron oxidant, leading to the formation of nitrososulfuric acid. In a flue gas scrubber, particularly when the gas-phase NO is converted to NO_2, the intermediate is much more likely to react with additional NO_2 due to its much higher concentration. Confirmation of the production of this intermediate and information on its chemical behavior are needed to fully assess its role in these systems.

The formation of a reactive intermediate in the reaction of NO_2 with SO_3^{2-} might also help explain the role of added Na_2SO_3 on the operation of a luminol-based NO_2 detector. The reaction of SO_3^{2-} with O_3 is a simple oxygen-atom transfer (*23*), leading to unreactive products:

$$O_3 + SO_3^{2-} \rightarrow O_2 + SO_4^{2-} \quad (17)$$

This explains the ability of SO_3^{2-} to reduce the interference due to O_3. When NO_2 is dissolved into a luminol solution, its reaction with luminol is in competition with the removal

of NO_2 due to disproportionation. If a large concentration of SO_3^{2-} is present, the NO_2 will react to form an intermediate. This intermediate, then, can proceed to react with the luminol, leading to chemiluminescence. An investigation into the nature of this intermediate would be useful in predicting possible complications in the luminol-based NO_2 detector.

Acknowledgments

We thank Dr. G. W. Harris of the Max Plank Institute for Chemistry, Mainz, FRG, for alerting us to the use of sulfite in the luminol-based NO_2 detector.

Registry No. NO_2, 10102-44-0; NO_x, 11104-93-1.

Literature Cited

(1) Chang, S. G. *ACS Symp. Ser.* **1986**, *No. 319*, 159
(2) Maeda, Y.; Aokl, K.; Munemorl, M. *Anal. Chem.* **1980**, *52*, 307.
(3) Wendel, G. J.; Stedman, D. H.; Cantrell, C. A. *Anal. Chem.* **1983**, *55*, 937.
(4) Nash, T. *Atmos. Environ.* **1979**, *13*, 1149.
(5) Rosenberg, H. S.; Grotta, H. M. *Environ. Sci. Technol.* **1980**, *14*, 470.
(6) Cofer, W. R.; Schryer, D. R.; Rogowski, R. S. *Atmos. Environ.* **1981**, *15*, 1281.
(7) Lee, Y. N.; Schwartz, S. E. In *Precipitation Scavenging, Dry Deposition, and Resuspension*; Pruppacher, H. R., Semonin, R. G., Slinn, W. G. N., Eds.; Elsevier: New York, 1983; p 453.
(8) Ellison, T. K.; Eckert, C. A. *J. Phys. Chem.* **1984**, *88*, 2335.
(9) Takeuchi, H.; Takahashi, K.; Kizawa, N. *Ind. Eng. Process Des. Dev.* **1977**, *16*, 486.
(10) Neta, P.; Huie, R. E. *EHP, Environ. Health Perspect.* **1985**, *64*, 209.
(11) Huie, R. E.; Neta, P. *J. Phys. Chem.* **1986**, *90*, 1193.
(12) Huie, R. E.; Clifton, C. L.; Altstein, N., submitted for publication in *Radiat. Phys. Chem.*
(13) Farhataziz; Ross, A. B. *Natl. Stand. Ref. Data. Ser.* (*U.S. Natl. Bur. Stand.*) **1977**, *NSRDS-NBS 59.*
(14) Graetzel, M.; Henglein, A.; Lilie, J.; Beck, G. *Ber. Bunsen-Ges. Phys. Chem.* **1969**, *73*, 646.
(15) Schwartz, S. E.; White, W. H. In *Trace Atmospheric Constituents: Properties, Transformations, and Fates*; Schwartz, S. E., Ed.; Wiley: New York, 1983; p 1.
(16) Goldberg, R. N.; Parker, V. B. *J. Res. Natl. Bur. Stand.* (*U.S.*) **1985**, *90*, 341.
(17) Huie, R. E.; Neta, P. *Atmos. Environ.* **1987**, *21*, 1743.
(18) Lee, Y. N.; Schwartz, S. E., Brookhaven National Laboratory, ref 7 and private communication.
(19) Oblath, S. B.; Markowitz, S. S.; Novakov, T.; Chang, S. G. *J. Phys. Chem.* **1982**, *86*, 4853.
(20) Oblath, S. B.; Markowitz, S. S.; Novakov, T.; Chang, S. G. *J. Phys. Chem.* **1981**, *85*, 1017.
(21) Nunes, T. L.; Powell, R. E. *Inorg. Chem.* **1970**, *9*, 1916.
(22) Littlejohn, D.; Hu, K. Y.; Chang, S. G. *Inorg. Chem.* **1986**, *25*, 3131.
(23) Hoffman, M. R. *Atmos. Environ.* **1986**, *20*, 1145.

Received for review June 25, 1987. Accepted December 14, 1987. Although the research described in this paper has been funded in part by the U.S. Environmental Protection Agency through Interagency Agreement DW13931327-01-0, it has not been subjected to the Agency's required peer and policy review and therefore does not necessarily reflect the views of the Agency, and no official endorsement should be inferred.

Environ. Sci. Technol. 1988, 22, 590–592

NOTES

Gran's Titrations and Ion Balances: Some Analytical Control Limits for Precipitation and Surface Waters

Neil R. McQuaker* and Douglas K. Sandberg

Environmental Laboratory, Ministry of Environment, 3650 Wesbrook Mall, Vancouver, British Columbia, Canada V6S 2L2

■ Analytical results provided by weakly buffered samples are used to define control limits for cation–anion balances when the combined cation plus anion concentration is below 700 μequiv/L. Application of the control limits can help identify when measurement processes are out of control. For acidic precipitation, an important component of the ion balance is free acidity, and in many applications, the determination of whether or not the free acidity exists principally as strong acidity becomes important. Use of Gran's titration in making this determination is discussed. The deviation from unity of the rate of change of $[H^+]$ with respect to the addition of titrant is used as a control limit that monitors the presence of interference.

Introduction

Use of an ion balance (anion – cation difference) has long been recognized as an important quality control check in the analysis of water samples (*1*). When control limits for the ion difference are available, they can be used to help identify when one or more of the laboratory measurement processes is out of control. Control limits for weakly buffered samples have evidently not appeared in the literature, and in this work analytical data provided by precipitation and surface waters of low alkalinity are used to determine typical values. The samples used were collected from some 30 sites that were approximately equally distributed between precipitation and surface water monitoring sites located in British Columbia. Procedures for sample collection and preservation appear elsewhere (*2*). All chemical analyses were carried out over a 6 month period at the Environmental Laboratory, Ministry of Environment, with routine procedures (*3*).

For acidic precipitation, an important component of the ion balance will be free acidity, and in order to assess the environmental impact of acidic precipitation it becomes important to know whether or not the free acidity exists principally as strong acidity. Recently, it has been suggested that the ratio $-\Delta[H^+]/\Delta C_B$ provided by Gran's titration could be used to make this determination (*4*); ΔC_B is the moles liter^{-1} of strong base required to produce a concentration change of $\Delta[H^+]$. In this approach, the deviation from unity of the rate of change of $[H^+]$ with respect to the addition of titrant becomes a control limit that monitors the presence of interference. Application of this approach to British Columbia precipitation samples is discussed.

Results and Discussion

Ion Balance. It was assumed that the major ions present in the samples are those appearing in Table I. Alkalinity was determined from Gran's titration, free acidity was determined from sample pH, and the balance of the ions was determined by either ion chromatography or inductively coupled plasma emission spectroscopy (Ca^{2+} and Mg^{2+} only). Detection limits for each of the parameters appearing in Table I are typically 1 μequiv/L or less (*3*), and participation in a series of interlaboratory comparison studies has suggested that the various analytical techniques used are free from significant measurement bias (*5*). Data from 233 samples provided the results shown in Table II for standard deviations of the anion – cation difference (A – C) associated with mean anion + cation concentrations (A + C) below 700 μequiv/L. The results are plotted, by using a least-squares linear regression fit, in Figure 1. They provide a "linear" relationship similar to that observed by earlier workers (*1*) at much higher ion concentrations (approximately 100 times higher) and are compatible with the expectation that the standard deviation will increase with increasing concentration.

Table I. Parameters Used in the Ion Balance

cations	anions	cations	anions
Ca^{2+}	SO_4^{2-}	K^+	F^-
Mg^{2+}	NO_3^-	NH_4^+	alkalinity
Na^+	Cl^-	free acidity	

When the results of Figure 1 are applied to individual samples, we expect that approximately 5% of the observed ion differences, A – C, will exceed plus or minus two standard deviations (±2 SD) and approximately 0.3% will exceed ±3 SD. The 5% that exceed ±2 SD should be flagged and all analytical results critically examined before the individual analyses for a particular sample are accepted or rejected. If a deviation of ±3 SD is exceeded (when major ions other than those of Table I are absent), then the measurement process for one or more analyses can be considered to be out of control. A summary of criteria for acceptable ion balances based on two standard deviations appears in Table III. It should perhaps be noted that the 2 SD and 3 SD control limits, which can be identified from Figure 1 (and Table III), are for samples collected in British Columbia and analyzed with the procedures employed by the Environmental Laboratory, Ministry of Environment. Samples collected in a different geographical area and analyzed at a different laboratory may provide slightly different control limits. This may be particularly true at low-ion concentrations (approximately 20–50 μequiv/L) where analytical detection limits and sample composition become limiting factors.

If we consider "duplicate" ion (i.e., cation–anion) analyses to be analogous to duplicate analyses of an individual analyte and if we designate the extrapolated standard deviation at zero concentration as S_0, then the "effective detection limit" for ion concentration may be estimated to be $(2\sqrt{2} \times 1.645)S_0$ (*6*). This provides a result of 17 μequiv/L when we use the S_0 value of 3.65 μequiv/L ob-

 0013-936X/88/0922-0590$01.50/0

Table II. Standard Deviation of Ion Difference as a Function of Ion Concentration[a]

	ion concentration, μequiv/L						
	40–70	70–100	100–150	150–200	200–300	300–500	500–700
no. of results	55	50	31	34	20	20	23
mean ion concn (A + C)	55	85	120	170	230	390	590
SD (A – C)	5.0	5.3	7.6	9.0	10.7	15.0	20.5

[a] (A + C) = anion + cation concentration; (A – C) = anion – cation difference.

Table III. Criteria for Acceptable Ion Balances[a]

ion concn (A + C), μequiv/L	ion diff (A – C), μequiv/L	(A – C)/(A + C)
20–50	8–10	0.40–0.20
50–200	10–19	0.20–0.10
200–700	19–49	0.10–0.07

[a] Based on two standard deviations; i.e., A – C = 2[0.0290(A + C) + 3.65].

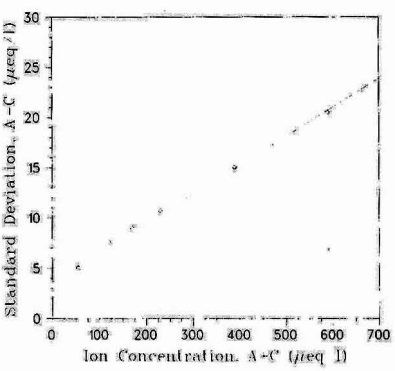

Figure 1. Standard deviation of the ion difference, A – C, versus the ion concentration, A + C. The curve is the least-squares linear fit $y = 0.0290x + 3.65$; $r = 0.996$.

tained from Figure 1 and suggests that, in our laboratory, ion balances are meaningful for only those samples where the ion concentration exceeds approximately 20 μequiv/L. Even so, an ion concentration of 20 μequiv/L is extremely dilute and will include essentially all weakly buffered samples, including precipitation. This compares with the earlier work (*1*) where the ion concentration requirement for a meaningful ion balance was approximately 500 μequiv/L (S_0 = 106.5 μequiv/L). The 500 μequiv/L concentration cannot include weakly buffered samples, and the S_0 ratio of 106.5:3.6 is a measure of the enhanced detection limits (i.e., 1–2 orders of magnitude) that currently make this possible.

Gran's Titration. Gran's titration curves may be generated by plotting $(V_0 + V)[H^+]$ versus V where V_0 is the original sample volume and V is the volume of titrant added. In the absence of interference, the intersection of the linear portion of the curve with the volume axis establishes the equivalence point V_e for strong acidity. The minimum requirement commonly used for establishing linearity is four successive data points with a correlation

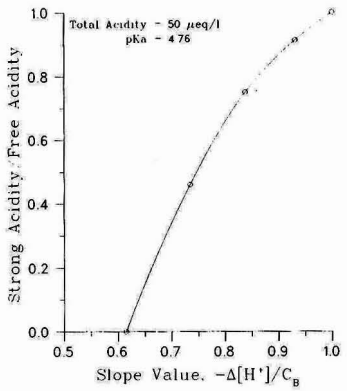

Figure 2. Strong acidity/free acidity ratio versus the slope value $-\Delta[H^+]/\Delta C_B$.

coefficient of at least 0.9995 (*7*, *8*). Recently, it has been pointed out that even though the curve is "linear", interference due to the dissociation of weak acids as the titration proceeds may be present (*2*, *9*). When dissociation of weak acids is absent, the slope value $-\Delta[H^+]/\Delta C_B$, which measures the rate of change of $[H^+]$ with respect to the addition of titrant, is expected to be unity. This suggests using a slope requirement, in addition to the linearity requirement, as a further analytical control limit. When $V_0 \gg V$, the initial titration point ($[H^+]$, zero) and the extrapolated end point (zero, V_e) may be used to approximate the slope (i.e., $-\Delta[H^+]/\Delta C_B \simeq [H^+]/(NV_e/V_0)$ = free acidity/Gran's acidity). Reference samples of 50 μequiv/L strong acidity (H_2SO_4 in distilled water) provided a slope value of 1.00 ± 0.10 where the deviation is expressed as 2 SD. This result was obtained from 23 successive replicate analyses carried out on separate analytical runs. The titrations were carried out with 0.01-mL incremental additions of 0.01 N NaOH (*7*).

Results provided by 70 acidic precipitation samples for the slope value $-\Delta[H^+]/\Delta C_B$ obtained from free acidity/Gran's acidity ratios are summarized in Table IV as a function of free acidity. The interval 15–80 μequiv/L free acidity shows a mean slope value of 0.95 ± 0.14 (which compares with the reference value of 1.00 ± 0.10). The observed deviation of the mean slope value from unity tends to suggest that some dissociation of weak acids may be occurring as Gran's titrations proceed. A graphical illustration of the effect of dissociation on the slope values appears in Figure 2. Here, slope values for mixtures of a weak acid of pK_a 4.76 (acetic acid) and a strong acid,

Table IV. Slope Values and Ion Ratios as a Function of Free Acidity

	free acidity, μequiv/L			
	15–20	20–30	30–80	15–80
no. of results	20	30	20	70
mean slope ($-\Delta[H^+]/\Delta C_B$)	0.94 ± 0.12	0.97 ± 0.15	0.96 ± 0.15	0.95 ± 0.14
mean ion ratio (C/A)	0.97 ± 0.11	0.96 ± 0.19	0.95 ± 0.19	0.96 ± 0.17

containing 50 μequiv/L total acidity, are plotted versus the strong acidity/free acidity ratio. The results show that if a 15% interference (i.e., a strong acidity/free acidity ratio of 0.85) is admitted, then the control limit for the slope is 0.890.

When the 85% strong acidity criteria is maintained, the control limit will tend toward higher/lower values as the pK_a value and/or total acidity decreases/increases. For example, at pK_a 4.76, the control limit shifts from 0.850 to 0.925 as the total acidity shifts from 80 to 15 μequiv/L. Application of these results to the mean slope values appearing in Table IV suggests that, within the limits of analytical precision, interference is not a significant factor for British Columbia precipitation samples. This conclusion is supported by mean cation/anion ratios, C/A (see Table IV), which give no evidence of the anion deficit expected if significant concentrations of partially dissociated weak acids were present. Even so, the small deviation of the mean slope values from unity does suggest marginal interference and is compatible with recent reports that the majority of precipitation samples are expected to contain weak organic acids (*9*). Within this context, the use of the slope value (or free acidity/Gran's acidity ratio) to monitor the presence of interference becomes important, and the principal appeal of Gran's titration is that it can be used (together with the ion balance) to help confirm whether or not the free acidity exists principally as strong acidity.

Registry No. H_2O, 7732-18-5.

Literature Cited

(1) Greenberg, A. E.; Navone, R. *J.—Am. Water Works Assoc.* **1958**, *50*, 1365.
(2) McQuaker, N. R. *Precipitation and Surface Water: Recommended Methods for Sampling and Site Selection*; Federal-Provincial Research and Monitoring Co-ordinating Committee for the Long Range Transport of Acid Pollutants; Environment Canada: Ottawa, Ontario, 1983.
(3) McQuaker, N. R.; Sandberg, D. K.; Keene, W. C.; Galloway, J. N. *Atmos. Environ.* **1986**, *20*, 1507.
(4) McQuaker, N. R. *A Laboratory Manual for the Chemical Analysis of Ambient Air, Emissions, Precipitation, Soil and Vegetation*; Ministry of Environment, Province of British Columbia: Victoria, 1983.
(5) Aspila, K. I.; Todd, S. *LRTAP Intercomparison Studies L1–L12: Major Ions, Nutrients and Physical Properties of Water*; Environment Canada: Ottawa, Ontario, 1983–1986.
(6) King, D. E. *Analytical Reproducibility*; Ministry of Environment, Province of Ontario: Toronto, 1976.
(7) McQuaker, N. R.; Kluckner, P. D.; Sandberg, D. K. *Environ. Sci. Technol.* **1983**, *17*, 431.
(8) McQuaker, N. R. *Measurement of Acidity and Alkalinity*; Federal-Provincial Research and Monitoring Co-ordinating Committee for the Long Range Transport of Acid Pollutants; Environment Canada: Ottawa, Ontario, 1986.
(9) Keene, W. C.; Galloway, J. N. *Atmos. Environ.* **1985**, *19*, 199.

Received for review July 15, 1986. Revised manuscript received April 6, 1987. Accepted December 11, 1987.

Remember when . . .

- ☐ The unknown unknown made you groan?
- ☐ Acid left you less than placid?
- ☐ It wasn't foreseen you could screen?
- ☐ You saved the hour with XRF power?

So your lab's running smoother these days? Your "total unknowns" are getting known quickly? Your fingers are the color of the rest of you again (not acid yellow)? And you're saving hours of costly lab prep by pre-screening your samples?

Splendid. Aren't you glad you added STXRF™ to your arsenal of analysis tools? Now all you need to remember: STXRF will analyze just about any substance, known or unknown. Solid, liquid, or any state between. You simply set the correct excitation to get a full composition rundown. This includes light elements.

And when it comes to substances like halogens or silicates (which AA and ICP techniques may miss) STXRF really shines, earning its keep a hundred times over.

Of course, your application may sometimes call for further analysis. In which case, STXRF can quickly tell you the dilution necessary to bring your sample within AA's or ICP's dynamic range, saving hours of guesswork.

If you haven't installed powerful STXRF yet, call Capt. Kev TOLL FREE at 1-800-227-0277 (In CA: 1-800-624-4374) for a demo or literature packet.

Be lab-merry not lab-wary.

*STXRF (source tuned X-ray fluorescence) is a trademark of Kevex Corporation.

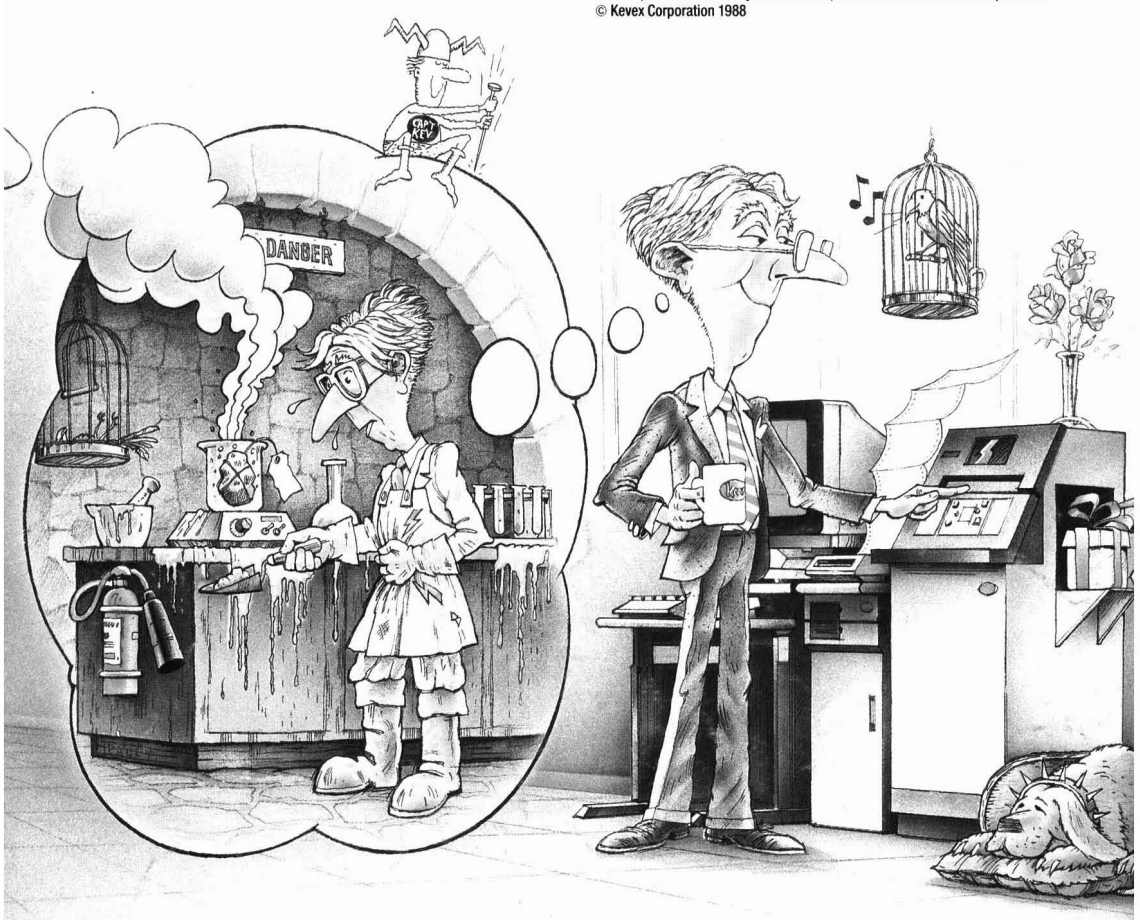

Kevex Corporation 1101 Chess Drive, Foster City, CA 94404 415-573-5866 1-800-227-0277 (In CA: 1-800-624-4374)
Kevex Affiliate (Getac GmbH) Tel 49-6131-40091 Kevex Canada, Ltd. Tel 416-731-2161 Kevex France (Fondis, S.A.) Tel 33-1-34810024 Kevex UK Tel 44-582-400596

kevex®